Engineering Sciences
New Trends, Concepts and Research

Editor
Assoc. Prof. Dr. Halil İbrahim Kurt

Engineering Sciences New Trends, Concepts and Research

livredelyon.com
livredelyon
livredelyon
livredelyon

Engineering Sciences

LIVRE DE LYON

Lyon 2021

ENGINEERING SCIENCES
New Trends, Concepts
and
Research

Editor
Assoc. Prof. Dr. Halil İbrahim Kurt

LIVRE DE LYON

Lyon 2021

Engineering Sciences New Trends, Concepts and Research

Editor • Assoc. Prof. Dr. Halil İbrahim Kurt • Orcid: 0000-0002-5992-8853
Cover Design • Clarica Consulting
Book Layout • Mirajul Kayal
First Published • December 2021, Lyon

ISBN: 978-2-38236-233-4

LIVRE DE LYON

PREFACE

The researches have contributed to the development of education and training definitions in various periods. Although the importance given to science and data-based academic studies is mentioned today, it is observed that the studies conducted are far from the scientific method. Disciplinary and/or interdisciplinary studies allow for synthesis of ideas and the synthesis of characteristics from many disciplines. At the same time it addresses scientists, engineers and students' individual differences and helps to develop important, transferable skills. These skills, like critical thinking, communication, analysis, interpretation and discussion are important and continually developing at all stages of life.

One of the major aims of this 'Engineering Sciences: New Trends, Concepts and Research' was to present evidence and gather together the results of research and development carried out on the engineering applications during recent years. The book project brought together scientists and engineers involved in assessing the various engineering areas, with particular emphasis on academic studies, applications and opinions.

The editor and editorial board hope that this book will be useful to engineers and to scientists working towards an understanding of and the resolution of the applications in the various fields of engineering that we have to face in near future.

Assoc. Prof. Dr. Halil İbrahim Kurt

CONTENT

CHAPTER 1

DETECTION AND CLASSIFICATION NATURAL DISASTERS USING TWITTER DATA WITH DEEP LEARNING APPROACH

Fatma KAHRAMAN[1] & Oğuzhan YARDIMCI[2] & Yunus DOĞAN[3]

[1](BSc) Dokuz Eylul University, Faculty of Engineering, Department of Computer Engineering, Izmir/Turkey,
e-mail: fatma.kahraman@ceng.deu.edu.tr
Orcid: 0000-0002-5231-9641
[2](BSc) Dokuz Eylul University, Faculty of Engineering,
Department of Computer Engineering, Izmir/Turkey,
e-mail: oguzhan.yardimci@ceng.deu.edu.tr
Orcid: 0000-0003-4915-1881
[3](Asst. Prof.) Dokuz Eylul University, Faculty of Engineering,
Department of Computer Engineering, Izmir/Turkey,
e-mail: y.dogan@deu.edu.tr
Orcid: 0000-0002-0353-5014

1.   Introduction

Twitter is a social networking service where users can post messages known as "tweets" of up to 280 characters, interact such as likes and retweet tweets. It has recently become a significant real-time source of information in natural disasters, major crises, or events. Twitter data can be used for detecting natural disasters or major crises. Nowadays, using Twitter data, studies about before, during and after natural disasters have become so popular.

Izmir has a geographical location where many natural disasters occur such as earthquakes, floods, storms. For this reason, various natural disasters often occur in Izmir. During these natural disasters, it has been observed that tweets

about natural disasters are posted by eyewitnesses. Therefore, there is a need for a study on natural disasters using Twitter data. In this study, particularly in locations where natural disasters occur frequently in Izmir natural disasters that occurred must be detected and classified.

There are two main problems in this thesis. The first problem is that millions of tweets are posted on Twitter every day. Many of these tweets may contain irrelevant or misleading text, so they should be filtered first. With this filtering, useful tweets should be obtained for our study. It is necessary to detect a disaster by analyzing whether these tweets contain panic in their content. The second problem is the classification of the type of natural disaster if a natural disaster that creates this panic environment after a panic situation is caught in the content of the tweet. This classification, which will be carried out with Machine Learning technique, creates another problem.

Recently, it is seen that many studies have been carried out about natural disasters using Twitter data. Studies managed in Turkey: A study was developed by (Cam & Duman, 2019) using artificial neural networks based on b value to predict earthquakes at earthquake regions in Turkey. However, it would be more effective to determine the natural disaster in real time instead of making an unrealized earthquake prediction. An advantage of our study is that it is developed with a deep learning approach. Although there is a study carried out using twitter and ekşi sözlük earthquake data (Yazan & Üsküdarlı, 2014), deep learning approach, machine learning techniques were not used in their study. One of the first reasons why our proposed study has been carried out is that when these studies were examined, there were not enough studies on natural disasters in Turkey using twitter data created by Twitter users.

While studies with deep learning have increased recently, there are many studies using existing machine learning techniques in natural disaster. Many studies have been developed to identify and classify the related disasters/ crisis tweets (Aipe, Mukuntha, Ekbal & Kurohashi, 2018). Their study was focused on classify in the 7 different categories using Deep learning CNN architecture. These classification classes are casualties and public impact, collateral damages, general awareness, voluntary services, sympathy and emotion, crisis-specific information and non-informative. Besides, if the type of natural disaster that occurred was predicted, a better project would come out. There are also lots of event detection with twitter data such as earthquakes, floods etc. developed by (Burel, Saif, Fernandez & Alani, 2017). Inspired by their work, for Turkish tweets posted at locations in Turkey have contributed to the realization of our

study. Moreover, there are studies that classify different types of eyewitness messages in twitter data during natural disasters using supervised machine models (Zahra, Imran & Ostermann, 2020). In this research, the classification model was based solely on the random forest algorithm. Deep learning has been carried out for social media text classification using specific hurricane cases (natural disasters) (Yu, Huang, Qin, Scheele, & Yang, 2019) (Sit, Koylu, & Demir, 2019). The twitter data of natural disasters occur frequently in Turkey in locations where it is desired to detect a variety of natural disasters. It is not just hurricane detection like their study. In addition, a study was developed that sentiment analysis of Twitter data during crisis events or natural disasters by Bayesian networks classifiers (Ruz, Henríquez, & Mascareño, 2020). Support vector machines and Random forests are used in their study. It would be better if natural disaster predictions were developed with deep learning after sentiment analysis was done. Location words in twitter data were extracted using a Convolutional Neural Network model during emergencies in this research (Kumar & Singh, 2019). Only earthquake-related studies have been conducted, but no studies have been conducted on other natural disasters. Therefore, all these studies enabled us to realize the project. Along with previous research in the world, studies have also been conducted in Turkey using Twitter data on natural disasters.

The main aim of this thesis is to detect and classify natural disasters by listening to the locations of natural disaster zones marked within the borders of Izmir via Twitter with tweets thrown in real time.

Firstly, it is aimed to investigate the regions where natural disasters occur frequently in Izmir and to obtain listening locations via Twitter. Tweets posted from these locations are collected in real time. It is aimed to make a panic situation analysis within the data obtained by our study.

Secondly, panic analysis consists of two prediction stages in our study. In the first stage, panic scores are calculated using a dictionary from tweet contents. As a result of panic score calculation, the filtering part is created. It is aimed to complete the filtering part using a dictionary. The second stage again has predicted the content of tweets filtered by the dictionary using deep learning. The result of this prediction categorizes which type of natural disaster occurred. It also has been prevented by incorrect evaluations at the filtering stage owing to the dictionary. In this way, the system is intended to make decisions with a high accuracy rate. Thus, both the double-verified natural disaster detection system and the determination of the type of natural disaster are included in the same application.

Finally, thanks to this architecture, artificial intelligence has been created that analyses the sense of panic that occurs on the twitter platform and predicts its results. With this result, the information that people create on social media can be automatically processed and turned into useful systems for people. During natural disasters, it is aimed to implement an alternative disaster detection system in case of inability of traditional emergency telephone lines (110, 112, 155 etc.) or collapse of telephone networks.

Specific natural disaster areas are listened to in real time on Twitter. Panic analysis is done with the ANEW dictionary without processing the data obtained from Twitter. Thus, the first prediction step, the filtering, is completed. Panic tweets from the dictionary move on to the next step, the deep learning model. Classification is made by predicting tweets with the deep learning model. Thanks to the classification model, the type of natural disaster that occurs is obtained and the natural disaster is determined.

Train and validation data are needed to train our deep learning model. In order to obtain the data, the time of natural disasters that occurred in the past is examined and the natural disaster data of those times can be accessed via Twitter. A deep learning architecture for multi-label classification in four different categories (earthquake, flood, storm, and no natural disaster) has been required to be realized.

Access to the twitter API has been provided by Twitter to access the Twitter data. Thanks to the Twitter API, tweets from certain natural disaster locations in Turkey have been accessed. Data obtained from Twitter has been stored by PostgreSQL database. Stream mining algorithms, text mining algorithms and Natural Language Processing (NLP) algorithms have been applied on these tweets. An ANEW dictionary has been used for analyzing panic situations. Deep learning has been tested using the TensorFlow and Keras frameworks in Python programming language to determine the type of natural disaster that has occurred. This project has been developed in Google Colab. Twitter data on natural disasters that have occurred so far has been tagged and created train and validation data. Classification model has been trained with Deep Learning technique. Classification predictive architecture has been convenient with multi-layer classification.

2.   Literature Review

In a study by (Fersini, Messina & Pozzi, 2017), a decision support system based on natural language processing was developed for earthquake management.

When earthquakes occur, social media users generate a huge amount of data. Thanks to the extraction of real twitter data, people can instantly respond to emergency calls through this decision support system. In addition, this study provides access to information such as earthquake damage, magnitude, location, and time references.

The purpose of a study developed by (Zahra, Imran & Ostermann, 2020) is to classify different types of eyewitness messages in twitter data during natural disasters. Each eyewitness type has characteristics, for these characteristics related keywords were used to detect kinds of eyewitness types. To learn whether a tweet was posted by an eyewitness or not, supervised machine learning models were used in this study. There are four different models (using textual features, using domain-expert features, using text and domain-expert features, and using text and domain-expert features with class balancing) to train for each event i.e. earthquake, flood etc. Also, related tweets were analyzed manually. As a contribution to science, this study has led to a lot of research that will contribute to the response of aid organizations by analyzing the content of tweets posted by people in case of natural disasters.

In a study by (Win & Aung, 2017), a tweet monitoring system was developed. This system defines tweets posted during natural disasters according to information categories and provides target information automatically according to the user's request. This system extracts and classifies the information actionable tweets from large amounts of raw tweets on Twitter using machine learning and natural language processing (NLP). In the feature extraction phase, only linguistic features, sentiment lexicon, and especially catastrophe lexicon-based features were used. The developers evaluated the performance of the system with four public datasets. As a result, classification accuracy on the proposed features set is higher than neural word embeddings and standard bag-of-words models.

The purpose of the study, developed by (Reynard & Shirgaokar, 2019), is to analyze tweets about Hurricane Irma in Florida to ensure efficient resource allocation in natural disasters using data on Twitter, a location-based social network. Machine learning and geospatial techniques were used to classify geolocated tweets. Sentiment analysis was carried out by classifying the tweets about damage as negative, neutral, and positive using the Python library, TextBlob in this article. The method in this research can be changed and used in areas other than the disaster area.

In a study by (Kaufhold, Bayer & Reuter, 2020), real-time sentiment analysis was performed on tweets that are posted from Twitter and time-based

analytics are provided to the user. Sentiment analysis feature-based sentiment classification and opinion summarization is focused on study. Sentiment classification feature-based classification and handling negations are problems in research. Efficient techniques are required for collecting a large amount of Twitter data and extract meaningful information. An interactive automatic system is provided predicting the sentiment of tweets on Twitter using Hadoop. A huge amount of data can be processed by Hadoop.

In a study by (Hagras, Hassan & Farag, 2017), tweets related to the 2011 Japan Tsunami were detected using Latent Dirichlet Allocation algorithm. In this study, it was checked whether the tweet content in the dataset contains "tsunami" or #tsunami. Latent Dirichlet Allocation algorithm was used for text mining and clustering to obtain knowledge from Twitter stream on natural disasters such as the time of the natural disaster, the location of the natural disaster, the number of injuries.

In a study by (Alam, Ofli, Imran & Aupetit, 2018), during the hurricanes Harvey, Irma and Maria, the textual and multimedia content of the related tweets were analyzed for making sense of large amounts of data about natural disasters. Different machine learning algorithms were used to process the data produced when natural disasters occurred and were carried out on Natural Language Processing and Artificial Intelligence techniques. LDA was used as a topic modeling technique, to generate topics from large amounts of textual data. It is to provide information that facilitates the development of automatic systems as a contribution to science.

In a study developed by (Poblete, Guzmán, Maldonado & Tobar, 2018), it was aimed to detect real-world events with the reactions of people in online social networks. Twitter has gained popularity among social networks, as real-time online access to real-time world events can be provided. Because of the noisy data in its content, Twitter-based event detection is at the heart of the challenges. Twitter-based event detection has challenges due to noisy data in its content. An online method is proposed to detect unusual crises that occur on Twitter. In addition, the projected approach is a method that can be applied to earthquake detection around the world. The proposed method has been compared with the latest technology used for earthquake tracking using social media.

The purpose of a study developed by (Yu, Huang, Qin, Scheele & Yang, 2019), is to apply a Convolutional Neural Networks model to classify tweets using labeled data from 3 different regions in hurricanes Sandy, Harvey, and Irma. This study has been done using Convolutional Neural Networks architectures. Keras library and TensorFlow were used to implement the model. The CNN

model was compared with the traditional machine learning support vector machine and logistic regression. As a result of the comparison, it was found that CNN models achieve more consistent and better accuracy in both single event and cross event evaluation scenarios. Additionally, in the study conducted in this article, knowledge such as geographical location and environmental conditions that affect the performance of the model can be added to increase the classification accuracy of the CNN model.

A study was developed by (ALRashdi & O'Keefe, 2019), using deep learning and domain-specific word placement to classify tweets for crisis response. The CrisisNLP dataset evaluated four different tweet classification models. These include 2 Convolutional Neural Networks and the other two of them as a deep learning architecture, Bi-LSTM. Crisis embedding and Glove embedding have been implemented separately in each deep learning architecture. In the results, it was seen that Glove, that is, general purpose word placement, achieved the highest performance with Bi-LSTM and can be used instead of field-specific embedding for text classification for crisis response.

In a study developed by (Romascanu, Ker, Sieber, Greenidge, Lumley, Bush & Brunila, 2020), machine learning, and social network analysis (SNC) are combined. A case study was presented using twitter data obtained from Nebraska floods in the United States in March 2019. Deep Learning (DL) was used to classify the content of the Twitter data. The Deep Learning model was trained with the Bert algorithm, which is the DL language technique, and then the model was trained with twitter data in crisis moments.

In a study developed by (Aipe, Mukuntha, Ekbal and Kurohashi, 2018), it is aimed to identify and classify the huge amount of data produced on Twitter during crisis scenarios. Convolutional Neural Network (CNN) was used for multi-labeled classification of crisis scenarios. Using the deep-CNN model, the extraction of various linguistic features is augmented.

In a study developed by (Nguyen, Joty, Imran, Sajjad & Mitra, 2016), Deep Neural Network (DNN) was used to identify and classify informative tweets that speed up decision-making processes during natural disasters. A new algorithm based on stochastic gradient descent has been proposed to train DNN. The trained model was tested using real world Twitter data. Using DNN in addition to NLP techniques has facilitated the challenging process of tweets processing.

In a study developed by (Sit, Koylu & Demir, 2019), first, a human-labeled training data set was created, and then Deep Learning networks and machine learning methods were trained for binary classification as disaster-related or

not. Long Short-Term Memory (LSTM) network was used for classification because the LSTM network was performed successfully to consider the whole text structure using long-term semantic word and feature dependencies. Second, unsupervised multi-label classification was employed with Latent Dirichlet Allocation (LDA) to identify latent categories such as affected individuals and disrupted services. Third, spatially adaptive kernel smoothing, and density-based spatial clustering were used to define relative prominence and domain for each information category. As a result of the steps taken, it was to highlight the areas where individuals affected by the disaster and infrastructure damage may be high.

In a study developed by (Kumar, Singh, Dwivedi, and Rana, 2020), a multi-modal approach was introduced to determine the informative content about the disaster by using the text and images in the tweets together. This approach was based on Long-short-term-memory and VGG-16 network bases. Seven different datasets related to disaster have been verified. In the F1 score range, results between 0.74 and 0.93 were obtained when tweet texts and images were used together, and between 0.61 and 0.92 when only tweet text was used. With the results obtained, it was stated that the multi-modal system had a good performance in determining the informative Twitter data about disasters.

In the study developed by (Laylavi, Rajabifard and Kalantari, 2017), it is aimed to determine whether the content of the tweets is related to the storm event in Sydney. So there is a specific event detection. To carry out this study, a method was applied to score the event relationship by comparing the relevant tweets with words specific to the predefined event. Streaming API was used as it was intended to listen to the tweets in real time. In this study, an API listener named tweepy is used to interact with the Stream API. Additionally, if deep learning were used, the study would become more comprehensive.

Developed by Arachie, Gaur, Anzaroot, Groves, Zhang & Jaimes, 2020), the aim of the study is to provide an alternative solution that detects sub-events thanks to unsupervised learning using posted twitter data during and after natural disasters such as earthquakes. A huge natural disaster causes a huge destruction, so it happens lots of significant sub-events during a huge natural disaster. Thus, lots of events were detected on Twitter and collected sub-events in this study. To detect sub-events, a method was used that consists of extraction of sub-events from text, ranking of candidate sub events and clustering. As a contribution to science, this study will contribute to determining the sub-events of natural disasters by using Twitter data in real time in the future.

In a study developed by (Kumar and Singh, 2019), enables the determination of geolocation using a Convolutional Neural Network to extract the location word used in the tweets. In addition, it allows us to detect emergencies, natural disasters early in services using location. Twitter provides three location information for sharing a user's location: user location, name of place, geographical coordinates. In this study, it is checked whether there is a location name in the content of the tweet and if there are these words are highlighted. Location names were estimated owing to the features of the location names in the tweets in the proposed model. This proposed architecture consists of 3 parts: word embedding that represents tweets in vector form, the convolutional model that learns the salient features from the tweet's representation and a fully connected layer interpreting the extracted features to predict the output.

In a study developed by (Burel, Saif, Fernandez and Alani, 2017), introduced the Dual-CNN deep learning model to understand the type of crisis using social media data in crisis situations. A layer of semantics was added to the CNN model to capture scarce semantic information from badly formatted social media messages. More than 79% of success has been achieved in classifying the new model event types they have created according to their results. While identifying fine-grained event-related information, a decrease was observed in the performance of the model.

In a study developed by (Madichetty, & Muthukumarasamy, 2020), it is aimed to detect situational tweets posted when a natural disaster occurs. The tweets posted during natural disasters are divided into situational and non-situational information categories. Convolution Neural Network (CNN), Long Short-Term Memory (LSTM), Bidirectional Long Short-Term Memory (BLSTM) and Attentive Bidirectional Long Short-Term Memory (BLSTM-attention) architectures were used in this study. Using various Deep learning architectures, a solution has been created on the problem of detecting situational tweets. In addition, the model was trained with tweets in English as well as in Hindi to identify situational tweets during the disaster. The results of deep learning models show that it outperformed traditional approaches such as the low-level SVM classifier for detecting situational tweets during natural disasters.

3.   Requirements / Requirement Engineering

With the "check missing values function", it is checked whether there is any missing value in the dataset. The removal of missing value data that is not useful for model training is performed. It takes the function parameter dataset and returns how many missing values are and which data they belong to.

With the "check duplicates function", duplicate data in the dataset is not meaningful for model training, so a function is needed to remove duplicate data with "remove duplicates" function. With this function, how many duplicate data are and what these duplicate data are obtained by the function.

With the "remove tokenizing word function", a machine cannot accurately process the language in its original form, so it must be processed to make the machine easier to understand. For this, the process of separating each tweet, which is called tokenizing, into words is performed. It is a function to separate every tweet in a data set, word by word. The return value of this function is the word string. With the "remove stop word function", the stop word function ensures that Turkish stop words are removed from the dataset. Stop words do not make sense to train the model. Thus, it is removed from the data set.

With this function, the dataset does not contain any stop words. With the "normalizing words – lemmatization function", it is a function in which the words that have the same root or have certain inflections suffix and derivational affix in the dataset are concentrated into a single form and normalization of words is done. The lemmatization normalization process is performed for each tweet in the dataset. With this function, the normalization requirement of the data is dealt with.

With the "vectorizing text function", Vectorization allows us to transform a token into a vector or a numerical array to represent various properties of a token in the context of the NLP. Vectors are performed to find word similarities, classify text, and other NLP operations. For the algorithms used to train machine learning models to work with text, the text needs to be converted to numbers first. There are three main approaches to doing this: Word Bag, TF-IDF, and Word2Vec. This function provides the conversion of words into numbers and training the model. With the "remove noise data function", noise data is removed from the data set. This function has fulfilled the requirement to remove punctuation marks and special characters from tweets. Performing all these procedures allows to reduce the inherent noise in the text and increase the accuracy of the results for modelling.

With the "under-sampling method function", the target attribute values that are unbalanced in the dataset are balanced. This function fulfils the requirement to prevent the model from being more inclined to any attribute value. This function takes the data set as a parameter. The function returns the balanced dataset. With the "split dataset function", the dataset is divided into test and train. This function fulfils the requirement to divide the dataset into two as a test and train before training the model. The parameter of this function is how

much the dataset is divided between train and test data as a percentage. This function returns the train and test set. With the "start training function", the training process of the model begins.

With this function, the training and confusion matrix requirements of the models are met. The parameters of the function are train set, Test set, and hyperparameter values of models. The function creates a confusion matrix that expresses the accuracy of the models and returns the values of the trained model. With the "read database function", data is read from the database. This function fulfils the requirement to read data from the database. The parameters of this function are the database query. With the "write database function", data is written from the database. This function fulfils the requirement to write data to the database. The parameters of this function are the database query.

With the "ANEW panic score calculation function", panic analysis is performed. It is calculated according to the dominance, arousal, variance values in ANEW. This function fulfils the requirement to filter the big data in Twitter according to whether it contains panic or not. With this calculated data, the function returns the panic score as the return value. The parameter of this function is the sentence whose panic value is calculated. With the "twitter listener function", the stream feature of twitter API is used. Thanks to this feature, the query always stays live on Twitter in real time. Each tweet that matches the query is notified in real time and instantly with the tweet API. Thus, every event that happens on Twitter can be followed. This function in run time, fulfils the requirement to listen to Twitter. The parameters of this function are the query for tweet queries.

With the "get tweet for train model function" - for the machine learning model where performed panic analysis and for the deep learning model where predicted the type of natural disasters - tweets to be used in the creation of the test, train and validation data set are collected. There is a Twitter API in this section. Tweets obtained with this function have been saved in the database. This function fulfils the requirement of data collection for model training. The parameters of this function are the query where tweet queries are made.

Firstly, it is necessary to filter this data, since there is a lot of data on Twitter. Since the subject of the project is to detect natural disasters and predict their types, capturing tweets involving panic situations on Twitter should fulfil the requirement at first. In the project, a model was created using the machine learning technique with the dataset labelled that there is a panic or no panic situation consisting of Twitter data. In addition, by using the ANEW dictionary, the panic score was calculated, and a text mining process was performed. In this

way, machine learning, and text mining are compared and it is decided which technique is more effective in removing a panic situation. By listening to Twitter in real time with the chosen technique, analyze the panic situation is fulfilled the requirement in the tweet content.

Secondly, the data containing panic situations are written to the database to be classified into classes in the deep learning model. The data kept in the database are the input values for the deep learning model. With the database, storing data with panic situations fulfils the requirement to be predicted by the deep learning model.

Thirdly, in the deep learning model, giving tweets containing panic as input enables the model to predict the tweets that are more prone to natural disasters. As a result of the deep learning model, these data received as input are determined to which type of natural disaster it belongs. In addition, as a result of the analysis of the panic situation, although it does not contain any natural disasters, misleading inputs can be found due to the high panic score. Thanks to the deep learning model, the result that these misleading inputs do not actually contain any natural disasters is revealed with the deep learning model.

Finally, in addition to using machine learning model and using ANEW dictionary as text mining technique separately, the use of the outputs obtained from one of these two techniques as input for the deep learning model fulfilled the requirement for 2-step prediction. Therefore, there is a 2-step prediction as a model for panic situation analysis and a model for classification of natural disaster type. The "data quality function" includes the operations by which the quality of the dataset is measured, and the data can be interpreted. This function fulfils the requirement to analyze distribution, size, and quality of the data set. With the "data visualization function", the dataset is visualized. The quality of the data is observed much better with graphs. In this function, charts such as bar charts, histograms, line charts are used in the project. This function fulfils the requirement for visualization of data for analysis. Function parameters are the dataset to be visualized and the type of graph to be observed.

4.   Design

4.1. Use Cases

In the project, twitter is listened to by Twitter Listener and tweets are captured. Panic analysis is performed by the Panic Prediction model with the captured tweets. Panic tweets were written into the database.
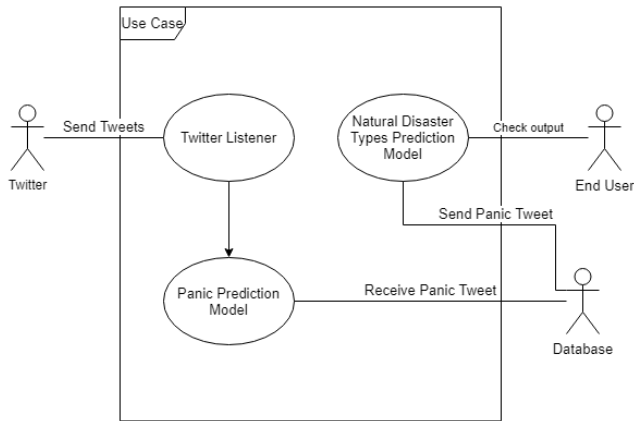
Figure 1: Use case diagram of tweet prediction system.

Later, these tweets were read from the database and panic tweets were given as inputs into the Natural Disaster Types of Prediction Model. Finally, the model's output was checked by an end user. All these phases are shown in the use case diagram (Figure 1). In this project, data analyst carries out all data pre-processing and natural language processing phases. In addition, data analyst starts train of the model. All these are shown in the use case diagram (Figure 2).
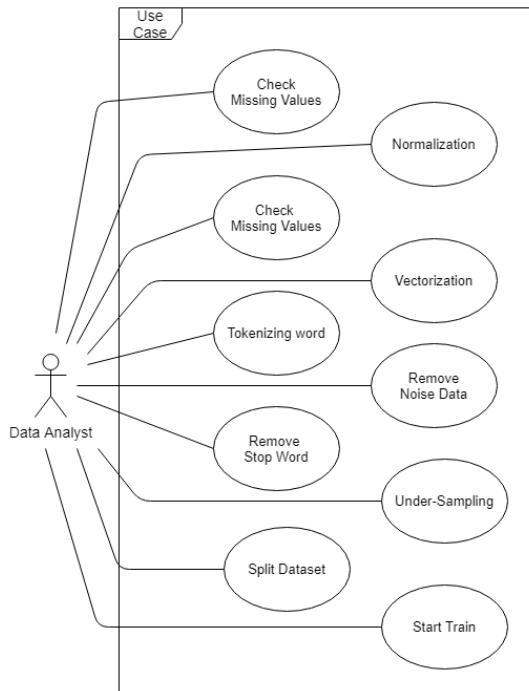
Figure 2: Use case diagram of data analyst's function.

4.2. Sequence Diagram

The sequence diagram is drawn in the project to show the progress of the tweets in run time between applications. The tweets captured by the twitter listener are divided into two by the panic prediction model, depending on whether they contain panic or not. Panic tweet is written to the database. Not-panic tweet is ignored. Natural Disaster Types Prediction Model predicts the tweet read from the database and produces whichever of 6 different outputs, the result is sent to the end user (Figure 3).
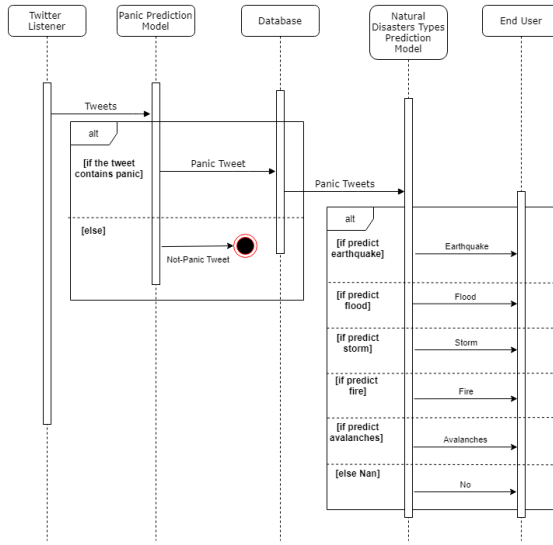
Figure 3: Sequence diagram of tweet prediction steps.

Figure 4: Sequence diagram of data analyst's steps.

The sequence diagram is drawn to indicate the data analyst's work steps. Tweets are collected by the data analyst using the twitter API. The quality of the collected tweets is controlled. Tokenizing and normalization are applied to tweets. Afterwards, the data set is prepared by applying the under-sampling method. The data set is divided into train dataset, validation dataset and test dataset before the model is trained. The model is trained. After the model is trained, the model is tested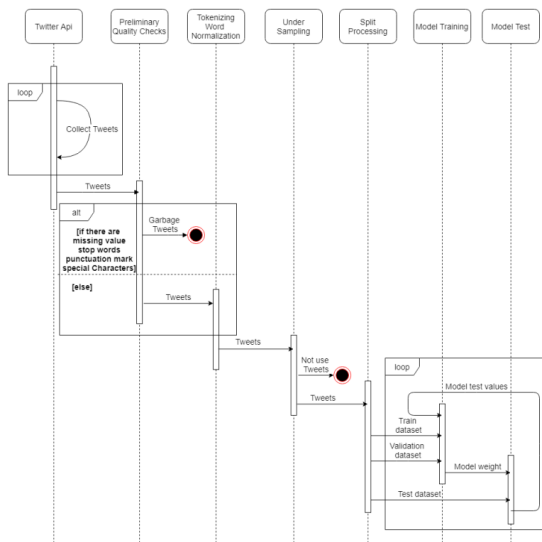 and according to the test result of the model, the model parameters are rearranged, and the model is retrained until the sufficient accuracy value is obtained (Figure 4).

4.3. Activity Diagram

After the data collection phase, the preliminary data quality was checked and the missing value, duplicate data, stop words, punctuation marks and special characters were removed. After the data pre-processing and NLP stages, the under-sampling method was applied to the data set. The dataset was divided as train, test, and validation dataset. Then, the test and training of the model interact with each other, and all these phases are shown in the activity diagram (Figure 5).
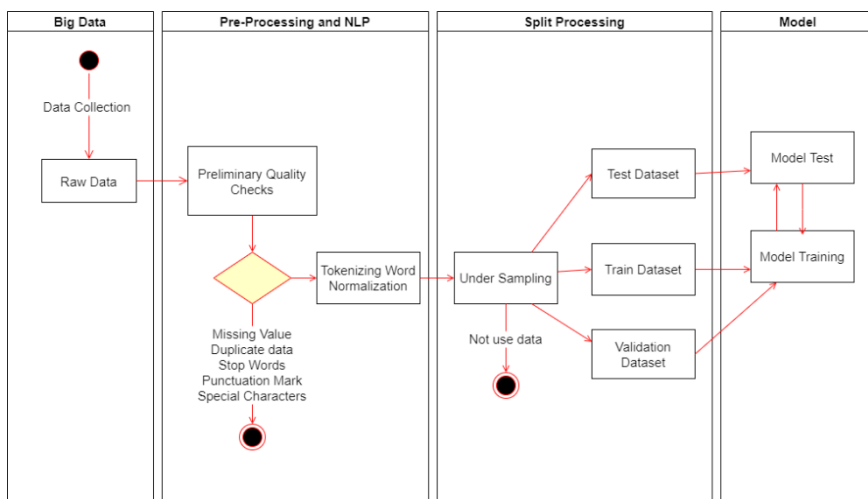
Figure 5: Activity diagram of model data processing steps.

First, data had been collected by listening to Twitter via the Twitter API to access tweets. Then, two techniques were created for the panic prediction model. While one of this technique were created by machine learning techniques, the other technique is a function which was obtained by the panic score using the ANEW dictionary. If the content of the tweet contains panic, it was written

to the database and a deep learning model was created to predict the type of natural disaster. As a result, the model ensures that each tweet is classified as earthquake, flood, avalanche, fire, storm, and no natural disaster. The activity diagram of this workflow is as follows (Figure 6).
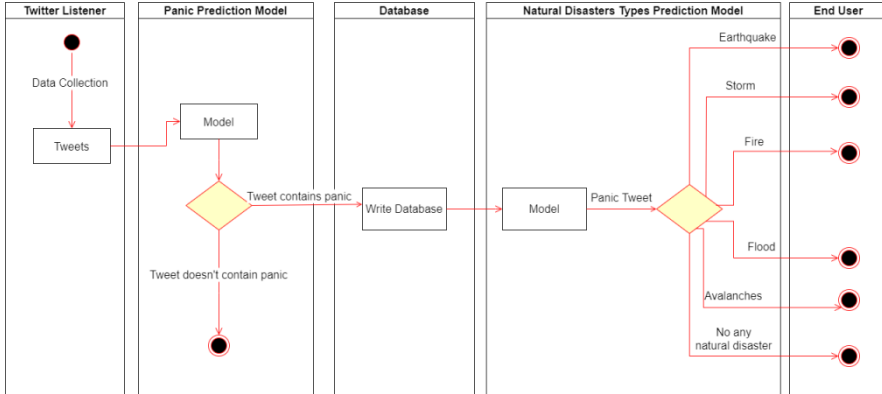
Figure 6: Activity diagram of model prediction system.

5. Implementation

5.1. Collection of Training Data from Twitter

Tweets are collected related to earthquakes, flood, storm using the keywords "deprem", "sel", "fırtına" and #deprem, #sel, #fırtına, #hortum from Twitter streaming API. For Deep Learning models to give high accuracy values, they need to be trained with a large amount of data. There is no ready data set to be used for this thesis. For this reason, when natural disasters occur, up-to-date twitter data is downloaded by using the twitter API. Current news sources are followed by television, web, or mobile news platforms to catch the times when earthquakes, floods or storm disasters occur. It is downloaded with the "getTweet.py" program, which is created to shoot tweets starting from the time of the disaster.

Program of "GetTweet.py" is used to download twitter data using tweepy library in python language. In the program, a session is opened to the twitter API with "consumer key", "consumer secret", "access token", "access token secret" tokens. The program filters the tweets according to the word to be searched, the language to be searched, the number of tweets to be extract, and most importantly, the date on which the tweets will be taken. Filtering is done with the tw.Cursor (api.search, q=new_search, lang="tr", count=50000, since=date_since) line in the program. It saves the data in csv files in utf-8

format to save the tweets downloaded by the program without losing data. Each data in the csv file is in the format <time>;<tweet>. The naming of the csv files is <disasterType> "Tweets_" <date_since> "_" <search_words>. The program can be run with the "python getTweet.py <disaster_type> <search_word> <date_since(year-mount-day)>" command on the command line (Figure 7).

```
2021-02-02 12:30:15,"b'#izmir\nBiz cok \xc5\x9f\xc3\xbck\xc3\xbcr evimizdeyiz\nAllahim
d\xc4\xb1\xc5\x9farda kalanlar\xc4\xb1 korusun\xf0\x9f\x99\x8f\xf0\x9f\x98\x94\nD
\xc3\xbcn deprem bugun sel, \xc4\xb0zmir yine felaketlerle m\xc3\xbccadele ediyor..'"

2021-02-02 12:30:04,"b""RT @laxalperrr: \xc4\xb0zmir'de Anl\xc4\xb1k Modumuz #izmir
https://t.co/OpIRBIRzJi"""

2021-02-02 12:30:01,"b'RT @rojin63_35: #izmirdeprem R\xc3\xbczgar, f\xc4\xb1rt
\xc4\xb1na, ya\xc4\x9fmur, garip bir s\xc4\xb1cak ve huzursuz bir hava...uyuyamiyorum
\xf0\x9f\x98\x91\xf0\x9f\x98\x96\xf0\x9f\x98\x9f\xf0\x9f\x98\xb4\xf0\x9f\x98\xb4#deprem
her\xc5\x9feyi ayni g\xc3\xbcnde y\xe2\x80\xa6'"

2021-02-02 12:29:51,b'#izmir #kadifekale\nSel oldu.. https://t.co/bH6Fx8e2J7'

2021-02-02 12:29:50,b'RT @hadimul_mumin: So\xc4\x9fukkuyu denize ba\xc4\x9flanm
\xc4\xb1\xc5\x9f \xf0\x9f\x98\xb1\n\nHerkese ge\xc3\xa7mi\xc5\x9f olsun\n\n#izmir
https://t.co/cQBTvFXLk0'

2021-02-02 12:29:47,b'Diyer \xc5\x9fehirler:    izmir:    #izmir
https://t.co/RFXZIE7XTu'
```

Figure 7: Uncleaned tweets in the file

Uncleaned tweets in the file are very dirty and unclear as can be seen. This is due to the emojis, and Turkish characters used in tweets. Data was collected through tweets for three months. During this period, around 100,000 tweets sent by twitter users during natural disasters were obtained.

5.2. Cleaning Twitter Data

Dirty twitter data that needs to be arranged are cleaned with the program "tweetCleaner.py". The program of "tweetCleaner.py" is written in python language and its purpose is to remove Retweets, remove meaningless http links in tweets and make tweets readable. While developing the program, the python "re" library was used in this project. Thanks to this library, unnecessary links have been removed and 'ş', ' ',' ç ',' ı ',' ö ',' ü 'Turkish characters have been arranged in the Twitter data.

The program of "tweetCleaner.py" can be run from the command line with the python tweetCleaner.py <source_file_name> <destination_file_name> <destination_folder_name> "command. In addition, there is a help file in the program. After the program has been run, data is organized and ready for labelling (Figure 8).

```
'Dün #Deprem bugün #sel geçmiş olsun #İzmir inş. cana mala zarar gelmeden atlatırsın bu
sıkıntıları \xf0\x9f\x99\x8f';;;
'Bugün #İzmir'de yaşanan #sel felaketinden etkilenen tüm vatandaşlarımıza geçmiş olsun
diliyoruz. \xf0\x9f\x99\x8f\xf0\x9f\x8f\xbb  #ethicasigorta';;;
'Yeni nesil toplu taşıma \xf0\x9f\x98\x92 #izmir #sel
'Balçova Barajı Kapaklarını açmak zorunda kaldı. #izmir #sel #yagmur
"""""'#İzmir'de yaşanan sel felaketinden etkilenen tüm vatandaşlarımıza geçmiş olsun
dileklerimizi iletiyor, can ve mal...
'İzmir'de aşırı yağışlarla birlikte gelen sel felaketiyle, zemin katta oturan
vatandaşların boğulmaktan son anda kur...
'#izmir de yaşanan felaketlerden sonra  hiç birseye hevesim kalmadı.. \xf0\x9f\x98\x92
#sel #deprem #balcova #izmiryağmur';;;|
'Meteorolojiden İzmirlilere önemli sel uyarısı!   #haberler  #izmir #sel #fırtına
#sonmühür
"""Minsolmaz Alpullu'daki 'Sel'in Ardından Bölgede!  #alpullu #sel @SMinsolmaz
#belediye #AFAD"""""""";;;
'Izmir bu yil var olma mucadelesi veriyor #deprem #sel #pandemi #izmir';;;
'Anlık İzmirliler :( #sel #deprem #Fırtına #yağmur #izmir
"""\xf0\x9f\x93\x8cİzmir'de sel suları nedeniyle denizin rengi değişti!  \xf0\x9f
\x94\x97  \xf0\x9f\x94\x8d#izmir #izmirhaber #sel...
'Kimse su depoları boş demesin bu saatten sonra\xf0\x9f\x98\xa1 #yağmur #izmir #sel';;;
'İlk can kaybımızı verdik #izmir #sel
'SON DAKİKA! Sel felaketi can aldı &gt;&gt;&gt;  #izmir #sel'
'Her an kapıda oturmuş felaketi bekliyoruz #sel';;;
```

Figure 8: Output of tweetCleaner.py

5.3. *Tagging Tweets*

Tagged data are needed to train the Deep Learning model. The more consistent the labelled data, the better the model will be performed. It is inconvenient to tag data obtained from Twitter according to hashtags without reviewing it. The reason it is inconvenient is that twitter users can post irrelevant tweets from the hashtag. To avoid this, the tweets are read by humans and a letter is added in front of the tweet to tell you which category it belongs to. The letter "f" means storm, the letter "d" means earthquake, the letter "s" for flood, and "y" for no disaster. The labels in the file content are shown below after the data is labelled (Figure 9).

```
s'#izmir Biz cok şükür evimizdeyiz Allahim dışarda kalanları korusun\xf0\x9f\x99\x8f
\xf0\x9f\x98\x94 Dün deprem bugun sel';;;
'@onrk1n @herseyplanliydi Bugün ögretim üyeleri. #AsagiBakmayacagiz  #izmir
'Bir yıla ne kadar acı sığdırmışsın \xe2\x98\x81\xef\xb8\x8f#izmir'
'#izmir Tabiat artık eskisi gibi değil.Her tarafta herşey olabilir.Bu da yazın
yaşanmıştı.
s'#izmir #kadifekale Sel oldu..
'Diyer şehirler:      izmir:     #izmir
f'#izmir ; yağmur,gök gürültüsü,fırtına.. İzlediğim film #fırtınaanı #Netflix'"
'Galatasaray-Başakşehir Bahis-MS 1 Galatasaray formda göllü maç olur ve kazanırlar.
#iddaa #DevletiminYabındayım...
s""Baskan, Venedik'i getirtmis begenmiyorsunuz! #izmir #ProvokasyonaDurDe
#DevletiminYanindayim
s"" İzmir'i vuran sel felaketiyle esnaf ve vatandaş çaresiz kaldı #izmir  #izmirsel"""
s'Bu yağmur duasını hangi muhterem yaptı arkadaş \xf0\x9f\x98\xa9 #izmir'
s'CEHAPE Nin sürekli kazandığı  #izmir afetlere ilk yenilen şehir oluyor galiba
önlemlerinizi keşke alsaydınız ve keş...
s'Güzel İzmir'immm benim \xe2\x9d\xa4\xef\xb8\x8f Dün deprem oldu .. bugün sel ... çok
geçmiş olsun \xf0\x9f\x99\x8f\xf0\x9f\x8f\xbb\xf0\x9f\xa7\xbf.....#kktc #izmir'
s'#izmir #izmirsel #izmirdeprem çekiciler parayı kırdı
s'Sel felaketi yaşanan İzmir'de, bir yurttaşımızın hayatını kaybettiğini üzüntüyle
öğrendik. Vatandaşımıza Allah'tan...
'Şubat ayına mükemmel bi başlangıç yaptın be İzmirim maşallah sağ çıkar mıyız ne dersin
#izmir'|
```

Figure 9: Tagging tweets according to categorize

5.4. Creating a Labelled Folder Structure

Before exporting the labelled data as data to the Deep Learning model, it must be placed in the labelled folder structure. "Tagger.py" program has been created to do this task. In addition, the tagged folders where the data will be placed are automatically generated owing to this program. Below is the code block that generates the required folder structure.

```
import os
main_dir = os.getcwd()
data_dir = main_dir + "/DataSet"
os.mkdir(data_dir)
os.mkdir(data_dir +"/Deprem")
os.mkdir(data_dir +"/Sel")
os.mkdir(data_dir +"/Fırtına")
os.mkdir(data_dir +"/Yok")
```

The program of python tagger.py is run on the command line in the directory where the data labelled with the python tagger.py command is located. Files with tagged data are read one by one by the program and moved to the relevant folder according to the label. In tag folders, tweets are in separate txt files and each txt names them with a unique id number. The view of the data in the "Sel" folder is shown below (Figure 10).


```
3.txt - Not Defteri                              —    □    ×
Dosya  Düzen  Biçim  Görünüm  Yardım
'izmir'de aşırı yağışlarla birlikte gelen sel
felaketiyle, zemin katta oturan vatandaşların
boğulmaktan son anda kur...
```
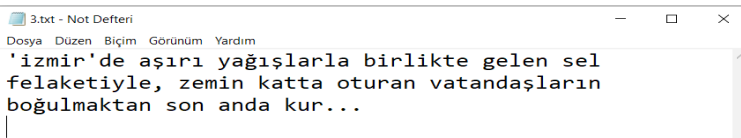
Figure 10: Clean and readability tweet from Sel folder 3.txt

5.5. Data Preposition and NLTK Library

Before using the tagged data as training data in the deep learning model, it must be cleaned by applying Natural Language Techniques. In this way, the data will become more suitable for model training. ""dataPreparation.py" " program was written to clean the data. The program is run on the command line with the python dataPreparation.py. With this program, the tagged data is read from the related files. Then, NLP transactions are applied by taking advantage of the capabilities of the NLTK library.

"""Deprem Fırtınası Devam Ediyor! 10 dk'da bir #deprem oluyor.   #izmir #istanbul #Yunanistan #Girit

Firstly, it is divided into data words. The form from nltk.tokenize library is used to split into words. Then, the tokenization process is performed with the import word_tokenize function.

['```', '```', 'Deprem', 'Fırtınası', 'Devam', 'Ediyor', '!', '10', "dk'da", 'bir', '#', 'deprem', 'oluyor', '.', '#', 'izmir', '#', 'istanbul', '#', 'Yunanistan', '#', 'Girit']

Secondly, the data is divided into punctuation marks. For this, punctuation marks are downloaded with the nltk.download('punkt') command.

['deprem', 'fırtınası', 'devam', 'ediyor', 'bir', 'deprem', 'oluyor', 'izmir', 'istanbul', 'yunanistan', 'girit']

Thirdly, the data is cleared of stop words. For this, from nltk.corpus import stopwords library is used.

['deprem', 'fırtınası', 'devam', 'ediyor', 'bir', 'deprem', 'oluyor', 'izmir', 'istanbul', 'yunanistan', 'girit']

Fourthly, the word roots must be found. For this, from TurkishStemmer import TurkishStemmer library is used. Thanks to this library, Turkish words can be separated into Turkish word roots.

['depre', 'fırtına', 'devam', 'ediyor', 'bir', 'depre', 'oluyor', 'izmir', 'istanbul', 'yunanistan', 'girit']

Finally, as in head 5.4 item the file structure is created by applying natural language processing data preparation processes to our data.

5.6. *Training the Deep Learning Model*

After all data are prepared for training, the deep learning model is started to be trained. TensorFlow Library is used to train the Deep Learning model. Data numbers in earthquake, flood, storm, and no disaster categories are equalized by using the under-sampling method of the data set. The reason for using this is to prevent the deep learning model from tending to any category. The data set is divided into three as 60% train, 20% validation and 20% test. Words are converted into numerical values by applying the text vectorization process. The Deep Learning model consists of 3 layers and the parameter information is specified in the table below. There are 4 neurons on the output layer. These neurons represent earthquake, flood, storm, and no disaster categories (Table 1).

Table 1: Layer – Output Shape – Param #

Layer (type)	Output Shape	Param #
embedding_3 (Embedding)	(None, None, 128)	640128
dropout_4 (Dropout)	(None, None, 128)	0
global_average_pooling1d_3	(None, 128)	0
dropout_5 (Dropout)	(None, 128)	0
dense_3 (Dense)	(None, 4)	516
Total params: 640644 Trainable params: 640644 Non-trainable params: 0		

In the first implementation phase of the Deep Learning model, low accuracy was obtained. The reason why the accuracy of the deep learning model is very small is that it was trained with a small data set. During the test phase, the data set will be enlarged.

5.7. Listening to Twitter Continuously in Real Time

Filtered Tweets matching the filtered stream endpoints are sent in real time, with a set of rules applied to the stream. Special rules have been created to get real-time data from Twitter with certain keywords. Filtered tweets matching the filtered stream endpoints have been improved with a set of rule updates applied to the stream. When building a rule, it was periodically tested with the stream endpoint to see what data it returns. Thus, within the scope of the project, more relevant tweets were taken to listen to the tweets about "flood", "storm", "earthquake" in real time.

Multiple rules can be applied to a stream using a POST /tweets/search/stream/rules endpoint. The rules are added and connected to stream using the GET /tweets/search/stream endpoint, only Tweets matching the rules in this project come in real time via a persistent streaming connection.

[{"value": "(deprem OR sallanmak OR sarsıntı OR artçı OR göçük OR zelzele) lang:tr -is:retweet -has:links -has:mentions"},

{"value": "(#deprem OR #sarsıntı OR #zelzele) lang:tr -is:retweet -has:links -has:mentions"},

{"value": "(fırtına OR hortum OR (şiddetli rüzgar) OR kasırga) lang:tr -is:retweet -has:links -has:mentions"},

{"value": "(#fırtına OR #hortum OR #kasırga) lang:tr -is:retweet -has:links -has:mentions"},

{"value": "(sel OR taşkın OR (su baskın)) lang:tr -is:retweet -has:links -has:mentions"},

{"value": "(#sel OR #taşkın OR #subaskın OR #taşkın) lang:tr -is:retweet -has:links -has:mentions"},

{"value": "(afet OR #afet) lang:tr -is:retweet -has:links -has:mentions"}]

5.8. *ANEW Dictionary Implementation*

ANEW is a database of 1034 English words (Bradley & Lang), which is used to analyze the sentiment of English words and is manually graded by many people based on three-dimensional emotional measurement. In this project, Turkish ANEW dictionary was used in Turkish twitter data due to semantic and morphological differences between Turkish and English languages. Thanks to the Twitter API, while listening to the Twitter in real time, filtering is performed to determine the panic state of each tweet. Panic scores of tweets are calculated using the ANEW dictionary, and tweets containing panic are saved in the database. Then, the tweets that pass the filter are classified with the deep learning model. Tweets that cannot pass through the filter will disappear.

5.9. *Two Stages Prediction System*

Twitter is listened in real-time with stream rules created. These rules consisted of the words most frequently used by people during natural disasters. No matter how much we query twitter with certain rules, dirty data can come to our system as input because twitter contains a lot of dirty data. A two-stage prediction system has been developed to deal with dirty data. As a result, tweets will be predicted by deep learning with higher accuracy. The first stage, the anew dictionary, detects the sense of panic with the tweet captured while Twitter is listened in real time. Here, a tweet with a low valence value, a high arousal value and a low dominance value is perceived as containing a sense of panic. At this stage, a study is carried out to determine the existence of a natural disaster in summary. The tweet that does not contain a sense of panic is removed from the system. After making an assessment of the presence of a natural disaster, the tweet with panic comes to the model trained with deep learning. At this stage, the tweet is classified in the categories of earthquake, storm, flood, and no natural disaster. The type of natural disaster is predicted with the output resulting from the estimation. Tweets that contain panic but do not contain natural disasters from the Anew filter are also noticed in the deep learning model and predicted as no natural disaster (Figure 11).
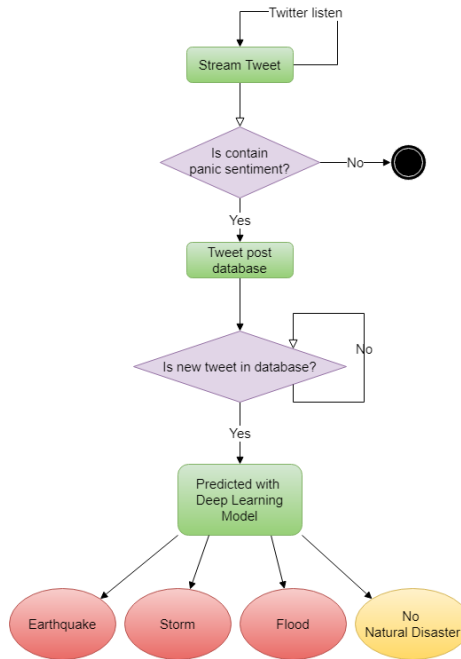
Figure 11: Two Stages Prediction System

6.   Tests / Experiments

6.1. Twitter Filtered Stream

Figure 12, Figure 13 and Figure 14 show that tweets captured while listening to twitter in real time with the twitter API. As can be seen in the figures, the filtered stream rules created in accordance with this project work successfully. In this way, relevant tweets can be captured in real time. In addition, there is a Turkish character problem in twitter stream data.


```
{
    "data": {
        "id": "1399535172178137089",
        "text": "Deprem oldu izmir #deprem"
    },
    "matching_rules": [
        {
            "id": 1399534793478619137,
            "tag": "dogal afet deprem"
        }
    ]
}
```

Figure 12: Sample 1 "deprem" tweet captured

```
{
    "data": {
        "id": "1399535258102607872",
        "text": "#deprem #MarmaraDenizi \n2021.06.01 03:51:23  40.69
63   27.4292      5.7      -.-  2.4  -.-   GUZELKOY ACIKLARI-TEKIR
DAG (MARMARA DENIZI)       \n\n2021.06.01 03:40:15  40.7082   27.435
5     10.8      -.-  2.2  -.-   GUZELKOY ACIKLARI-TEKIRDAG (MARMAR
A DENIZI)"
    },
    "matching_rules": [
        {
            "id": 1399534793478619137,
            "tag": "dogal afet deprem"
        }
    ]
}
```

Figure 13: Sample 2 "deprem" tweet captured

```
{
    "data": {
        "id": "1399535333994291201",
        "text": "\u201cBiz sevdik mi yer oluruz, biz sevdik mi sel o
luruz, biz sevdik mi l\u00e2l oluruz, biz sevdik mi can oluruz.\u201
d\n                On be\u015f\n#AlpNavruz Poyraz Demir\n#Ay\u00
e7aAy\u015finTuran Haziran Bozturk\n#AdaMasal\u0131 AdaMasal\u0131"
    },
    "matching_rules": [
        {
            "id": 1399534793478619136,
            "tag": "dogal afet sel"
        }
    ]
}
```

Figure 14: Sample 3 "deprem" tweet captured

6.2. Deep Learning Model Training Experiments

When the deep learning model was trained with 1500 train data, 500 validation and 500 test data, the validation accuracy value of 0.1562 was reached. This value, which is obtained because of training a deep learning model, is quite bad. The data set has been expanded to increase the accuracy value. In addition, the n-gram algorithm has been applied to increase accuracy (Figure 15).

Epoch 1/10 : 5/5 - 0s 31ms/step - loss: 1.3874 - accuracy: 0.2576 - val_loss: 1.3926 - val_accuracy: 0.1562
Epoch 2/10: 5/5 - 0s 34ms/step - loss: 1.3846 - accuracy: 0.2652 - val_loss: 1.3931 - val_accuracy: 0.1562
Epoch 3/10: 5/5 - 0s 30ms/step - loss: 1.3843 - accuracy: 0.2879 - val_loss: 1.3938 - val_accuracy: 0.1562
Epoch 4/10: 5/5 - 0s 30ms/step - loss: 1.3833 - accuracy: 0.2803 - val_loss: 1.3949 - val_accuracy: 0.1562
Epoch 5/10: 5/5 - 0s 30ms/step - loss: 1.3817 - accuracy: 0.2803 - val_loss: 1.3972 - val_accuracy: 0.1562

Figure 15: First model training experiment

In addition, tweets were collected for the no natural disaster category to increase the accuracy rate. Tweets pulled from Twitter were read and tagged with manpower. Thus, each tweet is classified. Thanks to the Twitter API, a total of 13926 tweets related to the storm were taken, while 12307 tweets were taken about the earthquake. While there were 8492 tweets about the flood, 16770 tweets were obtained in the no natural disaster category. For the deep learning model not to tend to a category, tweets belonging to each category were synchronized with sampling methods. Thus, a total of 48000 tweets were obtained from the categories of 12000 earthquakes, 12000 floods, 12000 storms, 12000 no natural disasters. 28800 of these tweets were used as training data, 9600 as validation data, and 9600 as test data (Figure 16, Figure 17 and Figure 18).
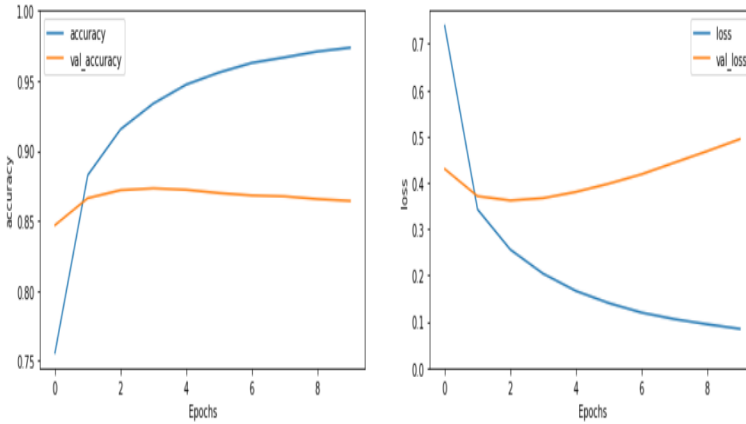

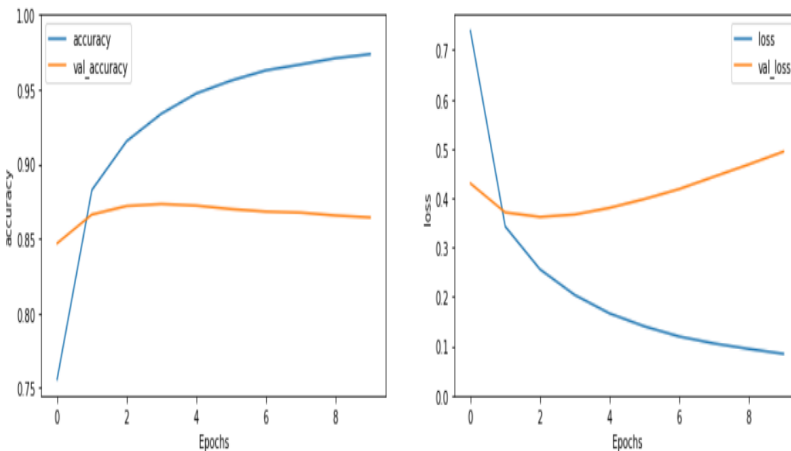Figure 16: Unigram text vectorization model accuracy

Figure 17: Unigram text vectorization model loss

300/300 - 2s 6ms/step - loss: 0.4570 - accuracy: 0.8649
Loss: 0.4570430517196655
Accuracy: 0.8648958206176758

Figure 18: Unigram text vectorization model loss and accuracy value

After the training trials of the deep learning model, accuracy reached 0.8648 and loss 0.457. To reach these values, the unigram algorithm was used, data vectorization was applied, the data set was expanded, and then the number of epochs was increased. "adam" is used for optimizer, "SparseCategoricalCrossentropy" is used for loss in the deep learning model. Figure 19 and Figure 20 were run with the same parameters, but the bigram algorithm was applied. As a result, while the bigram accuracy reached 0.8118, the loss value was 0.590 (Figure 21).
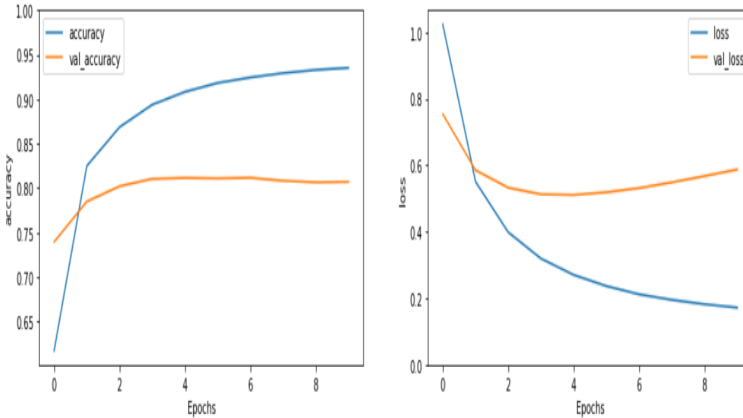

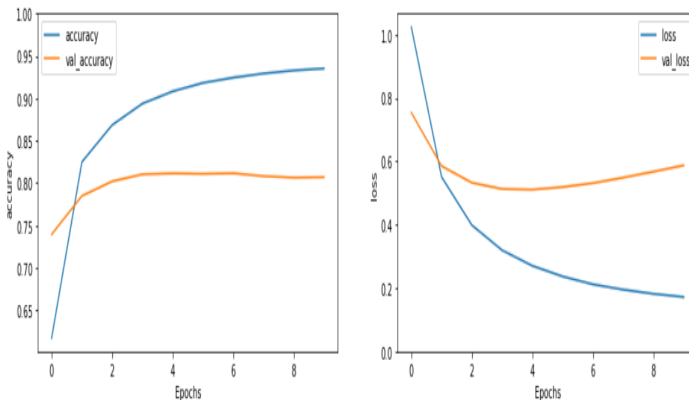Figure 19: Bigram text vectorization model accuracy

Figure 20: Bigram text vectorization model loss

300/300 - 2s 7ms/step - loss: 0.5903 - accuracy: 0.8118
Loss: 0.590300440788269
Accuracy: 0.8117708563804626

Figure 21: Unigram text vectorization model loss and accuracy value

7. Conclusion

Predicting natural disaster types of tweets was a challenging and tiring task as tweets had various noises due to streaming data, grammatical errors, difficulties in Turkish characters. In this project, only Turkish tweets were covered. It was discovered that the Twitter data was cleaned and the roots of some words in the text could not be found correctly, and the reason for this was the Turkish Stemmer library. This is also due to the scarcity and inadequacy of the studies in natural language processing on the Turkish language. In this thesis, two-stage filtering is proposed to make a highly accurate prediction. As the deep learning model, a model containing unigram text vectorization with high accuracy was used. Tweets were used in the flood, earthquake, storm, and "no natural disasters" category, and the deep learning model trained with these tweets has 3 layer 4 neurons. The highest accuracy value obtained is 0.86. In addition, it is aimed to implement an alternative disaster detection system in case of inability of traditional emergency during natural disasters.

In this project, although some tweets are tagged with earthquake, flood, and storm, since the tweet contains content independent of natural disaster in 3 categories, it has been tagged with manpower. It can be accomplished with less manpower using a semi-supervised approach rather than manual labeling. In addition, natural disasters and natural disaster types in Turkey can be determined by listening not only to the Izmir region, but also to the locations where possible natural disasters occur in Turkey. In addition, not only flood, earthquake, storm, and tornado, but also other natural disaster types can be predicted by expanding this study. For training the deep learning model, more natural disasters can be predicted by also collecting tweets about other natural disasters. This project can be used to follow economic trends and the popularity of any branch in the Olympics from social media or in different areas where people have dominant emotions by building different stream rules. It can be used in different projects by training the deep learning model with tweets specific to the relevant field. In addition, emotions specific to the relevant field can be filtered by changing the parameters of the ANEW dictionary in emotion analysis.

8. References

Aipe, A., Mukuntha, N., Ekbal, A., & Kurohashi, S. (2018). Deep Learning Approach towards Multi-label Classification of Crisis Related Tweets. In *Proceedings of the 15th ISCRAM Conference*.

Alam, F., Ofli, F., Imran, M., & Aupetit, M. (2018). A twitter tale of three hurricanes: Harvey, irma, and maria. *arXiv preprint arXiv:1805.05144*.

ALRashdi, R., & O'Keefe, S. (2019). Deep learning and word embeddings for tweet classification for crisis response. *arXiv preprint arXiv:1903.11024*.

Arachie, C., Gaur, M., Anzaroot, S., Groves, W., Zhang, K., & Jaimes, A. (2020, April). Unsupervised Detection of Sub-Events in Large Scale Disasters. In Proceedings of the AAAI Conference on Artificial Intelligence (Vol. 34, No. 01, pp. 354-361).

Bradley, M. M., & Lang, P. J. (1999). Affective norms for English words (ANEW): Instruction manual and affective ratings (Vol. 30, No. 1, pp. 25-36). Technical report C-1, the center for research in psychophysiology, University of Florida.

Burel, G., Saif, H., Fernandez, M., & Alani, H. (2017). On semantics and deep learning for event detection in crisis situations.

Cam, H., & Duman, O. (2019). Earthquake Prediction with Artificial Neural Network Method: The Application Of West Anatolian Fault In Turkey. arXiv preprint arXiv:1907.02209.

Fersini, E., Messina, E., & Pozzi, F. A. (2017). Earthquake management: a decision support system based on natural language processing. *Journal of Ambient Intelligence and Humanized Computing*, *8*(1), 37-45.

Filtered stream. (n.d.). Developer Twitter. Retrieved April 30, 2021, from https://developer.twitter.com/en/docs/twitter-api/tweets/filtered-stream/integrate/build-a-rule

Filtering Tweets by location. (n.d.). Developer Twitter. Retrieved April 30, 2021, from https://developer.twitter.com/en/docs/tutorials/filtering-tweets-by-location

Hagras, M., Hassan, G., & Farag, N. (2017, November). Towards natural disasters detection from Twitter using topic modelling. In *2017 European Conference on Electrical Engineering and Computer Science (EECS)* (pp. 272-279). IEEE.

Kaufhold, M. A., Bayer, M., & Reuter, C. (2020). Rapid relevance classification of social media posts in disasters and emergencies: A system and evaluation featuring active, incremental and online learning. *Information Processing & Management*, *57*(1), 102132.

Kumar, A., & Singh, J. P. (2019). Location reference identification from tweets during emergencies: A deep learning approach. International journal of disaster risk reduction, 33, 365-375.

Kumar, A., Singh, J. P., Dwivedi, Y. K., & Rana, N. P. (2020). A deep multi-modal neural network for informative Twitter content classification during emergencies. *Annals of Operations Research*, 1-32.

Laylavi, F., Rajabifard, A., & Kalantari, M. (2017). Event relatedness assessment of Twitter messages for emergency response. *Information processing & management*, *53*(1), 266-280.

Madichetty, S., & Muthukumarasamy, S. (2020). Detection of situational information from Twitter during disaster using deep learning models. Sādhanā, 45(1), 1-13.

Nguyen, D. T., S. Joty, M. Imran, H. Sajjad, and P. Mitra. 2016. "Applications of Online Deep Learning for Crisis Response Using Social Media Information." arXiv preprint arXiv:1610.01030.

Poblete, B., Guzmán, J., Maldonado, J., & Tobar, F. (2018). Robust detection of extreme events using twitter: worldwide earthquake monitoring. IEEE Transactions on Multimedia, 20(10), 2551-2561.

Reynard, D., & Shirgaokar, M. (2019). Harnessing the power of machine learning: Can Twitter data be useful in guiding resource allocation decisions during a natural disaster? *Transportation Research Part D: Transport and Environment*, *77*, 449-463.

Romascanu, A., Ker, H., Sieber, R., Greenidge, S., Lumley, S., Bush, D., ... & Brunila, M. (2020). Using deep learning and social network analysis to understand and manage extreme flooding. Journal of Contingencies and Crisis Management, 28(3), 251-261.

Ruz, G. A., Henríquez, P. A., & Mascareño, A. (2020). Sentiment analysis of Twitter data during critical events through Bayesian networks classifiers. Future Generation Computer Systems, 106, 92-104.

Sit, M. A., Koylu, C., & Demir, I. (2019). Identifying disaster-related tweets and their semantic, spatial, and temporal context using deep learning, natural language processing and spatial analysis: a case study of Hurricane Irma. International Journal of Digital Earth, 12(11), 1205-1229.

Temel metin sınıflandırması. (n.d.). TensorFlow. Retrieved April 30, 2021, from https://www.tensorflow.org/tutorials/keras/text_classification

Win, S. S. M., & Aung, T. N. (2017, May). Target oriented tweets monitoring system during natural disasters. In *2017 IEEE/ACIS 16th International Conference on Computer and Information Science (ICIS)* (pp. 143-148). IEEE.

Yazan, K., & Üsküdarlı, S. Sosyal Ağlar Üzerinden Deprem Tespiti.

Yu, M., Huang, Q., Qin, H., Scheele, C., & Yang, C. (2019). Deep learning for real-time social media text classification for situation awareness–using Hurricanes Sandy, Harvey, and Irma as case studies. *International Journal of Digital Earth*, *12*(11), 1230-1247.

Zahra, K., Imran, M., & Ostermann, F. O. (2020). Automatic identification of eyewitness messages on twitter during disasters. Information processing & management, 57(1), 102107.

MACHINE LEARNING-BASED ARTIFICIAL INTELLIGENCE IMPLEMENTATIONS IN THE MANUFACTURING CONTEXT

Büşra ALMA ÇALLI

(Dr), Sakarya University, Department of Management Information Systems, Sakarya, Turkey
E-mail: busraalma@sakarya.edu.tr
Orcid: 0000-0001-7411-4295

1. Introduction

Modern artificial intelligence (AI) is a large field of research that employs modern approaches to extract information from vast amounts of data. The core idea of AI is to teach machines to learn, analyze, and solve issues that people regularly encounter (Ambati et al., 2020). Machine learning (ML), which was introduced in the early twenty-first century, has accelerated AI research. This rise can be attributed to machine learning techniques' hardware and computing capability. Accordingly, advancements in the field of AI are accelerating as the capacity of processing power grows, and technologies in the future of AI will allow robots to learn and reason almost like humans (Lake et al., 2017)**.**

Despite all these developments and potential benefits in AI applications, the difficulties encountered in adopting and implementing these approaches are a matter of debate. Many obstacles related to AI-ML affect industrial processes and system adoption, including unpredictable behavior and complexity. Besides, artificial intelligence approaches (such as machine learning and deep learning) have changed how many specialists handle their jobs recently. Although manufacturers may use these technologies to solve real-world problems in new and creative ways, there are many

different algorithms and methodologies accessible, which makes selecting the proper AI methodology for the suitable manufacturing process difficult (Nti et al., 2021).

AI and ML have long been seen to be intertwined and, as a result, have been studied in conjunction throughout many areas and sectors. Being a part of AI, machine learning contributes to transforming many sectors. The utilization of ML allows for the detection of patterns within massive datasets, which results in appropriate solutions and accurate decision-making (Younis et al., 2021).

According to Oke (2008), since the intelligence of computers with machine learning skills has had tremendous consequences, the scope of AI has expanded dramatically (as cited in Cioffi et al., 2020). They also have an impact on global sustainability issues. AI has the potential to overcome challenges in the context of sustainable manufacturing. In this regard, Carvalho et al. (2019) stated a tendency in the field of smart production to integrate AI into green manufacturing practices to comply with tough environmental standards (as cited in Cioffi et al., 2020). Consequently, the advancement of machine learning as a field of AI is presently quite rapid. Its use has expanded to a variety of sectors, including smart manufacturing, agriculture, and medical science (Cioffi et al., 2020).

Notwithstanding their accomplishments, these mechanisms are fundamentally different from human intelligence. According to the contemporary cognitive science findings, machines that can learn and think like human beings will need to overreach modern engineering practices in terms of their learning power. Hence, instead of simply finding solutions to pattern recognition problems, these systems should establish models representing causality for enabling reasoning and understanding. Relevant theories of physics and psychology should be used for the learning mechanism in order to enrich the acquired knowledge. Further, learning-to-learn should be integrated to quickly capture and generalize information to new circumstances (Lake et al., 2017).

As a result, AI-ML approaches, which are used in a wide range of fields and are beneficial to competitiveness and efficiency when used correctly in businesses, should be criticized in terms of their use cases,

use cases, difficulties in these areas of use, their potential benefits, and limitations in the application. In this sense, this section aims to provide informative and explanatory information about these phenomena.

2. Artificial Intelligence-Machine Learning and Manufacturing

Depending on the fact that several knowledge-based systems have been used to automate various manufacturing tasks, collecting the necessary expert knowledge to execute these systems is an issue that ML techniques can solve by automating the processes. Further, machine learning has been widely adopted for classification issues, focusing on constructing models by learning from a previously classified dataset to categorize new instances. In this regard, several manufacturing issues apply classification through ML-based approaches for addressing manufacturing problems. Machine learning approaches are also beneficial for extracting new and hidden information; however, for their success, machine learning mechanisms should handle both structured and unstructured data, generate meaningful and understandable outcomes, and work with large volumes of data with high dimensionality. These systems should also be easy to apply and provide real-time data processing (Pham & Afify, 2005).

Specifically, in engineering and manufacturing, AI can be used for "fault diagnostics", "manufacturing monitoring", "robotics, autonomous functions", "anomaly detection", "predictive maintenance", "production", "machine vision", "virtual reality", and "wear and tear monitoring" (Nti et al., 2021). "Management of resources", "product design", "optimization", "prediction/ monitoring quality", "decision support", "parameter analysis", "analysing market demand", "scheduling", "analysing service issues from customers", "segmenting customers", and "optimization" are also mentioned as the benefits of data mining and machine learning in manufacturing environment. Besides, from the managerial aspect, machine learning supporting managers' decision-making process contributes to managing production resources more effectively (Dogan & Birant, 2021). Bauer et al. (2020) mentioned "recommender systems", "spare parts", "smart grids", "intrusion detection", "robotics", "warehouse inventory", and "chatbots" as machine learning implementations for different business use cases. Additionally, Fahle et al. (2020) mentioned the use of ML for assistance and learning systems for the employees.

de Jonge et al. (2017) and Leukel et al. (2021) emphasized failure prediction as essential maintenance goals. Failure prediction focuses on prohibiting

system failures and decreasing unexpected equipment, machine, and process malfunctions. Predictive maintenance is based on the ability to foresee future faults accurately. Accordingly, ML techniques based on failure prediction have been used for various systems in several domains, such as semiconductors, wind turbines, vehicle compressors, hard drive disks, aircraft components, metal machining, and electrical devices (Leukel et al., 2021).

These powerful machine learning approaches might be enforced in the future for small and medium-sized enterprises (SMEs) in manufacturing to assure improved quality control and monitoring of the output or to play a role as an assisting instrument. The use of predictive analytics of Gartner's four analytic phases would also be possible if AI-ML and IoT were combined (Hansen & Bøgh, 2021). In the case of the SME context, in order to achieve maturity for applying predictive analytics, four steps should be accomplished (Hagerty, 2016).

1. Descriptive analytics: Since many small businesses do not collect data from the system, the decision is usually based on expert opinion. In this context, collecting machine data from production will improve decision-making, and defects in the production line can be identified (Hagerty, 2016).
2. Diagnostic analytics: The transition to this stage requires applying AI-ML-oriented approaches. With these approaches, systems can now diagnose the detection of the problem and the source (Hagerty, 2016).
3. Predictive analytics: This stage requires AI-ML and IoT integration. In this context, the data to be collected through sensors is analyzed through models based on artificial intelligence and machine learning, and it is aimed to predict the probability of failure or malfunction of particular equipment and system (Hagerty, 2016).
4. Prescriptive analytics: According to Hagerty (2016), this stage is associated with the system's ability to make changes. The system can adjust how production takes place and uses better AI-ML models and more advanced sensor technologies. While production facilities that will operate autonomously can be given as an example in this context, the application area is very limited in today's conditions.

Machine learning's key advantage is its ability to learn from the past and respond to the changing contexts automatically. Thus, the machine learning system must be capable of adapting to changes in the dynamic production environment, and experts responsible for the system must offer quick fixes for all probable scenarios.

Another significant problem is obtaining reliable and relevant production data, which significantly impacts the effectiveness of machine learning algorithms. The pre-processing of data, which significantly influences the outcomes, is a frequent difficulty of ML applications in manufacturing. Another significant problem is deciding which machine learning approach and algorithm to use (Dogan & Birant, 2021).

From the innovations' perspective, AI use may impact knowledge production and the ability to acquire and absorb new information. Specifically, AI accelerates knowledge generation, contributes to enhancing R&D activities, improves investments in skills, develops learning and absorption aptitude, and increases the rate at which knowledge and technologies spread, leading to technological innovations (Liu et al., 2020).

Liu et al. (2020) reported that AI-ML is not just an advanced technology creating value as the outcome of technological innovations. It is also intricately related to existing technologies to establish a complicated network. AI-ML has become the underlying origin of other technological advances and the exterior reason supporting other technological innovations within these technologies. It is continually stimulating the invention of new technological advances and creating the circumstances for technological advancements. As a result, AI is a global technology that may aid in developing other advancements (Vocke et al., 2019).

2.1. Digital Twin-Driven Machine Learning

Digital twin (DT) implementations might provide advantages for smart manufacturing by incorporating the physical and virtual environment (Alexopoulos et al., 2020). According to Grieves (2014), digital twin models include the real world, virtual world, and the information linkages that link the physical and cyberspace. In this context, the digital twin acts as a control system for the physical production system. Rosen et al. (2015) suggest that DT-based approaches merging actual data with design simulation models enable forecasting the future behavior based on real-world data, which can boost the competence of manufacturing systems. Additionally, in the manufacturing environment, DT models contribute to enhancing the performance of ML-based artificial intelligence applications. Substantial amounts of data are necessary for ML approaches, and particularly for supervised machine learning, manual labeling is frequently required. Nevertheless, this method is costly, burdensome, and subject to problems in a very complex manufacturing environment. On the contrary, by providing appropriate training datasets and automatically labeling,

the digital twins approach may be used to speed up the training stage in ML and reduce user input (Alexopoulos et al., 2020).

3. Supply Chain Perspective

Additionally, AI-ML has proven to be helpful in improving SC, and as a result, the use of AI-ML in supply chain systems provides organizations with competitive advantages, and their tools and methodologies can harness the total value of the supply chain. AI-ML can help to lessen the bullwhip effect, which helps improve the supply chain's performance and responsiveness. The just-in-time process can be improved by optimizing the resources and accurate demand forecasting, and customer services can be enhanced by deploying chatbots and intelligent kiosks (Younis et al., 2021).

Nayal et al. (2021) reported that AI-ML has several benefits for the agricultural supply chains, which are represented in Table 1. However, there are obstacles in front of adoption in terms of the trust, interoperability, infrastructure, collaboration, scalability, training, costs, data security & privacy, standardization, infrastructure, skills, and vision and mission. Based on the research findings, the most important challenges were comprised of issues related to the lack of data security & privacy, rules & regulations, scalability, data availability and quality, interoperability, network design, and technological barriers (Nayal et al., 2021).

Table 1. Applications and Advantages of Artificial Intelligence-Machine Learning

Applications	Advantages
• drone and robotics use • use of digital twins • integration with big data analytics and Internet of things (IoT) • AI-enabled recommended systems • mobile applications • predictive risk management	• enhancement of food safety and quality • production planning • optimization of supply-demand • watching out plant, soil status • identification of fertilizer and water needs • less human intervention • improved traceability and visibility • improved monitoring • improved decision-making • customer satisfaction • cost elimination • customization of services • fast performance of repetitive tasks • eliminate food waste

Note: Adapted from Nayal et al. (2021)

According to Cioffi et al. (2020) AI-ML enhances innovativeness and quality and optimizes resources and processes. Sustainable development can occur by using these algorithms for production systems, supply chain, and inventory management. Materials can be used more effectively, energy consumption can be managed, and environmental footprint can be tracked. Accordingly, AI is considered one of the significant facilitators of smart logistics and production (Woschank et al., 2020).

In the context of smart logistics, Woschank et al. (2020) mentioned "cyber-physical systems", "intelligent transport logistics", and "enhancement of operational processes" as the implementation areas of AI-ML. Cyber-physical systems indicate the shift from traditional systems to smart logistics systems, while intelligent transport logistics focuses on enhancing the performance of activities through AI-based approaches and their incorporation with the other advanced technologies.

According to Wen et al. (2018), swarm robotics can be utilized for green logistics, route monitoring, and smart warehousing within the context of smart logistics. Accordingly, optimization of smart warehouses can be performed (as cited in Woschank et al., 2020). Additionally, Laux et al. (2018) proposed that sound location systems can develop visibility, monitoring, and tracking processes (as cited in Woschank et al., 2020).

The Covid-19 pandemic has caused uncertainties and fluctuations in the agricultural supply chains. Uncertainties in demand and pricing, panic buying, disruptions in production, processing, and distribution channels have endangered global food security. While the supply chain risks that are not managed well reduce profitability and increase costs for the producer, they are reflected to the consumers as price increases or shortage of food (Nayal et al., 2021).

In several industries, supply chains have suffered significantly from handling high demand volumes, resulting in overpricing (Kumar et al., 2021). To eliminate the influence of risks, artificial intelligence and machine learning (AI-ML) is reported as a considerable driver of accurate predictions in supply chains due to enhanced decision-making under uncertainties. In addition to traditional AI approaches, big data and machine learning techniques have a remarkable potential to mitigate risks proactively by enabling robust predictions (Nayal et al., 2021).

3.1. Intelligent Automation and Supply Chain

Intelligent automation is defined as a mix of robots and artificial intelligence that works in tandem to bring digital transformation. The term "intelligent" now encompasses a wide range of characteristics that have been added to the classic automation that has been in use for several years. By combining machine learning and data analytics, it has the capacity to learn from itself. An intelligent manufacturing system incorporates the components represented in Figure 1 (Kumar et al., 2021). Artificial intelligence contributes to the smart systems environment by offering the learning mechanism for independent decision-making processes. Hence, AI achieving analytical tasks likewise data processing and analysis well might be used instead of the human being or might assist employees for improving the efficiency of production systems (Liu et al., 2020).
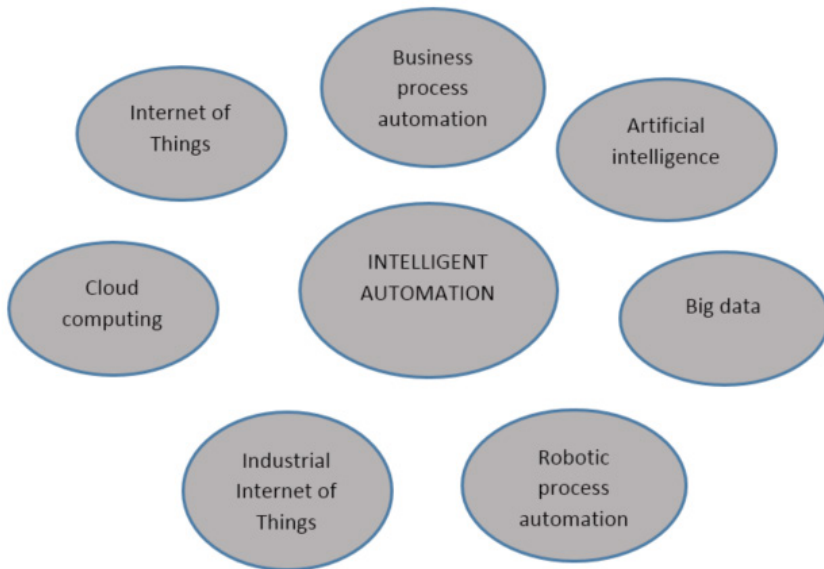

Figure 1. Components of Intelligent Automation (Source: Kumar et al. (2021))

The term "automation" had become increasingly popular in all industrial domains during the post-COVID-19 recovery of the economy, as the manufacturing industry confronted a significant labor shortage. As more uncertainties are expected due to global crises, the economy, and unexpected events, automation now seems the only option in manufacturing. It has been proved that automating the production of goods lowers operating costs. For the next ten years, many academics expect that AI will replace humans in a variety of tasks (Dogan & Birant, 2021; Kumar et al., 2021). A robot exhibits higher performance by providing more accuracy and uniformity (Kumar et al., 2021).

According to McKinsey & Company (2018), robotic process automation, machine learning, and computer vision are the most widely implemented AI skills. Almost 20% of respondents reported that their organizations have already integrated these capabilities based on a survey. Autonomous vehicles and physical robots are the least widely used technologies because they are primarily significant to organizations where they have obvious applicability. However, companies operating in industries suitable for using these technologies report that they use these technologies widely and effectively. Particularly in the automotive and assembly industries, physical robots are used in at least one function or department.

4. Intelligent Automation and Human Resources Management (HRM)

According to Vrontis et al. (2021), artificial intelligence for HR practices includes recruitment, training, and job performance. Besides, from strategies perspective AI can be utilized for enhancing decision-making processes in enterprises, creating job-replacement concerns, providing human and robot (artificial intelligence) collaboration, and providing employees learning chances. Consequently, intelligent automation has both impacts on employees and organizations in terms of innovations, automation of processes, creation of new products/services, decreasing costs, increasing quality of decisions, contributions to productivity, and the increase of customer satisfaction (Vrontis et al., 2021).

AI is capable of learning, reasoning, seeing, and making decisions on its own. It may substitute a portion of physical and mental labor while also providing users with useful auxiliary tasks like data processing and technical analysis, which can help boost job and production performance (Liu et al., 2020).

Employee considerations, likewise, the fear of job loss, resistance to change, or any technology-related difficulties might make AI adoption challenging in an enterprise. The top management has the responsibility of raising awareness, minimizing extra work burden, and setting the vision. Understanding employee-related issues preventing avoidance from AI adoption increases acceptance (Ambati et al., 2020).

5. Machine Learning and Energy Systems

Smart sensors Internet of Things (IoT), and smart grids, have allowed big data, presenting new problems and opportunities for energy systems. Accordingly, ML models have become popular to use big data for better decision-making

and creating effective models. The most prevalent machine learning algorithms for model construction include artificial neural networks, support vector machines, MPL, an advanced form of ANN, deep learning, extreme learning machine, decision trees, hybrid, and ensemble models. These models can be used for predicting power demand, cost, solar radiation, risk, consumption, and demand, forecasting the speed of wind and power generation, and monitoring and controlling energy (Mosavi et al., 2019). Besides, AI in the field of energy offers the advantages of "smart infrastructure maintenance", "smart metering", and "effective grid operations" (Vocke et al., 2019). Flick et al. (2020) developed a machine learning-based approach for managing energy systems in the factory context. Temporal shifts of energy states are evaluated by means of prediction-based ML techniques. Further research into the capabilities of several machine learning models revealed that advanced hybrid models outperform the performance of more traditional ML models. Hybrid ML models will keep evolving, delivering more excellent performance and implementing more complex energy models (Mosavi et al., 2019).

6. Critical Success Factors and Barriers

Bughin et al. (2018) reported that according to current predictions, AI can boost global GDP by a total of 1.2 percentage points every year by 2030. As a result, AI outperforms the yearly growth impact of some other technologies (as cited in Vocke et al., 2019). As a result, businesses in all industries are urged to explore the efficient utilization of AI to harness AI's potential fully, and this understanding appears to have grown in businesses. Based on PwC (2018) findings, almost 70% of CEOs expect that merging artificial intelligence with human intellect will significantly influence business enterprises, and half of them affirm that AI has already enhanced productivity in their companies. AI is expected to be an important element of competitiveness soon (as cited Vocke et al., 2019).

ML technologies are well-established in corporate applications, and there is a lot of interest in them. However, the technology's predominance is medium, and the technologies implemented generally have a medium level of complexity. On the other side, some organizations are already using highly sophisticated approaches. Small and medium-sized enterprises are far less prone to have ML implementations since their existing obstacles are different from those faced by more prominent companies and indicate lower ML maturity levels. Insufficient adoption of ML among key actors and inadequate know-how are major barriers for these companies. Further data availability, governance policies, inadequate ML outcomes, limited employee qualifications,

lack of expertise, labor division, and technical skills were reported as obstacles to implementing machine learning practices (Bauer et al., 2020).

Specifically for artificial intelligence, lack of an apparent strategy for AI, inadequate skills, poor leadership and commitment, unawareness regarding the benefits of AI outcomes, data availability and accessibility issues, insufficient technological infrastructure, subjective decision-making tendency instead of artificial intelligence-assisted decision-making mechanism, no changes to front-line processes in parallel with AI applications, limited resource utilization for artificial intelligence in the case of line organization, and functional silo syndrome are among the most considerable challenges that business enterprises encounter (McKinsey & Company, 2018).

The effects of AI-ML-based applications on productivity and efficiency are obvious. Businesses with difficulties in terms of the changing demand structure and the form of competition in today's economies are looking for ways to achieve large-scale transformations such as Industry 4.0. In this regard, the adoption of AI-ML applications should be considered together with the technologies it will interact with within an ecosystem (Lee et al., 2018).

The advancement of a company's digitalization journey is a major facilitator of AI. The companies that have advanced in digitalizing fundamental business operations are also at the forefront of AI use. AI has been integrated into routine business practices and operations at most digital companies. Machine learning, robotic process automation, computer vision, virtual agents, physical robotics, natural-language understanding (text or speech), and autonomous vehicles, for example, are most likely to have been implemented by the organizations with a higher level of digitalization (McKinsey & Company, 2018).

When looking at AI-ML applications from the perspective of industry 4.0 and digital transformation, it is necessary to discuss the basic requirements for AI applications within the ecosystem. Big data and cloud computing are important requirements since they constitute the data source and the platform. Further, domain knowledge is critical to anticipate the problem and analyze the system for acquiring the right data, and labeling is also required to verify the models and the learning capability. Analytics is another significant enabler, which can only be useful if other requirements are fulfilled (Lee et al., 2018).

In order to close the gap between business enterprises collaborations with external partners and between employees, commitment, standardized data interfaces, quick decision-making process, the existence of a qualified data science team, and implementation of ML projects in an incremental manner which brings achievement motivation are essential (Bauer et al., 2020).

References

Alexopoulos, K., Nikolakis, N., & Chryssolouris, G. (2020). Digital twin-driven supervised machine learning for the development of artificial intelligence applications in manufacturing. *International Journal of Computer Integrated Manufacturing*, *33*(5), 429–439. https://doi.org/10.1080/0951192X.2020.1747642

Ambati, L. S., Bishop, D., & Bishop, D. (2020). Factors Influencing the Adoption of Artificial Intelligence in Organizations – From an Employee's Perspective. *MWAIS 2020 Proceedings*, *April*.

Bauer, M., van Dinther, C., & Kiefer, D. (2020). Machine learning in SME: An empirical study on enablers and success factors. *26th Americas Conference on Information Systems, AMCIS 2020*.

Cioffi, R., Travaglioni, M., Piscitelli, G., Petrillo, A., & De Felice, F. (2020). Artificial intelligence and machine learning applications in smart production: Progress, trends, and directions. *Sustainability MDPI*, *12*(2), 1–26. https://doi.org/10.3390/su12020492

de Jonge, B., Teunter, R., & Tinga, T. (2017). The influence of practical factors on the benefits of condition-based maintenance over time-based maintenance. *Reliability Engineering and System Safety*, *158*(October 2016), 21–30. https://doi.org/10.1016/j.ress.2016.10.002

Dogan, A., & Birant, D. (2021). Machine learning and data mining in manufacturing. *Expert Systems with Applications*, *166*(September 2020), 114060. https://doi.org/10.1016/j.eswa.2020.114060

Fahle, S., Prinz, C., & Kuhlenkötter, B. (2020). Systematic review on machine learning (ML) methods for manufacturing processes - Identifying artificial intelligence (AI) methods for field application. *Procedia CIRP*, *93*, 413–418. https://doi.org/10.1016/j.procir.2020.04.109

Flick, D., Keck, C., Herrmann, C., & Thiede, S. (2020). Machine learning based analysis of factory energy load curves with focus on transition times for anomaly detection. *Procedia CIRP*, *93*, 461–466. https://doi.org/10.1016/j.procir.2020.04.073

Grieves, M. (2014). Digital Twin : Manufacturing Excellence through Virtual Factory Replication. In *White Paper* (Issue March). https://www.researchgate.net/publication/275211047_Digital_Twin_Manufacturing_Excellence_through_Virtual_Factory_Replication

Hagerty, J. (2016). *2017 Planning Guide for Data and Analytics*. https://www.gartner.com/en/documents/3471553/2017-planning-guide-for-data-and-analytics

Hansen, E. B., & Bøgh, S. (2021). Artificial intelligence and internet of things in small and medium-sized enterprises: A survey. *Journal of Manufacturing Systems*, *58*(October 2019), 362–372. https://doi.org/10.1016/j.jmsy.2020.08.009

Kumar, R., Singh V, K., Harish, K., & Bhavish, R. K. (2021). Importance of Intelligent Automation in Post COVID Era: A Study. *2nd International Conference on Computation, Automation and Knowledge Management (ICCAKM)*, 204–209.

Lake, B. M., Ullman, T. D., Tenenbaum, J. B., & Gershman, S. J. (2017). Building machines that learn and think like people. *Behavioral and Brain Sciences*, *40*(2017). https://doi.org/10.1017/S0140525X16001837

Lee, J., Davari, H., Singh, J., & Pandhare, V. (2018). Industrial Artificial Intelligence for industry 4.0-based manufacturing systems. *Manufacturing Letters*, *18*, 20–23. https://doi.org/10.1016/j.mfglet.2018.09.002

Leukel, J., González, J., & Riekert, M. (2021). Adoption of machine learning technology for failure prediction in industrial maintenance: A systematic review. *Journal of Manufacturing Systems*, *61*(September), 87–96. https://doi.org/10.1016/j.jmsy.2021.08.012

Liu, J., Chang, H., Forrest, J. Y. L., & Yang, B. (2020). Influence of artificial intelligence on technological innovation: Evidence from the panel data of china's manufacturing sectors. *Technological Forecasting and Social Change*, *158*(May). https://doi.org/10.1016/j.techfore.2020.120142

McKinsey & Company. (2018). *AI adoption advances, but foundational barriers remain*. https://www.mckinsey.com/featured-insights/artificial-intelligence/ai-adoption-advances-but-foundational-barriers-remain

Mosavi, A., Salimi, M., Ardabili, S. F., Rabczuk, T., Shamshirband, S., & Varkonyi-Koczy, A. R. (2019). State of the art of machine learning models in energy systems, a systematic review. *MDPI Energies*, *12*(7). https://doi.org/10.3390/en12071301

Nayal, K., Raut, R. D., Queiroz, M. M., Yadav, V. S., & Narkhede, B. E. (2021). Are artificial intelligence and machine learning suitable to tackle the COVID-19 impacts? An agriculture supply chain perspective. In *International Journal of Logistics Management*. https://doi.org/10.1108/IJLM-01-2021-0002

Nti, I. K., Adekoya, A. F., Weyori, B. A., & Nyarko-Boateng, O. (2021). Applications of artificial intelligence in engineering and manufacturing: a systematic review. *Journal of Intelligent Manufacturing*, *2019*. https://doi.org/10.1007/s10845-021-01771-6

Pham, D. T., & Afify, A. A. (2005). Machine-learning techniques and their applications in manufacturing. *Proceedings of the Institution of Mechanical Engineers, Part B: Journal of Engineering Manufacture*, *219*(5), 395–412. https://doi.org/10.1243/095440505X32274

Rosen, R., Von Wichert, G., Lo, G., & Bettenhausen, K. D. (2015). About the importance of autonomy and digital twins for the future of manufacturing. *IFAC-PapersOnLine*, *48–3*, 567–572. https://doi.org/10.1016/j.ifacol.2015.06.141

Vocke, C., Constantinescu, C., & Popescu, D. (2019). Application potentials of artificial intelligence for the design of innovation processes. *Procedia CIRP*, *84*, 810–813. https://doi.org/10.1016/j.procir.2019.04.230

Vrontis, D., Christofi, M., Pereira, V., Tarba, S., Makrides, A., & Trichina, E. (2021). Artificial intelligence, robotics, advanced technologies and human resource management: a systematic review. *International Journal of Human Resource Management*, *0*(0), 1–30. https://doi.org/10.1080/09585192.2020.1871398

Woschank, M., Rauch, E., & Zsifkovits, H. (2020). A review of further directions for artificial intelligence, machine learning, and deep learning in smart logistics. *Sustainability MDPI*, *12*(9). https://doi.org/10.3390/su12093760

Younis, H., Sundarakani, B., & Alsharairi, M. (2021). Applications of artificial intelligence and machine learning within supply chains:systematic review and future research directions. *Journal of Modelling in Management*. https://doi.org/10.1108/JM2-12-2020-0322

THE STATE OF GENETIC ALGORITHM OPTIMIZATION IN ANTENNA DESIGN

Ali Recai CELİK

(*Dr.*), *Dicle University, e-mail: eeealicelik@gmail.com*
Orcid: 0000-0002-6917-5170

1. Introduction

In this chapter, the state and importance of the 'Genetic Algorithm (GA)' optimization in antenna design process are mentioned. For this purpose, firstly the optimization is defined in general terms. Then, the GA is explained in details. The stages of the GA such as identification, generation, adaptation, evaluation, mutation are introduced. The properties and advantages of using GA are mentioned. After that, some antenna design studies with GA are summarized. As a result, it is emphasized that the GA method can perform difficult operations efficiently in a short time and provides convenience to designers.

1.1. What is Optimization?

Optimization can be defined as a system that is applied to advance and develop the ideas, and that changes the initial parameters using existing information. The input parameters included in the optimization process are found as fitness values at the output of the process. The 'root finding' process searching the place where the derivative is zero can be preferred as an optimization method. Although there are many types of algorithms, optimizations can be generally divided into six groups. These are 'single and multi-objective optimization', 'continuous and discrete optimization', 'limited and unlimited optimization', 'static and dynamic optimization', 'trial and error optimization', 'random search and minimization optimization' (Haataja, 1994; Wurtz, et.al., 1997).

Various optimization processes can be used for many purposes nowadays. One of these purposes is to increase the performance of the antennas. Many

features of an antenna such as bandwidth, gain, radiation diagram can be reached to desired values by optimizing different design parameters such as patch size, ground structure, feeding position etc. In this chapter, the optimization method using the GA is mentioned. The features, advantages and application stages of this method are given. The state and importance of the GA optimization in antenna design are emphasized by reviewing some studies related with this field.

1.2. *Optimization with Genetic Algorithm*

Optimization using the GA is achieved by modelling a biological process. Input parameters in the GA represent genes in biology. Genes can be thought as binary encoding of the problem variants, and the string of genes is defined as a chromosome. Another term is population which is a set of chromosomes. Each chromosome of the population has a fitness value calculated with a fitness function. After examining the fitness values, the chromosomes are ranked from best to worst. In the next step, it is desired to create a new population with better characteristics than the individuals in the previous generation. For this, the higher ranked chromosomes are matched. Mutation is allowed to occur at a small probability. These steps are repeated until a desired fitness is achieved or a certain number of generations have occurred (Wyant, 2007).

It is determined whether the population is suitable or not by performing maximization or minimization operations according to the certain rules. The survivors are determined in the sequences obtained by random information exchange. As a result of bringing them together, the new generations are formed (Angeline, 1995).

There are many advantages of using the GA. In summary:

- The derivative transactions are not required,
- GA can be run with parallel processors,
- It can optimize both continuous and discrete parameters,
- GA can reach optimum results even when working with many parameters,
- It can explore a wide range of the objective function and optimize the complex objective functions without difficulty (Fertas, et.al., 2020; Sahal and Tejpal, 2021).

Before starting the GA optimization cycle, the input parameters are converted to the desired form by 'encoding'. As seen in Figure 1, the variables can be written as the binary or real numbers. The 'binary coded GA' is commonly used, and its flow chart is given in Figure 2. As seen from the figure, the objective function, parameters and limits are set for optimization at first. Then, the fitness values are

calculated by adapting the parameters to the GA. After the matching, crossover and mutation stages, the algorithm is completed by checking the convergence criteria.
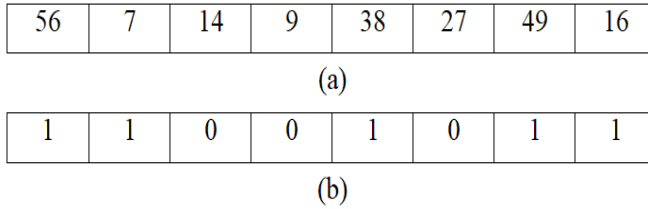
56	7	14	9	38	27	49	16

(a)

1	1	0	0	1	0	1	1

(b)

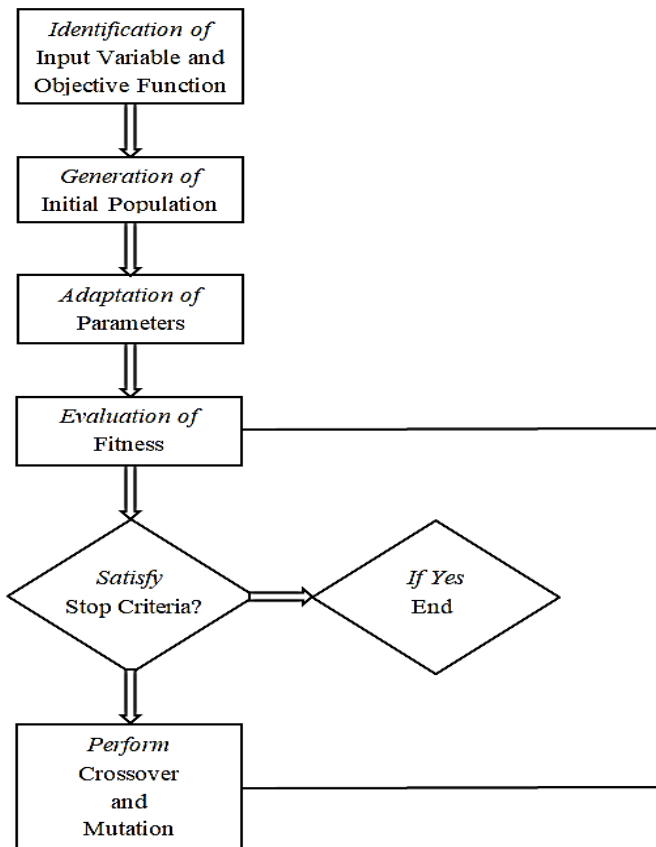Figure 1. Encoding of the Parameters; a) Real, b) Binary

Figure 2. Flow Chart of the Binary GA

2. GA Optimization in Antenna Design

While designing the antenna, besides the optimization options of the simulation programs, different optimization methods such as Quasi-Newton, Particle-

Swarm, Nelder-Mead, GA etc. can be used. GA is one of the powerful techniques that can be preferred in solving the electromagnetic problems that cannot be easily handled by other traditional methods. Since it has the ability to successfully handle a large number of different parameters, using the GA is a logical choice when designing multivariable antennas.

GA can be used to determine the length and width of a patch, thickness and permittivity of the dielectric slabs, feeding point of the designed antenna, shape of the ground structure etc. The fitness function can be derived from the cavity model and evaluate some antenna characteristics (Robinson and Rahmat-Samii, 2004).

2.1. Related Works

Different antenna design works using the GA optimization can be found in the literature. Some of these studies are mentioned in this section. In the study conducted by Johnson and Rahmat-Samii (1997), the shape and size of the antenna patch was optimized for the bandwidth (BW) enhancement, but the gain was not taken into account. After the optimization process, the fractional bandwidth value of 20% was reached. It was concluded in the study that the GA is applicable to a broad class of optimization problems.

A quad-band patch antenna for the wireless communications was proposed in the paper of Jayasinghe and Uduwawala (2012). Both the patch geometry and feed position were considered as the optimization parameters in the design process. The antenna resonated at 2.4 GHz and 5 GHz with BW of 4.1% and 33.5%, respectively. However, the radiation pattern was not considered in the optimization.

In another study, a square shaped microstrip antenna was designed by using the GA technique to obtain a wide BW for the X-band applications. The optimized antenna had a high gain of 8.35 dB. It was emphasized that the shape simplicity and size reduction were achieved thanks to the GA optimization (Mishra, et.al., 2018).

In the study of Zhang, et.al. (2019), both the GA optimization method and the defected ground structure (DGS) were used to design an antenna so that it could be ultra-wideband. After the rectangular patch structure had been optimized and DGS had been applied, the values of S_{11} were obtained under -10 dB between the 2.5 GHz and 10.6 GHz. It was concluded that the GA provided automatic debugging of the errors in antenna design and finding the most suitable design values in a short time.

The GA was used to design of a thin-wire antenna in another study for using in the radar and telecommunication systems. The wire topology and branching tree methods were investigated in the study. Developing process of an objective function for any desired pattern was also mentioned (Smith and Baginski, 2019).

In another study, it was shown that the designs which are difficult to make manually can be easily realized and the simulation process can be accelerated by using GA (Gulati, et.al., 2018). The dimensions of the patch were calculated, and the S-parameters and radiation pattern were obtained experimentally. The planar antenna proposed in the study operated in the 3.1-9 GHz frequency range.

Another UWB antenna having compact size was designed with GA optimization in (Fertas, et.al., 2017). The return loss, radiation pattern and gain of the proposed antenna were investigated in that study. It had the working frequencies between the 2.4 GHz and 9.8 GHz. The results of the fabricated antenna showed a good agreement with the simulations. The importance of using the GA for the design of UWB antennas was emphasized in the study.

A fractal square microstrip antenna for using in the S-band and C-band applications was proposed by Rasheda, et.al. (2021). The GA was applied to design the patch and partial ground of the antenna. Accordingly, the size of the designed antenna was reduced by cutting the edges and center of the patch. An improvement was observed in the return loss and gain results after the optimization process. It was reported that the optimized and presented antenna operated at 3.5 GHz and 6 GHz.

In the study of Derbal, et.al. (2020), the GA was used to optimize the ground plane of an UWB antenna. Two notched bands were obtained at the WiMAX and WLAN bands through the DGS design. It was concluded that the GA optimization method provided a good performance to create band rejection and prevented the complex problem.

In another study, an antenna was designed and fabricated for operating in DSRC band. The GA was used to optimize the ground structure in order to reach high gain and obtain omnidirectional radiation pattern. Therefore, the gain was measured as 5.6 dB and the desired radiation pattern was obtained after optimization (Kanni and Brinda, 2019).

3.   Conclusions

In this chapter, firstly, the definition of optimization was made and its types were mentioned. It was stated that the GA has an important place among the optimization methods. The advantages of the GA were emphasized and the

necessary stages for its use were explained. Afterwards, the importance of the GA optimization in antenna design was explained and some studies such as microstrip antenna, planar antenna, UWB antenna, thin-wire antenna whose dimensions had been determined by using GA were summarized.

In conclusions, it is understood that the GAs can be used successfully in the decision mechanisms of the antenna designs, and they can perform difficult operations efficiently in a short time by providing convenience to the designers. It can be said that the GA method will become more popular and remain on the agenda for a long time both in antenna designs and solving other electromagnetic problems.

References

Angeline, P.J. (1995). Evolution revolution: An introduction to the special track on genetic and evolutionary programming. *IEEE Expert Intelligent Systems and Their Applications,* vol. 10, 6-10.

Derbal, M.C., Zeghdoud, A., Mourad., N. (2020). A dual band notched UWB antenna with optimized DGS using genetic algorithm. *Progress In Electromagnetics Research*. vol. 88, 89-95.

Fertas, K., Kimouche, H., Challal, M., Ghanem, F., Fertas, F., Aksas, G. (2017). Development of a novel UWB planar antenna using a genetic algorithm. In *Proceedings of 5th International Conference on Electrical Engineering-Boumerdes*. 1-4.

Fertas, K.,Tebache, S.,Ghanem, F., Tedjini, S., Aksas, R. (2020). Non-conventional multiband patch antenna design with filtering aspect based on genetic algorithm. *IETE Journal of Research.* vol. 66(6), 815-822.

Gulati, M., Siddhartha, S., Vedi, Y., Susila, M. (2018). genetic-algorithm based planar antenna design, In *Proceedings of International Conference on Wireless Communications, Signal Processing and Networking.*1-2.

Haataja, J., (1994). Solving optimization problems. CSC- Center for Scientific Computing Ltd, Yliopistopaino. First Edition. ISBN 952-9821-02-6

Jayasinghe J.M.J.W., Uduwawala D.N. (2012). Novel quad-band patch antenna design for wireless communications in 2.4, 5.2, 5.6 and 5.8 GHz bands using genetic algorithm optimization. *International Journal of Engineering and Technology.* vol. 1(4), 466-471.

Johnson J.M., Rahmat-Samii Y. (1997). Genetic algorithms in engineering electromagnetics. *IEEE Transactions on Antennas and Propagation*, vol. 39, 7-21.

Kanni, R., Brinda, R. (2019). Design of high gain microstrip antenna for vehicle to vehicle communication using genetic algorithm. *Progress In Electromagnetics Research M*. vol. 81, 167-179.

Mishra, R.G., Mishra, R., Kuchhal, P., Kumari, N.P. (2018). Optimization and analysis of high gain wideband microstrip patch antenna using genetic algorithm. *International Journal of Engineering & Technology*. vol. 7, 176-179

Rasheda, H. M. Q., *et al*. (2021). An optimization of fractal microstrip patch antenna with partial ground using genetic algorithm method. In *Proceedings of International Congress of Advanced Technology and Engineering*. 1-6.

Robinson, J., Rahmat-Samii, Y. (2004). Particle swarm optimization in electromagnetics. *IEEE Transactions on Antennas and Propagation*. vol. 52(2), 397-407.

Sahal M., Tejpal, V.T. (2021). Optimization algorithms for antenna design, array thinning, and radiation pattern synthesis. In *Proceedings of International Conference on Communication and Computational Technologies*. Springer, Singapore.

Smith, J. S., Baginski, M. E. (2019). Thin-wire antenna design using a novel branching scheme and genetic algorithm optimization. *IEEE Transactions on Antennas and Propagation*. vol. 67(5), 2934-2941.

Wurtz, F., Richomme M., Bigeon J., Sabonnadiere J.C. (1997). A few results for using genetic algorithms in design of electrical machines. *IEEE Transactions on Macgnetis*. vol. 33(2), 1892-1895.

Wyant, A. (2007). Genetic algorithm optimization applied to planar and wire antennas. Msc Thesis, Rochester Institute of Technology.

Zhang, Z., Yang, S., Liu, M., Deng, S., Li, L. (2019). Design of an UWB microstrip antenna with DGS based on genetic algorithm. In *Proceedings of 21st International Conference on Advanced Communication Technology*. 228-232.

A NOVEL TOPSIS INTEGRATED DSS FOR PERFORMANCE ASSESSMENT OF CITY HOSPITALS

Yeliz BURUK SAHİN[1] & Hilal DEMİREL[2]

[1](Asst. Prof. Dr.) Department of Industrial Engineering, Eskisehir Osmangazi University, email: yelizburuk@ogu.edu.tr Orcid: 0000-0002-6215-5193

[2](Graduate Student) Department of Industrial Engineering, Eskisehir Osmangazi University, email: hilaldemirel932@gmail.com Orcid: 0000-0002-3453-8904

1.   Introduction

The result of an aging population and the increase in chronic and epidemic diseases make the acquisition of appropriate health care more valuable. With the determination of the right strategies, it may be possible to take measures to improve public health. (Ahmad et al., 2021). In this sense, it is important to analyze the performance of the country, hospital, and all health units and to investigate which policies can be improved. With performance-oriented benchmarking, it is also possible to examine competitors anywhere in the world, adapt their successful processes and increase performance.

Today, decision problems are frequently encountered in the rapidly developing world. For this reason, decision makers' need for MCDM techniques in the decision making process has increased. The use of MCDM problems is a necessary field, as the subject of evaluating health systems requires considering multiple conflicting criteria. There are many studies in the literature using MCDM techniques (Stojčić et al., 2019).

Some of the Multi-Criteria Decision Making (MCDM) techniques frequently used by decision makers in literature are as follows: Analytical Hierarchy Process (AHP) (Schmidt et al., 2015), Analytic Network Process (ANP) (Saaty and Vargas, 2013), Elimination and Choice Expressing Reality (ELECTRE) (Govindan and Jepsen, 2016), Complex Proportional Assessment (COPRAS) (Dhiman and Deb, 2020), Technique for Order Preference by Similarity to Ideal Solution (TOPSIS) (Nilashi et al., 2019), Multi-Objective Optimization Method by Ratio Analysis (MOORA) (Abdel-Basset et al., 2019), Vise Kriterijumska Optimizacija Kompromisno Resenjemeaning (VIKOR) (Gupta, 2018), Data Envelopment Analysis (DEA) (Charnes vd., 1978) and Best Worst Method (BWM) (Rezaei, 2015).

In the literature, MCDM techniques are frequently used in the evaluation of performance in the health sector. The studies examined in the recent literature review is summarized as follows:

Araujo et al. (2018) evaluated the relative performance of hospitals in the municipality of Rio de Janeiro between 2008 and 2013 with TOPSIS. Afterward, TOPSIS results were combined with neural networks to create a predictive performance model. Hospital outpatient and inpatient treatment services were the subjects of the study.

Jafari, Seyedjavadi, and Zaboli (2020) selected bed turnover rate, patient stay, bed turnover interval, inpatient discharge time, outpatient discharge time, operating room capacity, bed occupancy rate, and the number of emergency patients as criteria for hospital performance evaluation. The TOPSIS method was used in the study and it was deduced from the results that the weights of the bed turnover rate, number of emergency patients, and length of stay criteria were higher and that the relevant criteria were the three main indicators in the study.

Ortiz-Barrios et al. (2020) used FAHP to determine the weights of thirty-six sub-criteria related to six main criteria in disaster preparedness. FDEMATEL is used to reveal interdependences. They applied the TOPSIS method to rank hospitals by disaster preparedness. Thus, it was aimed to identify the weak points of each institution.

Khambhati et al. (2021) evaluated the service quality of public health facilities with TOPSIS. They conducted a conceptual performance assessment in a fuzzy environment with TOPSIS and proposed a model.

İnce and Güre (2021) evaluated the health performance of 18 OECD countries on the basis of rare diseases, taking into account health indicators. The

performance of rare diseases in selected OECD countries was analyzed using three MCDM methods.

The application of methods in problems with many criteria and alternatives takes considerable time. By considering that the number of decision problems encountered is increasing day by day, it is aimed to reduce the workload of decision makers and save time by developing a Decision Support System (DSS) based on MCDM methods. In this study, a DSS-based evaluation was carried out to determine the performance level of city hospitals in the health sector, which is one of the sectors with the highest expectation for continuous improvement.

2. Method

2.1. SWARA Method

SWARA (Step-wise Weight Assessment Ratio Analysis) was introduced to the literature in 2010 by Kersuliene, Zavadskas, and Turskis. It makes the weighting of the criteria by providing a more accurate evaluation process by taking into account the expert opinion on the relevant subject.

The expert, with the experience he has gained, ranks all the discussed criteria from the most important to the least important criteria. After this ranking, the expert determines how much more important a criterion is than the next criterion, under the name of "relative importance level", by subjective evaluation. The method steps are as follows:

Step 1: The criteria to be evaluated in the problem $(c_1, c_2, …, c_n)$ and the experts who will evaluate these criteria with knowledge about the subject $(k_1, k_2, …, k_m)$ are determined.

Step 2: Decision makers rank the n criteria, with the most important (best) criterion in the first place.

Step 3: Considering the order made in the previous step, the "relative importance levels" (s_j) that show how important each criterion (criterion j) are than the next criterion (criterion (j+1)) are determined.

Step 4: Based on the s_j value, that is, the relative importance levels, the "k_j" coefficient is determined according to equation 1.

$$k_j = \begin{cases} 1 & j = 1 \\ s_j + 1 & j > 1 \end{cases} \tag{1}$$

Step 5: For the criteria, "q_j" weight values are calculated as seen in equation 2.

$$q_j = \begin{cases} 1 & j = 1 \\ \dfrac{k_{j-1}}{k_j} & j > 1 \end{cases} \tag{2}$$

Step 6: The relative weights of the criteria "w_j" are calculated by considering equation 3. In the case of more than one decision maker, the final weight value for the relevant criterion is determined by taking the geometric/arithmetic average of the relative weight values.

$$w_j = \frac{q_j}{\sum_{k=1}^{n} q_k} \tag{3}$$

2.2 BWM

One of the powerful techniques used to determine criteria weights is the BWM developed by Rezaei (2015). The method depends on the selection of the best and worst decision criteria made by the decision maker and the evaluation of other decision criteria by scoring in the range of 1-9.

Here, 5 steps of the BWM method has been explained (Rezaei, 2015, 2016):

Step 1: Determine a set of criteria ($c_1, c_2, ..., c_n$).

Step 2: Determine the best and the worst criterion.

Step 3: Compare preferences of the best criterion to the other criteria. Preferences are defined on a scale of 1-9 and "1" means i is of equal importance to j, "9" means i is extremely important relative to j. Best to Others (BO) Vector $A_B = (a_{B1}, a_{B2}, ..., a_{Bn})$ is defined with comparisons. a_{Bj} is the preference of best criterion B to criterion j.

Step 4: Compare preferences of the other criteria to the worst criterion. Scale is the same with the previous step. Others to Worst (OW) vector $A_w = (a_{1w}, a_{2w}, ..., a_{nw})^T$ and is defined with comparisons. a_{1w} is the preference of criterion j to the worst criterion w.

Step 5: To determine the optimal weights, the following model is used:

$$\left| w_B - a_{Bj} W_j \right| \le \xi^L \quad \forall j \tag{4}$$

$$\left| w_j - a_{jw} W_w \right| \le \xi^L \quad \forall j \tag{5}$$

$$\sum_j w_j = 1 \tag{6}$$

$$w_j \geq 0, \qquad \forall j \tag{7}$$

indicates better consistency with results close to zero.

2.3   TOPSIS Method

TOPSIS, first developed by Hwang and Yoon (1981), is the most widely used MCDM method. This method is based on the view that the best alternative is close to the positive ideal solution (PIS) and farthest from the negative ideal solution (NIS).

TOPSIS method implementation steps are explained as follows: Step 1: Construct a decision matrix with m attributes and n criteria. The intersection of every alternative and criteria is shown as x_{ij}. Then, using equation 8, the decision matrix is normalized.

$$R_{ij} = \frac{x_{ij}}{\sqrt{\sum_{i=1}^{m} x_{ij}^2}} \tag{8}$$

Step 2: The weighted normalized decision matrix (V) is constructed by equations 9-10 by considering the importance levels of each criterion (w_j: weight of criterion j).:

$$V = (v_{ij})_{mxn} = (w_j r_{ij})_{mxn} \tag{9}$$

$$\sum_{j=1}^{n} w_j = 1 \tag{10}$$

Step 3: PIS ($A^+ = v_1^+$, v_2^+, … , v_n^+) and NIS ($A^- = v_1^-$, v_2^-, … , v_n^-) are determined depending on the purpose direction (maximization and minimization) represented by the criteria. While j_b represents benefit criteria set and j_c represents cost criteria set, PIS and NIS are calculated by equations 11-12.

$$v_j^+ = \left\{ \left(\underset{i}{max} \; v_{ij} \; \Big| \; j \in j_b \right), \left(\underset{i}{min} \; v_{ij} \; | \; j \in j_c \right) | i \in \lfloor 1..m \rfloor \right\} \tag{11}$$

$$v_j^- = \left\{ \left(\underset{i}{min} \; v_{ij} \; \Big| \; j \in j_b \right), \left(\underset{i}{max} \; v_{ij} \; | \; j \in j_c \right) | i \in \lfloor 1..m \rfloor \right\} \tag{12}$$

Step 4: The deviation values (s_i^+, s_i^-) representing the distances of the alternatives from the PIS and the NIS can be calculated using the formulas 13-14.

$$s_i^+ = \sqrt{\sum_{j=1}^{n}(v_{ij} - v_j^+)^2} \quad \forall i \in \lfloor 1..m \rfloor \qquad (13)$$

$$s_i^- = \sqrt{\sum_{j=1}^{n}(v_{ij} - v_j^-)^2} \quad \forall i \in \lfloor 1..m \rfloor \qquad (14)$$

Step 5: To calculate the relative closeness of the alternatives to the ideal solution, formula 15 is used:

$$C_i = \frac{s_i^-}{s_i^+ + s_i^-} \quad \forall i \in \lfloor 1..m \rfloor \qquad (15)$$

Step 6: Calculated C_i values are ordered from largest to smallest, and the largest of these values, ranging from 0 to 1, represents the best option based on the criteria evaluated according to all alternatives.

3. Results and Discussion

In this part of the study, a DSS supported by MCDM was developed. The performance evaluation of 13 city hospitals in the borders of the Republic of Turkey was carried out using the TOPSIS. Criteria weights were obtained by BWM and SWARA methods. Six criteria have been determined and these criteria are as follows: Hospital bed (HB), Operating Room (OR), Critical Care Bed (CCB), Burn Unit (BU), Outpatient Clinic (OC), and Leave Delivery Room Patient (LDRP).

In the selection of criteria, the criteria discussed in the studies examined in the literature research were taken into consideration. The data used in the study were obtained from the website of the General Directorate of Public Hospitals, Department of City Hospitals Coordination (https://khgmsehirhastaneleridb. saglik.gov.tr/).

TOPSIS, BWM, and SWARA methods used in this study were integrated with the DSS that was coded in MS Office Excel software. The DSS can retrieve the data non-manually by opening a text document containing the data via the Excel program.

Performance evaluation was carried out with the TOPSIS method, and the weights of the criteria are calculated by using the BWM and SWARA methods to determine the effect of the criteria on the decision problem, by including the opinions of different decision makers about the criteria. These calculated weights are determined by taking geometric/arithmetic averages for each criterion in the case of more than one decision maker. These determined criteria weights provide input to the TOPSIS method weighted standard decision matrix, providing more realistic results compared to the case where all criteria weights are taken equally. The data of the designated hospitals regarding the criteria discussed are given in **Appendix-1.**

In this study, for the developed DSS, firstly "BWM" or "SWARA" can be used up to decision-maker preferences, finally, for performance evaluation, the "TOPSIS" method is used.

3.1   DSS (BWM-TOPSIS)

When the DSS developed in the Excel program is run and the "DSS" button that appears on the screen is clicked, the "User Data Entry Pages" user interface shown in Figure 1 is displayed. By using the button named "Data Input" on the first page of the interface named "Data" by the user, the text document containing the relevant data set should be selected.
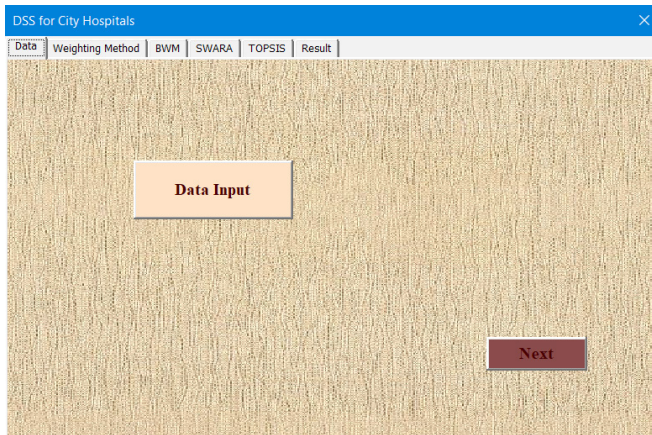

Figure 1. User data selection page

After data selection is completed, the "Next" button on the screen switches to the "Weighting Method" page, and the "BWM" and the number of decision makers are selected on this page. The number of decision makers whose opinions were evaluated in the study was determined as two. When the button named "Next" is clicked, the interface page named "BWM" becomes active.

The best and worst criteria should be selected over the interface in Figure 2. Then, the criteria are scored by the first decision maker in the range of 1 to 9 to create BO and OW vectors in line with these selections. The interface pages are displayed again for the second decision maker to score the criteria after the evaluation of the first decision maker.

Figure 2. BWM scoring screen for the first decision-maker

While the first decision maker chooses the number of the outpatient clinic as the best criterion, the number of burn units is defined as the worst criterion. According to the first decision maker, the score values given in the BO vector are as follows: 3, 4, 5, 8, 1, 6. OW vector scoring is as follows: 6, 5, 4, 1, 8, 3. While the second decision maker chooses the critical care bed as the best criterion, the LDRP is selected as the worst criterion. According to the second decision maker, the score values given in the BO vector are as follows: 4, 3, 1, 5, 6, 7. OW vector scoring is as follows: 5, 6, 8, 4, 3, 1.

After entering the opinions of the second decision maker on the criteria, the "TOPSIS" page is accessed with the help of the "Next" button. When the "TOPSIS" button is clicked, the interfaces where the decision maker will choose the benefit-cost regarding the objective function direction of the criteria become active. Since the criteria discussed within the scope of the study are for the capacity of the hospitals, the purpose function aspect was chosen as benefit for all criteria. After this selection, the performance values of city hospitals are determined with the TOPSIS method and ranked from the highest to the lowest. The performance ranking of city hospitals is given in Figure 3.
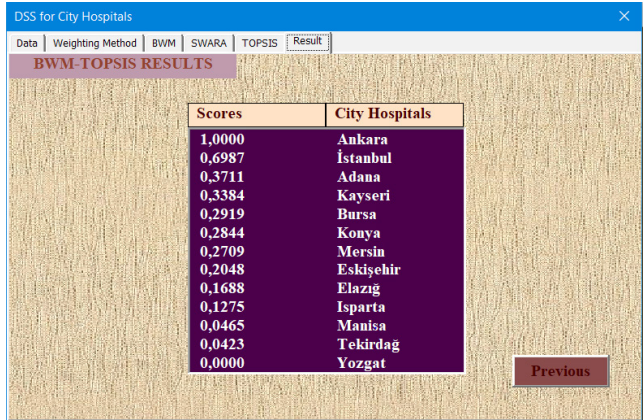
Figure 3. BWM-TOPSIS Results

3.2. DSS (SWARA-TOPSIS)

When the SWARA method was used to weight the criteria while evaluating the performance in the developed DSS, the "SWARA" method and the number of decision makers were selected as "2" on the "weighting method" page. After this selection process, when the "Next" button is clicked, the "SWARA" page of the interface component becomes active. When the "SWARA" button on the interface is clicked, the interfaces where the decision makers sort the criteria and determine their relative importance levels (s_j) are displayed respectively for each decision maker. The order of importance determined by the first decision maker for the criteria discussed in the study is shown in Figure 4.
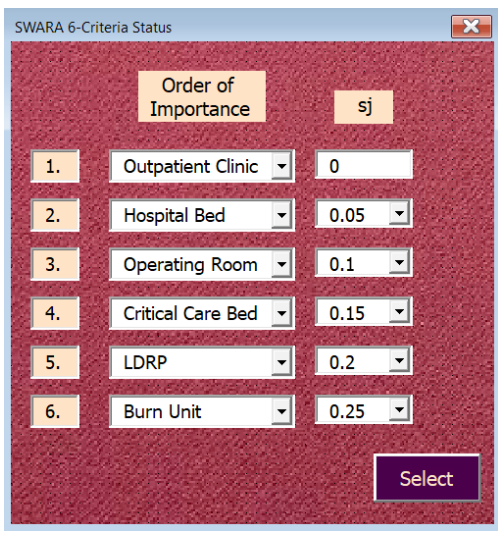

Figure 4. SWARA Data input interface for the first decision-maker

The first decision maker ranked the criteria from the most important to the least important as follows: Outpatient clinic (s1=0), hospital bed (s2=0.05), operating room (s3=0.1), critical care bed (s4=0.15), LDRP (s5= 0.2), burn unit (s6=0.25). The second decision maker ranked the criteria from the most important to the least important as follows: Critical care bed (s1=0), operating room (s2=0.1), hospital bed (s3=0.15), burn unit (s4=0.05), outpatient clinic (s5 =0.25), LDRP (s6=0.2).

After determining the criteria weights using the SWARA method, "benefit" selection is made for all criteria. When this selection process is completed, the performance ranking of the criteria is created with the TOPSIS method. The performance ranking of city hospitals when criteria weighting is obtained with the SWARA method is shown in Figure 5.
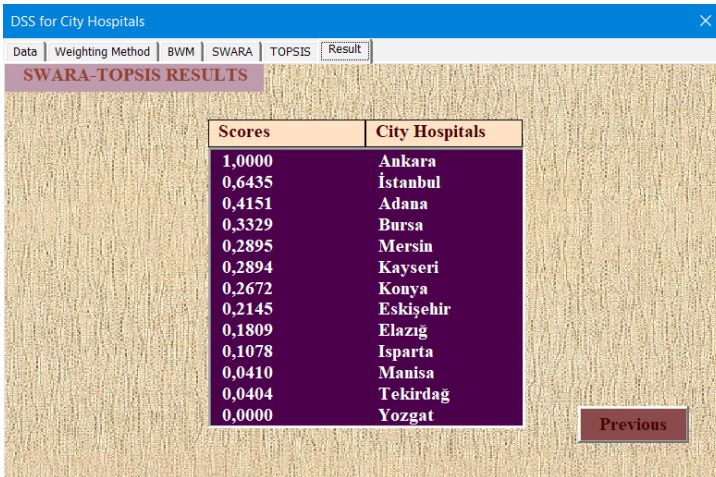

Figure 5. SWARA-TOPSIS Results

5. Conclusion

A dynamic DSS has been created over the Microsoft Excel program for the MCDM Techniques used in the study. Data entry to the DSS is designed to be transferred via text documents and it is aimed to prevent errors that may arise from manual data entry. Two different criteria weighting methods (BWM and SWARA) have been integrated into the DSS to obtain the criteria weights.

Within the scope of the study, performance evaluation of thirteen city hospitals in Turkey was carried out with the TOPSIS method. BWM and SWARA methods are used to determine selected six criteria weights. After these weights are determined, a preference order is created to evaluate the performance with

the TOPSIS method. While determining the criterion weights, common criterion weights can be calculated for a variable number of decision makers.

When the BWM method is performed to weight the criteria and the TOPSIS method is used for performance evaluation, the order of preference and score values of the city hospitals are as follows: Ankara (1), Istanbul (0.6987), Adana (0.3711), Kayseri (0.3384), Bursa (0.2919), Konya (0.2844), Mersin (0.2709), Eskişehir (0.2048), Elazig (0.1688), Isparta (0.1275), Manisa (0.0465), Tekirdağ (0.0423) and Yozgat (0).

When the SWARA method was used to weight the criteria and the TOPSIS method was used in the performance evaluation, the order of preference and score values of the city hospitals from the highest to the lowest were found as follows: Ankara (1), Istanbul (0.6435), Adana (0.4151), Bursa (0.3329), Mersin (0.2895), Kayseri (0.2894), Konya (0.2672), Eskişehir (0.2145), Elazığ (0.1809), Isparta (0.1078), Manisa (0.0410), Tekirdağ (0.0404) and Yozgat (0).

From the performance evaluations made using BWM-TOPSIS and SWARA-TOPSIS methods, it can be interpreted that Ankara, Istanbul, and Adana City Hospitals are the hospitals with the highest performance, and Yozgat, Tekirdağ, Manisa City Hospitals are the hospitals with the lowest performance levels.

Although the most important, best, and least important, worst criteria selections were made the same in two different weighting methods, different preference rankings were obtained for Bursa, Kayseri, Mersin, and Konya City hospitals as a result of the performance ranking due to the differences in scoring and relative importance levels between the methods.

Different weighting techniques can be integrated into the developed DSS to solve the problem. In addition, by increasing the variety of sequencing techniques, sensitivity analyzes can be performed and the results of the methods can be compared.

Appendix-1. Data Set for City Hospitals

Alternatives	Criteria					
	H.B.	O.R.	C.C.B	B.U.	O.C.	LDRP
Eskişehir City Hospital	1235	37	181	12	254	13
Adana City Hospital	1595	60	231	29	407	27
Mersin City Hospital	1330	51	236	12	260	26
Isparta City Hospital	800	20	176	4	167	9
Yozgat City Hospital	475	18	70	0	114	8
Kayseri City Hospital	1607	43	263	5	395	10
Manisa City Hospital	558	19	103	2	146	10
Elazığ City Hospital	1038	37	160	10	227	14
Ankara City Hospital	3332	115	688	34	761	80
Bursa City Hospital	1355	49	225	26	300	15
İstanbul City Hospital	2682	90	456	24	710	28
Konya City Hospital	1250	36	240	15	334	14
Tekirdağ City Hospital	605	18	102	2	134	10

References

Abdel-Basset, M., Manogaran, G., Gamal, A., & Smarandache, F. (2019). A group decision-making framework based on neutrosophic TOPSIS approach for smart medical device selection. *Journal of medical systems*, 43(2), 38.

Ahmad, N., Hasan, M. G., & Barbhuiya, R. K. (2021). Identification and prioritization of strategies to tackle COVID-19 outbreak: A group-BWM based MCDM approach. *Applied soft computing*, 111, 107642.

Araujo, C. A. S., Wanke, P., & Siqueira, M. M. (2018). Performance analysis of Brazilian public health: TOPSIS and neural networks application. *International Journal of Productivity and Performance Management*, 67, 9,1526-1549.

Charnes, A., Cooper, W. W., & Rhodes, E. (1978). Measuring the efficiency of decision-making units. *European journal of operational research*, 2(6), 429-444.

Dhiman, H. S., & Deb, D. (2020). Fuzzy TOPSIS and fuzzy COPRAS-based multi-criteria decision making for hybrid wind farms. *Energy*, 202, 117755.

Govindan, K., & Jepsen, M. B. (2016). ELECTRE: A comprehensive literature review on methodologies and applications. *European Journal of Operational Research*, 250(1), 1-29.

Gupta, H. (2018). Evaluating service quality of airline industry using hybrid best worst method and VIKOR. *Journal of Air Transport Management*, 68, 35-47.

Hwang, C.L., & Yoon, K.P. (1981). Multiple attribute decision making: methods and applications. New York: Springer-Verlag.

İnce, Ö., Güre, M.D.P. (2021). Evaluation Of Rare Diseases Policy Performance Of OECD Countries Using MCDM Methods. Health Policy and Technology, 100537.

Jafari, M., Seyedjavadi, M., & Zaboli, R. (2020). Assessment of performance in teaching hospitals: Using multicriteria decision-making techniques. *Journal of Education and Health Promotion*, 9(1), 5.

Khambhati, R., Patel, H., & Kumar, S. (2021). A performance evaluation and comparison model for urban public healthcare service Quality (Urbpubhcservqual) By fuzzy TOPSIS Method. *Journal of Nonprofit & Public Sector Marketing*, 1-20. https://doi.org/10.1080/10495142.2020.18 65232

Nilashi, M., Mardani, A., Liao, H., Ahmadi, H., Manaf, A. A., & Almukadi, W. (2019). A hybrid method with TOPSIS and machine learning techniques for sustainable development of green hotels considering online reviews. *Sustainability*, 11(21), 6013.

Ortiz-Barrios, M., Gul, M., López-Meza, P., Yucesan, M., & Navarro-Jiménez, E. (2020). Evaluation of hospital disaster preparedness by a multi-criteria decision making approach: The case of Turkish hospitals. *International journal of disaster risk reduction*, 49, 101748.

Rezaei, J. (2015). Best-worst multi-criteria decision making method. *Omega*, 53, 49-57.

Rezaei, J., 2016, "Best-worst multi-criteria decision making method: Some properties and a linear model", *Omega*, 64, 126-130.

Saaty, T. L., & Vargas, L. G. (2013). The analytic network process. In *Decision making with the analytic network process*, 1-40, Springer, Boston, MA.

Schmidt, K., Aumann, I., Hollander, I., Damm, K., & von der Schulenburg, J. M. G. (2015). Applying the Analytic Hierarchy Process in healthcare research: A systematic literature review and evaluation of reporting. *BMC medical informatics and decision making*, 15(1), 1-27.

Stojčić, M., Zavadskas, E. K., Pamučar, D., Stević, Ž., & Mardani, A. (2019). Application of MCDM methods in sustainability engineering: A literature review 2008–2018. *Symmetry*, 11(3), 350.

NATURAL VENTILATION IN DAIRY CATTLE BARNS

Busra YAYLI[1*] & Ilker KILIC[2]

[1](Phd. Student), Bursa Uludag University, e-mail:busrayayli@uludag.edu.tr
Orcid: 0000-0002-0198-3550
[2](Assoc. Prof.), Bursa Uludag University, e-mail:ikilic@uludag.edu.tr
Orcid: 0000-0003-0087-6718
[*]Corresponding author: E-mail:busrayayli@uludag.edu.tr

1. Introduction

As the population of the world increases, the needs of people for nutrients also increase. Foods of animal origin have an essential share for a healthy and balanced diet. Today, products of animal origin are considered strategic products. People show a tendency to eat healthier diets due to the Covid-19 pandemic that started in 2020. Milk and dairy products are essential elements of a balanced diet, and there is an increase in demand during the pandemic. While some disruptions such as milk production, supply, and distribution are expected due to the Covid-19 pandemic, global milk production increased by 1.3% and reached 874 million tons in 2020. There was an increase in all geographical regions except Africa, where production remained stable. The world's milk production was mainly in Asia. In the Asian continent, it constituted 379 million tons with an increase of 2.6% in 2020, and India, China, Pakistan, and Turkey are leading in these increases (FAO, 2021). World dairy cattle stock was 1.3 billion heads in 2020. In Turkey, it increased by 1.6% in 2020 and reached 17 million 965 thousand heads (TUIK, 2020). In the first half of 2021, 5 million 574 tons of milk production was realized, increasing 2.5% compared to the same period of the previous year (TUIK, 2021).

Genetics, nutrition, physiology, and environmental conditions are the main factors in realizing production at high productivity levels in dairy cattle barns. In order to obtain high-quality milk and meat production, it is essential that the production with productive breeds, as well as the environment in which the animals are raised, comply with the wishes of the animals, ensure optimal

climatic conditions, and are well designed (Uğurlu and Şahin, 2010). In order to obtain the highest efficiency, climatic (temperature, relative humidity, ventilation, lighting) and structural (stall, feeder, milking parlor, tie-stall types, special compartments) conditions must be provided at an optimum level.

It is imperative to create ideal environmental conditions to reduce the adverse effects of shelter climatic conditions on animals. It is also effective in the construction of barns as it affects animals from different perspectives (Mundan et al., 2018). In barns where suitable climatic conditions cannot be provided, adverse effects occur by creating stress in animals. In cases where high temperature and relative humidity occur in the barns, there will inevitably be a decrease in the yield, as the desire to eat feed will decrease in the animals. Providing clean air by removing heat, humidity, and odor in livestock barns is essential for animal productivity, animal welfare, and economic profitability. By throwing out the harmful gas, odor, polluted and dusty air in the barns, ensuring the entry of fresh air reduces the detrimental effects of temperature and relative humidity on animals. In addition, it prolongs the use of the barn, protects the building elements, and prevents fodder from spoiling. Therefore, good ventilation is required in the barns.

Natural ventilation; is the movement of air through special openings left in the building with the help of natural forces caused by wind effects and temperature differences (Olgun, 2016). Ventilation can be done in two ways to discharge the polluted air inside the barns and provide fresh air: natural ventilation and mechanical ventilation. Natural ventilation is a more advantageous method than mechanical ventilation in energy conservation, health, environmental and economic aspects.

2.   Importance of Ventilation in Dairy Barns

Dairy cattle spread much moisture in the air during their breathing and rumination in the barn, and the ambient temperature increases. The average body temperature of the cattle is about 38.5°C, and there are significant adverse effects on the yield when it rises above 39°C (Thatcher et al., 2010). Typical 600 kg dairy cattle produce 25-30 m^3 of gas per day due to fermentation, and this gas mixes with the barn air by respiration (Göncü et al., 2015). Fertile breeds with a high milk yield produce more heat. With the increase in ambient temperature, cows maintain the average temperature level and homeostasis in the body by breathing more and sweating through evaporation. If this situation does not relieve the cow, heat stress occurs in the animal. Heat stress creates unfavorable conditions such as decreased feed intake, low yield and deterioration of milk quality, weakening of the immune system, and low fertility in animals (Alkoyak, 2016).

To reduce the effects of heat stress in dairy cattle, regulation of genetic and environmental factors will contribute to the solution at a rate of 65% (Dinçel and Dikmen, 2013). Where genetic factors and nutritional conditions are provided, production performance will directly depend on the environment. The most effects of indoor conditions in dairy barns are temperature, relative humidity, ammonia (NH_3), carbon dioxide (CO_2), methane (CH_4), and hydrogen sulfide (H_2S) concentrations (Zou et al., 2020). Manure and urine are produced by animals result of digestion, the amount of moisture emitted to the environment increases, and gases such as ammonia are produced. If adequate ventilation is not provided, polluted ambient air occurs.

When the barn environment is warm, it retains more moisture than in cold conditions in the air. Humidity in the barn environment creates high relative humidity when it is not adequately ventilated. High humidity causes more dust and gas to be retained in the environment. With a good ventilation system, the temperature of the barınağın is controlled, the relative humidity is kept within the desired limit, and moisture condensation is prevented.

Ventilation in their farms provides airflow between cows by reducing the heat load on animals in hot climates or periods. In cold climatic regions or periods, heat increase, and moisture condensation occur if adequate ventilation is not provided. While this creates an unhealthy environment for animals, it can cause a corrosive effect on building materials. Thus, the life of the building is reduced.

3. Natural Ventilation

Natural ventilation in the animal barn aims to constantly expel the heat, polluted and harmful gases, humidity, and microorganisms in the indoor environment, to take fresh air into the barn instead, and standard distribution ventilation at the proper speed/flow is aimed. Natural ventilation is generally recommended in cattle and sheep barns. Mechanical ventilation is more widely used because natural ventilation may be insufficient in poultry farms, where the animal density is high and sensitive to heat.

It is advantageous to have natural ventilation in dairy cattle barns, as there is no need for energy consumption, no additional budget, noiseless operation, and resistance against low air temperatures. Adequate ventilation in the barn is essential in terms of maintaining a healthy production. Since dairy and beef cattle are not sensitive to ambient temperature, natural ventilation is generally preferred in these enterprises.

The environmental, economic, and health benefits of natural ventilation in buildings are better understood than barns with mechanical ventilation. While the thermal environment and gas emissions in dairy cattle barns directly affect product performance, they also affect the global ecological environment (Zou et al., 2020). It is at the end of the right design, the proper placement, and the suitable construction to make good natural ventilation in livestock farms.

4. Effective Factors for Good Natural Ventilation

For adequate natural ventilation in animal barns, it is necessary to remove the polluted air inside the barn, take the clean air into the building, and ensure a uniform distribution of the clean air in the building. Well-designed natural ventilation systems can be more beneficial than conventional designed mechanical ventilation in weather-favorable areas (Gürdil et al., 2005). With the help of special openings left inside the buildings where natural ventilation is made, the polluted air in the indoor environment is thrown to the outside, and the fresh air is taken into the indoor environment with the help of wind and indoor-outdoor temperature differences. The location of the building, the prevailing winds and direction of the region, the surrounding structure, hills, and trees, and the settlement direction of the building play the primary role in the natural ventilation system. The velocity of the ventilation flow is between 0.2-0.5 m/s, indicating that the ventilation success is high in the barn. It is recommended to build the structure on high ground as it will make the most of the effect of the wind and create an advantageous situation for drainage.

4.1. Ventilation with the effect of wind

It creates an airflow on the surface where the wind contacts the structure and towards the back of the structure. On the contact surface of the building, positive pressure (+) is formed on the windward side, and harmful (-) pressure zones are created on the leeward side of the building (Figure 1). While the part with positive pressure creates a high-pressure area, the leeward part and the roofs form a low-pressure region. The wind effect is more effective in the summer months.

By placing openings of different types and sizes in low and high-pressure areas, the air in the building can flow at the desired level and direction. The air outlet openings should be placed on the structure's negative pressure (pressing) surfaces and the air intake openings on the positive pressure (absorption) surfaces in natural ventilation. The air entering with high pressure from the inlet openings throws the polluted air out through the outlet openings.
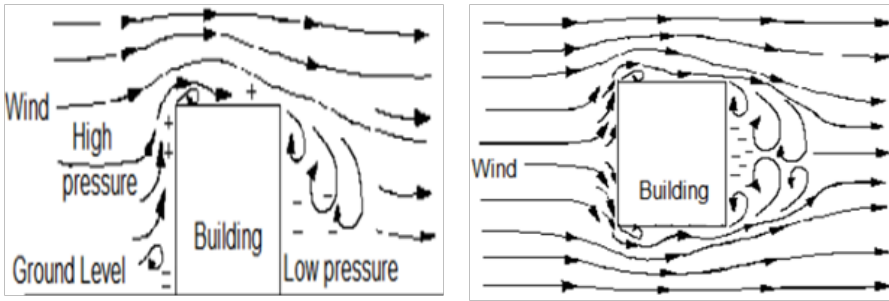
Figure 1: The effect of the wind on the structure (Anonymous, 2021a)

For the wind effect to be effective in natural ventilation, the settlement direction of the long axis of the building, the direction and speed of the prevailing wind, and the positioning of the air inlet and outlet openings must be planned and considered very well.

4.2. Ventilation with Temperature Difference (Chimney Effect)

The chimney effect is more effective in the winter months when the temperature difference between the indoor and outdoor temperatures created by the heat generated by the animals in the barns is higher. As the indoor and outdoor temperature differences increase, it will cause a pressure difference and cause changes in air density. When the indoor temperature of the shelter is higher than the outdoor temperature, the rising hot air will go out from the exit opening at the top of the building, and the fresh air will enter from the lower elevations of the building (Figure 2). If the indoor air temperature is lower than the outdoor air temperature, it will be reverse the airflow direction. Ventilation with this effect is adequate only if the animals produce enough heat in the barn.
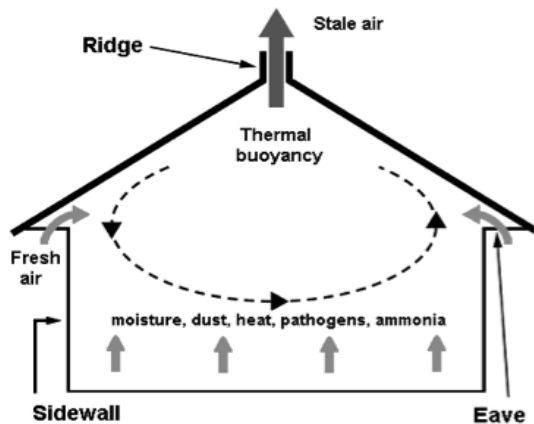

Figure 2: Natural ventilation with chimney effect (Anonymous, 2021b)

For the chimney effect to be more effective in natural ventilation, the indoor and outdoor temperature difference should be at least 5-7°C. It is recommended that the vertical distance between the air inlet opening and the outlet openings be at least 2 m, and the height of the air outlet opening from the ridge should be at least 0.50 m (Olgun, 2016).

4.3. *Air Inlet and Outlet Spaces*

In barns with natural ventilation, air inlet openings are placed on the discharge surfaces of the building, and air outlet spaces are placed on the suction surfaces. Natural ventilation is done with adjustable or continuous openings, especially in cold barns. Natural ventilation entrance openings in dairy cattle barns are usually provided by air intake spaces left under the eaves, windows, doors, and specially designed spaces that open in or out (Figure 3). The first factor to be considered in ventilation design is the prevailing wind direction. The inlet spaces should be in the prevailing wind direction and in another direction to provide proper ventilation. Especially in rectangular structures, when the long sides are against the wind, more surfaces are under maximum pressure, and the suction effect is more effective on the rear wall.
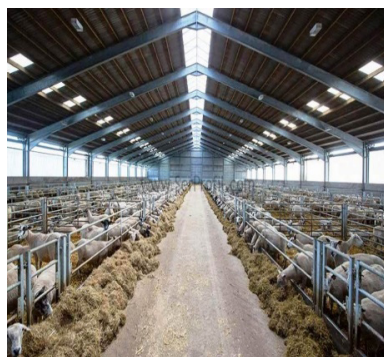
Figure 3: Ventilation openings in the dairy cattle barn

If the windows on the sidewalls of the building are also used for ventilation, it is recommended to use transom windows (Figure 4). With transom windows, fresh air is directed towards the roof, preventing direct airflow on the animals. Thus, the fresh air is heated in the barn, and heated air reaches to animals.
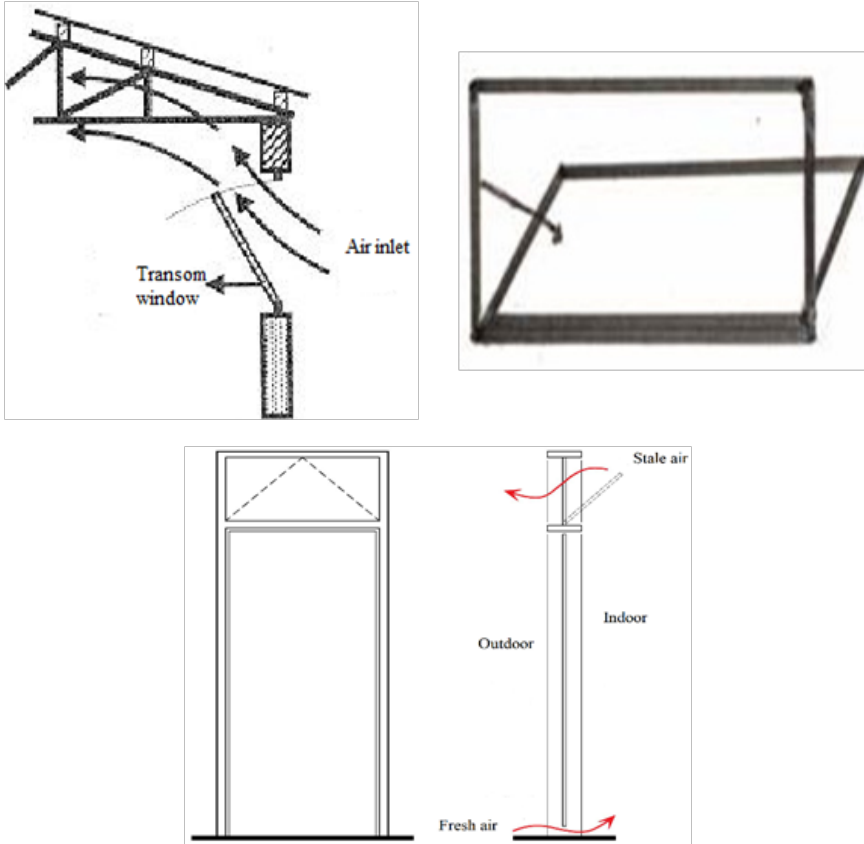

Figure 4: Natural ventilation with transom type windows (Anonymous, 2007; Darçın, 2008; Kendirli, 2016)

Air outlet in dairy cattle barns is provided by windows, chimneys, spaces in the roof, and openings along the ridge. Their arrangement affects indoor air circulation. The inlet opening where the clean air enters is smaller than the space where the polluted air exits, providing adequate ventilation (Darçın and Balanlı, 2012). The fact that ventilation spaces are more extensive in regions with tempered or hot climates increases the effect of wind on natural ventilation (Yüksel and Şişman, 2015). If the ventilation inlet openings are in the dominant wind direction, the outlet openings should be on the sidewall or the opposite wall, not facing each other. Figure 5a shows situations where air velocity is

high but air circulation is insufficient. The movement of the air throughout the barn by changing the direction of the air at the appropriate speed increases the efficiency of natural ventilation (Figure 5b, 5c). Airflow circulation in the barn differs according to the placement of the exit windows and their relative positions. The fact that the output windows are located on the sidewall enables the airflow to circulate in the indoor environment more effectively. When the entrance and exit windows are far from each other, fresh air can circulate more in the barn. More effective and efficient natural ventilation is provided in cases where the air can change its position in the building.
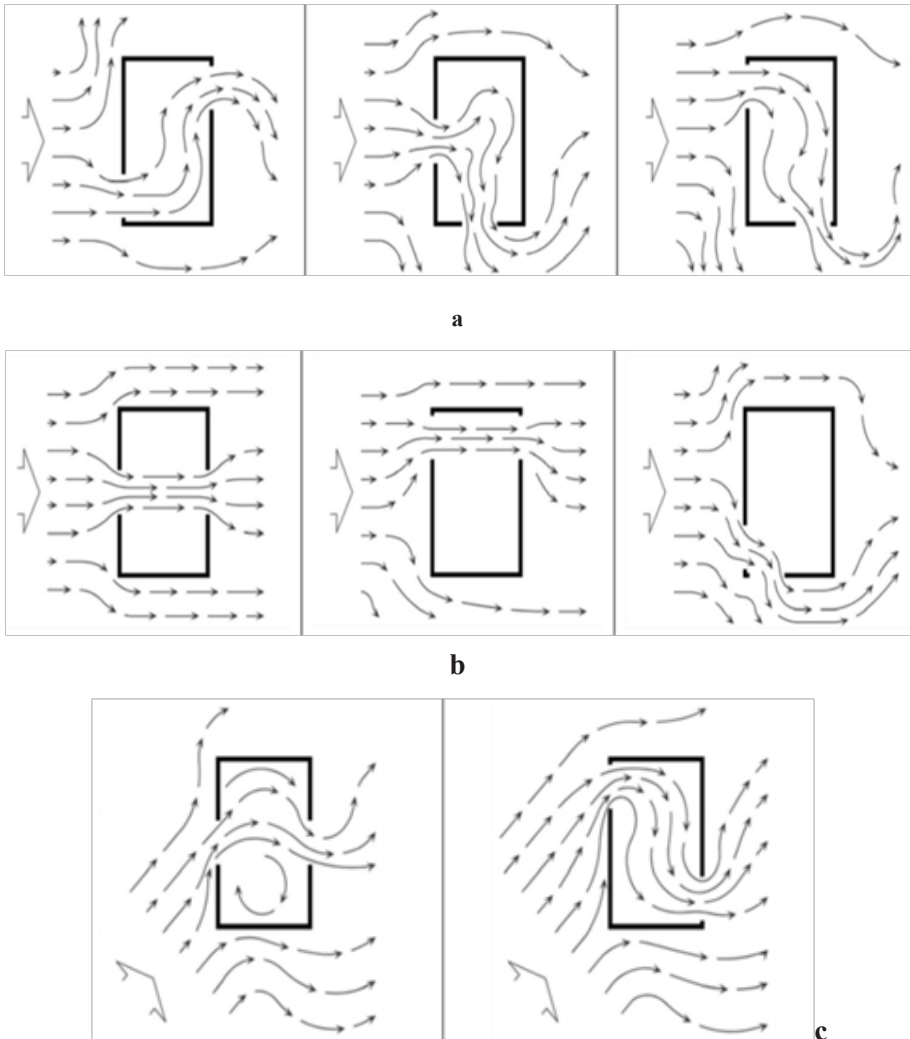

a

b

c

Figure 5: Directing the air currents in the structure (Darçın and Balabanlı, 2012)

Ventilation openings located along the roof ridge in shelters are mainly applied on the monitor roof and gable roofs (Yağanoğlu, 1990; Yüksel and Şişman, 2015). The openings left along the ridge can be designed in different ways (symmetrical or asymmetrical structures, rectangular section orifice, chimney shape, etc.) (Figure 6).
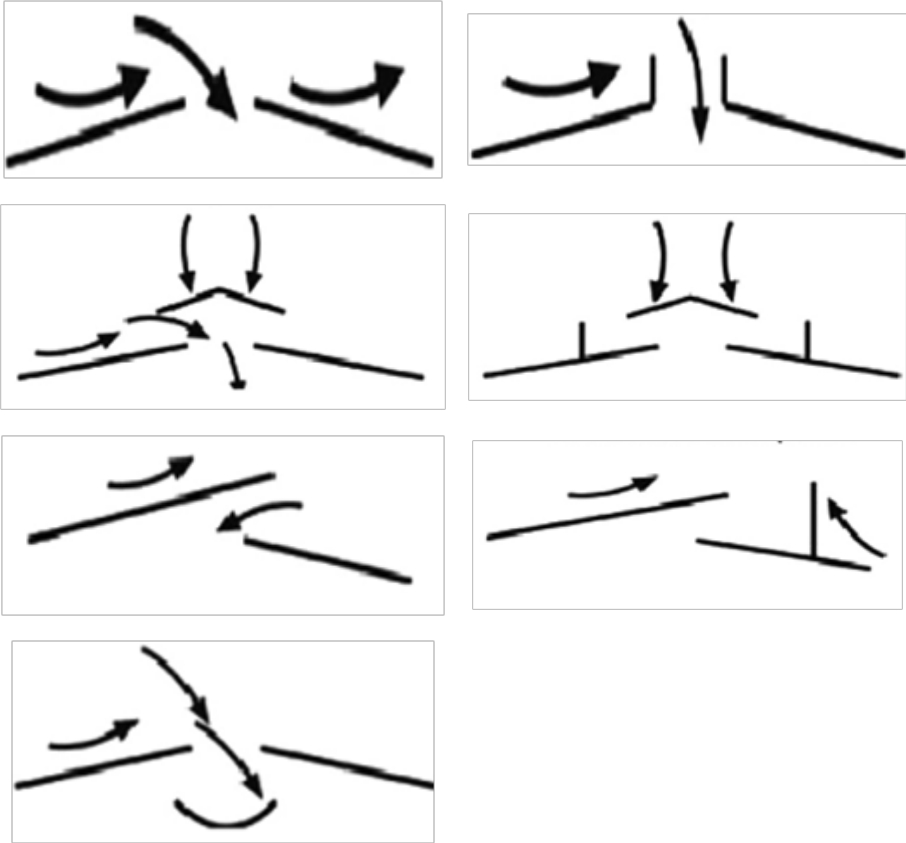

Figure 6: Ridge openings in roofs (Firfiris et al., 2019)

A chimney should be designed for every 100 m² of floor area in shelters. It should cover it with a chimney cap to prevent rain and snow waters from entering. The effective chimney height (air inlet opening and chimney top-level) must be at least 4 meters to ensure adequate ventilation. The height of the chimney from the ridge must be at least 50 cm. The chimney should be located at the top of the structure, and its dimensions should not be less than 25 x 25 cm (Figure 7) (Usta, 2011; Olgun, 2016). The cross-sections of the chimneys can be rectangular, circular, and square. However, since the losses due to friction in the airflow are less in circular chimneys, circular chimneys are preferred.

In summer, hot air comes out through openings along the ridge or through openings near the roof. With large openings or windows in the sidewalls of the building, fresh airflow is allowed, and cross-air flow is provided within the structure (Figure 8a).
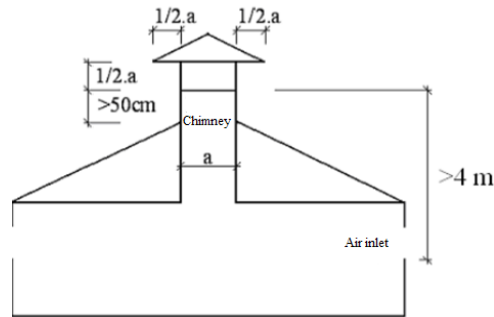

Figure 7: Chimney dimension in natural ventilation (Göncü and Gökçe, 2018)

Warm and fresh air enters the building through the openings along the eaves in windy weather during the winter months. The polluted air is expelled from the ridge opening, and a gentle airflow is created inside the shelter (Figure 8b). In warmer winter days, when the wind speed in the outdoor environment falls below the average seasonal value, the hot and polluted air inside the building receives water vapor and rises, heading towards the air outlet openings and expelled by the chimney effect (Figure 8c).
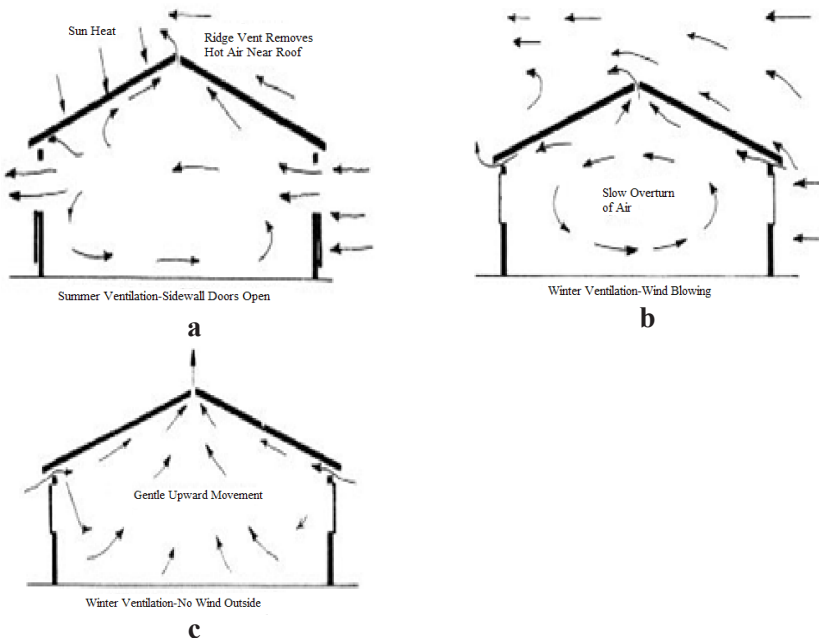

Figure 8: Natural ventilation with wind and indoor-outdoor temperature difference (Jones et al., 2015)

5. Conclusion

The discharge of polluted air to the outside in animal barns and the supply of fresh air without air current have multifaceted importance in animal health, employee health, structure life, and economic profitability. Since dairy cattle are resistant to outdoor conditions, the natural ventilation system is very effective when correctly planned. Natural ventilation is provided by taking in a sufficient amount of fresh air into the building, circulating it effectively, and removing the polluted warm air.

References

Alkoyak, K., & Çetin, O. (2016). Heat stress and prevention ways in dairy cattle. Journal of Bahri Dagdas Animal Research, 5(1), 40-55.

Anonymous, (2007). Sığır Barınakları-2. Retrieved from http://www.tarimkutuphanesi.com/sigir_barinaklari_-_2_00135.html

Anonymous, (2021a). HVAC – Natural Ventilation Principles and Practices. Retrieved from https://www.cedengineering.com/userfiles/HVAC%20-%20Natural%20 Ventilation%20Principles%20R1.pdf

Anonymous, (2021b). Retrieved from https://nurturewithprovimi.com/phases/pre-weaning/

Darçın, P. (2008). Natural ventilation guidelines for removing indoor air pollution. (Master Science thesis).

Darçın, P., & Balanlı, A. (2012). Yapılarda doğal havalandırmanın sağlanmasına yönelik ilkeler. Tesisat Mühendisliği Dergisi, 128, 33-42. Retrieved from https://www.mmo.org.tr/sites/default/files/aec6225f614230a_ek.pdf.

Dinçel, D., & Dikmen, S. (2013). Assessment of heat stress, effects on production traits and protection methods in dairy cows. Uludag University Journal of the Faculty of Veterinary Medicine, 32(1), 19-30.

FAO, (2021). Food and Agriculture Organization of the United Nations, Overview of global dairy market developments in 2020. Retrieved from https://www.fao.org/3/cb4230en/cb4230en.pdf.

Firfiris, V. K ., M artzopoulou, A . G ., & K otsopoulos, T. A . (2019). Passive cooling systems in livestock buildings towards energy saving: A critical review. Energy and Buildings, 202, 109368.

Göncü, S., & Gökçe, G. (2018). Kış Koşullarında Sığır Barınak Özelliklerinde Öncelikli Konular. Retrieved from https://www.ruminantbesleme.com/wp-content/uploads/2018/08/K%C4%B1s%CC%A7-kos%CC%A7ullar%C4%B1nda-s%C4%B1g%CC%86%C4%B1r-bar%C4%B1nak-o%CC%88zellikleri.pdf

Göncü, S., Önder, D., Koluman, N., & Mevliyaoğulları, E. (2015). Sıcak ve nemli koşullara uygun hayvan barınak özellikleri. Tüsedad, 5(30), 42-47. Retrieved from https://www.ruminantbesleme.com/wp-content/uploads/2020/03/S%C4%B1cak-Ko%C5%9Fullarda   Bar%C4%B1nak-Ozellikleri.pdf.

Gürdil, G., Selvi, K. Ç., Fuat, L., & Yeşiloğlu, E. (2005). Developing a software   for determination of natural ventilation rate in animal house. Anadolu Journal of Agricultural Sciences. 20(1), 30-36.

Jones, D. D., Friday, W. H., & DeForest, S. S. (2015). Natural ventilation for livestock housing. Retrieved from https://docs.lib.purdue.edu/cgi/viewcontent.cgi?article=2043&context=agext.

Kendirli, B. (2016). Tarımsal Yapılar ve Sulama Dersi Notu, Tarımsal yapılarda çevre koşullarının denetimi.

Mundan, D., Atalar, B., Meral, B. A., & Yakışan, M. M. (2018). A research on the determination of the structural and technical characteristics of modern dairy cattle enterprises. *Atatürk University Journal of Veterinary Sciences*, 13(2), 201-210.

Olgun, M. (2016). Tarımsal Yapılar. Ankara Üniversitesi Yayınları, Üçüncü Basım.

Thatcher, W. W., Flamenbaum, I., Block, J., Bilby, T. R., (2010). Interrelationships of Heat Stress and Reproduction in Lactating Dairy Cows. High Plains Dairy Conference Amarillo, Texas.

TUIK, (2020). Turkish Statistical Institute, Livestock Statistics. Retrieved from https://www.tuik.gov.tr/

TUIK, (2021). Turkish Statistical Institute, Milk and Milk Products. Retrieved from https://www.tuik.gov.tr/

Uğurlu, N., & Şahin, S. (2010). The structural properties of dairy cattle barns in Kayseri. Selçuk Tarım ve Gıda Bilimleri Dergisi, 24(2), 23-26.

Usta, S. (2011). Free stall dairy cattle farms architectural layout plan principles and suggestions for the nature of manufacturer type residential development plans. *Suleyman Demirel University Journal of Tecnical Sciences*, 1(2), 29-42.

Yağanoğlu, A.V. (1990). Ridge vent, wind direktion and wind velocity *effects on closed, naturally ventilated, cattle building ventilation. Atatürk University Journal of Agricultural Faculty, 21(1). Retrieved from https://dergipark. org.tr/tr/pub/ataunizfd/issue/3002/41652.*

Yüksel, A.N., & Şişman, C.B. (2015). Hayvan Barınaklarının Planlanması. Hasad Yayıncılık Ltd. Şti.

Zou, B., Shi, Z., & Du, S. (2020). Gases emissions estimation and analysis by using carbon dioxide balance method in natural-ventilated dairy cow barns. *International Journal of Agricultural and Biological Engineering,* 13(2), 41-47.

STRESS MEASUREMENT ON TRAIN WHEELS

Emre *GÖRGÜN*[1] & Mehmet Baki KARAMIS[2]

[1]*(Asst.Prof.Dr.), Sivas Cumhuriyet University,*
emregorgun@cumhuriyet.edu.com.tr
Orcid: 0000-0002-1971-456X

[2]*(Prof. Dr.), Erciyes University*
Orcid: 0000-0002-2156-2016

1.   Introduction

Ultrasonic velocity is a type of mechanical pulse or longitudinal waves which bring about a state of alternative transmit and receive of the textures in the material. The velocity of sound is constant for any given medium although it changes from medium to medium. The pulses of sound can be described as seperatilly events within the material following a waveform. Bigger the density, the interior the velocity. The higher the elasticity, the higher the velocity.

1.1. Longitudinal or Compression Waves

Residual stresses from manufacturing affect the material more than thermal productions.(Fajoui vd., 2018) Longitudinal ultrasonic waves like sound consist of alternate compression of pressure waves and these pulses go on the same direction as the energy of spread. Specially mechanism related on the elastic interactions, so as each particule moves from equilibrium, it transmits at the velocity of ultrasound.

1.2. Compression Wave Probes

The base of longitudinal wave probe is the mono crystal probe that can do as the transmitter of ultrasonic sound as waves in addition to the receiver, When using a single crystal probe do as both the transmitter and receiver.The waves during the unpropagate delay between spread each pulse. TR probes (Transmit-Recieve) crystal probe is especially the same as the single crystal

probe.Useing one probe for continuously transmitting pulses and other for receiving, To interrupt 'cross-talk' between the two piezo-element a cork isolator is used to propagate the probe into two, and the thickness of the plexiglass wedge is enhanced. Ultrasound echos into the sample at proper angles to the surface of the sample. No refraction happen at the first surface and just longitudinal sounds go into the material. So longitudinal probes are used when normal compression probes are used for convational ultrasonic thickness measurement. Each crystals in transmitter propagate compression waves. But, a transmitter can be designed to perform in the shear wave propagating by having a wedged shaped frontal member so that the probe directs longitudinal waves at an angle to the surface of the sample. The angle of portion is such that only shear waves go into the sample. Briefly, the angle propagated on the probe refers to the angle from the vertical in material.

1.3. Stress measurement techniques

It is now possible to measure residual stress with destructive testing or non-destructive testing methods. The temperature fields and the cutting-induced and welding-induced residual stresses are numerically investigated.(Zhou, Li, He, He, & Li, 2018) The following methods can be said as destructive and destructive stress measurement techniques.

- Sectioning
- Hole Drilling
- X-Ray Diffraction
- Magnetic elastic and neutron Diffraction.(Tebedge, Alpsten, & Tall, 1973)

Stress measurement methods are generally used to measure stresses on the surface of the material.(Watanabe, Oguro, Minegishi, Awaji, & Nishijima, 2010) X-ray diffraction method can define the surface stress by measuring the crystal distance according to the Bragg law of a crystal structure.(Ruibin, Wenjiao, Fei, Min, & Weigang, 2015) It is a non-destructive method, but allows stretching to a depth of only 10 μm. The one of the stress measurement tecniques neutron diffraction method is so similar to the X-ray measurement as it is based on elastic deformations in a multi-crystal material.(Palkowski, Brück, Pirling, & Carradò, 2013) The magnetic elastic method is based on the Barkhausen effect however, magnetizing conditions are necessary in addition to necessary complex equipment.(Mierczak, Jiles, & Fantoni, 2010)

1.4. Stress measurement technique of medium carbon steels

The one of the wheel material is described in EN 13262 standart that ER7 type steel was selected as solid wheel material. Ultrasonic probes that generate longitudinal waves measured sound speeds for ER7 type steel. In this study it was used 1MHz, 2MHz and 4 MHz longitudinal probes were used. One of probes was fixed to specimen during perform tensile test. 4 specimens were prepared for 3 probes as reference.

2. Theory

2.1. Theory of Pulse- Echo

The mostly used as a system in ultrasonic thickness measurement and ultrasonic defect detection is the pulse-echo. In the PET method, ultrasonic sound waves are repeated in short periods.. There is a delay of too little time between each transmit, The ultrasonic wave pulses propagate through the material during test until they encounter an interface, where pulses are reflected back. So waves meets the interface at proper angles. Waves turning back to the probe are converted into electrical inputs and the time between transmitting the pulse and receiving the echo is electronically measured. The convantional ultrasonic equipment for the spread speed in the material the equipment can display A certain amount of time is needed for the sound wave to propagate through the material.

2.2. Theory of simple linear regression

Linear Regression is one of the simplest supervised learning algorithms assumes that there is a linear relationship between the Y variable being tried to predict and the other variables X1, X2, ..., Xn. Although this method seems simple, it is extremely useful both conceptually and practically.

$$Y=\beta_0+\beta_1X+\varepsilon \tag{1}$$

As we do here, the models we try to calculate a response variable (Y) with a single predictor variable (X) are called simple linear regressions. In this form, β_0 and β_1 are unknown constants and represent intercept and slope respectively. They are also called regression coefficients / parameters. ε represents the error term. Normally we do not know β_0 and β_1. We try to estimate them using the inear regression method. We have applied this method as an example and calculated β_0 and β_1 which are our predictions for real coefficients. We can estimate the result as follows.

$$y"=\beta_0"+\beta_1"x \tag{2}$$

Here we show our prediction for the real Y value when X = x.(Lonsdale, Demilly, & Fabbro, 2000) Calculation of intermediate values were used linear regression method

2.3. Past Research Efforts

When we look at the literature, it is seen that many studies have been done on residual stress measurement techniques. Cameron Lonsdale and friends presented the paper were shown residual stress state using the portable PET and EMAT systems according to wheel type. (Table 1.)

Table 1. Residual stress measurement results
in PET and EMAT systems.*(Lonsdale vd., 2000)*

Wheel Type	Depth below tread (mm)	PET stress (MPa)	EMAT stress (MPa)
D42	10	-155	-140
	20	-112	-115
	25	-65	---
	35	0	-40
	45	---	16
E40	10	-185	-170
	15	-112	-120
	20	-69	-83
	25	-64.5	-60
H36	15	-164	-140
	25	-108	---
	Near ID	---	-35
32RD	15	-190	-143
	25	-151	-95
	35	-56	-45
	40	-39	-12

In same study Table 2 shows the data for train wheels of CEVHER and VMS wagons after 150,000 km of operation. It has been calculated by considering the given deviation amounts shown in the table. The outward bending of the wheel plate, which occurred in the axial direction, was caused by heating during braking.

Table 2. Residual stress measurement results at the wheel.(Lonsdale vd., 2000)

Values after 150,000 km	ORE Wheels, %	VMS Wheels, %
Residual Stress		
0 to 100 MPa	11	54
100 to 200 MPa	32	38
200 to 300 MPa	43	8
300 to 400 MPa	14	0
Deflection		
Over + 1.5 mm	87	0
Over + 2.0 mm	11	0

3.   Material and Method

3.1. Material

3.1.1.   Wheel Sample Material

Wheel materials employed for solid wheels in Europe are commonly restricted to unalloyed steels with a maximum cabon content of 0,56% - after appropriate heat treatment of the tread – tensile strengths of at least 820 to 980MPa in maximum.(Neslušan, Minárik, Grenčík, Trojan, & Zgútová, 2019) The surface quality of the wheels that remain in operation for a long time changes. We obtained sample from used wheelset are shown Fig 1.

3.1.2. UT Inspection Device and Probes

A portable conventional flaw detector was used in this study. and also as 1MHz. ,2MHz. and 4MHz. probes were used. For each probe have different frequence values are shown below Table 5.

Table3.Probe Values

	1MHz	**2MHz**	**4MHz**
Prob Type	P1-10L	P2-6L	P2-6L
Prob Dia.(mm)	10,00	6,00	6,00
GAWidth(%)	30,00	30,00	30,00
Gain(dB)	60,00	48,50	60,00
Zero(μsn)	19,61	19,64	19,64
GATresh(%)	50,00	50,00	50,00
Range(mm)	31,00	31,00	31,00
Sample Thikness	14,10	14,10	14,10
Probe Delay	0,00	0,00	0,00

3.2. Method

For measuring the strain of steel type ER7 by ultrasonic compression wave we performed following process. Sample obtain from used railway wheels. Heat treatment carried out of railway wheel. Test specimen placed to tensile machine. During the tensile machine start ultrasonic velocity measured for each probes. (1MHz, 2MHz and 4MHz). Strain and longitudinal wave speed derived from test for each frequencies. Velocity results by using only longitudinal wave adopted Table 1 and Table 2.

4. Results and Discussions

4.1. Relationship Between Strain and Ultrasonic Compression Wave Velocity

This paper present how compress wave apply to residual stress measurement on wheel. Probes of different frequencies were used. Stress values vary according to depth from tread surface. In this study indicate how can stress measurement prices decrease. Compression wave probes are used commonly and prices lower from EMAT probes. We used probe which propagates only longitudinally wave probes. We have achieved significant results in some wheel sets. This stress values in Table 6. derived from tensile test resuls. Calculation of intermediate values were used linear regression method.

Table 4. Relationship of Stress-Probe Velocity

Wheel Type	Depth Below Tread (mm)	PET Stress (Mpa)	Velocity-1MHz(mm/s)	Velocity-2MHz(mm/s)	Velocity-4MHz (mm/s)
D42	10	-155	5367,75	5866,05	6060,45
	20	-112	5938,00	6009,66	6061,61
	25	-65	5940,27	6018,35	6074,81
	35	0	5938,00	6065,00	5940,00
	45	X	X	X	X
E40	10	-185	5370,40	6010,76	6060,53
	15	-112	5938,00	6009,66	6061,61
	20	-69	5938,59	6011,51	6074,81
	25	-64,5	5940,48	6019,20	6074,81
H36	15	-164	5367,80	5650,76	6059,23
	25	-108	5938,00	6009,08	6062,17
	NearID	X	X	X	X
32RD	15	-190	5366,21	6012,90	6058,43
	25	-151	5369,43	6009,71	6062,13
	35	-56	5947,69	6026,29	6074,81
	40	-39	5941,30	6038,20	6045,20

Table 5. The tensile stress values according to the probe frequency

Probe Frequency	Tensile stress measurement results
1MHz	140,84MPa
2 MHz	160,92MPa
4MHz	80,48MPa

probe. Specially 1MHz probes were particularly flourished in residual stress measurements. The lower the frequency values, the higher the response to stress. It was thought that these probes might be sufficient for residual stress measurements. Particularly in the H36 type, a linear curve on the wheels can be encourage the studies.Fig2., Fig3., Fig 4. And Fig 5.
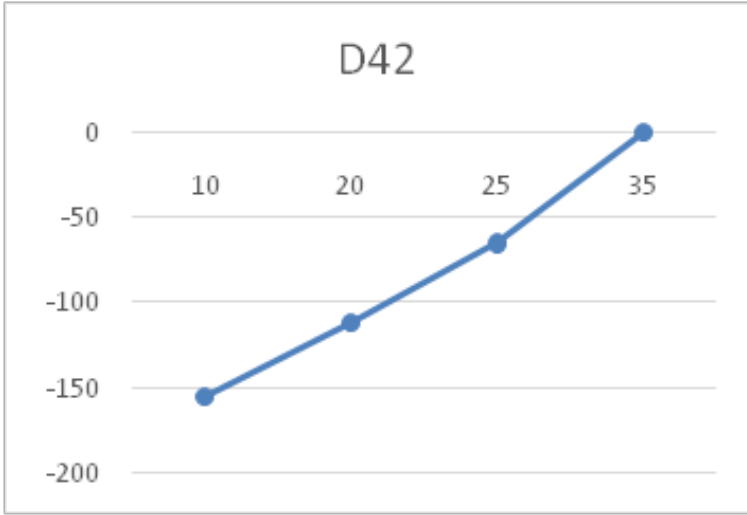
4.2. Discussions

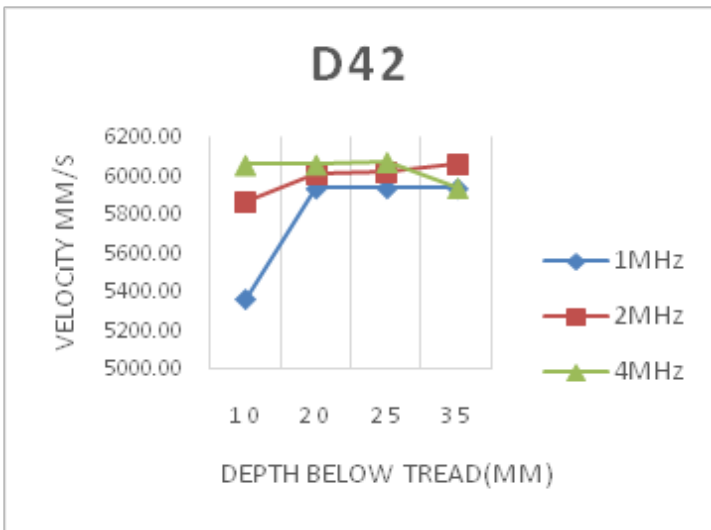Figure 1.D42 PET Stress of depth below tread. (Lonsdale vd., 2000)

Figure 3.D42 velocity of depth below tread
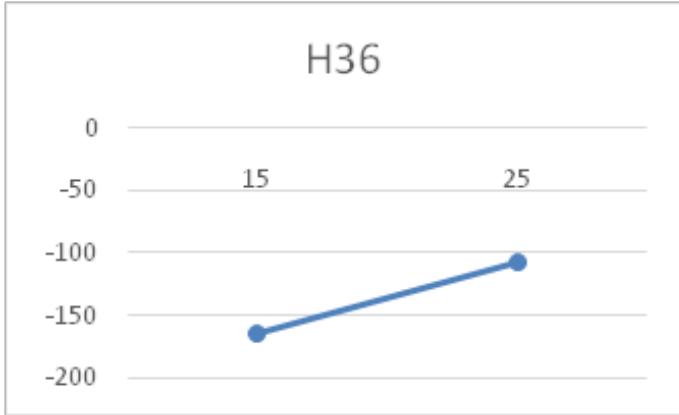
Figure 4 H36 PET Stress of depth below tread.(Lonsdale vd., 2000)
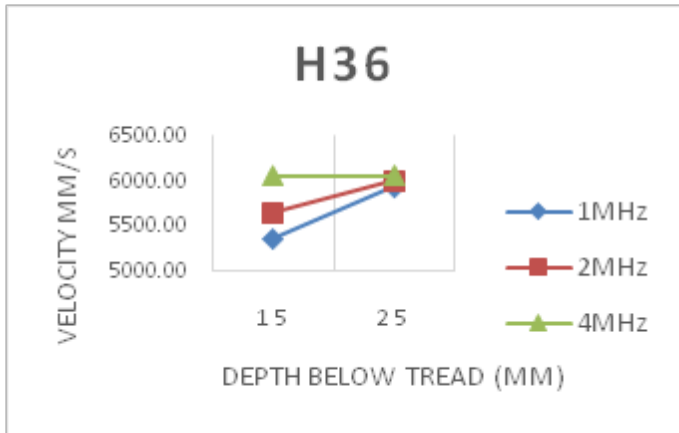
Figure 5 H36 velocity of depth below tread
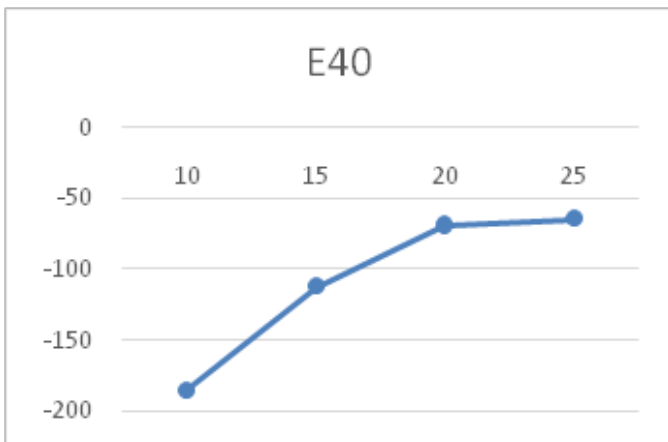
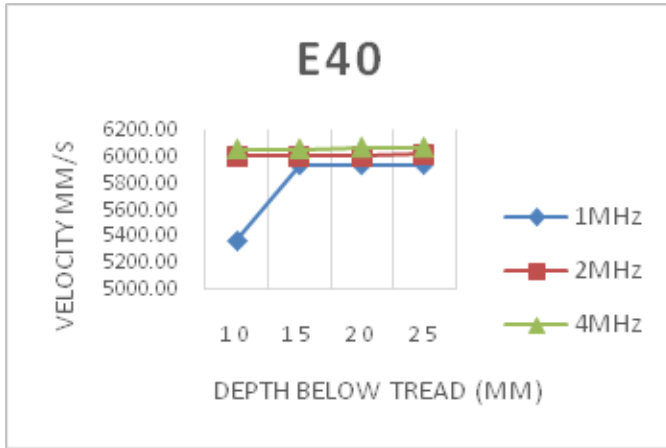**Figure 6.** E40 PET Stress of depth below tread.(Lonsdale vd., 2000)

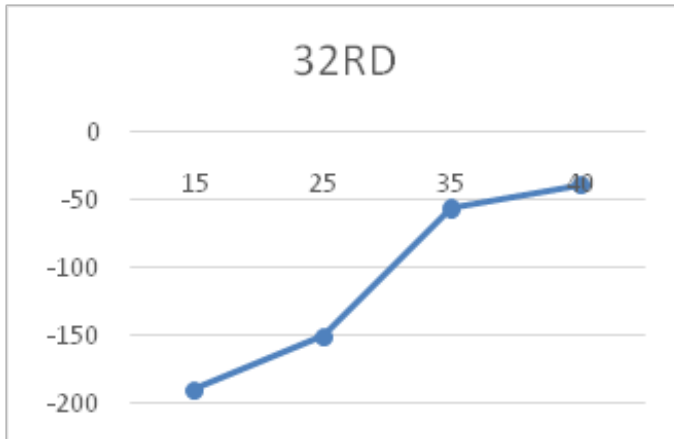**Figure 7.** E40 velocity of depth below tread

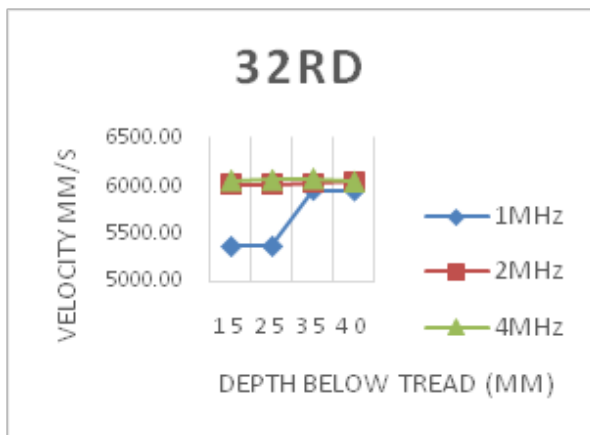**Figure 8.** 32RD PET Stress of depth below tread.(Lonsdale vd., 2000)

Figure 9. 32RD velocity of depth below tread

Lonsdale, C and friends find relations of PET and Residual Stress in previous study.(Fig.2,Fig.4,Fig.6 and Fig.8). In this study possible to find residual values using just compress probes. It could be understood ;

- In this figüre we can use 1MHz. probes to measure resudual stress
- It can be understood as the wave frequency decreases, the results are improving.
- 1MHz probe give well results specially 15-25mm depth below tread
- We can use 1MHz. and 2MHz. probes in their best results depth.
- This method can use in plant which have no EMAT

5. Conclusion

The conclusions derived from this study can be follow as

1) It was seen that there were how compress wave apply to residual stress measurement on wheel tread surface.
2) Linear curve on the wheels can be encourage the studies like H36 types. Specially some of wheel types show sudden drop in stress value state according to depth of tread surface.
3) The lower the frequency values gave response to stress accurately.
4) This probes cab use measurement of residual stress instead of EMAT probes or Bırefrıngence Theory.
5) Residual stress measurement can be applied by conventional ultrasonic detector.As Compression wave probes are used commonly and prices lower from EMAT probes,
6) The velocity of the sound is increased so the depth from the tread surface is getting increase of the wheel surface.

It can be understood from this paper ; if this study improve the longitudinal wave can be used to measurement of the residual stress. There can not be used ultrasonic detector other than conventional detector. The staff work any railway plant can use the detector all related inspection. The conventional detector can be used to measure of residual stress thus measurement prices could be decreased.

6. References

Fajoui, J., Kchaou, M., Sellami, A., Branchu, S., Elleuch, R., & Jacquemin, F. (2018). Impact of residual stresses on mechanical behaviour of hot work steels. *Engineering Failure Analysis*, *94*, 33-40.

Lonsdale, C., Demilly, F., & Fabbro, V. D. (2000). Wheel rim residual stress measurements. *Proceedings of the Railway Wheel Manufacturer's Engineering Committee Technical Conference, CP Lonsdale., eds., Chicago, Illinois*. Citeseer.

Mierczak, L., Jiles, D. C., & Fantoni, G. (2010). A new method for evaluation of mechanical stress using the reciprocal amplitude of magnetic Barkhausen noise. *IEEE Transactions on Magnetics*, *47*(2), 459-465.

Neslušan, M., Minárik, P., Grenčík, J., Trojan, K., & Zgútová, K. (2019). Non-destructive evaluation of the railway wheel surface damage after long-term operation via Barkhausen noise technique. *Wear*, *420*, 195-206.

Palkowski, H., Brück, S., Pirling, T., & Carradò, A. (2013). Investigation on the residual stress state of drawn tubes by numerical simulation and neutron diffraction analysis. *Materials*, *6*(11), 5118-5130.

Ruibin, G., Wenjiao, D., Fei, Q., Min, Y., & Weigang, Z. (2015). Welding residual stress measurement of an urban buried gas pipeline by X-ray diffraction method. *Insight-Non-Destructive Testing and Condition Monitoring*, *57*(10), 556-561.

Tebedge, N., Alpsten, G., & Tall, L. (1973). Residual-stress measurement by the sectioning method. *Experimental mechanics*, *13*(2), 88-96.

Watanabe, K., Oguro, H., Minegishi, K., Awaji, S., & Nishijima, G. (2010). Strain Gauge Method for Evaluating a Three-Dimensional Residual Strain State in $${$$\backslash$\rm Nb$}$ $ _ ${$3$}$$${$$\backslash$\rm Sn$}$ $ $ Wires. *IEEE Transactions on Applied Superconductivity*, *20*(3), 1420-1423.

Zhou, X., Li, J., He, Y., He, Z., & Li, Z. (2018). Finite element analysis of thermal residual stresses in castellated beams. *Journal of Constructional Steel Research*, *148*, 741-755.

ENHANCEMENT OF PHOTOCATALYTIC ACTIVITY OF WO$_3$ BY COUPLING TIO$_2$

Hafize Nagehan KÖYSÜREN[1] & Özcan KÖYSÜREN[2]

[1](Asst. Prof. Dr.), Environmental Engineering,
Engineering and Architecture Faculty, Kırşehir Ahi Evran University,
e-mail: nagehan.koysuren@ahievran.edu.tr,
Orcid: 0000-0002-7115-2250

[2](Assoc. Prof. Dr.), Energy Engineering, Engineering Faculty, Ankara
University, e-mail: koysuren@ankara.edu.tr,
Orcid: 0000-0001-7100-0399

1.   Introduction

Organic dye contamination in water and wastewater is harmful to aquatic life and indirectly to human health. Photocatalytic degradation of the organic pollutants in wastewater by semiconductor photocatalysts has attracted remarkable interest owing to the benefits of low cost, high photosensitivity, and strong oxidizing activity (Mohammadi et al., 2016). The main goal of a photocatalyst is to generate highly reactive hydroxyl radicals, superoxide and hydroxyl radicals. These radicals can react with liquid-dissolved organic pollutants and convert them to harmless small molecules like H_2O and CO_2 (Zerjav et al., 2017). Tungsten oxide (WO$_3$), which has a narrower optical band gap (2.4-2.8 eV) than the commonly used photocatalysts, is a highly ranking semiconductor with many advantages such as sensitivity to visible light, nontoxicity and chemically stability. WO$_3$ can absorb a significant part of the solar spectrum (Nagarjuna et al., 2017; Thwala and Dlamini, 2020). In addition, WO$_3$ is highly resistant to acid environment and can show moderate resistance to photocorrosion (Thwala and Dlamini, 2020). Owing to the specified features, WO$_3$ has been extensively applied to gas sensors, photochromic and electrochromic devices. It is also considered as a suitable anode material for oxygen generation reaction in photoelectrochemical water splitting process (Nagarjuna et al., 2017).

The researchers have studied on varying strategies for the synthesis of WO$_3$ nanoparticles such as sol-gel method (Nagarjuna et al., 2017), template

method (Gibot et al., 2011), hydrothermal method (Puga et a., 2021; Govindaraj et al., 2021) and co-precipitation method (Thilagavathi et al., 2021). Among the specified methods, the co-precipitation method is a simple and low-cost method. Depending on the heat treatment temperature applied in the hydrothermal synthesis method, WO_3 can be synthesized in various crystal structures such as triclinic, monoclinic, orthorhombic and tetragonal (Thilagavathi et al., 2021) and in different morphological shapes such as spherical (Puga et al., 2021), nanorod (Govindaraj et al., 2021) and nanoplate (Thilagavathi et al., 2021).

Although WO_3 can absorb the significant portion of the visible light and the sunlight, the photocatalytic efficiency of the semiconducting material is low due to the position of the valence and conduction bands (Thwala and Dlamini, 2020). In addition, the use of pure WO_3 in photocatalytic energy conversion and wastewater treatment applications is limited due to the high recombination rates of the photoinduced charge carriers on WO_3 (Ai et al., 2020). Various efforts have been performed to improve the photocatalytic activity of WO_3, and forming a semiconductor p-n heterojunction is one of the most effective ways. Such a structure allows the photogenerated electron-hole pairs to be separated by the electric field formed between the n-type and p-type semiconductors and reduces the recombination rate of the photogenerated charge carriers (Zhou et al., 2020). Many attempts have been performed to promote the separation of the photoexcited carge carriers on WO_3 and enhance the photocatalytic performance. Accordingly, one common approach is to form a heterojunction by coupling WO_3 with TiO_2 (Carvalho et al., 2021), SiO_2 (Soares et al., 2018), SnS_2 (Li et al., 2014), CdS (Zhang et al., 2017), $CuFe_2O_4$ (Sayadi et al., 2021) and Ag_2MoO_4 (Wang et al., 2019). The idea of combining WO_3 with another metal oxide with suitable edge positions of the valence band and the conduction band can be followed as a possible way to improve the photogenerated charge separation. In fact, by coupling WO_3 with a metal oxide possessing the valence band edge more negative in level than the valence band edge of WO_3, the photoinduced holes can move from the valence band of WO_3 to that of the other metal oxide, while the photogenerated electrons remain trapped within the WO_3 phase of the heterostructure, resulting an enhancement in the photogenerated charge separation on the WO_3 phase. Also, if the conduction band edge of the metal oxide is more negative in level than the conduction band edge of WO_3, the photoinduced electrons of the metal oxide can move to the conduction band of WO_3 to contribute to the photocatalytic activity (Dozzi et al., 2016). Among the specified semiconductor photocatalysts, titanium dioxide (TiO_2) has a suitable conduction band and valence band edges promoting the transfer of the photoinduced holes from the valence band of WO_3 into the

valence band of TiO_2 and the transfer of the photoinduced electrons from the conduction band of TiO_2 into the conduction band of WO_3 (Dozzi et al., 2016).

TiO_2 has been widely used as a photocatalyst for the degradation of organic pollutants within the aqueous medium owing to its high photocatalytic performance, nontoxicity, stability and low cost. The major drawback of this photocatalyst is its wide optical band gap, which is between 3.2-3.4 eV. Due to its wide optical band gap, TiO_2 can absorb only UV light with a wavelength less than 387 nm. Another drawback of TiO_2 is the fast recombination of the photoexcited charge carriers. Combining TiO_2 with WO_3 can solve the stated drawbacks of both TiO_2 and WO_3. Coupling of TiO_2 with WO_3 can provide to form a heterojunction between the photocatalysts, enhancing the charge separation. In addition, the energy range of photoexcitation can be expanded from UV to the visible range (Zerjav et al., 2017).

Within the scope of this study, WO_3 was combined with TiO_2 within the composite structure. The photocatalytic activity of the composites were analyzed and compared with pure WO_3 and pure TiO_2 by monitoring the degradation of the model organic dye in aqueous solution, which was exposed to UV light irradiation. Coupling WO_3 with TiO_2 seemed to be an efficient way to improve the photocatalytic performance of WO_3.

2.   Experimental

2.1. Preparation of TiO2/WO3 Composites

WO_3 nanoparticles and TiO_2/WO_3 composites were used as photocatalyst for the photocatalytic decompostion of the model dye, methylene blue. Co-precipitation technique was followed to synthesize WO_3 nanoparticels and TiO_2/WO_3 composites. For this purpose, sodium tungstate dihydrate ($Na_2WO_4 \cdot 2H_2O$) (3 g) was dissolved in 20 ml of distilled water and then the solution was kept under stirring at room temperature. 20 ml of HCl solution was prepared and added into the as-prepared solution. Afterwards, the solution was stirred for 2 h at 80 °C. After cooling to room temperature, the as-prepared slurry was separated from the acid solution and washed several times with distilled water. Then the cleaned slurry was dried at 80°C for 12 hours. After drying, the obtained product was calcined at 600°C for 1 hour. Following grounding, WO_3 nanoparticles were obtained (Thilagavathi et al., 2021). TiO_2/WO_3 composites in different compositions (25/75, 50/50 and 75/25 wt./wt.) were synthesized following the same procedure. Only difference was that certain amount of TiO_2 nanoparticles, depending on the composition of TiO_2/WO_3, was dispersed in sodium tungstate dehydrate solution for half an hour and then HCl solution was added into the solution, containing TiO_2 nanoparticles.

2.2. *Characterization of TiO$_2$/WO$_3$ Composites*

The optical properties were investigated using UV-Vis absorption spectroscopy (Genesys 10S, Thermo Scientific). The photocatalytic activity was characterized on the basis of the degradation of the model dye, methylene blue, under UV light irradiation (12 W UVA). The degradation of the model dye was evaluated by monitoring the decrease of its concentrations, which was measured by using a Genesys 10S UV-Vis spectrophotometer (Thermo Scientific) before and after UV light irradiation. In order to evaluate the photocatalytic activity, 50 mg of a photocatalyst sample was added into 100 ml of methylene blue solution (10 mg/l). Before UV light irradiation, methylene blue solution, containing the photocatalyst sample, was stirred using a magnetic stirrer in the dark for 30 min. to attain adsorption/desorption equilibrium between the photocatalyst and the organic dye molecules. The methylene blue solution was also stirred during the UV light irradiation. The dye solution was irradiated with a UV lamp (UVA lamp, 12 W) for 80 minutes. Aliquots (3 ml) of the dye solution were collected at regular time intervals (20 min) during irradiation and then separated from the photocatalyst nanoparticles using a centrifuge at 4000 rpm. Methylene blue concentration in the aliquots was determined by colorimetric method using the UV–Vis spectrophotometer. In addition, ammonium oxalate (1 mM), potassium persulfate (1 mM), tert-butanol (1 mM) and ascorbic acid (1 mM) were studied as scavengers for hole (h^+), electron (e^-), •OH and •O_2^-, respectively and added into the dye solution with the TiO$_2$/WO$_3$ (50/50 wt./wt.) composite.

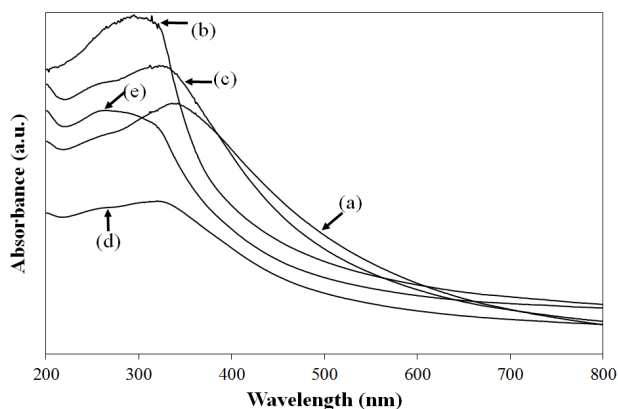## 3. Results and Dicussion

3.1. *UV-Vis absorption spectroscopy*

Figure 1: UV-Vis absorbance spectra of (a) WO$_3$, (b) TiO$_2$, (c) TiO$_2$/WO$_3$ (25/75 wt./wt.) (d) TiO$_2$/WO$_3$ (50/50 wt./wt.) and (e) TiO$_2$/WO$_3$ (75/25 wt./wt.)

Figure 1 illustrates the absorption spectra of the photocatalysts. All samples exhibited wide absorption starting from UV light (~200 nm) to visible light up to 700 nm. The absorption band of WO_3 was shifted towards UV region with TiO_2 contribution. As the TiO_2 ratio in the composite structure increased, this shift effect also increased. The optical band gap energy of the photocatalysts was calculated implicating Tauc's formula given by (Basumatary et., 2022):

$$\alpha h\upsilon = A(h\upsilon - E_g)^{1/2} \tag{1}$$

where A, α, E_g and $h\upsilon$ are, the absorption coefficent, the band gap energy and the photon energy, respectively. The optical band gap energy was estimated by extrapolating the linear part of the curve to $(\alpha h\upsilon)^2 = 0$ on the plot of $h\upsilon$ versus $(\alpha h\upsilon)^2$ (Figure 2) (Basumatary et al., 2022). The estimated band gap energy for pure WO_3 and TiO_2 were 3.35 eV and 2.65 eV, respectively. On the other hand, the band gap energy of TiO_2/WO_3 composites, containing 25wt.% 50 wt.% and 75 wt.% TiO_2, was 2.85 eV, 2.95 eV, and 3.25 eV, respectively.
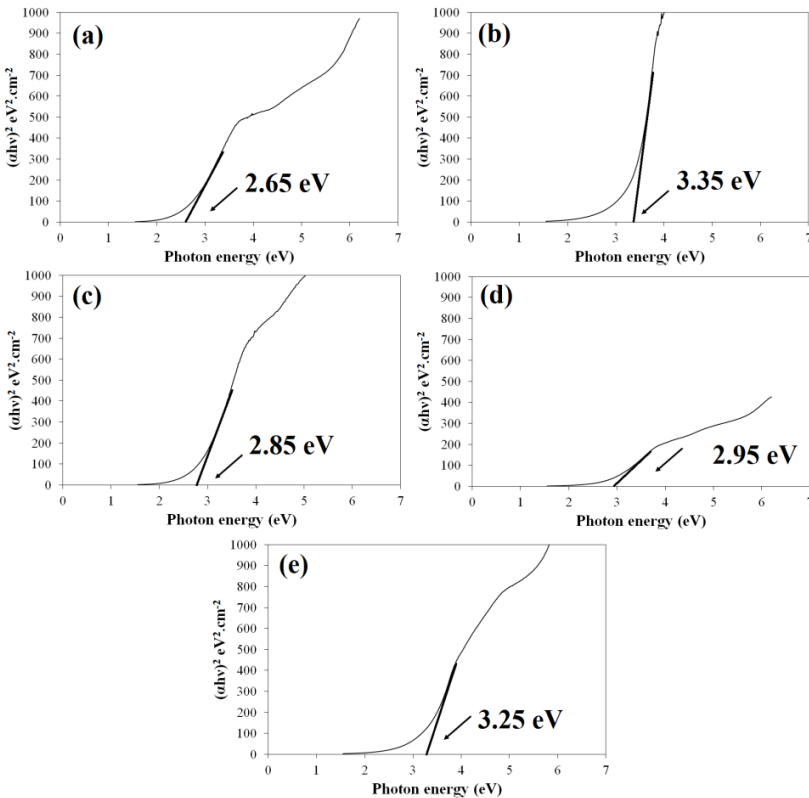

Figure 2: Tauc's plot for (a) WO_3, (b) TiO_2, (c) TiO_2/WO_3 (25/75 wt./wt.) (d) TiO_2/WO_3 (50/50 wt./wt.) and (e) TiO_2/WO_3 (75/25 wt./wt.)
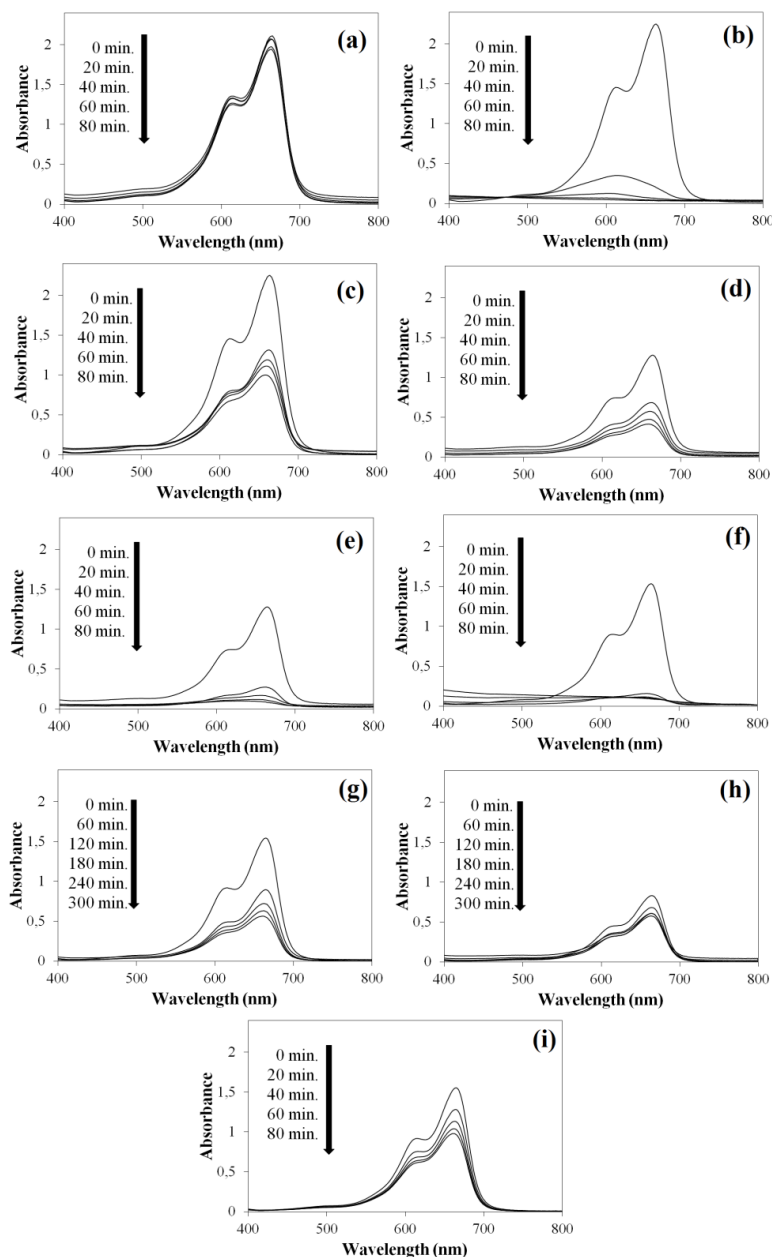
3.2. *Photocatalytic activity*

Figure 3: The variation in the UV–visible spectrum of the dye solution including (a) WO_3, (b) TiO_2, (c) TiO_2/WO_3 (25/75 wt./wt.) (d) TiO_2/WO_3 (50/50 wt./wt.), (e) TiO_2/WO_3 (75/25 wt./wt.), (f) TiO_2/WO_3 (50/50 wt./wt.) with e^- scavenger, (g) TiO_2/WO_3 (50/50 wt./wt.) with h^+ scavenger, (h) TiO_2/WO_3 (50/50 wt./wt.) with $•O_2^-$ scavenger and (i) TiO_2/WO_3 (50/50 wt./wt.) with $•OH$ scavenger

The photocatalytic activity of all samples was tested through the degradation of a model dye, methylene blue, in aqueous solution. Figure 3 exhibits the reduction in the absorption of methylene blue under UV light irradiation. When compared with the TiO$_2$/WO$_3$ composites, pure WO$_3$ nanoparticles exhibited low photocatalytic activity. The model dye, methylene blue, was degraded 7.9% with pure WO$_3$ nanoparticles within 80 minutes. The low photocatalytic performance with the WO$_3$ nanoparticles might be attributed to the limited oxidative decomposition ability of the pure photocatalyst. The low reduction potential of electrons in the conduction band of WO$_3$ may have slowed down the photocatalytic decomposition reaction (Jia et al., 2017).
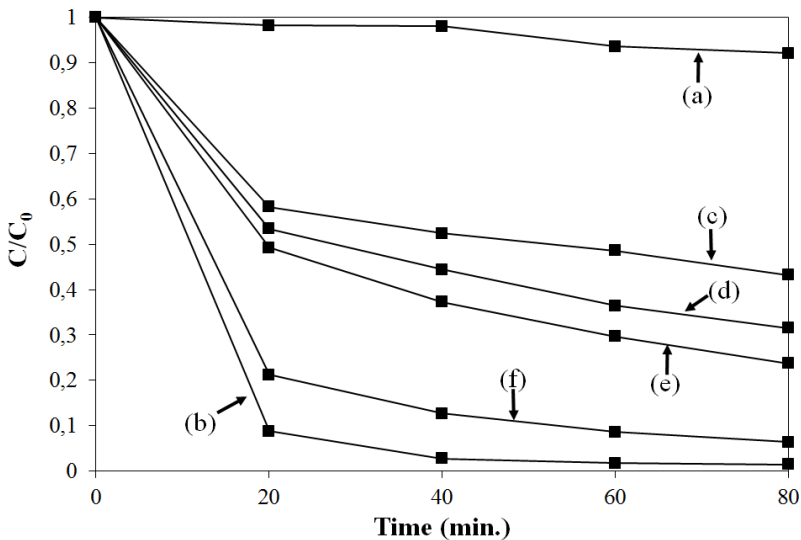

Figure 4: Degradation efficiency of methylene blue, over (a) WO$_3$, (b) TiO$_2$, (c) TiO$_2$/WO$_3$ (25/75 wt./wt.) (d) TiO$_2$/WO$_3$ (50/50 wt./wt.) and (e) TiO$_2$/WO$_3$ (75/25 wt./wt.) under UVA light irradiation

In the photocatalysis of WO$_3$, electrons in the valence band can be excited to the conduction band through absorption of photons with energy equal or greater than the optical band gap energy of the photocatalyst. The photoexcited holes in the valence band can oxidize and the photoexcited electrons in the conduction can reduce molecules adsorbed on the surface of WO$_3$. Another possibility is that the photoexcited charge carriers can recombine without the redox reactions. When the photocatalytic performance of the photocatalyst is worse than expected, it is generally attributed to the rapid recombination of the photoinduced charge carriers. (Zerjav et al., 2017). The photocatalytic degradation of the model dye

in the presence of TiO_2/WO_3 composites was enhanced. Methylene blue was degraded 56.8%, 68.4% and 93.6% with TiO_2/WO_3 composites, containing 25 wt.%, 50 wt.% and 75 wt.% TiO_2, respectively (Figure 4). The maximum photocatalytic activity was achieved with pure TiO_2. 98.5% of the methylene blue molecules were decomposed on pure TiO_2 nanoparticles after 80 minutes of UVA irradiation. High photocatalytic efficiency was obtained with the composites compared to pure WO_3. This could be attributed to the reduction in the recombination rate of the photogenerated electron-hole pairs formed on WO_3 within the composite structure and the photocatalytic performance of TiO_2 phase.

According to the literature, the valence band edge of WO_3 is more positive compared to the valence band edge of TiO_2. Thus, the photogenerated holes of WO_3 might preferably migrate towards the valence band of TiO_2. In addition, the conduction band edge of WO_3 is more positive compared to the conduction band edge of TiO_2, which results in the migration of the photoinduced electron from the conduction band of TiO_2 to the conduction band of WO_3. Hence, coupling WO_3 with TiO_2 might result in the suppression of the recombination of the photoexcited electron-hole pairs due to the mentioned differences in the band energy levels of both WO_3 and TiO_2 (Basumatary et al., 2022).

When the detail of the photocatalytic decomposition mechanism of methylene blue is examined, the electrons present in the conduction band of TiO_2 can react with surface adsorbed O_2, which gives rise to the formation superoxide anion radicals ($\bullet O_2^-$). With the following reactions, the superoxide radical can first turn into a peroxide (H_2O_2) molecule and then into a hydroxyl radical ($\bullet OH$) or the superoxide radical can react with the organic dye molecule. Similarly, the holes present in the valence band of both TiO_2 and WO_3 can react with surface adsorbed H_2O molecules, resulting in the formation of hydroxyl radicals ($\bullet OH$), which can react with the organic dye molecules. (Basumatary et al., 2022). To investigate the photocatalytic mechanism of the TiO_2/WO_3 (50/50 wt./wt.) composite in detail, the effects of different scavengers on the decomposition of methylene blue molecules were studied. According to Figure 5, the addition of superoxide ($\bullet O_2^-$) and hydroxyl ($\bullet OH$) scavengers inhibited the decomposition of methylene blue molecules. 30.8% and 37.5% of methylene blue were decomposed within 80 min. with $\bullet O_2^-$ and $\bullet OH$ scavengers, respectively. The reduction in the photocatalytic decomposition indicated that both radicals were similarly effective in photocatalytic decomposition reactions. The addition of the hole scavenger also inhibited the decomposition of the model dye at a certain extent. Methylene blue was degraded 64.1% within 80 min. by TiO_2/WO_3 (50/50

wt./wt.) composite in the presence of the hole scavenger. In contrast to the hole scavenger, the addition of the electron scavenger enhanced the photocatalytic decomposition. Methylene blue was degraded 93.5% within 80 min. by the TiO$_2$/WO$_3$ composite in the presence of the electron scavenger. There might be two possibilities for this increase in the photocatalytic efficiency. There might be an increase in the number of active holes to participate in the photocatalytic decomposition reaction, as the electron-hole recombination was inhibited due to the retention of the photoexcited electrons by the scavenger. Another possibility was that potassium persulfate added into the solution as an electron scavenger might contribute actively to the decomposition reaction of the model dye.
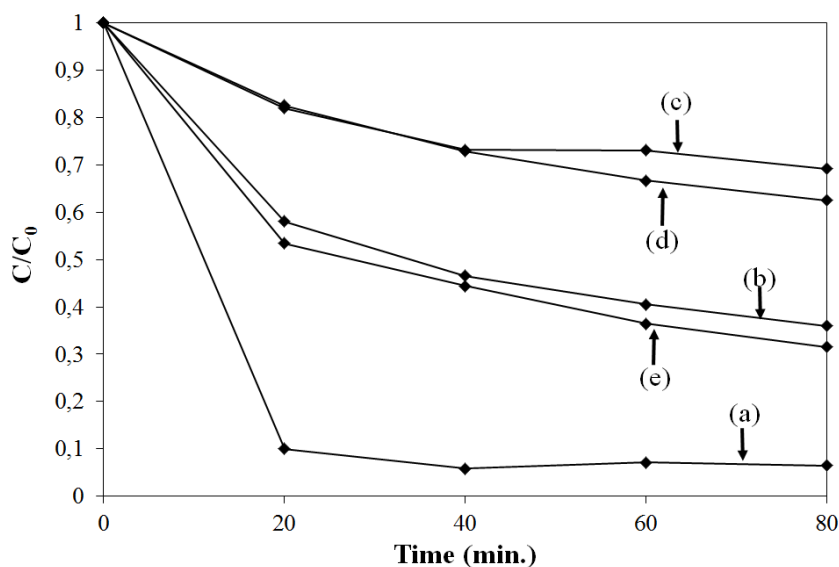

Figure 5: Degradation efficiency of methylene blue, over (a) TiO$_2$/WO$_3$ (50/50 wt./wt.) with e⁻ scavenger, (b) TiO$_2$/WO$_3$ (50/50 wt./wt.) with h⁺ scavenger, (c) TiO$_2$/WO$_3$ (50/50 wt./wt.) with •O$_2^-$ scavenger, (d) TiO$_2$/WO$_3$ (50/50 wt./wt.) with •OH scavenger and (e) TiO$_2$/WO$_3$ (50/50 wt./wt.) without a scavenger under UVA light irradiation

To investigate the photocatalytic degradation kinetics of methylene blue in the presence of the photocatalysts, the following pseudo-first order kinetic model was studied (Hasan et al., 2020):

$$\ln(C_0/C_t) = kt \qquad (2)$$

where C$_0$ and C$_t$ are the concentration of methylene blue in aqueous solution before and after UV light irradiation, t is the time and k is the rate constant, which was obtained from the slope of the plot of $\ln(C_0/C_t)$ versus t

(Figure 6). The rate constant values were illustrated in Table 1. The rate constant values were found to be 0.001 min^{-1} and 0.0643 min^{-1} for pure WO_3 and TiO_2, respectively. On the other hand, the rate constant values were found to be 0.0123 min^{-1}, 0.0165 min^{-1}, and 0.0401 min^{-1} for the TiO_2/WO_3 composites, containing 25 wt.%, 50 wt.% and 75 wt.% TiO_2, respectively.
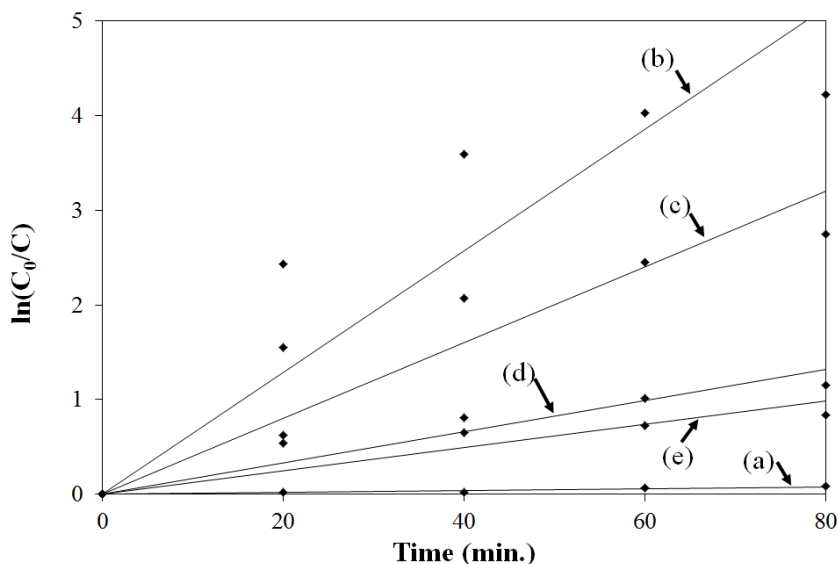

Figure 6: Photocatalytic degradation kinetics of methylene blue onto
(a) WO_3, (b) TiO_2, (c) TiO_2/WO_3 (25/75 wt./wt.) (d) TiO_2/WO_3 (50/50 wt./wt.)
and (e) TiO_2/WO_3 (75/25 wt./wt.) under UVA light irradiation

Table 1: The discoloration rate of methylene blue for
WO_3, TiO_2 and TiO_2/WO_3 composites

Sample	k (min-1)	R2
WO_3	0.001	0.909
TiO_2	0.0643	0.7337
TiO_2/WO_3 (25/75 wt./wt.%)	0.0123	0.6897
TiO_2/WO_3 (50/50 wt./wt.%)	0.0165	0.8277
TiO_2/WO_3 (75/25 wt./wt.%)	0.0401	0,7899

4. Conclusions

TiO_2/WO_3 composites were synthesized through co-precipitation technique in the presence of TiO_2 nanoparticles and their photocatalytic activity for the decomposition of methylene blue was evaluated. Methylene blue decomposition

studies showed that the TiO$_2$/WO$_3$ composites presented enhanced photocatalytic activity compared to pure WO$_3$, which was attributed to the reduction in the recombination rate of the photogenerated electron-hole pairs formed on the WO$_3$ phase of the composites. Coupling WO$_3$ with TiO$_2$ also enhanced the reaction rate of the photocatalytic decomposition. In addition, the optical band gap energy of WO$_3$ was widened by coupling with TiO$_2$.

References

Ai, L., Jia, D., Guo, N., Xu, M., Zhang, S., Wang, L., Jia, L. (2020). Cl-doped Bi2S3 homojunction nanorods with rich-defects for collaboratively boosting photocatalytic reduction performance. *Applied Surface Science*, 529, 147002.

Basumatary, B., Basumatary, R., Ramchiary, A., Konwar, D. (2022). Evaluation of Ag@TiO2/WO3 heterojunction photocatalyst for enhanced photocatalytic activity towards methylene blue degradation. *Chemosphere*, 286(2), 131848.

Carvalho, L. M., Soares, A. F., Lima, M. S., Cruz-Filho, J. F., Dantas, T. C. M., Luz, G. E. (2021). 2,4-Dichlorophenoxyacetic acid (2,4-D) photodegradation on WO3-TiO2-SBA-15 nanostructured composite. *Enviromental Science and Pollution Research*, 28(7), 7774-7785.

Dozzi, M. V., Marzorati, S., Longhi, M., Coduri, M., Artiglia, L., Selli, E. (2016). Photocatalytic activity of TiO2-WO3 mixed oxides in relation to electron transfer efficiency. *Applied Catalysis B-Environmental*, 186, 157-165.

Gibot, P., Comet, M., Vidal, L., Moitrier, F., Lacroix, F., Suma, Y., Schnell, F., Spitzer, D. (2011). Synthesis of WO3 nanoparticles for superthermites by the template method from silica spheres. *Solid State Sciences*, 5(13), 908-914.

Govindaraj, T., Mahendran, C., Marnadu, R., Shkir, M., Manikandan, V. S. (2021). The remarkably enhanced visible-light-photocatalytic activity of hydrothermally synthesized WO3 nanorods: An effect of Gd doping. *Ceramics International*, 47(3), 4267-4278.

Hasan, J., Li, H., Tian, G., Qin, C. (2020). Fabrication of Cr2S3-GO-TiO2 composite with high visible-light-driven photocatalytic activity on degradation of organic dyes. *Chemical Physics*, 539, 110950.

Jia, J., Taniyama, K., Imura, M., Kanai, T., Shigesato, Y. (2017). A visible-light active TiO2 photocatalyst multilayered with WO3. *Physical Chemistry Chemical Physics*, 19(26), 17342-17348.

Li, J., Du, X., Yao, L., Zhang, Y. (2014). Synthesis of SnS2/WO3 nanocomposite with enhanced photocatalytic activity. *Materials Letters*, 121, 44-46.

Mohammadi, S., Sohrabi, M., Golikand, A. N., Fakhri, A. (2016). Preparation and characterization of zinc and copper co-doped WO3 nanoparticles: Application in photocatalysis and photobiology. *The Journal of Photochemistry and Photobiology B: Biology*, 161, 217-221.

Nagarjuna, R., Challagulla, S., Sahu, P., Roy, S., Ganesan, R. (2017). Polymerizable sol-gel synthesis of nano-crystalline WO3 and its photocatalytic Cr(VI) reduction under visible light. *Advanced Powder Technology*, 28(12), 3265-3273.

Puga, F., Navio, J. A., Hidalgo, M. C. (2021). Features of coupled AgBr/WO3 materials as potential photocatalysts. *Journal of Alloys and Compounds*, 867, 159191.

Sayadi, M. H., Ahmadpour, N., Homaeigohar, S. (2021). Photocatalytic and Antibacterial Properties of Ag-CuFe2O4@WO3 Magnetic Nanocomposite. *Nanomaterials*, 11(2), 298.

Soares, A. F., Cruz, J. F., Lima, M. S., Carvalho, L. M., Silva, L. K. R., Costa, J. S., Dantas, T. C. M., Luz, G. E. (2018). Photodegradation of 17 alpha-Ethynylstradiol (EE2) on Nanostructured Material of Type WO3-SBA-15. *Water Air and Soil Pollution*, 229(8), 268.

Thilagavathi, T., Venugopal, D., Marnadu, R., Chandrasekaran, J., Alshahrani, T., Shkir, M. (2021). An Investigation on Microstructural, Morphological, Optical, Photoluminescence and Photocatalytic Activity of WO(3) for Photocatalysis Applications: An Effect of Annealing. *Journal of Inorganic and Organometallic Polymer and Materials*, 31(3), 1217-1230.

Thwala, M. M., Dlamini, L. N. 2020. "Photocatalytic reduction of Cr(VI) using Mg-doped WO3 nanoparticles", Environmetal Technology, 41 (17), 2277-2292.

Wang, H. L., Wang, Y. F., Xu, A. L., Yang, Q. P., Tao, F. J., Ma, M. L., Song, Z. W., Chen, X. B. (2019). Facile synthesis of a novel WO3/Ag2MoO4 particles-on-plate staggered type II heterojunction with improved visible-light photocatalytic activity in removing environmental pollutants. *RSC Advances*, 9(60), 34804-34813.

Zerjav, G., Arshad, M. S., Djinovic, P., Zavasnik, J., Pintar, A. (2017). Electron trapping energy states of TiO2-WO3 composites and their influence on photocatalytic degradation of bisphenol A. *Applied Catalysis B-Environmental*, 209, 273-284.

Zhang, J., Guo, Y., Xiong, Y., Zhou, D., Dong, S. (2017). An environmentally friendly Z-scheme WO3/CDots/CdS heterostructure with remarkable

photocatalytic activity and anti-photocorrosion performance. *Journal of Catalysis*, 356, 1-13.

Zhou, G., Long, L., Wang, P., Hu, Y., Zhang, Q., Liu, C. (2020). Designing CuO/ZnO nanoforest device toward optimal photocatalytic performance through structure and facet engineering. *Materials Letters*, 273, 127907.

STATE OF THE ART REVIEW ON THE LATEST WELDING TECHNOLOGIES FOR ALUMINUM

Halil Ibrahim KURT[1] & Engin ERGUL[2] & Aziz Baris BASYIGIT[3] & Murat ODUNCUOGLU[4]

[1]*(Assoc. Prof. Dr.) Metallurgy and Materials Engineering Department, Engineering Faculty, Gaziantep University, e-mail: hiakurt@gmail.com*
Orcid: 0000-0002-5992-8853
[2]*(Dr.) Mechanical Department, Izmir Vocational High School, Dokuz Eylul University, e-mail: engine.ergul@deu.edu.tr*
Orcid: 0000-0003-3347-5400
[3]*(Assist. Prof. Dr.) Metallurgical and Material Engineering Department, Engineering Faculty, Kirikkale University, e-mail: abbasyigit@kku.edu.tr*
Orcid Id: 0000-0003-1544-3747
[4]*(Dr.) Physical Department, Science Faculty, Yildiz Technical University, e-mail: oduncuoglu@gmail.com*
Orcid: 0000-0002-3130-5646

1. Introduction

Due to rapidly depleting fossil fuels, the demand for higher performance vehicles, global warming, and stringent emission standards, automotive and aviation manufacturers are continuously looking for new strategies to further increase the fuel efficiency (Giampieri et al., 2020). Although these are important problems for manufacturers, weight reduction method is one of the strategies in solving these problems. If the weight of a vehicle is reduced by 10%, the specific fuel consumption will be reduced by 3 to 7% (Manladan et al., 2017). Therefore, the need for lightweight materials is increasing in the automotive and aerospace industries.

Aluminum is of great importance among light materials, with its low density (2.7 gr/cm^3), low melting temperature (660.3 °C), low cost, high

corrosion resistance and good recycling properties. Moreover, while the mechanical properties of aluminum can be enhanced by alloying, there is no big difference between the thermal conductivity, thermal expansion and melting points of these aluminum alloys (Cao et al., 2020; Dursun & Soutis, 2014; Kurt et al., 2020; Manladan et al., 2017; Omar Cooke, 2020; Pratap et al., 2021). As shown in Figure 1, there are eight series of aluminum and many aluminum alloys derived from them. With the development of precipitation hardening, the mechanical properties of aluminum have improved enormously and it has gained a great importance in the metal industry (Starke & Staley, 1996). Thanks to these properties, aluminum ranks second in the metal market of the world (Onat, 2018). On the other hand, aircraft and automotive manufacturers are trying to reduce the number of parts in vehicles and avoid screw or rivet joints. One method of achieving these is by using the welding process.
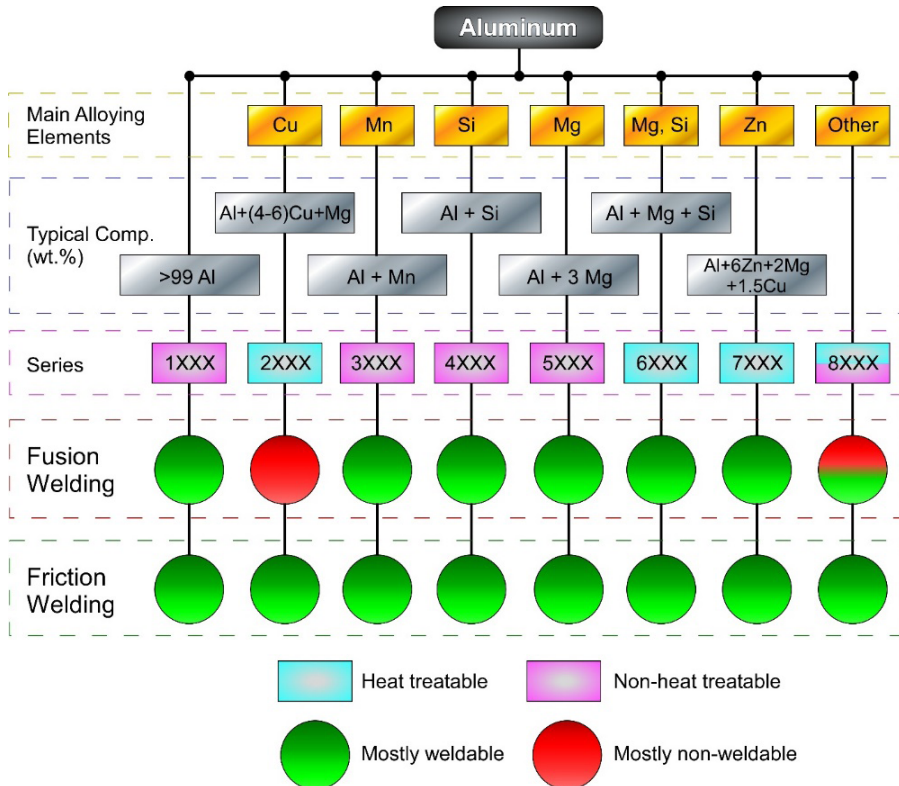

Figure 1: Main alloying elements, typical compositions, series and weldability of aluminum alloys.

In its most general definition, welding process is the combination of two or more materials with the help of heat, pressure or both. However, the application

of traditional welding methods in the joining of aluminum alloys poses huge problems. These problems can be classified as follows:

1. Mechanical properties of the welding zone of aluminum alloys treated with precipitation hardening significantly decrease.
2. Hot cracking may occur in the welding zone of high strength aluminum alloys.
3. Due to the oxygen affinity of aluminum, there is an aluminum oxide layer (having melting point about 2200 °C) on its surface and this layer prevents the flow of molten metal from the welding pool into the material, causing a weak welded joint. In addition, this weld zone contains oxide inclusions.
4. Since molten aluminum can absorb large amounts of hydrogen, the solidified welding zone contains hydrogen porosities (Bagautdinova et al., 2019; Kah, 2014).

In order to minimize these problems, the availability of new (complex and/or technological) welding technologies in the welding of aluminum and its alloys is an important research subject. High or very low heat input to a material in a very short time is the most important advantage of new welding technologies. Welding processes, such as electron beam welding or laser welding, due to high heat input for a very short time, fast cooling take place in the welded materials. This situation prevents or minimizes damages resultant the recrystallization of the welded materials. In the case of low heat input processes such as friction stir welding, the negative effects of high temperature on the material can be eliminated. Furthermore, it is possible to weld dissimilar alloys and metals using new welding techniques (Mishra & Ma, 2005; Ni & Ye, 2018; Pratap et al., 2021; Selvi, Vishvaksenan, & Rajasekar, 2018; Wang et al., 2021).

In this study, the use of new welding techniques such as laser beam welding, laser-arc hybrid welding, electron beam welding, cold metal transfer welding, magnetic pulse welding and friction stir welding in aluminum and its alloys are compiled and evaluated in the light of relevant articles containing the most recent developments on this subjects. The effects of welding techniques on the properties of aluminum alloy are discussed by taking into consideration mechanisms, advantages and disadvantages.

2.   Laser Beam Welding

After the first working laser system was introduced in the 1960s, high power lasers were developed in the 1990s, which are more suitable for use in industry

and welding (Katayama, 2009, 2020). Laser beam welding (LBW) is a fusion welding technique in which two metal parts are joined using a laser beam. The main source parameter is laser power. This determines both the penetration depth and the welding speed. Other basic parameters are beam diameter, focal point position on the material surface, wire diameter and feed rate. During the process, melting and in some cases even evaporation occurs on the surface of the irradiated welding region. High quality and precise welding of aluminum alloys is possible thanks to LBW (Mathers, 2002; Yilbas, Akhtar, & Shuja, 2013). As seen in Figure 2, there are two types of LBW mechanisms called as keyhole mode and conduction mode. The difference between these two mechanisms is related with the power density (laser power densities for keyhole and conduction modes are 10^4-10^6 W/cm^2 and higher than 10^6 W/cm^2, respectively (Sánchez-Amaya et al., 2012; Xiao & Zhang, 2014)higher specific strength and rigidity, better corrosion and fatigue crack growth resistance properties, compared to conventional aluminum alloys. Laser beam welding (LBW) applied to the welding zone. Therefore, different welding pools are formed in both mechanisms.
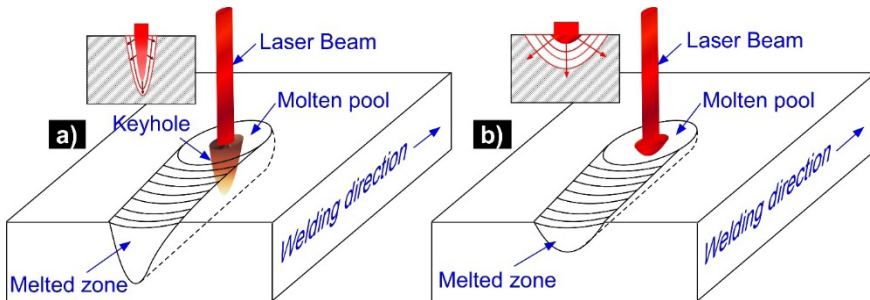

Figure 2: Schematic representations of laser beam welding mechanisms. Key hole mechanism (a) and conduction mode mechanism (b).

In the keyhole mechanism, the energy density of the applied laser is high enough to cause evaporation in the materials. In this way, the penetration depth is high and a keyhole gap is created in the weld zone. During this process, partial ionization of the metal vapor usually takes place and therefore laser-induced plasma can be formed just above the weld pool. In the case of conduction mechanism, the energy density of the applied laser is sufficient to trigger the boil of the material. Therefore, the weld pool is wider and the penetration depth is less than the keyhole mechanism (Sánchez-Amaya et al., 2017). In particular, the keyhole mode laser source produces a very narrow heat affected zone (HAZ). This minimizes the deterioration and loss of strength in the HAZ of aluminum alloys hardened by work or precipitation. In addition, the loss of alloying elements

having low-boiling temperature such as magnesium is reduced (Mathers, 2002; Xiao & Zhang, 2014).

As the wavelength of the laser beam increases, the strength of the weld gets weaker, a special case in welding aluminum and its alloys. Since the wavelength of the CO_2 laser (10.6 µm) is higher than the wavelength of the Nd-YAG laser (1.06 µm), the Nd-YAG laser is more suitable for welding aluminum and alloys (Mathers, 2002). High power diode laser welding is also possible for aluminum alloys. In the laser welding of aluminum alloys, it is stated that alloying elements such as magnesium, zinc and silicon improve weldability. Among these, the most important in terms of laser beam weldabilitiy is magnesium. Because these elements reduce the thermal conductivity and melting point of the alloy (Sánchez-Amaya et al., 2012)a highpower diode laser has been employed to weld six aluminum alloys (1050, 2017, 2024, 5083, 6082, and 7075.

One of the biggest problems in laser welding of aluminum alloys is pore formation in the weld zone. This situation occurs due to the metal vapor which cannot escape from the narrow keyhole and this metal vapor is trapped in the molten weld pool. The use of super imposed laser beams is an effective method in solving pore formation. In this way, larger vapor capillaries are formed and the metal vapor coming from the keyhole can easily leave the weld pool. The use of different distributions of laser beam intensity (see Figure 3) is also an effective method to reduce porosity formation in laser welding of aluminum alloys.
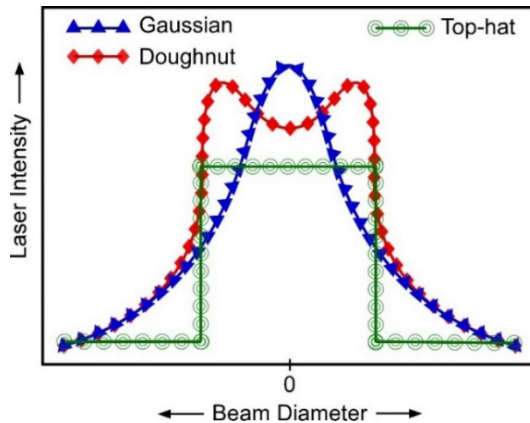

Figure 3: Different distributions of laser beam intensity.

Porosity formation is less when using Gaussian distribution of laser beams than top-hat and doughnut distribution of laser beams. These distributions can be created by using concentrically arranged laser beams. Moreover, some properties

of the welding like spatter formation and pore formation can be controlled by using different concentrically arranged dual laser beams (Punzel et al., 2020). In this technique, two disk or fiber laser beams are superimposed with advanced optical fiber technologies (Kang & Kim, 2020).

On the other hand, Ke et al. (2021) investigated the effect of laser oscillating welding on keyhole induced porosity formation during welding of 5A06 aluminum alloy by using a spiral and infinity oscillation patterned laser beam. In the laser welding process performed under protective argon gas at a flow rate of 15 l/min, the diameter, power, longitudinal velocity and oscillating amplitude of the laser were selected as 4 mm, 4 kw, 0.03 m/s and 2 mm, respectively. They showed that, infinity oscillation mode was superior than circular oscillation mode in terms of porosity elimination. A non-porous structure can be obtained at an oscillation frequency of 200 Hz. In the case of oscillating laser beam, the molten pool moves back and forth. Due to this movement, the air bubbles coalesce and out flow from the molten pool. In a similar study which was carried out by Li, Mi, & Wang(2020), researchers determined that as laser diameter and oscillation frequency increase, weld depth and porosity decrease significantly of 5083 Al alloy. In addition, they have experimentally proved that the tensile strength of the welded alloy by laser beam oscillation is higher than the welded material without laser beam oscillation. They explained this situation by the elimination of porosities due to the oscillation. In the analysis performed by Hagenlocher et al. (2020), it is stated during the LBW of aluminum sheets having residual stresses, low welding speed and line energy of 20 to 25 J/mm2for per depth should be applied to obtain maximum reliability in terms of hot crack formation. In another study (Fritzsche et al., 2018), an electromagnetic system was developed to reduce porosity in laser beam welding of die casted AlSi9MnMg aluminum alloy. In this system, it is aimed to move the gases to the surface during the laser beam welding process by using the electromagnetic system by taking advantage of the difference between the electrical conductivity of the gases and the molten aluminum. Lorentz forces were created in the welding pool by means of the generated magnetic field and it was determined that a serious decrease in porosity was achieved. Another method developed to reduce porosity in the laser welded aluminum alloys is the use of concentrically arranged laser beams. As seen in Figure 4, in this method, the energy density of the laser beam in the inner core is higher than the outer ring. During welding of 5083 Al alloy, by using laser power of 900 W for inner core and 100 W for outer ring, it is possible to decrease the porosity from 12 to 8 %. This decrease in the porosity is attributed to the increase in the keyhole opening. The high pressure

and other instabilities caused by boiling bubbles are reduced by larger keyhole opening and this causes the porosity to decrease (Punzel et al., 2020).
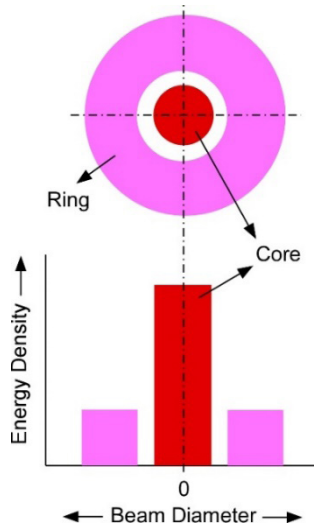

Figure 4: Schematic explanation of concentrically arranged lasers beams and differences in energy densities between outer ring and inner core laser beams.

3.   Laser-arc hybrid welding

The use of an additional electric arc with the laser beam in material processing took place in the early 1980s. Since then, there have been important developments in the welding of materials with the successful synergistic effect of laser beam and arc (Oladimeji & Taban, 2016). In laser welding (CO2, Nd-YAG, diode, disk or fiber laser) of aluminum alloys, with the application of an additional heat source (TIG, MIG, MAG, plasma or another arc heat source), it is possible to directionally control the structure and properties of the HAZ. The process enables to welding at high speeds. In addition, thermal conditions in the welding pool can be controlled. The low coefficient of absorption of laser radiation value of aluminum alloys, which is another problem in laser welding of aluminum alloys, increases with hybrid laser arc welding by reducing the surface reflectivity. Thanks to the additional arc, the metal is preheated and so the hydrogen content and other impurities in the melt can be controlled, which causes porosity formation (Katayama, 2020; Shiganovet al., 2017). A schematic presentation of laser-arc hybrid welding process can be seen in Figure 5. If the direction of the arc and/or wire feeding is in the welding direction, this process is called as "forward angle", while the direction of the arc and/or wire feeding

is opposite to the welding direction, this process is called as "backward angle". Figure 5 represents the situation of "backward angle".
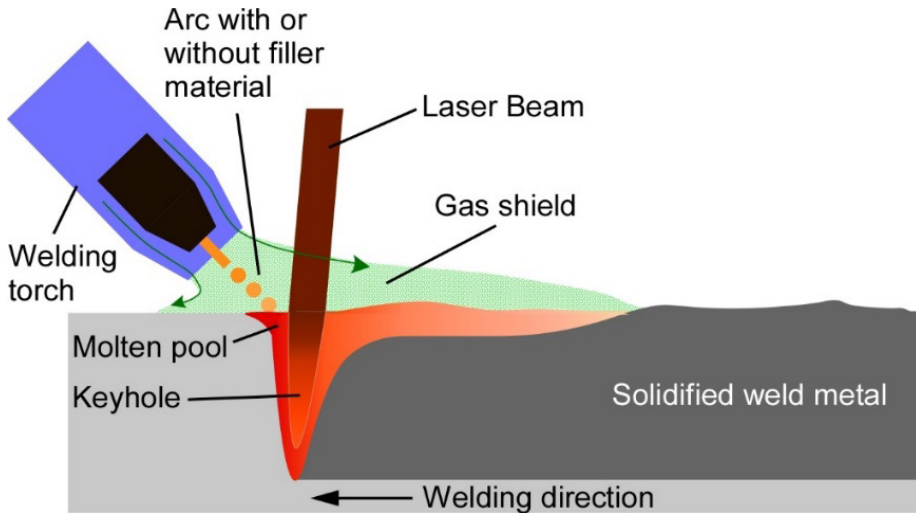

Figure 5: Schematic representation of laser-arc hybrid welding process.

The first effect of laser beam and electric arc on improving the welding of aluminum alloys is related to the interaction of the laser beam with the arc, which transforms the energy level of electron into a transition state. In this way, more photon emission occurs and the heat input into the material increases. The second effect is that the amount of spatter is less in laser-arc hybrid welding. Because, in this technique, droplets are absorbed more easily by the weld pool thanks to the larger weld pool opening and the downward melt flow (Zhang, Gao, & Zeng, 2019). It is reported that 20% melting efficiency can be obtained by laser-TIG hybrid welding process (Liu, Yuan, & Li, 2012).

Möller, & Thomy (2013) investigated a coaxial laser-plasma hybrid welding process on 6016 aluminum alloy. The researchers created a system consisting of a coaxial plasma that surrounds the laser beam. They determined that during welding with this system, the plasma arc was affected by the aluminum evaporated by the laser. It is stated that the plasma arc becomes stable when removed the dielectric layer on the aluminum surface by the laser or plasma. Zhang et al. (2017) welded an AA6068 aluminum alloy by using a fiber laser beam and MIG system having filler wire. They determined that the amount of porosity decreased with the increase of arc current and/or laser power. This decrease in the porosity positively affected the fatigue life of AA6082 aluminum alloy (Zhang, Gao, & Zeng, 2016). Casalino, & Ludovico (2013) studied the effect of direction of arc in the welding AA5754 aluminum alloy. According

to their results, using a fiber laser and TIG welding system in the "backward angle" position, there is less penetration, larger HAZ area and welding defects. On the other hand, it is possible to obtain a better structure, a stable melting pool and a narrower HAZ in the "forward angle" position welding. In another study (Wang, Liu, Yang, & Gao, 2021), the authors concluded that it is possible to obtain porosity-free welds in the welding of AA6082 aluminum alloy by using high-frequency oscillating (100-500 Hz) laser-arc hybrid welding system (fiber laser-MIG weld system with Al filler wire). In that study, the beam was oscillated and it was stated that the porosities completely eliminated in the range of 100-300 A arc. Obtaining the weld without porosity has been explained by three mechanisms. (1) The keyhole oscillating at a high frequency captures the bubbles in the molten pool. (2) Thanks to the high frequency oscillation on the keyhole, the diameter of the keyhole is larger and its stability increases. (3) Thanks to the vortex created by the high-frequency oscillation in the molten pool, the bubbles moved away from the structure.

However, besides all these advantages, in laser-arc hybrid welding method, many parameters need to be adjusted and it involves complicated physical processes. Therefore, the optimization process is difficult and this situation creates a disadvantage in terms of laser-arc hybrid welding method (Xu et al., 2018).

4. Electron beam welding

Electron beam welding is a kind of high technological welding process in which the two or more materials are melted and combined with a high speed electron beam (Vogel, 2011). The use of electron beam in welding started in 1958 (Schultz, 1993). In the processing of electron beam welding, a high energy density electron beam with a diameter of around 0.25 – 2.5 mm is used to obtain the energy required for welding. The process is carried out in a vacuum environment. As seen in Figure 6, the electron beam produced by heating the filament to high temperature is accelerated and magnetically focused on the surface of the material to be welded. This allows precise and high speed welding with deep keyhole penetration and a low heat input. The accelerating voltage, current of electron gun filament and travel speed are basic parameters during welding (Mathers, 2002). Thanks to the high density of the electron beam, very fast heating and cooling occurs. Besides, the HAZ occurs in a very narrow area. Thus electron beam welding is very suitable technique for joining aluminum alloys and has a great potential in this regard (Wanjara & Brochu, 2010).
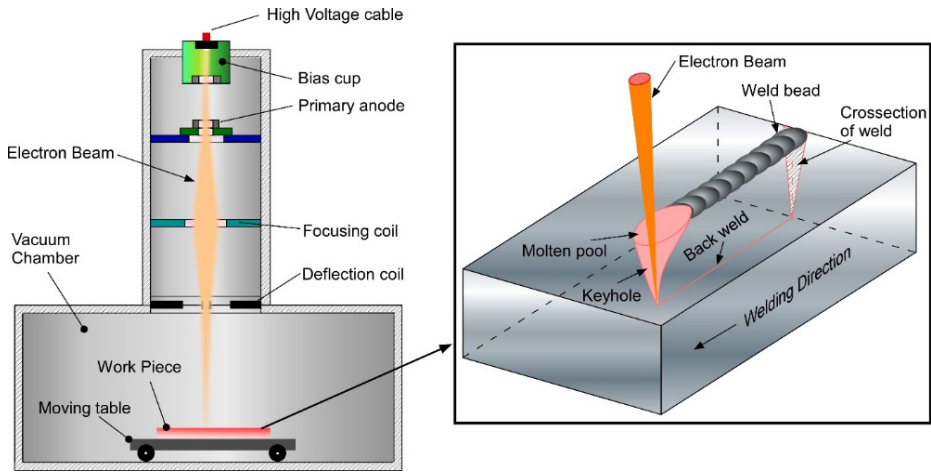
Figure 6: Electron beam welding, schematic explanation of keyhole mode.

The biggest problem in electron beam welding is metal vapor coming from the molten pool, which causes arc formation in the electron beam gun, especially in the presence of alloying elements with low melting temperature such as magnesium and zinc. This arc in the gun interrupts the electron beam and causes cavities in the weld (Mathers, 2002). Chen et al. (2019) conducted some numerical and experimental researches in electron beam welding of 2A12 aluminum alloy. According to the results, it was determined that there is a relationship between the welding speed and the escape of metal vapor from the melt pool. In addition, the large heat input causes the metal to vaporize heavily and waves the keyhole. The flow behavior of the liquid metal is mainly related with keyhole penetration and welding speed. During low speed welding, a flat molten pool wall is formed and liquid metal at the wall edge flows to the bottom of the molten pool, preventing the escape of metal vapor. By increasing the welding speed, the slope of the molten pool increases and the stability of the keyhole is improved. Therefore, the metal vapor cavity is reduced and it is recommended that the high welding speed is useful to the decrease of pores during the electron beam welding of aluminum alloys.

In the study which was carried out by Sobih et al. (2016), a 2219 aluminum alloy was welded by electron beam welding method. When working with a small beam diameter, it was determined that full penetration was achieved and the weld seam width was 3.51 mm. Due to the rapid heating and cooling characteristic of the electron beam welding method, a small HAZ was acquired and a tensile strength of 295 MPa, corresponding to 62% of the base metal,

was obtained. It was concluded that this decrease in tensile strength was due to micro size solidification cracks. Alexopoulos et al. (2016) state that the mechanical strength of the weld zone of electron beam welded 6156 aluminum alloy is significantly improved by artificial aging carried out post welding. The solution treatment and aging treatments after electron beam welding have a significant effect on improving the fatigue strength of AA2219 aluminum alloys (Malarvizhi, Raghukandan, & Viswanathan, 2008). In a study (Chen et al., 2019)which reduced the strength of the joint via conventional EBW (CEBW in which oscillating electron beam was tested in the welding of 2A12 aluminum alloy, it was determined that porosity decreased in the weld zone and, tensile strength improved and fatigue life was satisfactory thanks to oscillating beam.

Another disadvantage of electron beam welding is the investment cost of the process. The necessity of welding in a vacuum chamber requires expensive diffusion pumps and large airtight chambers.

5. Cold Metal Transfer Welding

Cold metal transfer welding was developed in 2004 and the method is basically a short circuit transfer modified MIG welding process. The difference of this process from the MIG welding method is the mechanical droplet cutting of the cold metal transfer welding system. This process is predicted to be a milestone in aluminum welding (Gungor et al., 2014). The most advantageous feature of cold metal transfer welding is low heat input to the material to be welded due to low current of short circuit (Furukawa, 2006; Selvi et al., 2018). Thanks to this low heat input, it is a very suitable method for welding dissimilar metals such as aluminum-stainless steel (Babu et al., 2019). It is stated that cold metal transfer welding method creates a sputter-free weld seam in the joining of 1.2 mm thick AlSi5 alloy plates, good gap filling can be made due to low heat input and the deformations that may occur due to welding are at a minimum level (Feng, Zhang, & He, 2009). During the process, a normal arc and therefore a weld pool is formed (Figure 7 (a)). Then, the electrode wire tip moving towards to the weld pool contacts with the weld pool (Figure 7 (b)) and the electrode wire end is immediately retracted by the servo motor of the system (Figure 7 (c)). Metal transfer occurs in the form of droplets, during which time the current drops to almost zero. After metal transfer, the arc re-ignites and the process continues in this way (Figure 7(d)).
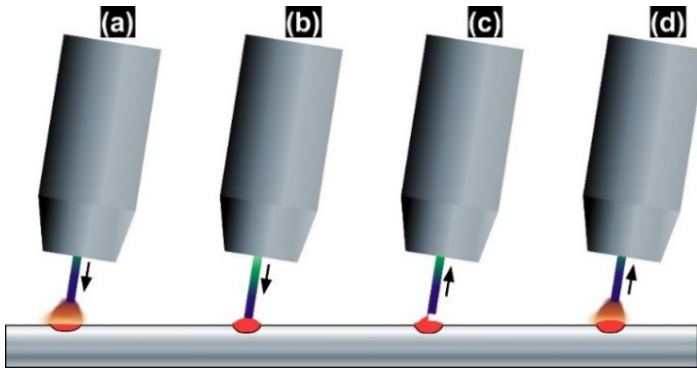
Figure 7: Cold metal transfer welding process and electrode wire movement.

As can be seen in Figure 8, in cold metal transfer welding of aluminum and its alloys, the relationship between metal transfer and heat transfer is a hermetic phenomenon due to the complex wave shape of the welding current and the mechanical effects of metal transfer by withdrawing the electrode wire (Mezrag, Deschaux, & Benachour, 2015; Selvi et al., 2018). First of all, thanks to the high pulsed current at peak time, the welding arc easily ignites and the wire electrode heats up. Then, the background time phase starts and the current is reduced by the system. In this way, the transfer of the small droplet at the wire electrode tip is prevented. The last stage is the short circuit stage. Arc voltage at this stage is almost equal to zero. Thanks to this stage, the liquid material in the wire electrode flows into the weld pool. At the same time, the pullback signal is given to the step motor of the wire feeder (Feng et al., 2009).
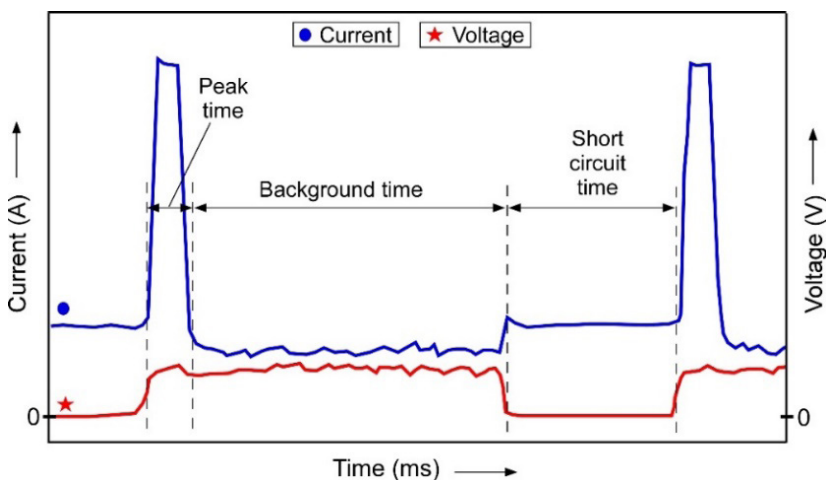

Figure 8: Relationship between current
and voltage in cold metal transfer welding and welding phases.

It is stated that it is possible to eliminate welding gas porosities of AA2219 aluminum alloy by applying low heat input in cold metal transfer welding (wire feed speed, welding speed and heat input: 7.5 m/min, 0.5 m/min and 273.4 J/mm, respectively) (Baoqiang et al., 2016). Gungor et al. (2014) showed that the yield strength of 5083 and 6082 aluminum alloys welded with cold metal transfer welding applied by robotic system is better than the alloys welded by traditional welding method. Liu et al. (2015) generated Lorenz Force in the weld zone by applying an external magnetic field during cold metal transfer welding of aluminum/steel materials. This magnetic field applied during welding homogenized the heat distribution in the weld zone and effected the metal flow. As a result, it was determined that the maximum load force in the tensile strength is 45% more than the aluminum/steel pair welded by cold metal transfer method without magnetic field. Increasing the current, voltage and welding speed parameters in order to increase welding efficiency in aluminum alloys is not recommended as it causes gas bubbles in the weld (Matusiak & Pfeifer, 2013).

6.   Magnetic pulse welding

Magnetic pulse welding was invented in the 1970s (Miranda, Tomás, Santos, & Fernandes, 2014). As can be seen in Figure 9, a typical magnetic pulse welding system usually consists of a power supply, a switching system and a coil. In the method, very high electric current is generated by the sudden discharge of the capacitors through the coil around the materials to be welded. Eddy currents oppose the magnetic field in the bond, thereby generating a high-speed pulsed Lorentz force. This Lorentz force causes to impact the flayer to the target material at high speed (Faster than 1000 km/h) and creates an impact type of weld (Czerwinski, 2011; Zhu, Liu, Wu, & Gao, 2020)which is mainly used in the lap joining of similar and dissimilar materials. It has broad application prospects in aerospace, automotive and appliance industries. In this paper, the corrosion-resistant 5052 aluminum alloy (Al. Due to this high impact speed, the welded regions of the materials undergo a very localized plastic deformation at stress ratios in the range of $10^{-6} - 10^{-7}$ s^{-1} (Y. Zhang, Suresh, & Daehn, 2010). This is a kind of a solid state welding. During impact, a jet is formed in a thin layer at the interface that cleans the surface contaminants. In this way, atomic contact and joint strength are improved (Pereira et al., 2017). In the welding of aluminum alloys, the wavy structure of the weld interface and material flow from one work piece to another can be regarded as an indicator of jet formation

(S. Mishra et al., 2017). There is no need for a protective atmosphere and filling material. In addition, since it is a cold welding process, HAZ does not occur in the material.
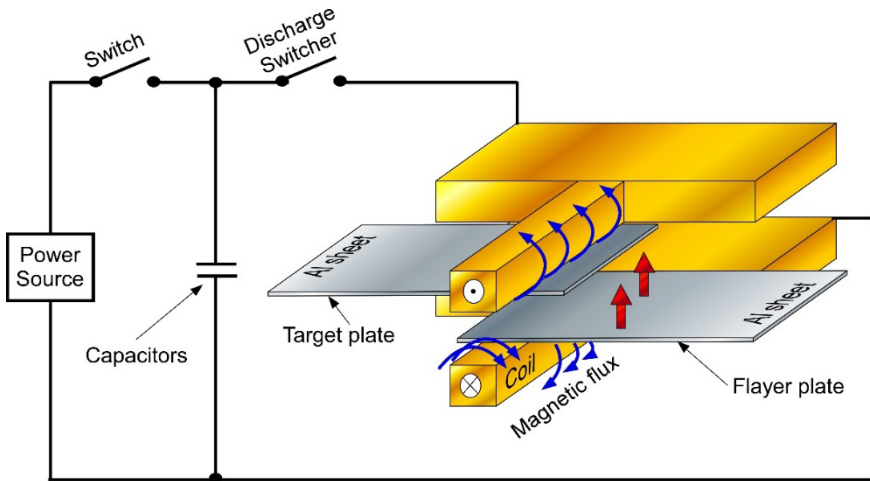

Figure 9: Schematic explanation of magnetic pulse welding.

Easily controllable process parameters, ability to make repeated welding for mass production, energy efficiency and environmentally harmlessness are important advantages of magnetic pulse welding. However, since its parts such as positioning systems and coils have a certain life time, their replacement costs are the disadvantages of the technique (Pereira et al., 2017).

Zhang et al. (Y. Zhang et al., 2010), welded the AA6061 aluminum alloy and copper plates by magnetic pulse welding method. The researchers found that the hardness of the weld interfaces was higher than the base metals. They explained this situation with the ultra-fine grained structure, intermediate dislocation density and deformation twins of the weld interface. In another study (Pereira et al., 2017), AA6083-T6 tubular materials were welded and it was determined that the welded joint exhibits mechanical properties close to the base material. Cui et al. (2019) welded carbon fiber-reinforced plastic and 5A02 aluminum alloy tubes by magnetic pulse welding method. As a result of their experiments, they determined that the tension and torsional strengths of the weld zone were better than the aluminum base material.

7.   Friction stir welding

Friction stir welding is an important metal joining technique, which was invented in 1991 and continues to gain importance day by day. With this technique, all

aluminum alloys can be welded. In addition, aluminum alloys that are impossible to be welded with fission welding methods such as 2XXX and 7XXX can be effectively welded by friction stir welding technique (Khan, Siddiquee, & Khan, 2017; Mishra, De, & Kumar, 2014). The heat required in friction stir welding is obtained from the friction between a non-consumable rotating tool and work piece, and the plastic deformation of the materials to be joined. Due to this plastic deformation, the material flows and recrystallizes simultaneously. Therefore, ultra-fine coaxial grains are formed in the welding area (McNelley, Swaminathan, & Su, 2008). As seen in Figure 10, welding equipment consists of a special cylindrical shoulder and a pin on it, and the design of this tool is the most important phenomenon of the friction stir welding system.
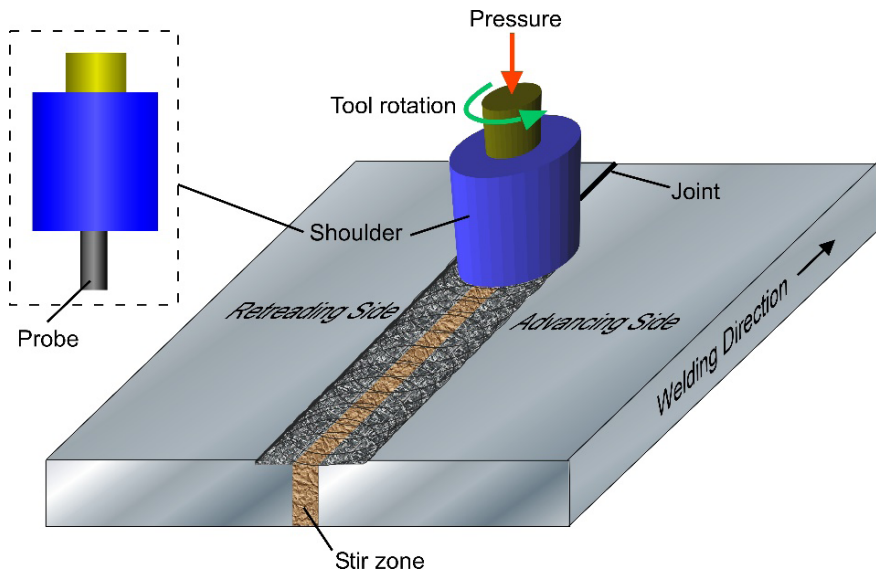

Figure 10: Schematic representation of friction stir welding.

Pin or probe is a special protrusion on the shoulder that makes the friction process by plunging into the material. At the beginning of the welding, by applying sufficient pressure to the shoulder and turning it, the pin is plunged into the surfaces of materials to be welded, and when the shoulder touches to the surfaces of materials to be welded, tool starts to be moved along the welding direction. Rotation of the welding tool in the material heats the material and this localized heating softens material around the pin. In this way, the materials flow from the advancing side towards the retreading side and consolidate behind the pin. Upward flow of the material is restricted by the shoulder. The area where the stirring take place by the pin in the material is called as "nugget". Dynamic

recrystallization takes place in the stir zone and thus grain refinement occurs. The size of the stir zone is slightly larger than the tool pin. Around of the stir zone is the thermo-mechanically affected zone. Grain growth occurs in this area and the hardness is minimum. There is a heat affected zone (HAZ) in between the base metal and thermo-mechanically affected zone. Generally, the hardness of HAZ is lower than the base metal as it is affected by the welding heat (Khan et al., 2017).

In a study conducted Wang et al. (2021), microstructural characterization of friction stir welded joint of 7055-T6 aluminum alloy was performed. They showed that grain refinement occurs due to friction stir welding. The average particle size of the stir zone was 5.9 μm, while the average particle size of the thermo-mechanical effected zone was 6.3 μm. The mechanism of grain refinement has been explained as continuous dynamic recrystallization and geometric dynamic recrystallization. It has been determined that the friction zone and thermo-mechanical effected zone have higher nano-hardness and elastic modulus than the base metal. This change in mechanical properties was attributed to the precipitation in the grain interior. Moreover, it was determined that the HAZ and the thermo-mechanical effected zone had higher creep resistance than the stir zone, and this was ascribed by coarse precipitates. Yu et al. (2021) analyzed the dynamic recrystallization mechanism of 1060 aluminum sheet during friction stir welding. For this, they combined finite element analysis and Monte Carlo simulation with EBSD (Electron Backscatter Diffraction Analysis) characterization results. It was determined that the HAZ region on the retreading side was larger and the microstructure differences were less obvious. It is stated that this is due to the strain and temperature differences on the advancing and retreading sides. As the tool rotation speed increases, the welding temperature increases and the grain boundary movement becomes easier, so coaxial grains may occur. As the welding temperature increases further, strain-free grains grow, the deformed grains disappear, and nucleation and growth stages occur. When the tool rotation speed is slowed down, this provides low heat input and so it is possible to produce the microstructure having finer dynamic recrystallization grains. In another study investigating the of mechanical behavior of friction stir welded AA6083 aluminum alloy (Sivabalan et al., 2021), it was observed that the grain orientation in the nugget region was along the direction of tool movement and the joints produced at a welding speed of 72 mm/min had maximum tensile strength. The ultimate tensile strength of AA-6351 aluminum alloy increases with the friction stir welding speed up to 160 mm/min. However, this is a limit value and the ultimate tensile strength of AA-6351 aluminum decreases above

the this welding speed value (Kumar et al., 2020). In friction stir welding of AA6061 aluminum alloy, it is reported that the pin geometry as well as the tool rotational speed have an important effect on the strength of the weld. It was concluded that a pin having square geometry is better than pins having cylindrical or triangular geometries in terms of tensile strength and bending strength of the weld (Mohapatra & Sarangi, 2020). In friction stir welding of 6061-T6 aluminum alloy (Kalinenko et al., 2020), it was observed that the temperature of the stir zone was between 254 and 416 °C and generally below 300 °C in different welding parameters such as tool rotation speed and welding speed. Therefore, temperature of the weld zone was below the dissolution threshold of the strengthening phase (beta-phase). It is also stated that the main parameter determining the strength of the weld is the welding speed. On the other hand, it is possible to obtain a defect free weld joints in friction stir welding process of AA2014-T6 aluminum alloys with a tool tilt angle varying in between 1 and 3 ° (Rajendran, 2019).

8. Conclusions

In this study, a review was carried out on the application of new welding technologies to aluminum alloys by focusing on laser beam welding, laser arc hybrid welding, electron beam welding, cold metal transfer welding, magnetic pulse welding and friction stir welding techniques. Mechanisms, problems, solutions, advantages and disadvantages of new welding techniques were evaluated in the light of current studies. The general conclusions can be summarized as follows.

- Laser beam welding in aluminum alloys is an important technique for producing high quality and precise joints. The biggest problem in this technique is the formation of pore in the weld zone. On the other hand, the solution to this problem is possible with the modifications such as superimposed beams, oscillating beam and concentrically arranged beams.
- Thanks to the laser-arc hybrid welding technique, the structure and properties of the HAZ region can be directionally controlled. Moreover, the low laser absorption value of aluminum is improved by this technique and spatter formation is minimal.
- In electron beam welding technique, it is possible to obtain a very narrow HAZ region. The biggest problem in this method is the metal vapor cutting the electron beam during welding. Setting the welding speed correctly (usually working at low welding speeds) is the most effective way to solve this problem.

- In cold metal transfer welding of aluminum alloys, it is possible to combine dissimilar aluminum alloys because of the low heat input to the material to be welded. In addition, a welding zone having porosity and sputter-free can be obtained.
- In magnetic pulse welding of aluminum alloys, there is no need for a protective atmosphere and filling material. In addition, HAZ does not occur in the material and the mechanical properties of the welding zone are at a high level.
- Friction stir welding is applicable to all aluminum alloys. It is also a very effective method for joining 2XXX and 7XXX aluminum alloys that cannot be welded with fusion welding techniques. Thanks to this technique, it is possible to obtain welding zones with mechanical properties better than base aluminum alloy.

References

Alexopoulos, N. D., Examilioti, T. N., Stergiou, V., & Kourkoulis, S. K. (2016). Tensile mechanical performance of electron-beam welded joints from aluminum alloy (Al-Mg-Si) 6156. *Procedia Structural Integrity*, 2, 3539–3545. Retrieved from https://doi.org/10.1016/j.prostr.2016.06.441

Babu, S., Panigrahi, S. K., Janaki Ram, G. D., Venkitakrishnan, P. V., & Suresh Kumar, R. (2019). Cold metal transfer welding of aluminium alloy AA 2219 to austenitic stainless steel AISI 321. *Journal of Materials Processing Technology*, 266(November 2018), 155–164. Retrieved from https://doi.org/10.1016/j.jmatprotec.2018.10.034

Bagautdinova, L. N., Basyrov, R. S., Galimzyanov, I. I., Gaysin, A. F., Gaysin, A. Z. F., Gaysin, F. M., & Fakhrutdinova, I. T. (2019). New technology for welding aluminum and its alloys. *Materials Today: Proceedings*, 19, 2566–2567. Retrieved from https://doi.org/10.1016/j.matpr.2019.08.239

Baoqiang, C., Ruijie, O., Bojin, Q., & Jialou, D. (2016). Influence of Cold Metal Transfer Process and Its Heat Input on Weld Bead Geometry and Porosity of Aluminum-Copper Alloy Welds. *Rare Metal Materials and Engineering*, 45(3), 606–611. Retrieved from https://doi.org/10.1016/S1875-5372(16)30080-7

Cao, X., Zhou, X., Wang, H., Luo, Z., & Duan, J. (2020). Microstructures and mechanical properties of laser offset welded 5052 aluminum to press-hardened steel. *Journal of Materials Research and Technology*, 9(3), 5378–5390. Retrieved from https://doi.org/10.1016/j.jmrt.2020.03.064

Casalino, G., Campanelli, S. L., Maso, U. D., & Ludovico, A. D. (2013). Arc leading versus laser leading in the hybrid welding of aluminium alloy using a fiber laser. *Procedia CIRP*, 12, 151–156. Retrieved from https://doi.org/10.1016/j.procir.2013.09.027

Chen, G., Liu, J., Shu, X., Gu, H., & Zhang, B. (2019). Numerical simulation of keyhole morphology and molten pool flow behavior in aluminum alloy electron-beam welding. *International Journal of Heat and Mass Transfer*, 138, 879–888. Retrieved from https://doi.org/10.1016/j.ijheatmasstransfer.2019.04.112

Chen, G., Liu, J., Shu, X., Gu, H., Zhang, B., & Feng, J. (2019). Beam scanning effect on properties optimization of thick-plate 2A12 aluminum alloy electron-beam welding joints. *Materials Science and Engineering A*, 744(December 2018), 583–592. Retrieved from https://doi.org/10.1016/j.msea.2018.12.034

Cui, J., Li, Y., Liu, Q., Zhang, X., Xu, Z., & Li, G. (2019). Joining of tubular carbon fiber-reinforced plastic/aluminum by magnetic pulse welding. *Journal of Materials Processing Technology*, 264(June 2018), 273–282. Retrieved from https://doi.org/10.1016/j.jmatprotec.2018.09.018

Czerwinski, F. (2011). Welding and Joining of Magnesium Alloys. In *Magnesium Alloys - Design, Processing and Properties* (p. 23). IntechOpen. Retrieved from https://doi.org/10.5772/13947

Dursun, T., & Soutis, C. (2014). Recent developments in advanced aircraft aluminium alloys. *Materials and Design*, 56, 862–871. Retrieved from https://doi.org/10.1016/j.matdes.2013.12.002

Feng, J., Zhang, H., & He, P. (2009). The CMT short-circuiting metal transfer process and its use in thin aluminium sheets welding. *Materials and Design*, 30(5), 1850–1852. Retrieved from https://doi.org/10.1016/j.matdes.2008.07.015

Fritzsche, A., Hilgenberg, K., Teichmann, F., Pries, H., Dilger, K., & Rethmeier, M. (2018). Improved degassing in laser beam welding of aluminum die casting by an electromagnetic field. *Journal of Materials Processing Technology*, 253(November 2017), 51–56. Retrieved from https://doi.org/10.1016/j.jmatprotec.2017.10.021

Furukawa, K. (2006). New CMT arc welding process – welding of steel to aluminium dissimilar metals and welding of super-thin aluminium sheets. *Welding International*, 20(6), 440–445. Retrieved from https://doi.org/10.1533/wint.2006.3598

Giampieri, A., Ling-Chin, J., Ma, Z., Smallbone, A., & Roskilly, A. P. (2020). A review of the current automotive manufacturing practice from an energy perspective. *Applied Energy*, 261(October 2019). Retrieved from https://doi.org/10.1016/j.apenergy.2019.114074

Gungor, B., Kaluc, E., Taban, E., & SIK Ş.Ş, A. (2014). Mechanical and microstructural properties of robotic Cold Metal Transfer (CMT) welded 5083-H111 and 6082-T651 aluminum alloys. *Materials and Design*, 54, 207–211. Retrieved from https://doi.org/10.1016/j.matdes.2013.08.018

Hagenlocher, C., Wagner, J., Michel, J., Weber, R., Bachmann, M., Karadogan, C., … Graf, T. (2020). The influence of residual stresses on laser beam welding processes of aluminium sheets. *Procedia CIRP*, 94, 713–717. Retrieved from https://doi.org/10.1016/j.procir.2020.09.124

Kah, P. (2014). Automation of aluminum alloy welding. *International Review of Mechanical Engineering*, 8(1), 145–152. Retrieved from https://doi.org/10.15866/ireme.v8i1.1253

Kalinenko, A., Kim, K., Vysotskiy, I., Zuiko, I., Malopheyev, S., Mironov, S., & Kaibyshev, R. (2020). Microstructure-strength relationship in friction-stir welded 6061-T6 aluminum alloy. *Materials Science and Engineering A*, 793(July), 139858. Retrieved from https://doi.org/10.1016/j.msea.2020.139858

Kang, M., & Kim, C. (2020). Evaluation of hot cracking susceptibility on laser welded aluminum alloy using coaxially arranged multiple-beam laser. *Journal of Laser Applications*, 32(2), 022072. Retrieved from https://doi.org/10.2351/7.0000107

Katayama, S. (2009). Advantages and disadvantages of arc and laser welding. In F. O. Olsen (Ed.), *Hybrid laser–arc welding* (pp. 28–46). Wasgington: Woodhead Publishing Limited.

Katayama, S. (2020). *Fundamentals and Details of Laser Welding*. Singapore: Springer.

Ke, W., Bu, X., Oliveira, J. P., Xu, W. G., Wang, Z., & Zeng, Z. (2021). Modeling and numerical study of keyhole-induced porosity formation in laser beam oscillating welding of 5A06 aluminum alloy. *Optics and Laser Technology*, 133(July 2020), 106540. Retrieved from https://doi.org/10.1016/j.optlastec.2020.106540

Khan, N. Z., Siddiquee, A. N., & Khan, Z. A. (2017). *Friction Stir Welding: Dissimilar Aluminum Alloys*. Taylor & Francis.

Kumar, P., Kumar, R., Hembram, B. K., Murugan, M., Arif, A., & Veerababu, M. (2020). Study of microstructure and mechanical properties of aluminium alloy (AA-6351-T6) using friction stir welding. *Materials Today:*

Proceedings, 27, 1733–1737. Retrieved from https://doi.org/10.1016/j.matpr.2020.03.650

Kurt, H. I., Ergul, E., Yilmaz, N. F., & Oduncuoglu, M. (2020). The Theoretical Overview of the Selected Optimization and Prediction Models Useful in the Design of Aluminum Alloys and Aluminum Matrix Composites. In *Aluminium Alloys* (pp. 1–22). IntechOpen. Retrieved from https://doi.org/10.5772/intechopen.93608

Li, S., Mi, G., & Wang, C. (2020). A study on laser beam oscillating welding characteristics for the 5083 aluminum alloy: Morphology, microstructure and mechanical properties. *Journal of Manufacturing Processes*, 53(January), 12–20. Retrieved from https://doi.org/10.1016/j.jmapro.2020.01.018

Liu, L. M., Yuan, S. T., & Li, C. B. (2012). Effect of relative location of laser beam and TIG arc in different hybrid welding modes. *Science and Technology of Welding and Joining*, 17(6), 441–446. Retrieved from https://doi.org/10.1179/1362171812Y.0000000033

Liu, Y., Sun, Q., Liu, J., Wang, S., & Feng, J. (2015). Effect of axial external magnetic field on cold metal transfer welds of aluminum alloy and stainless steel. *Materials Letters*, 152(2), 29–31. Retrieved from https://doi.org/10.1016/j.matlet.2015.03.077

Malarvizhi, S., Raghukandan, K., & Viswanathan, N. (2008). Fatigue behaviour of post weld heat treated electron beam welded AA2219 aluminium alloy joints. *Materials and Design*, 29(8), 1562–1567. Retrieved from https://doi.org/10.1016/j.matdes.2007.11.005

Manladan, S. M., Yusof, F., Ramesh, S., Fadzil, M., Luo, Z., & Ao, S. (2017). *A review on resistance spot welding of aluminum alloys*. International Journal of Advanced Manufacturing Technology (Vol. 90). Retrieved from https://doi.org/10.1007/s00170-016-9225-9

Mathers, G. (2002). *The welding of aluminium and its alloys*. *Kemampuan Koneksi Matematis (Tinjauan Terhadap Pendekatan Pembelajaran Savi)* (Vol. 53). Abington: Woodhead Publishing Limited.

Matusiak, J., & Pfeifer, T. (2013). The research of technological and environmental conditions during low-energetic gas-shielded metal arc welding of aluminium alloys. *Welding International*, 27(5), 338–344. Retrieved from https://doi.org/10.1080/09507116.2011.600040

McNelley, T. R., Swaminathan, S., & Su, J. Q. (2008). Recrystallization mechanisms during friction stir welding/processing of aluminum alloys. *Scripta Materialia*, 58(5), 349–354. Retrieved from https://doi.org/10.1016/j.scriptamat.2007.09.064

Mezrag, B., Deschaux-Beaume, F., & Benachour, M. (2015). Control of mass and heat transfer for steel/ aluminium joining using cold metal transfer process. *Science and Technology of Welding and Joining*, 20(3), 189–198. Retrieved from https://doi.org/10.1179/1362171814Y.0000000271

Miranda, R. M., Tomás, B., Santos, T. G., & Fernandes, N. (2014). Magnetic pulse welding on the cutting edge of industrial applications. *Soldagem & Inspeção*, 19(1), 69–81. Retrieved from https://doi.org/10.1590/s0104-92242014000100009

Mishra, R. S., & Ma, Z. Y. (2005). Friction stir welding and processing. *Materials Science and Engineering R: Reports*, 50(1–2), 1–78. Retrieved from https://doi.org/10.1016/j.mser.2005.07.001

Mishra, Rajiv Sharan, De, P. S., & Kumar, N. (2014). *Friction Stir Welding and Processing Science and Engineering*. Sprin.

Mishra, S., Sharma, S. K., Kumar, S., Sagar, K., Meena, M., & Shyam, A. (2017). 40 kJ magnetic pulse welding system for expansion welding of aluminium 6061 tube. *Journal of Materials Processing Technology*, 240, 168–175. Retrieved from https://doi.org/10.1016/j.jmatprotec.2016.09.020

Mohapatra, S., & Sarangi, H. (2020). Experimental investigation of tool probe shape and rotational speed on weld quality of friction stir welding of aluminium alloy. *Materials Today: Proceedings*, (xxxx). Retrieved from https://doi.org/10.1016/j.matpr.2020.10.009

Möller, F., & Thomy, C. (2013). Interaction effects between laser beam and plasma arc in hybrid welding of aluminum. *Physics Procedia*, 41, 81–89. Retrieved from https://doi.org/10.1016/j.phpro.2013.03.054

Ni, Z. L., & Ye, F. X. (2018). Ultrasonic spot welding of aluminum alloys: A review. *Journal of Manufacturing Processes*, 35(July), 580–594. Retrieved from https://doi.org/10.1016/j.jmapro.2018.09.009

Oladimeji, O. O., & Taban, E. (2016). Trend and innovations in laser beam welding of wrought aluminum alloys. *Welding in the World*, 60(3), 415–457. Retrieved from https://doi.org/10.1007/s40194-016-0317-9

Omar Cooke, K. (2020). Introductory Chapter: Structural Aluminum Alloys and Composites. In *Aluminium Alloys and Composites*. IntechOpen. Retrieved from https://doi.org/10.5772/intechopen.90569

Onat, A. (2018). Effects of artificial aging heat treatment on mechanical properties and corrosion behaviour of AA6XXX aluminium alloys. *Journal of Chemical Engineering and Materials Science*, 9(2), 17–23. Retrieved from https://doi.org/10.5897/jcems2018.0319

Pereira, D., Oliveira, J. P., Pardal, T., Miranda, R. M., Santos, T. G., Oliveira, J. P., … Santos, T. G. (2017). Magnetic pulse welding : machine optimisation for aluminium tubular joints production. *Science and Technology of Welding and Joining*, 0(0), 1–8. Retrieved from https://doi.org/10.1080/13621718.2017.1355425

Pratap, S., Agrawal, G. K., Nagpal, S., & Kumar, A. (2021). Dissimilar aluminum alloy joint strength is effected by heat addition in friction stir welding (FSW). *Materials Today: Proceedings*, In Press. Retrieved from https://doi.org/10.1016/j.matpr.2020.11.639

Punzel, E., Hugger, F., Dinkelbach, T., & Bürger, A. (2020). Influence of power distribution on weld seam quality and geometry in laser beam welding of aluminum alloys. *Procedia CIRP*, 94, 601–604. Retrieved from https://doi.org/10.1016/j.procir.2020.09.086

Rajendran, C., Srinivasan, K., Balasubramanian, V., Balaji, H., & Selvaraj, P. (2019). Effect of tool tilt angle on strength and microstructural characteristics of friction stir welded lap joints of AA2014-T6 aluminum alloy. *Transactions of Nonferrous Metals Society of China*, 29(9), 1824–1835. Retrieved from https://doi.org/10.1016/S1003-6326(19)65090-9

Sánchez-Amaya, J. M., Boukha, Z., Amaya-Vázquez, M. R., & Botana., F. J. (2012). Weldability of aluminum alloys with high-power diode laser. *Welding Journal*, 91(5), 155–161.

Sánchez-Amaya, Jose Maria, Pasang, T., Amaya-Vazquez, M. R., Lopez-Castro, J. de D., Churiaque, C., Tao, Y., & Botana Pedemonte, F. J. (2017). Microstructure and mechanical properties of Ti5553 butt welds performed by LBW under conduction regime. *Metals*, 7(7). Retrieved from https://doi.org/10.3390/met7070269

Schultz, H. (1993). *Electron beam welding*. *First published in German*. Cambridge: Abington Publishing.

Selvi, S., Vishvaksenan, A., & Rajasekar, E. (2018). Cold metal transfer (CMT) technology - An overview. *Defence Technology*, 14(1), 28–44. Retrieved from https://doi.org/10.1016/j.dt.2017.08.002

Shiganov, I. N., Misyurov, A. I., Trushnikov, A. N., Kholopov, A. A., & Blinkov, V. V. (2017). Hybrid laser-arc welding of aluminium alloys. *Welding International*, 31(1), 67–70. Retrieved from https://doi.org/10.1080/09507116.2016.1213043

Sivabalan, S., Sridhar, R., Parthiban, A., & Sathiskumar, G. (2021). Experimental investigations of mechanical behavior of friction stir welding on aluminium

alloy 6063. *Materials Today: Proceedings*, (In press). Retrieved from https://doi.org/10.1016/j.matpr.2020.07.236

Sobih, M., Elseddig, Z., Almazy, K., & Sallam, M. (2016). Experimental Evaluation and Characterization of Electron Beam Welding of 2219 AL-Alloy. *Indian Journal of Materials Science*, 2016, 1–6. Retrieved from https://doi.org/10.1155/2016/5671532

Starke, E. A., & Staley, J. T. (1996). Application of modern aluminum alloys to aircraft. *Progress in Aerospace Sciences*, 32(2–3), 131–172. Retrieved from https://doi.org/10.1016/0376-0421(95)00004-6

Vogel, N. (2011). *Numerical Simulation and Experimental Investigation of the Fracture Behaviour of an Electron Beam Welded Steel Joint*.

Wang, L., Liu, Y., Yang, C., & Gao, M. (2021). Study of porosity suppression in oscillating laser-MIG hybrid welding of AA6082 aluminum alloy. *Journal of Materials Processing Technology*, 292(May 2020), 117053. Retrieved from https://doi.org/10.1016/j.jmatprotec.2021.117053

Wang, S., Xu, L., Sun, T., Li, G., & Cui, J. (2021). Effects of process parameters on mechanical performance and interfacial morphology of electromagnetic pulse welded joints between aluminum and galvanized steel. *Journal of Materials Research and Technology*, 10, 552–564. Retrieved from https://doi.org/10.1016/j.jmrt.2020.12.047

Wang, W., Yuan, S., Qiao, K., Wang, K., Zhang, S., Peng, P., … Yang, J. (2021). Microstructure and nanomechanical behavior of friction stir welded joint of 7055 aluminum alloy. *Journal of Manufacturing Processes*, 61(December 2020), 311–321. Retrieved from https://doi.org/10.1016/j.jmapro.2020.11.016

Wanjara, P., & Brochu, M. (2010). Characterization of electron beam welded AA2024. *Vacuum*, 85(2), 268–282. Retrieved from https://doi.org/10.1016/j.vacuum.2010.06.007

Xiao, R., & Zhang, X. (2014). Problems and issues in laser beam welding of aluminum-lithium alloys. *Journal of Manufacturing Processes*, 16(2), 166–175. Retrieved from https://doi.org/10.1016/j.jmapro.2013.10.005

Xu, G., Li, P., Cao, Q., Hu, Q., Gu, X., & Du, B. (2018). Modelling of fluid flow phenomenon in laser+GMAW hybrid welding of aluminum alloy considering three phase coupling and arc plasma shear stress. *Optics and Laser Technology*, 100, 244–255. Retrieved from https://doi.org/10.1016/j.optlastec.2017.10.009

Yilbas, B. S., Akhtar, S., & Shuja, S. Z. (2013). *Introduction to Laser Forming and Welding Processes*. (J.P. Davim,Ed.). Springer. Retrieved from https://doi.org/10.1007/978-3-319-00981-0_1

Yu, P., Wu, C., & Lei, S. (2021). Analysis and characterization of dynamic recrystallization and grain structure evolution in friction stir welding of aluminum plates. *Acta Materialia*, In Press, 116692. Retrieved from https://doi.org/10.1016/j.actamat.2021.116692

Zhang, C., Gao, M., Wang, D., Yin, J., & Zeng, X. (2017). Relationship between pool characteristic and weld porosity in laser arc hybrid welding of AA6082 aluminum alloy. *Journal of Materials Processing Technology*, 240, 217–222. Retrieved from https://doi.org/10.1016/j.jmatprotec.2016.10.001

Zhang, C., Gao, M., & Zeng, X. (2016). Effect of microstructural characteristics on high cycle fatigue properties of laser-arc hybrid welded AA6082 aluminum alloy. *Journal of Materials Processing Technology*, 231, 479–487. Retrieved from https://doi.org/10.1016/j.jmatprotec.2016.01.019

Zhang, C., Gao, M., & Zeng, X. (2019). Influences of synergy effect between laser and arc on laser-arc hybrid welding of aluminum alloys. *Optics and Laser Technology*, 120(August). Retrieved from https://doi.org/10.1016/j.optlastec.2019.105766

Zhang, Y., Suresh, S., & Daehn, G. S. (2010). Interfacial ultrafine-grained structures on aluminum alloy 6061 joint and copper alloy 110 joint fabricated by magnetic pulse welding, 4645–4651. Retrieved from https://doi.org/10.1007/s10853-010-4676-0

Zhu, C., Liu, Q., Wu, Z., & Gao, W. (2020). Interfacial microstructure characterization of aluminum/aluminum-lithium joints fabricated by magnetic pulse welding. *Materials Characterization*, 167(July), 110530. Retrieved from https://doi.org/10.1016/j.matchar.2020.110530

A TECHNICAL EVALUATION OF TWO CERAMIC CLAYS FROM THE REGIONS OF INNER WEST AND MID-ANATOLIA

Özgür CENGİZ[1] & Pınar UYAN[2,3]

[1](phD, Assist.Prof.), Afyon Kocatepe University,
Faculty of Fine Arts, Ceramic Department, 03200, Afyonkarahisar, Turkey
e-mail: ocengiz@aku.edu.tr/ ocengiz1@gmail.com
Orcid: 0000-0002-8075-7470

[2](phD, Assist.Prof.), Bilecik Seyh Edebali University, Vocational School,
Metallurgy Programme, 11210, Bilecik, Turkey
[3]Bilecik Seyh Edebali University, Biotechnology Application and Research
Centre, 11230, Bilecik, Turkey
e-mail: pinar.uyan@bilecik.edu.tr
Orcid: 0000-0003-0411-9773

1. Introduction

The combination of ceramic clays in optimal proportions is the main parameter of ceramic tile compositions. Clay and clay-based raw materials are preferred due to the fact that they provide plasticity and raw strength during the shapng process. They greatly affect the color development of the fired product due to the impurity oxide content. As a rule, two types of clay are used: non-plastic (china clay) ceramic clay and thin plastic clay (ball clay). It is a clay containing iron oxide and titanium oxide as minor impurities, along with quartz mineral as the dominant impurity (pollution), both of which have kaolinitic properties. Fine- plastic ball clays are mostly defined as plastic clays because they have fine properties and provide more plasticity in ceramic structures than white sintered kaolinitic china clay (Das, 2005). Although clay minerals give

plasticity (formability) to the ceramic product to be formed, non-plastic raw materials reduce the plasticity of ceramic paste. They generally increase water absorption by reducing the dry resistance of sludge, the dry shrinkage and the shrinkage of firing. Several non-plastic raw materials (feldspar, pegmatite, calcite, etc.) have melting effect in the paste largely due to the effect of the firing temperature and additive ratios and thus provides early sintering of the ceramic paste (Kibici, 2002).

From an archaeological point of view, ceramic products are products that ensure the permanence of clays (raw materials) by firing and are obtained as a result of the natural hardening of their structures under the influence of heat of clays. During firing, a number of chemical and structural modifications (such as dehydration, dehydroxylation, decomposition and formation of new phases, vitrification) occur in clay-containing bodies. These changes completely transform the clay-containing body. This process consists of high temperature and chemical and mineralogical composition of clay, grain size distribution and low pressure mineral transformations affected by the maximum heat treatment temperature, heating rate, firing time and furnace reduced atmosphere. Neo-ormed high-temperature minerals can be nucleated and growth occurs both by replacing them with mineral phases with a complementary chemical structure at the grain boundaries of clay, and by the resulting high-temperature phases. In the mineralogical transformation studies carried out with fired clays, calcium-rich and poor clays were usually emphasized; neoformed phases were recorded as gehlenite, volastonite and anorthite. In the study conducted with dolomite-rich clays in which illite is mainly a mineral alone, the acermanite, monticellite, forsterite, periclas and spinel phases are the neoformed phases after sintering (Trindade 2009). In a similar study, it was again examined whether the mineralogical transformations of calcium-rich and calcium-poor clays were affected by the firing conditions, and it was determined that the initial composition of clay according to temperature was the main factor catalyzing the phases formed during firing (Duminuco, 1998).

The selection of raw materials for ceramic tiles is the most important factor determining the quality of the tile product. Clay type minerals (such as illite, kaolinite, montmorillonite) provide strength in green tile properties (Kumar et al. 2001). Besides, the mineralogical and granulometric properties of raw materials, many factors such as the forming or shaping stage of the production process, firing conditions and thermal variables determine the properties of ceramic products. This is especially significant for illitic-chloritic clays, which are used in the production of floor and wall tiles, bricks, tiles, and in some cases

may contain limestone. It is known that the properties of these ceramic products in the production process depend on the raw material composition and firing temperature (Carretero, 2002). There are many studies aimed at improving the raw material supply area by adding alternative raw materials to the raw materials used in the ceramic industry. According to these studies, in general, raw materials obtained from different places are examined and compared in terms of their physical, mineralogical and chemical properties and the possibilities of use in ceramics, pottery and brick-tile products are evaluated (Correia, 2005).

In one of the studies in which phase changes occurring in kaolinite and illite-rich ceramic bodies were investigated, detailed XRD studies of phases occurred at different temperatures in the developed bodies were carried out and evaluated (Aras, 2004). In another study, the effect of chemical composition on microstructural and mechanical properties of porcelain body was investigated. Accordingly, it has been determined that mechanical strength increases as the amount of alumina in the composition increases (Dondi, 1995). In another similar study, it was shown that the addition of alumina in feldspar significantly increased the bending strength in porcelain bodies (Harada, 1996). It has been found that the addition of fly ash with alumina, silica and iron in its composition increases the hardness, fracture strength and wear resistance of porcelain tiles (Kumar, 2001). Another investigation was carried out regarding the use of Afyon clays in porcelain tile compositions (Tarhan, 2019).

Sanchez-Soto et al. (1994) investigated the effects of kaolinite-pyrophyllite-illite mixtures on grinding and formation of mullite. In their study, the effects of dry grinding (mechanochemical) on the natural mixture consisting of kaolinite, pyrophyllite and illite were investigated. The developments of the materials used were determined using XRD, DTA-TG, SEM techniques and nitrogen absorption devices. The grinding process creates a strong structural alteration of the silicates forming the mixture, creating effects that can be determined by XRD and SEM such as surface area increase, grain size decrease and agglomeration. Significant changes in the DTA and TG curves were observed with grinding. The presence of an exothermic peak at 985 °C, where weight losses and an increase in density and sharpness values occur at low temperatures, was observed with DTA. At least 325 min after grinding using pure silicates such as kaolinite, pyrophyllite and illite. regardless of the presence of kaolinite and illite until grinding, an increase in the density and sharpness values in the exothermic direction was found due to the presence of pyrophyllite in the mixture. This effect is due to the thermal and mechanical properties of the raw materials from pyrophyllite to the formation of mullite. Kaolinite also contributes to the formation of mullite,

but there has been no increase after grinding. It has been determined that the structure of cristobalite is undesirable for grinding longer than 120 min, and it has been considered that this cristobalite is the factor due to the crystallization of amorphous silica. The thermomechanical and microstructural properties of talc-doped porcelain composition containing illite-like clay have been investigated. It was found that there is an optimal amount of talc with the addition of feldspar to ensure complete vitrification at low temperature. It was observed that there was an increase in strength and density values, a decrease in water absorption values with the addition of 3% (wt.) talc. Due to the increase in the high-expansion glassy phase with increased talc addition, a decrease in the residual quartz content, a decrease in thermal expansion values up to 3% (wt.) talc addition and an increase in the high-expansion glassy phase with the addition of large amounts of talc, the opposite effects have begun to be observed (Mukhopadyay, 2003). The addition of talc had little effect on the electrolyte content of the fired body (Kayacı, 2007).

Ferrari and Gualtieri (2005) evaluated the effects of illitic clay on the production of porcelain tile ceramics. In their study, eight clay raw materials with illite content up to 70% (wt.) were added to mixtures containing albite, feldspar and quartz, which are widely used in the production of porcelain tiles at a rate of 35% (wt.). The physical, chemical, mineralogical and thermal properties of each clay are characterized individually. In the study, changes in technological properties due to the presence of illite were studied mineralogically in fired and unfired bodies. The increase of the illite catalyzed the formation of a lower water absorption due to the decrease of the melting point of the glassy phase percentage. Pyroplastic deformation and shrinkage of firing decreased with the content of illite. The presence of illite prevented the formation of the structure of mullite and cristobalite.

According to Sidjanin et al. (2007) investigated the Vickers micro and macro hardness of ceramic floor tile samples consisting of two types of clay materials; kaolinite and illite, carbonate. The samples were prepared separately for all types of clay, pressed dry at a pressure of 25 MPa, fired under laboratory conditions at 960°C and 1050°C, and subjected to freezing and melting regimes for microstructure comparison and hardness comparison before and after firing. According to the results, it was observed that the Vickers microstructure increased due to the increase in the firing temperature, but the expected microstructure was not achieved. The results observed after freezing and melting were the same. In addition, the notch length effect was also studied within the low load hardness test. It should be noted that the hardness has increased as a result of the freezing and melting cycle in samples containing illite-carbonate-based clay material.

In the production of ceramic tiles, clays with oxide-rich content obtained by reducing the firing shrinkage and obtaining high strength values when using iron-containing raw materials below 1% (wt.), the total of these oxides should not be above 6% (wt.) when they are to be used in the production of ceramic products (Mahmoudi, 2008). Sedmale et al. (2013) in their studies, in which they examined the activation of alkali with potassium and sodium hydroxide in illitic clays, it was observed that illitic-quaternary clay changed the illite-type structure with KOH treatment, but did not disrupt it. The main changes occurred in relation to the changes in the A-OH groups O-, where there is a neighbouring Si-layer. This results in a decrease of the sintering temperature and increases the amorphous (glassy) phase development of ceramic samples sintered at 600-700ºC. In addition, it increases the total porosity. In another study, the shrinkage and strength behaviours of quartz and kaolinitic clays in ceramic tile structures were determined and it was found that the bodies containing high kaolinitic clay have the lowest water absorption value and show the highest strength value due to better densification (Das, 2005). There are several studies according to the literatüre, however, there is not any detailed investigation regarding a comparative technical evaluation of illite-based local raw materials which are suitable for use in ceramic industry (Khalfaouri,2006; Khalfaouri, 2009, Khalfaoui, 2011). In a study in which kaolinitic clay (derived from Istanbul) was added to ceramic floor tiling materials instead of clays obtained from Afyonkarahisar and the surrounding region and determined to be illitic, there was no change in the final water absorption values of the tiles; it has been observed that there is some decrease in bending strength. As a result of the study, it was determined that the clays obtained from Afyonkarahisar and Eskişehir and the surrounding region have the potential to be used in the ceramic tile production industry (Çelik, 2010).

Illite is the basic clay-based component used in the preparation of mixtures of traditional ceramic products. Ceramics, especially white-fired porcelain products, generally contain feldspar, quartz and kaolin, smectite and illite clay minerals (Ferrari, 2006). Turkey is a country where there are significant amount of deposits of clay and clayey raw materials. Mostly in Central Anatolia and Inner Western Anatolia, along with Afyonkarahisar, Kütahya, Eskişehir and the surrounding area of Bilecik are the most developed area of Turkey in terms of ceramic production. Illitic-kaolinitic clays are commonly found in Afyonkarahisar and surrounding provinces. In this study, the effect of locally obtained clays on the production process and final product properties of the ceramic bodies to which they were added was investigated. For this purpose,

the clays that are considered to have illitic-kaolinitic properties found in Afyonkarahisar from Inner West Anatolia and Eskişehir from Mid-Anatolia regions of Turkey which were examined in detail and a preliminary evaluation is made on the potential for use for ceramic tile production.

2. Materials and Methods

2.1. Clay Sampling Provinces of Turkey

The clay samples were collected from different areas in two districts of Afyonkarahisar and Eskişehir, Turkey (Figure 1). Codes of the collected samples are A-2 and E.K-2, respectively. The purpose of the selection of the selected two districts was evaluation of the potential of two local raw materials.
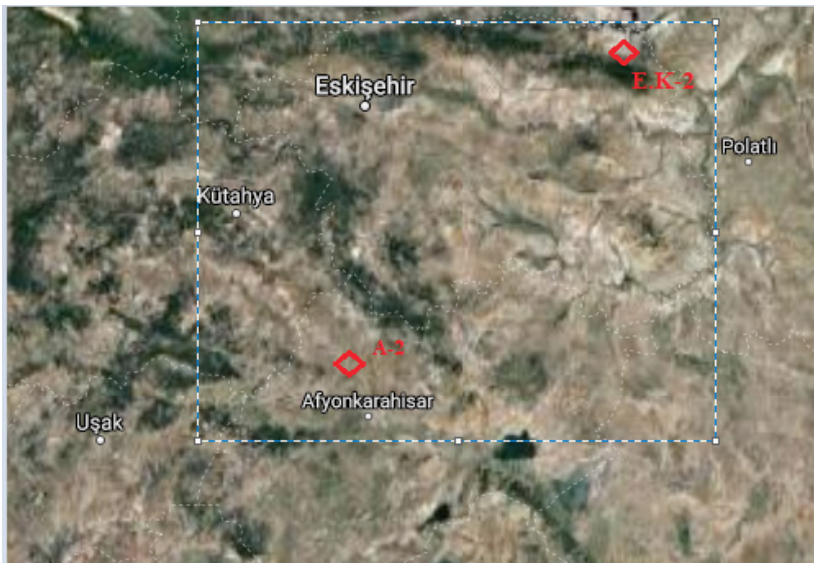
Figure 1. Representative map of the areas and
the provinces of the collected clay samples.

2.2. The Chemical Characterisation of the Evaluated Clays

The chemical composition of the studied clay samples are given in Table 1. It can be concluded that A-2 clay is a type of soft clays, illitic clays regarding the high ratio of K_2O/Na_2O while low ratio of SiO_2/Al_2O_3 the clay minerals are major compared to quartz minerals as well as low particle size distrubition (Trindade, 2009). E.K-2 clay could be evaluated as magnesium-bearing clay owing to high amount of MgO content and high loss on ignition values.

Table 1: Chemical analysis of the clays.

Oxide Content (% wt.)	Raw Material Codes	
	E.K-2	A-2
SiO_2	12.20	77.95
TiO_2	0.12	0.08
Al_2O_3	2.35	13.40
Fe_2O_3	1.10	1.30
CaO	6.77	0.28
MgO	32.87	0.11
Na_2O	0.19	0.29
K_2O	0.32	4.22
SO_3	0.10	0.14
LoI*	41.98	2.20
Total	98.00	99.97

LoI: Loss on Ignition.

3. Results and Discussion

3.1. Technological Properties of the Evaluated Clays

It is already known that he technological properties such as physical, chemical and mineralogical properties effect the entire pre-sintering process (Correia, 2005). The samples were prepared and fired in evaluated temperatures and firing regimes and then mineralogical transformations of the clays were observed.

3.1.1. Thermal Behaviours of the Analysed Clays

DTA curves (Figure 2) demostrate that two differently treated clays samples remarkable changes of curves is observed in the temperature range up to 500ºC. It was reported that this characteristic endo-peak for illite normally is connected with the structural water losing and is visible only for untreated clay in previous studies carried out by Das et al. (2005). Between the temperatures of 500-600ºC, a small amount of dimensional change is observed and the endothermic peak detected at 522.3 ºC and a dehydroxylation occured during α → β quartz inversion. The observed endothermic peak occured at 692.1ºC indicated that the

dehydroxylation occured in the clay sample which contain montmorillonite. The transformation of metakaolin to γ-Al$_2$O$_3$ spinel phase occured at 920 ºC could be observed as an exothermic peak.
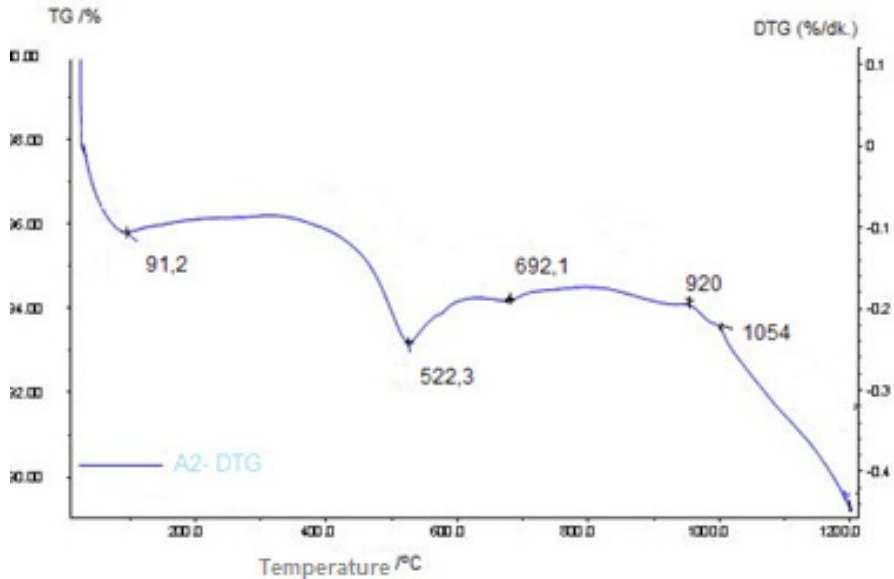

Figure 2. Thermal Analysis of the clay sample A-2.

The properties of the clay sample treated with a temperature of 1000ºC are given in Figure 2. Accordingly, it is observed that the linear shrinkage values increase significantly in proportion to the temperature. Fe$_2$O$_3$ and K$_2$O content in clays affect shrinkage by increasing vitrification. This is evidenced with the several studies conducted, as well (Mahmoudi, 2008; McConville, 2013). However, due to the fact that the clays are illitic, the total shrinkage rates are not relatively high. There are no observed changes for the temperatures between 1050 C and 1070ºC. The behaviour of clays with increasing temperature shows compatibility with the results of the study in which the thermal applications of illitic-chloritic clays were studied (Dondi, 2002). In this case, it can be said that the clays, if they are used in the production of ceramic tiles, meet the characteristics expected in the final samples in order to be used in the production of ceramic tiles (Figure 2 and Figure 3).
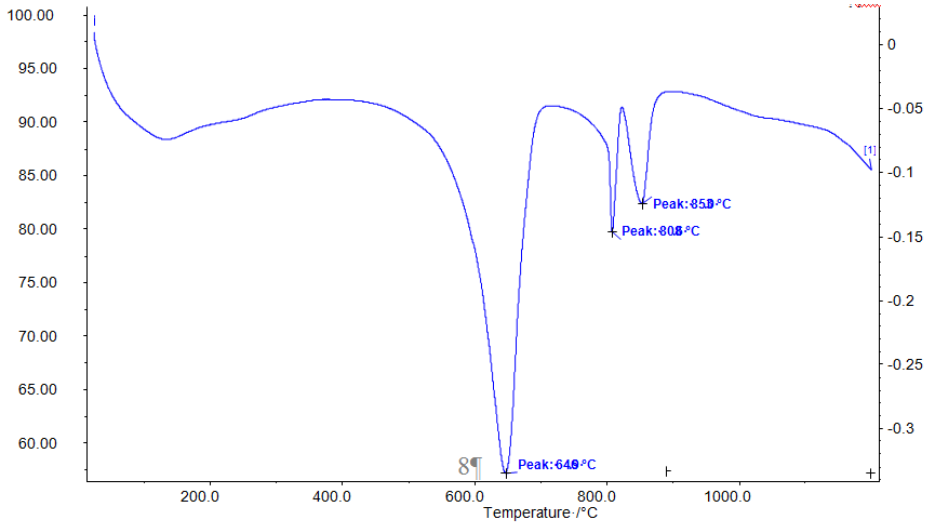
Figure 3. Thermal analysis of the clay sample E.K-1.

Below the temperature of 600ºC, an endothermic peak is detected with a small loss on weight. The weight loss occured due to the water removal below the temperature of 200ºC. Above the temperature of 600ºC, the endothermic reactions were occured due to the quartz and illite content of the clay along with considerable mass change. The detected endothermic peak at temperature of 640ºC indicates the dehydroxylation of kaolinite which is slightly shifted to the higher temperatures above 550ºC related to the illite content of the clay which acts as an inhibitory between the temperatures of 550-900ºC. According to this, the shrinkage and deformation behaviours should be arranged for the preparation of ceramic tile recipes. The endothermic peaks detected at temperatures of 808ºC and 853ºC are related to quartz and illite compounds, respectively.

3.1.2. Phase Analysis of the Evaluated Clays

Clays have a low content of calcium oxide, magnesium oxide and sodium oxide. In addition, the clays contain a certain amount of potassium oxide and iron oxide, as well as a large amount of silicon dioxide and aluminum oxide (Table 1). In the XRD patterns of clays, it is observed that A1 clay contains mainly illite-kaolinite, as well as kaolinite, quartz, and also orthoclase and montmorillonite content (Figures 4 and 5).

According to the results of the XRD analysis given in Figures 4 and 5, it was seen that the clays are predominantly illitic in structure, as well as containing monmorillonite, quartz and kaolinite and orthoclase. Therefore,

it can be said that potassium is found as major oxide which forms layers and sodium or calcium were replaced by potassium in the layers.
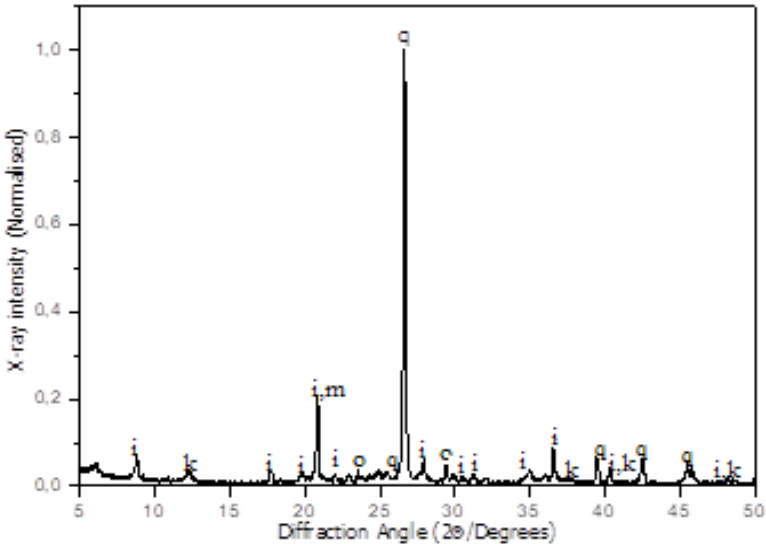

Figure 4. Phase analysis of the clay sample A2
(q: quartz, m: montmorillonite, i: illite, k: kaolinite, o: orthoclase).

Afyonkarahisar and Eskişehir provinces are being evaluated in terms of local and alternative raw material sources and should be evaluated in terms of their suitability for the production process due to the fact that they are close to the region, which is an important base for the production of ceramic tiles and other products. In this study, a technical investigation of the clays that have been carried out to determine whether the clays are suitable for use within the context of the potential reserves of Afyonkarahisar and the surrounding region. Thus, the amount of reserves should be determined in terms of the fact that the region is located near the primary ceramic material production center, the availability of a sustainable resource in production, the producers of the relevant manufacturing industry should be evaluated. In this study, the technical properties of clays, which are known to be suitable for ceramic porcelain and floor tile production process, are evaluated. In this aspect of the investigation, it can be said that this is a preliminary study that will serve as a source for other uses of clays. However, further studies can also be carried out to determine the most suitable clays for the development of the ceramic properties to meet the standards (EN ISO 10545).
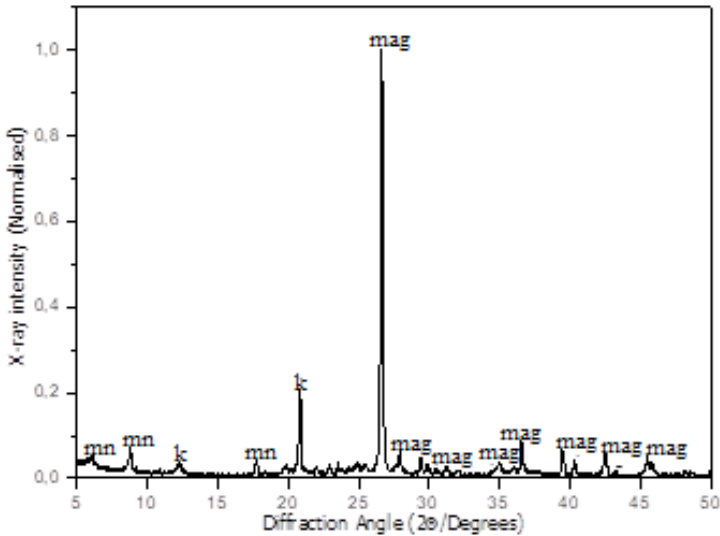
Figure 5. Phase analysis of the clay sample
E.K.-2 (mag: magnesite, k: kaolinite, mn: montmorillonite).

4. Conclusion

i. It has been determined that it is appropriate to use mica-type and/or illite-kaolinitic clays found in Afyonkarahisar and surrounding deposits as potential ceramic raw materials in accordance with the analyzes carried out.

ii. The samples were examined by scanning electron microscope (SEM) in order to determine the amount of glassy phase and the degree of crystallisation. It has been observed that the recrystallised phases (recrystallisation) formed together with the viscous (liquid) phase are controlled mainly by minerals containing potassium and clay minerals containing iron oxide.

iii. It is known that the phases formed by neo-formation process have a small amount of influence on the development of technological properties. In addition, the firing behavior of clays can be adjusted for the purpose of their use in the ceramic industry.

iv. As a result of detecting the transformations that occur with the firing of illitic-kaolinitic clays, it was determined that these clays with existing deposits are potential ceramic raw materials in terms of the advantage of low-cost transportation due to the fact that the reserves where they are supplied are close to the production sites.

Acknowledgement

References

Aras, A. (2004). The change of phase composition in kaolinite and illite- reach clay-based ceramic bodies. *Applied Clay Science*, 24, 257-269. doi: 1016/j.clay.2003.08.012

Carretero, M.I., Dondi,M., Fabbri, B., Raimondo, M. (2002). The influence of shaping and firing technology properties of calcereous and non-calcareous illitic, chloritic clays. *Applied Clay Science,* 20(6), 301-306. doi: 10.1016/S.0169-1317(01)00076-X

Correia, S.L., Curto, K.A.S., Hotza, D. Segadaes, A.M. (2005). Clays from southern Brazil: Physical, chemical and mineralogical characterization. *Materials Science Forum*, 498-499, 447-452, 2005. doi: 10.4028/www.scientific.net/MSF.498-499.447

Cuevas, J., Leguey, S., Garralon, A., Rastrero, M.R., Procopio, J.R., Sevilla, M.T., Jimenez, N.S., Abad, R.R., Garrido, A. (2009). Behavior of kaolinite and illite-based clays as landfill barriers. *Applied Clay Science*, 42(3-4), 497-509. doi: 1016/j.clay.2008.06.017

Çelik, H. (2010). Technological characterization and industrial application of two Turkish clays for the ceramic industry. *Applied Clay Science,* 50, 245-254. doi: 1016/j.clay.2010.08.005

Das, S., Dana, K., Singh, N., Sarkar, R. (2005). Shrinkage and strength behaviour of quartzitic and kaolinitic clays in wall tile compositions, *Applied Clay Science*, 29, 137-143. doi: 10.1016/j.clay.2004.10.002

Dondi M., Fabbri B., Manfredini T., Pellacani G.C. (1995). Microstructure and mechanical properties of porcelainised stoneware tiles. *Proceedings of the Fourth Euro-Ceramics, Floor and Wall Tiles*, 319-321.

Duminuco, P., Messiga, B., Riccardi, M.P. (1998). Firing process of natural clays: Some microtextures and related phase compositions. *Thermochimica Acta*, 321(1-2), 185-190. Doi: 10.1016/S0040-6031(98)00458-4

Ferrari, S., Gualtieri, A.F. (2006). The use of illitic clay in the production of stoneware tile ceramics. *Applied Clay Science*, 32(1-2), 73-81. doi: 10.1016/j.clay.2005.10.001

Harada, R., Sugiyama, N., Ishida, H. (1996). Al_2O_3-Strengthened feldspathic porcelain bodies: Effects of the amount and particle size of alumina. *Ceram. Eng. Sci. Proc.*, 17(1), 88-98. doi: 10.1002/9780470314807.ch14

EN ISO 10545 (2018). Ceramic Tiles: Standardization, The International Organization for Standardization.

Jordan, M.M., Sanfeliu, T., de la Fuente, C. (2001). Firing transformations of Tertiary clays used in the manufacturing of ceramic tile bodies. *Applied Clay Science*, 20(1-2), 87-95. doi: 10.1016/S0169-1317(00)00044-2

Kayacı, K. (2007). *Karaköy (Bilecik) yöresi mikrogranitinin jeolojisi ve seramik bünyelerde kullanım olanaklarının araştırılması.* (Unpublished masters thesis). İstanbul Teknik Üniversitesi, Fen Bilimleri Enstitüsü, İstanbul.

Kacim, S., Hajjaji, M. (2003). Firing transformations of a carbonatic clay from the High-Atlas, Morocco. *Clay Minerals*, 38, 363-367. doi: 10.1180/0009855033830102

Khalfaouri, A., Kacim, S., Hajjaji, M. (2006). Sintering mechanism and ceramic phases of an illitic-chloritic raw clay. *Journal of European Ceramic Society*, 26, 161-167. doi: 10.1016/j.jeurceramsoc.2004.10.30

Khalfaouri, A., Hajjaji, M. (2009). A chloritic-illitic clay from Morocco: Temperature-time-transformation and neoformation. Applied Clay Science, 45, 83-89. doi: 10.1016/j.clay.2009.03.006

Khalfaouri, A., Hajjaji, M. (2011). Effect of heating time on phases transformation of an illitic-chloritic clay. *Journal of Optoelectronics and Advanced Materials*, 3 (3), 127-128.

Kibici, Y. (2002). *Seramik hammaddeleri ve teknolojik özellikleri.* Afyonkarahisar: Afyon Kocatepe Üniversitesi Yayınları.

Kumar, S., Singh, K.K., Ramachandrarao, P. (2001). Effects of fly ash additions on the mechanical and other properties of porcelainised stoneware tiles. *Journal of Materials Science*, 36, 5917-5922. doi: 10.1023/A:1012936928769

Mahmoudi, S., Srasra, E., Zargouni, F. (2008). The use of Tunisian Barremian clay in the traditional ceramic industry: Optimization of ceramic properties. *Applied Clay Science*, 42, 125-129. doi: 10.1016/j.clay.2007.12.008

McConville, C., Lee, W.E. (2005). Microstructural development on firing illite and smectite clays compared with that in kaolinite. Journal of the American Ceramic Society, 88 (8), 2267-2276. doi: 10.1111/j.1551-2916.2005.00390.x

Sedmale, G., Korovkins, A., Seglins, V., Lindina, L. (2013). Application of chemical treated illite clay for development of ceramics products. *IOP Conf. Series: Materials Science and Engineering*, 47 (1), 012056. doi: 10.1088/1757-899X/47/1/012056

Sidjanin, L., Ranogajec, J., Rajnovic, D., Molnar, E. (2007). Influence of firing temperature on mechanical properties of roofing tiles, *Materials and Design*, 28, 941-947. doi: 10.1016/j.matdes.2005.10.002

Tarhan, M., Tarhan, B. (2019). Afyon kilinin porselen karo bünyelerde kullanımının araştırılması, *Uluslararası Mühendislik Araştırma ve Geliştirme Dergisi,* 11(1), 275-281. doi: 10.29137/umagd.433307

Trindade, M.J. (2009). Mineralogical transformations of calcerous rich clays with firing: A comparative study between calcite and dolomite rich clays from Algarve, Portugal. *Applied Clay Science*, 42, 345-355. doi: 10.1016/j.clay.2008.02.008

AN ECONOMICAL AND SUSTAINABLE TYPE OF ASPHALT PAVEMENT: CHIP SEALS

Cahit GÜRER[1]

[1](Assoc.Prof.) Afyon Kocatepe University
Engineering Faculty, Department of Civil Engineering,
03200, Afyonkarahisar, Turkey
Eposta: cgurer@aku.edu.tr
ORCID: 0000-0003-1413-2357

1.   Introduction

Chip seals is a type of thin layer asphalt pavement generally used in the low volume roads in countries such as Turkey, New Zealand, South Africa and Australia. It comprises a uniformly sized stone, aggregate or "sealing chip" embedded in a 1 to 2 mm thick film of bituminous binder, provide smooth and thin waterproofing layer as the top surface of a pavement. It can be applied on the granular base layer, as well as widely used on asphalt pavements for preventive and maintenance purposes. Generally, chip seals are used to provide a smooth rolling surface, to create a waterproof surface on the pavement, and to increase the friction resistance of road surfaces (Gürer 2010). It is not taken into account when calculating the load-bearing capacity of the pavement, as it has a very limited load-bearing capability. The fact that their thickness is less than 25 mm has an effect on the limited load carrying capacity. Chip seals are a good road pavement type if used correctly. It consists of a single layer of asphalt binder that is then covered by a single layer of aggregate. The aggregate is then embedded into the binder by rolling, and that process is followed by sweeping the excess stone from the surface of the road using rotary brooms (Gransberg and James, 2005).

Important factors such as aggregate, bitumen, available materials such as ground condition, and traffic capacity should be carefully assessed before

deciding whether to use a chip seal (Asphalt Institute, 1989). Generally, chip seals are applied on roads where the average daily number of heavy commercial vehicles is less than 500 in both directions or the total number of equivalent standard axle loads in one direction during the project is less than 3,000,000. However, the weather conditions, operator, and equipment usage during the construction affect the chip seal's performance. Preventive and maintenance purposed chip seals on HMA not only correct the appearance of the old pavement by filling the capillary cracks, but also provide the structural stability of the pavement by protecting it against external effects such as oxidation and aging (Banihatti, 1994).

Because of the easy application, good durability, a significant increase in road surface friction resistance, application with limited materials, rapid opening to traffic of roads, and importantly low-cost mostly preferred by the road construction administrations on the rural roads. (Gürer 2010, Nam et al. .2014). The fact that chip seals require less material to manufacture is also important in terms of sustainability, resource conservation, and the environment.

2. Materials and Construction of Chip Seals

2.1. Aggregates

Aggregate selection is important to determining which type of chip seal to use, which type of binder to design for, and which type of construction procedures to specify. The quality of aggregate is important to the general success of the chip sealed road pavement, and quality involves a number of constructability issues about using aggregates that are clean, durable, and abrasion resistant.

The percent of flat particles used in chip seals must be within the values specified in the specification and resistant to abrasion, fragmentation, and weather effects. In addition, the aggregates used in the chip seals should have enough stripping strength and adhesion properties. Otherwise, the chip-sealed pavement will not be able to provide the desired impermeability and it will deteriorate rapidly. The adhesion properties of aggregates also depend on whether the material is clean and does not contain organic and soft materials. In order for the aggregate particles to provide good adhesion, it must be crushed stone and cubic shape. Cubical aggregate tend to lock together and provide better long-term retention and stability (Gransberg and James, 2005).

The gradation values of the aggregate should also be in accordance with the values specified in the technical specifications of the roads. These values may vary according to the climatic characteristics of each region. Table 1. shows

the specification limits of Turkey for the aggregates to be used in surface coating (KGM, 2013). The five different chip seal gradations applied in Turkey and US are given in Table 2 and 3 as respectively. Generally uniform type gradation is used in chip seals.

Table 1. Chip seal aggregate properties for
Turkish Highway Specifications (KGM 2013)

Aggregate Properties	Standard	Limit Value
Los Angeles Abrasion Loss, Maximum %	CEN EN 1097-2 (ASTM C-131)	35
Na_2SO_4 Soundness loss, maximum %	CEN EN 1367-1	12
Crushing Value, minimum % (by weight) - At least two sides of the 4.75 mm sieve for Type 1, Type 2,	-	60
- At least two sides of the 2.00 mm sieve for Type 3, Type 4,	-	60
Stripping Resistance, minimum %	KGM 2013	50
Vialite Adhesion Test, max dropped aggregate particle	KGM 2013	12
Flakiness Index, maximum %	CEN EN 933-3	30
Polishing Stone Value, minimum	BS 812	0,50

Table 2. Typical chip seal gradations applied in Turkey (KGM 2013)

Sieves		% Passing				
inch	mm	Type A	Type B	Type C	Type D	Type E
1	25	100	100			
¾	19	0-20	90-100	100		
½	12,5	0-10	0-20	90-100	100	
3/8	9,5		0-10	0-20	90-100	100
¼	6,3					90-100
No:4	4,75	0-2	0-2	0-2	0-20	60-85
No:10	2,0				0-2	0-2

Table 3. Typical chip seal gradations applied in US (Gransberg and James 2005)

Sieve Size (inch)	Alaska	Arizona (Low Traffic)	Arizona (High Traffic)
½	100	100	100
3/8	90-100	100	70-90
¼	-	70-90	0-10
No:4	10-30	1-10	-
No:8	0-8	0-5	0-5
No:40	-	-	-
No:200	0-1	0-1	0-1

2.2. Binders

Bituminous binder acts as the material that adheres the aggregates to the surface. To construct a good chip sealed road pavement is only possible with the selection of suitable bituminous binders. Binders generally consist of penetration bitumen and bituminous emulsions, which must be heated to the appropriate fluidity in order to be sprayed. For chip seals, it is necessary to choose a suitable bituminous binder for the climatic conditions of each region. When choosing binder material:

- climatic conditions of the region where chip seal will be performed,
- Weather conditions at the time of application,
- Humidity and wind conditions,
- Condition of the surface to be applied,
- Type, type and condition of the aggregate to be applied,
- Machine park and machine type and etc.

should be taken into account (McLeod 1969, Gürer 2010). Generally, binder types for chip seals are given in Table 4. Binder application amounts although it varies according to the factors such as traffic, aggregate maximum diameter etc. it is approximately 0.75-1.75 l/m².

   The disadvantage of using penetration bitumen is that it must be heated and applied hot. Usually, soft penetration bitumen is used. On the other hand, if penetration bitumen is used, it is possible to form the aggregate layer to be spread on second layer of chip seal is coarser grained material.

Table 4. Binder types used in chip seal constructions (KGM, 2013)

Prime Coat Binder	Binder Type	Standard
Fm 2 B 2, Fm 2 B3	Cutback Bitumen	TS EN 15322
C50B9-4, C50B9-5, C55B9-4, C55B9-5, C60B9-4, C60B9-5	Cationic Bitumen Emulsions	TS EN 13808
Chip Seal Binder	**Binder Type**	**Standard**
B 70/100, B 100/150, B160/220	Penetration Bitumen	TS EN 12591
C60B2-3, C60B2-4, C60B2-5 C65B2-3, C65B2-4, C65B2-5	Cationic Bitumen Emulsions	TS EN 13808 Table 400
C60BP2-3, C60BP2-4, C65BP2-3, C65BP2-4	Cationic Modified Bitumen Emulsions	TS EN 13808

Primer coat layers are used on an unbound granular basecourse to control dust and provide impermeability (Gürer 2010). Generally, cutback bitumen or asphalt emulsions are used in primer coat layers. The application rate is changed between 1.00-2.50 l/m^2.

3. Construction Methods

Chip seals are pavements that can be constructed quickly by using more than one construction machine by a method known as train operation. However, the type of machines and operator experience are very effective in chip sealed road performance. Figure 1 shows a chip sealed road surface with aggregates locked under traffic loads.

Figure 1. Single layer chip sealed road surface on unbound base layer

How the voids between the spread chip sealing aggregates changes over time can be seen in Figure 2.
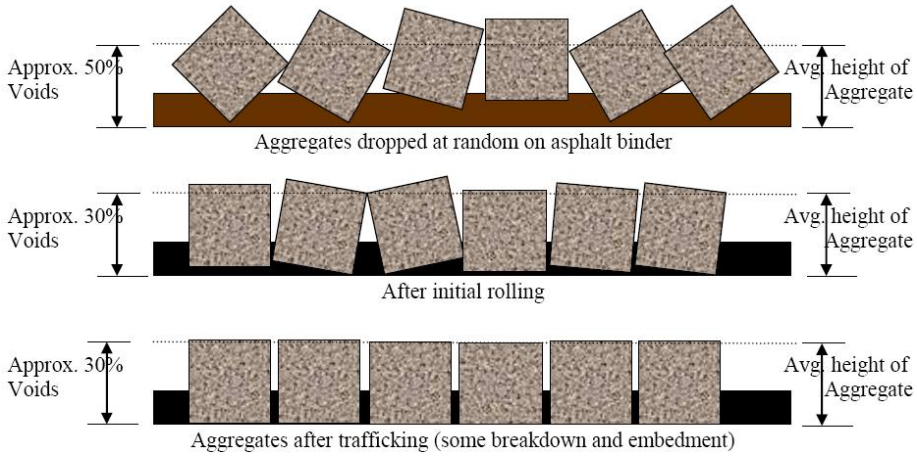

Figure 2. Voids between the spread chip
sealing aggregates changes over time (Islam 2010)

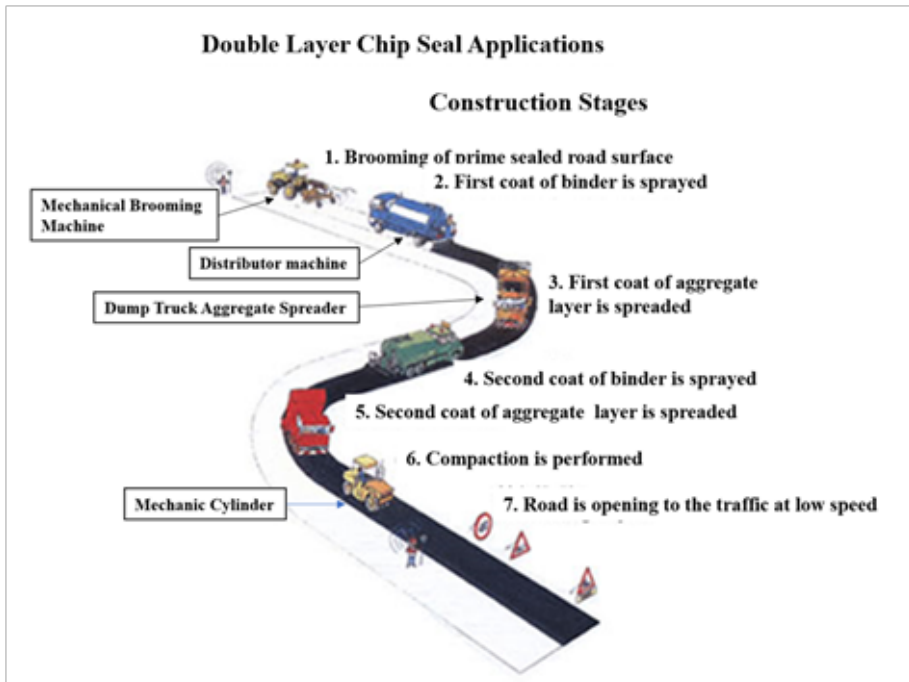Double layer chip seal's construction stages were shown in Figure 3.

Figure 3. Double layer chip seal's construction stages (Gürer 2007)

The construction of a single layer chip sealing consists of the following steps:

Surface preparation: Surface defects, such as potholes, are repaired and the existing surface is cleaned (e.g., by a brooming machine).

Prime coat application: It is the uniform application of low viscosity bitumen emulsion or cutback bitumen onto the compacted granular basecourse. If a prime coat is used, its main function is to ensure a good bond between the larger Stones in the basecourse and the road surfacing (TNZ 2005).

Binder application: Typically, an asphalt emulsion is applied from a spray truck to the surface of the existing pavement.

Aggregate application: A thin aggregate cover is spread over the asphalt material before it has set (see Figure 2). The aggregate usually has a uniform gradation. The aggregate application rate varied from 11 to 12 kg/m2 (Griffith and Hunt 2000).

Aggregate embedding: A roller (usually a pneumatic tire roller) is used to push the aggregate into the asphalt material and seat it firmly against the underlying pavement. Generally, about 50 percent of each aggregate particle should be embedded in the asphalt material (see Figure 4) after final rolling. About 70 percent of each aggregate particle will be embedded after several weeks of traffic. It is common to place an aggregate "choke stone" on top of the uniformly graded larger aggregates after embedment. Choke stone is essentially a finer aggregate gradation (e.g., less than 12.5 mm) used to make a denser aggregate matrix at the level of embedment. This denser matrix helps prevent excessive aggregate loss due to traffic loads.

3.2. Equipment Used in the Chip Seals Construction

3.2.1. Asphalt Distributors

Asphalt distributor is the most important equipment for chip sealing applications. It is used to apply a certain amount of binder material to the road surface homogeneously. The distributor bar and spray nozzles should be adjusted to give a uniform binder application to the road surface. The dimensions of the sprayed binder tracks, the aperture angles are directly related to the position and height of the spray bar (Robert et al.1991) (Figure 4). Asphalt distributor consists of an insulated tank with a capacity of 3000 to 20000 liters mounted on a truck or trailer. Many distributors also have a heating system to keep the binder at the proper spray temperature.
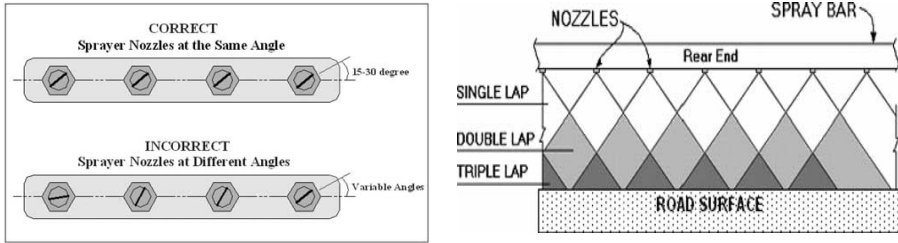
Figure 4. Spray bar nozzle alignment and
spraying lab coverage (Gransberg and James 2005).

3.2.2. Aggregate Spreader

The aggregate spreader is the most important equipment after the asphalt distributor. Provided that it is used correctly, a good aggregate spreader prevents aggregate loss and makes a uniform paving. Aggregate pavers consist of three main types: the dump truck paver, which is attached to the tailgate of the back of the truck, and another type, which is attached to the rear door of the truck; but it is a pave box mounted on wheels to support the aggregate spreader. A third type is the self-propelled aggregate paver, which is mounted on a wheel that pulls the truck and provides the power needed for paving (Figure 5). (KGM, 2013; Asphalt Institute, 1989).

a

b

c

d

Figure 5. Equipment Used in Chip Sealing: a) Asphalt distributor b)Aggregate spreader (NCDOT 2015) c) Mechanical brooming machine (NCDOT 2015) d) Pneumatic tire and static steel wheel roller (NCDOT 2015)

3.2.3. Mechanical Brooms

If the surface to be coated is not completely clean, the binder may not adhere to the road surface. Therefore, it is necessary to clean the surface before spraying the bituminous binder. When using brooms; It may be necessary to clean with water to meet clean air criteria or to remove loose aggregate particle. Sweeping can be used to remove loose particles after the pavement is complete or the bituminous binder was cured properly. Light broom pressures are used to prevent the displacement of aggregate particles embedded in the bituminous binder. The most used ones are the rotary brooms pulled by a rubber wheel tractor (Gürer 2010).

3.2.4. Bitumen Relay Tank

These machines are used to transport the required bituminous material from the main tanks or mobile ground tanks to the distributors, to heat them to the desired degree, and to mix some additives uniformly before the distributor. They are available in various models and sizes.

3.2.5. Rollers

The compaction of aggregate particles is an important part of chip sealing construction. The purpose of the rolling is to ensure that the aggregate has a good connection with the binder and to correct the irregularities that occur during the aggregate spreading. Thus, the destructive effect of traffic is reduced. For this, it is sufficient to pass the roller once or twice. Increasing the number of passes causes segregation due to the breaking of small and soft aggregate particles. Therefore, a pneumatic tire roller with tire pressures of 415-620 kPa is recommended for chip sealing applications. If it is not possible to supply a pneumatic tire roller, steel bandaged rollers weighing not more than 8 tons should be used and the compaction should be performed very carefully.

4.   Types of Chip Seals

4.1. Single Layer Chip Sealed Road Pavement

Single-layer chip seals are consists of the application of a single layer of bituminous material to the road surface followed by a single layer of aggregate

spreading with as much one dimension gradation as possible. It is the most economical type of asphalt pavement type. It is generally preferred on roads with low and medium traffic volumes (Holtrop, 2008). The chip-sealed road pavement thickness is equal to the nominal maximum size of the aggregate thickness. In this type of chip sealing, the aggregate sizes are almost the same (Figure 6).
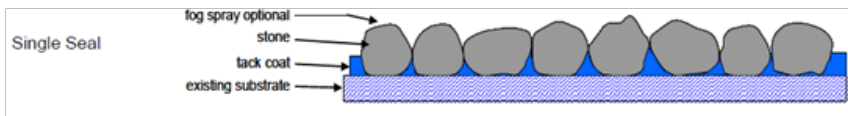

Figure 6. Single-layer chip sealed road pavement cross-section (SANRAL 2007)

4.2. *Double Layer Chip Sealed Road Pavements*

Double layer chip seals are formed by constructing two or more chip seals on top of each other. Multi-layer chip seal is more durable than single-layer chip seals. Its impermeability against water is also better than a single-layer chip seal (Asphalt Institute, 1989). The noise level in traffic is also less. For this reason, double-layer surface coatings are preferred on sloping road sections where heavy traffic volume is high (Gransberg and James, 2005). (Figure 7).
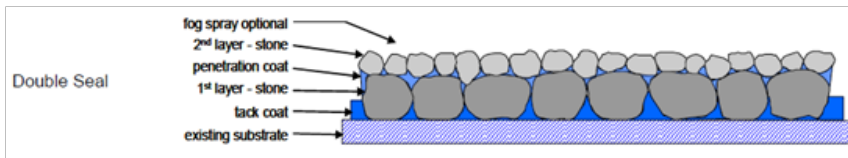

Figure 7. Double-layer chip sealed road pavement cross-section (SANRAL 2007)

There are also Choked, Cape, sandwich type inverted double seal chip sealing applications applied with different techniques. Slurry seals and sand seals are surface coatings that are generally applied over the asphalt concrete layers. These seal coating types are known as preventive and maintenance purposed seal coatings (Gürer 2010). In the Choked type chip seal application, it is the seal coat application that is carried out by spreading and compacting the second aggregate with a smaller diameter without using binders on the voids formed in the single-layer chip seal (Figure 8). Smaller-diameter aggregates are locked into the space between coarser aggregates by the moving of the axle loads. The application of Choked type chip sealing, especially in the areas where the traffic is rotating, prevents the aggregates from premature raveling before the curing of the chip seal is completed (Gransberg and James, 2005).
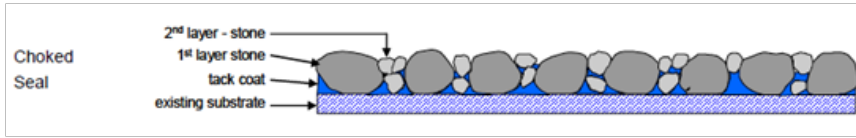
Figure 8. Choked type chip sealed road pavement cross-section (SANRAL 2007)

Another double-layer chip sealing application is the Cape type chip sealing. Since this type of chip sealing was developed in the Cape region of South Africa, it takes its name from that region (Gransberg and James, 2005). It is a dense, smooth-surfaced, and long service life chip sealed pavement with good skid resistance when applied correctly. This type of pavement provides a durable and impermeable surface. The rich mortar mixture on a single-layer chip sealing eliminates the problem of loose aggregates, locking the aggregates in place well, and reducing traffic noise (Solaimanian and Kennedy, 1998). In Cape-type chip sealing, a single or double-layer slurry seal or micro-surfacing is applied on the first layer chip sealing with one-dimensional gradation. If a single layer slurry type seal coating is to be applied, a single layer chip sealing is applied using aggregate with a nominal diameter of 13.2 mm. If a double layer slurry sealing is to be applied, a chip sealing application is performed using an aggregate with a nominal diameter of 19 mm. Generally, the slurry seal application is applied manually until the voids between the single-layer chip sealing layer are filled. It is successfully applied on roads with 20000 equivalent light vehicles in one direction according to SANRAL (one heavy vehicle is equivalent to 40 light vehicles according to South African Specifications). Figure 2.6. shows the Cape-type chip sealed road pavement section (Distin, 2008).
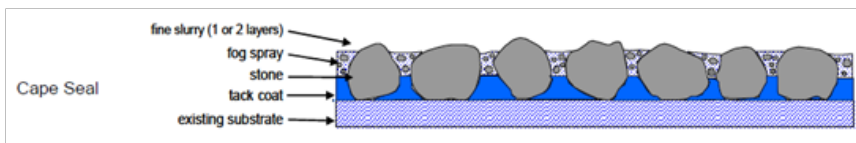

Figure 9. Cape type chip sealed road pavement cross-section (SANRAL 2007).

It is a double-layer seal coating application in inverted chip sealing. Since the aggregate spread in the first layer is smaller in size than the aggregate in the second layer, this type of seal coating is called an inverted chip sealing. This type of chip seals is generally used for the repairing of bleeding surfaces. Australian Highways Administration successfully apply it on the routes with an average daily traffic of 30000.

These chip seals are also used to repairing the deteriorated surface texture uniformity in the transverse direction (Gransberg and James, 2005). Inverted chip seals are used, especially in areas where there is a high risk of aggregate embedment and soft base material (Distin, 2008; Holtrop, 2008). Figure 10 shows a cross section of the inverted chip sealed road sections.
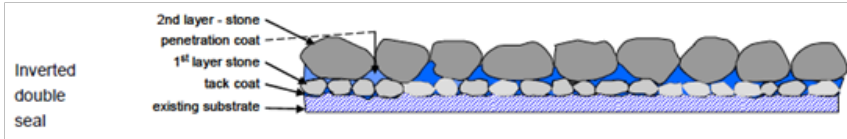

Figure 10. Inverted type chip sealed road pavement cross-section (SANRAL 2007)

In sandwich type chip sealing, a single layer of binder layer is applied between two sandwich-shaped aggregate layers (Figure 2.8.). This type of chip sealing is especially used to repairing the surface texture that was raveled (Gransberg and James, 2005).
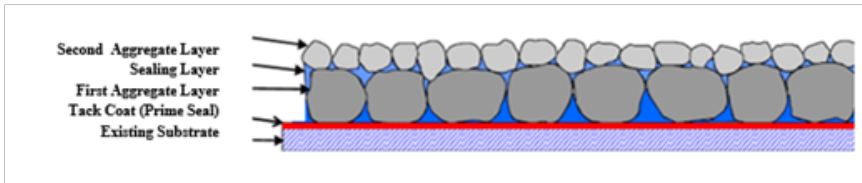

Figure 11. Sandwich type chip sealed road
pavement cross-section (SANRAL 2007)

Especially on asphalt surfaces that are highly oxidized and have capillary cracks, single layer chip seals reinforced with geotextiles are applied for protective and preventive maintenance purposes. During the application, after the first layer of bitumen, the geotextile is carefully laid and rolled, then a single layer of chip sealing is applied on the geotextile (Gransberg and James, 2005). The use of geotextiles in low volume roads such as chip sealing greatly improves it's performance (Marienfeld, 1997). Figure 12 shows the section of surface coating reinforced with geotextile.
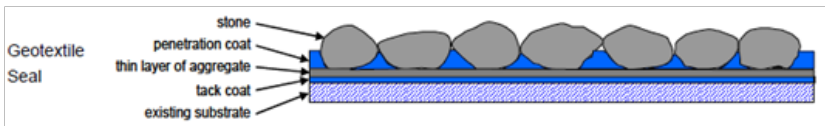

Figure 12. Geotextile reinforced chip
sealed road pavement cross-section (SANRAL 2007)

Slurry type seal coats are a type of surface coating generally used for protective and preventive maintenance (Figure 13). They are especially used in the renewal

of aged asphalt pavement surfaces and it's surface texture, in filling the rutting deformations before surface regeneration, and in the construction of Cape type chip sealing (Rasmussen, 2002; Distin, 2008). In this type of sealing, emulsion bitumen is used as binder, and different gradations and types of aggregates are used depending on the application. Aggregate and binder are mixed in a mobile mixing machine. Portland cement, hydrated lime or aluminum sulfate can be added to cure the mixture. The slurry type seal coat is spread and paved on the surface with a paving box attached to the rear of a mixing truck (Jahren et.al., 1999).
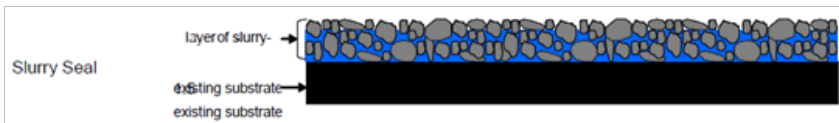

Figure 13. Slurry type seal coating's cross-section (SANRAL 2007)

Another type of chip sealing, which is considered as a double layer chip sealing, is a type of asphalt pavement performed by using aggregates with a certain gradation, developed in the Norwegian Road Research Laboratories in 1963-1966 therefore known as Otta type seal coating (Figure 14). The thickness of this type of chip sealing varies between 12-30 mm. Two types of gradation are applied in the first layer as open and dense gradation. The highest and smallest grain diameters of the aggregates used is 19 mm and 2 mm as respectively. After applying the aggregate layer in a certain gradation, if desired, the second layer of binder layer and then sand sealing layers are applied and the production of graded chip sealing is completed (Pinard and Obika, 1997).
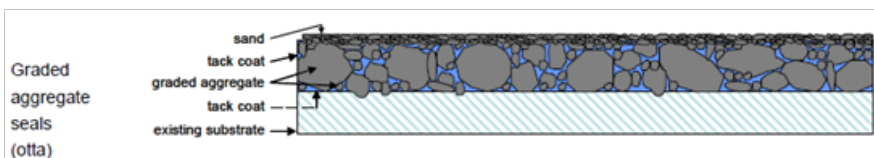

Figure 14. Graded (Otta) type chip sealed road
pavement cross-section (SANRAL 2007)

Another type of seal coating used for preventive and maintenance purposed is the sand or sandstone seal coat layer (Figure 15). Sand seal is the application of asphalt emulsion by spraying, followed by the spreading of clean sand or fine aggregate on the road surface. Generally, after the sand application, compaction is performed with a pneumatic cylinder and then the loose aggregates remaining on the surface are broomed. While providing additional skid resistance to the sand sealing, it also prevents fragmentation. With this application, only capillary cracks can be filled, and large cracks could be reappearing within 1 year (Yamada, 1999).
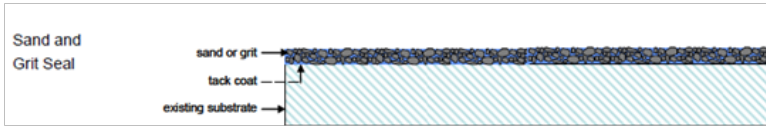
Figure 15. The sand or sandstone chip sealed road
pavement cross-section (SANRAL 2007)

Fog seal is the application of sprayed bitumen emulsion with or without sand on the pavement surface. The asphalt pavement surface can deteriorate erosion, raveling, loss of aggregate, honeycombing, and sulphate attacks over time due to weather conditions such as frost, sunlight, heat, and also road salting, snow removal, as well as the effects of excessive loading and friction, especially caused by tire chains and snowplow blades. Failing to repair asphalt in due time will allow damages to expand, leading to complete destruction of the road surface and even the underlying layers. The use of protective layers is recommended to prevent intensification of asphalt wear out, postpone overlay installation, maintain the existing conditions, and fill the cracks. Fog seal is one of the seal coat applications used for this (Reha bitumen 2021). In fog seal application, the emulsion is diluted to a suitable consistency to cover the entire road surface, but it should not be too thick to avoid slippery surface. The fog seal layer works better on surfaces composed of coarse aggregate by filling in between the aggregate particles. If the fog seal is not applied properly and a slippery surface occurred, sand or aggregate with a diameter of less than 6.3 mm is spread on the surface.

Figure 16. Fog seal application (Reha bitumen 2021)

5. Chip Seal Deteriorations and Performance

Although the factors affecting the chip sealing performance are known from the literature, there is no detailed information in the literature about the size of

the parameters (TNZ 2005, Gransberg and James 2005, SANRAL 2007, Gürer 2010, Gürer et al. 2012, Aktaş et al. 2013, Karaşahin et al. 2016). If the factors affecting the performance of the pavements are well known by the application engineers, the chip sealed road pavements will have a longer service life and also be comfortable. Parameters that are thought to directly or indirectly affect the performance of chip seals are given in Figure 17.
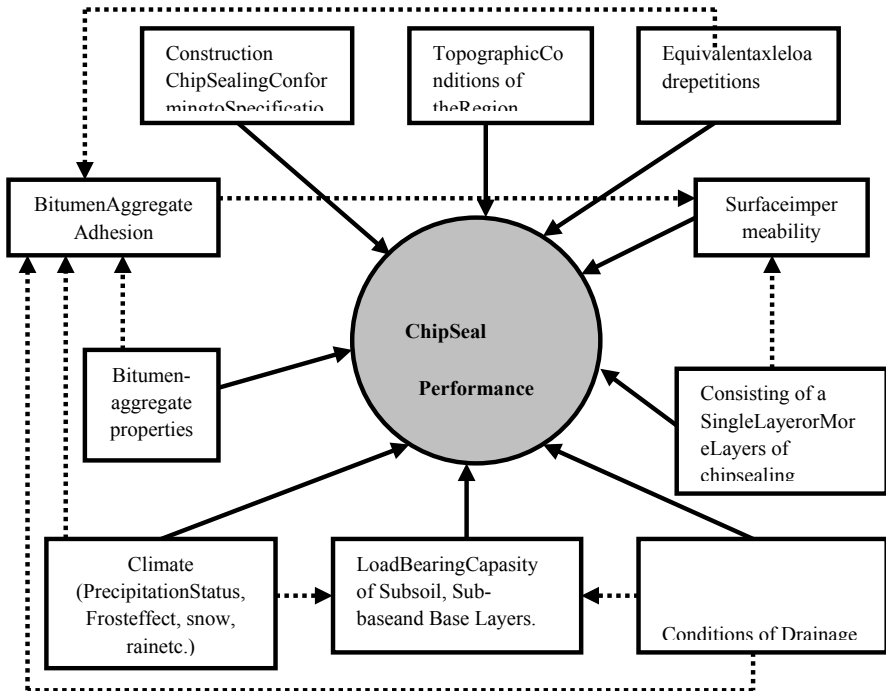
Figure 17. Parameters considered directly or indirectly affecting surface coating performance (Gürer, 2010)

While traffic volume, standard axle load, number of repetitions and climate-temperature effects are the most important reasons for the deterioration of the pavement, the lack of construction, design and use of inappropriate materials also affect the performance of chip seals.

5.1. Deteriorations in Chip Seals

5.1.1. Aggregate Retention, Segregation and Fragmentations

Aggregate loss occurs as a result of the deterioration of aggregate-asphalt adhesion with the effect of heavy traffic and surface moistures. It is the formation of a permeable surface as a result of the loss of the aggregate pieces

on the surface over time. Over time, the moisture on the surface passes through these parts, causing the loosening of the base layer and the deformation of the road pavement. As a result, the asphalt film becomes open to external factors. In Figure 10, aggregate raveling and segregations occurring on a chip sealed surface was shown in Figure 18 and 19. As a result of the loss of aggregate particles on the road surface, the formation of potholes and accumulation of water in these parts (ACMA, 1992.).

Figure 18. Aggregate raveling on a chip sealed road surface (a) and segregation occurring on the surface (b).

Various factors can also cause aggregate loss, these are:

- Aggregate spreading after the bitumen is over-cooled,
- Using dusty and humid aggregate,
- Delaying the rolling operation of the aggregate after spreading,
- Steel wheel rollers could cause aggregate degradation,
- Early opening to traffic of newly constructed chip seals,
- Using insufficient or wrong bitumen grade or the surface is excessively porous,
- Ignoring the air temperature, wind, precipitation, etc. (Gürer 2010).

Figure 19. Segregation and fragmentations in chip seals (a and b) (Karaşahin and Gürer, 2007)

5.1.2. *Rutting, Consolidation and Swelling*

In chip sealed road pavements, rutting is formed as a result of lateral movements, consolidation (compression or settlement) of the subgrade or foundation-subbase layers under the pavement caused by axle loads and moisture. The main reasons for consolidations are;

• Insufficient selection of base and sub-base thicknesses,
• Settlements on the base layer,
• Inadequacy of lateral supports (slope stability of road fillings)
• The height of the underground water level,
• Insufficient drainage, filling of the voids of the base and sub-base materials with clay or fine material due to capillary effect.

Generally, this type of deterioration is seen in the parts where the wheel tracking is concentrated (Figure 20.).

Figure 20. Settlements and consolidations in the chip sealed road pavements

5.1.3. *Loss of Skid Resistance*

It generally occurs as a result of the bleeding of the bitumen and the polishing of the gravel particles over time with the effect of traffic and moisture. One of the most important properties for aggregates is skid resistance. As a result of reduced skid resistance, the probability of traffic accidents increases, especially in rainy weather conditions. At each stage of the pavement's service life, some roughness must be maintained between the road surface and the vehicle tire. Skid resistance is defined as the measurement of the resistance of the pavement surface against the slipping of the vehicle. This is a relationship between the vertical and horizontal forces generated as the tire slides along the pavement surface. Skid resistance depends on the macro and micro texture of the pavement surface. Micro texture is the small-scale roughness of the pavement aggregate

component (controlled by the contact between the wheel tire and pavement surface). Macro texture is the large-scale pavement roughness and depends on the distribution of aggregate particles on the pavement surface (it controls the removal of water from under the vehicle tire on the asphalt pavement surface) (Figure 21.) (Asi, 2005).

Figure 21. Micro and macro texture of the road surface (Tremblay et al., 1995)

Polishing of aggregates reduces micro-texture, resulting in smooth and smooth surface aggregates. Road surface roughness characteristics are shown in Figure 13 (Tremblay et al., 1995). The roughness of the pavement surface and its resistance to the polishing effect of traffic is extremely important. Polishing of aggregates is the reduction or loss of micro-roughness as a result of the roughness of the aggregates on the surface being destroyed. This process takes place on a microscopic scale, with the grinding action of small abraded aggregate particles. Aggregates, especially some types of limestone, become polished more quickly under traffic loads. Naturally, river bed aggregates, which are polished and smooth, also pose a slip hazard if they are used on pavement without crushing. Such aggregates, whose surfaces have become polished, become completely slippery when moisture (Shahin, M.Y.; 2002, Asi, 2005; Fwa T. et al. 2003).

5.1.4. Bleeding

Bleeding or bitumen rises occurred when excess bitumen rises to the surface of the road pavement, especially in hot weather and heavy traffic loads, and has a negative impact on traffic safety. It is a complex form of deterioration and could be occurred as a result of any combination of the following factors:

- Applying more bituminous binder,
- Embedding of aggregates on the road surface; in this case, the binder between the aggregates causes it to rise relatively. (Figure 22).
- The disintegration of aggregates; some aggregate particles break down (at least into two pieces) under compaction or traffic loads. The resulting loss of aggregate leads to a change in the binder-aggregate ratio, thus causing bleeding problems. The problem encountered here is that the compressive strength of aggregates with high shear resistance is low.

- Dust absorption by the binder; Binders with high durability tend to absorb dust particles falling on them. The effective volume of the binder, which absorbs a high amount of dust, increases. As it is embedded in its aggregates, this effect leads to the loss of surface texture (Whiteoak, 1990; ACMA, 1992).
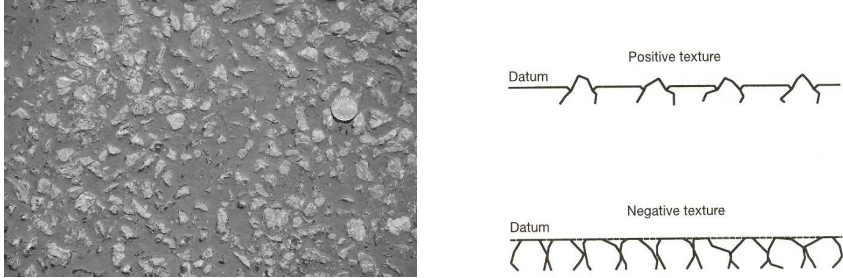

Figure 22. Negative surface texture due to bleeding in chip seals and illustrations of the positive and negative surface textures (Whiteoak D. 1990).

5.1.5. *Traffic Conditions*

Although weather and traffic are two important factors that deteriorate the road surface, traffic also plays a very important role in the formation of a smooth and good locked chip sealed road surface. The tire wheels of heavy-duty vehicles exert a kneading action on the aggregates, which causes the aggregates to form an interlocked mass and resists their individual breakage. Since this process will occur slowly on roads with light traffic, a large amount of binder must be applied in order to keep the aggregate on the surface on such roads (Gürer 2010). For this reason, the configuration of the traffic is as important as the volume in the chip seals. Although the use of chip sealing on heavy traffic intercity roads gives good results, chip seals cannot withstand variable accelerations during turning, braking, and acceleration on heavy-traffic urban streets. If the newly constructed chip-sealed road sections need to be opened to traffic immediately, the traffic speed should be controlled (it should be ensured that it is passed at a speed of 23-30 km/h). The safest way is to open the traffic at least one hour after compaction operation (Gürer and Karaşahin 2007).

5.1.6. *Road Pavement Surface Condition*

If chip sealing is applied on an old pavement, the road surface must be free of dust and loose material. The surface is should be carefully swept with a mechanical broom before applying the binder. The embedding of aggregate particles in the existing pavement surface or foundation layer depends on the hardness of the

existing base layer and the volume of heavy vehicle traffic. When determining the amount of binder, the porosity and roughness of the old surface should be considered. If the old surface shows a lack of binder and is porous, it will be necessary to use more binders. In addition, if the existing pavement surface is very cracked, it should be expected that these cracks will reflect on the chip-sealed surface over time. If the surface is very porous, the aggregate loss will occur on the surface as the binder material will penetrate excessively.

5.1.7. Climate and Whether Conditions

The viscosity of the bituminous binder is highly dependent on temperature. If a very low viscosity binder is used to ensure that the binder can adhere to the aggregate in the winter, deterioration becomes inevitable when the temperature rises in the spring. Air temperature changes during manufacturing may adversely affect chip seal performance. Therefore, the chip sealing construction season is limited.

5.1.8. Binder

It should be sufficient to close the cracks and bind the aggregate particles to the substrate, but not enough to create a slippery surface. The viscosity of the binder should be fluid enough to envelop the aggregate particles at the time of application, low enough to not cause bleeding at high temperatures, and high enough to not be brittle at low temperatures.

5.1.9. Topographic Conditions of the Road Section

Especially at the intersections and curves of the road route, a little more aggregate should be applied and a little more rolling should be performed. Aggregate particles should not be removed in climbing lanes with slow traffic movements. Consideration should also be given to the drainage conditions of the road sections.

6. Chip Seal and Environmental Impacts

Chip seals are preferred by road authorities, especially on rural, undivided roads. They are not suitable roads for high speed due to reasons such as relatively high wheel noise and high friction coefficient. Therefore, they should be among the pavement types that should be preferred in terms of minimizing the wildlife crossing crash losses caused by the roads (Figure 23). Since less material is required for the construction of the unit area of chip seals compared to other

road pavements, it provides better protection of natural resources. Transportation infrastructure contributes 23% of global carbon dioxide (CO_2) emissions, making it the second largest contributor, only behind electricity generation (Ang and Marchal 2013). For this reason, this type of asphalt pavement makes a significant contribution to sustainability.

Figure 23. Chip sealed pavements are safer for wild life crossings (wolfcenter 2021)

7.   Conclusions

Chip seals are among the most important asphalt pavement types for road pavements due to reasons such as constructing quickly, requiring limited materials for their construction, being low cost and not suitable for high traffic speeds, being safe due to their high skid resistance surface, and increasing the service life of asphalt concrete coatings. So, it will continue to be widely used by road administrations for many different purposes in the future.

8.   References

ACMA Product Group of the British Aggregate Construction Materials Industries (BACMI). (1992). Bituminous Mixes and Flexible Pavements. London.

Aktaş, B., Karaşahin, M., Saltan, M., Gürer, C., Uz, V.E. (2013). Effect of Aggregate Surface Properties on Chip Seal Retention Performance. *Construction and Building Materials*, *44,* 639-644.

Ang, G., Marchal, V. (2013) Mobilising Private Investment in Sustainable Transport: The Case of Land-Based Passenger Transport Infrastructure. *OECD Environment Working Papers, 56.*

Asi, I.M. (2007). Evaluating Skid Resistance of Different Asphalt Concrete Mixes. Building and Environment. *Building and Environment, 42(1),* 325-329.

Asphalt Institute. (1989). The Asphalt Handbook. Manuel Series No:4 (MS-4), Edition.

Banihatti, N.V., 1994. Design and Durability of Asphalt Seal Coats. M.Sc. Thesis. University of Arkansas, Arkansas.

Distin, T. (2008). Spray Sealing Practice in South Africa. 1st Sprayed Sealing Conference. Adelaide Australia.

Fwa, T., Cho Y., Liu, Y. (2003). Effect of Aggregate Spacing On Skid Resistance Of Asphalt Pavement. *The Journal of Transportation Engineering,129(4),* 420–6.

Gransberg, D., James, D.M.B. (2005). Chip Seal Best Practices. National Cooperative Highway Research Program. Transportation Researh Board. Washington, D.C.

Gürer, C. (2010). Determination of Parameters Affecting Seal Coat Performance And Development A Performance Model.(Unpublished Ph.D. Thesis). Suleyman Demirel University, Natural and Applied Science Institute, Department of Civil Engineering, Isparta, Turkey.

Gürer, C., Karaşahin, M., Çetin, S., Aktaş, B.(2012). Effects of Construction-Related Factors on Chip Seal Performance. *Construction and Building Materials, 35,* 605-613.

Holtrop, W. (2008). Sprayed sealing practice in Australia. 1st Sprayed Sealing Conference. Adelaide Australia.

Islam, M.S. (2010). Evaluation of Lightweight Aggregates in Chip Seal. Kansas State University, Department of Civil Engineering, College of Engineering. M.Sc. Thesis. Manhattan, Kansas.

Karaşahin M., Gürer C., Saltan M., Taciroğlu M.V., Uz V.E. (2016). Investigation of Chip Seal Performance Under Cold Climate Conditions, Science and Engineering of Composite Materials. 23(6), 649-658.

Karaşahin, M., Ağar, E. (2004). An Evaluation on Seal Coats.4th National Asphalt Symposium, 131-140. Ankara, Turkey (in Turkish).

KGM (Turkish General Directorate of Highways). (2013). Republic of Turkey Highway Specification, Ankara, Turkey. (In Turkish).

Marienfeld, M.L. (1997). Geotextiles Improve Low Volume Roads. International Symposium of Thin Pavements, Surface Treatments, Unbound Roads. University of New Brunswick. Fredericton, New Brunswick, Canada.

Nam, B.H.N., Golestani, B., Noori M., Tatari ,O., An, J. (2014). Investigation of Reflective Cracking Mitigation Techniques. Final Report. FDOT Contract No.: BDK78-977-17. Department of Civil, Environmental, and Construction Engineering University of Central Florida. 138p.

NCDOT.(2015). Chip seal best practices manual. North Carolina Department of Transportation.

Pinard, M.I., Obika, B.O. (1997). Low Cost Bituminous Seals For Low Volume Roads: the Otta (graded aggregate) Weal. UNB International Symposium on Thin Pavements, Surface Treatments, and Unbound Roads, New Brunswick, Canada.

Reha Bitumen. https://rahabitumen.com/bitumen-emulsion-fog-seal/ Accessed 10.09.2021

SANRAL (The South African National Roads Agency Ltd.). (2007). Technical Recommedations For Highways, Design and Construction of Surfacing Seals. TRH3 2007. Pretoria, Republic of South Africa.

Shahin, M.Y. (2002). *Pavement Management for Airports, Roads and Parking Lots*. US: Kluwer Academic Publishers.

Solaimanian, M., Harvey, J., Tahmoressi, M. and Tandon, V. (2003). *Test methods to predictmoisture sensitivity of hot mix asphalt pavements*. Moisture sensitivity of asphalt pavements: A national seminar. San Diego, CaliforniaWashington DC: National Academies Press.

Transit New Zealand (TNZ). (2005). Chipsealing in New Zealand. Wellington, New Zealand: Road Controlling Authorities, Roading New Zealand.

Tremblay, G.S., Julien, A., Leclerc, and Auger, B. (1995). The Role of Aggregates in Road Surfacing Texture and Skid Resistance. In Proceedings, Transportation Association of Canada, Victoria, British Columbia.

Whiteoak, D. (1990). The Shell Bitumen Handbook. UK: Shell bitumen.

Wolf Center. https://www.wolfcenter.org/can-wildlife-crossings-help-animals-cross-highways-more-safely/ Accessed 20.09.2021

Yamada, A. (1999). *Asphalt Seal Coat Treatments.* San Dimas, California: San Dimas Technology and Development Center,

CHAPTER 11

UTILIZATION OF PHASE CHANGING MATERIALS (PCM) IN BUILDING APPLICATION

Esra GÜÇKIR[1] & Kadir GÜÇLÜER[1*] & Osman GÜNAYDIN[2]

[1](MSc. Student) Adıyaman University, Graduate Education Institute, Dept. of Civil Engineering, Turkey.
esraguckir@gmail.com
Orcid: 0000-0002-5049-7778
[1](Asst. Prof. Dr.) Adıyaman University, Vocational Schools of Technical Sciences, Dept. of Construction, Turkey.*
kgucluer@adiyaman.edu.tr
Orcid: 0000-0001-7617-198X
[2](Prof. Dr.) Adıyaman University, Engineering Faculty,, Dept. of Civil Engineering, Turkey.
gunaydin@adiyaman.edu.tr
Orcid: 0000-0001-7559-5684

1.   Introduction

While Stanford Ovshinsky is often referred to as the inventor of phase-changing materials, the work done by Alan Tower Waterman of Yale University on the phase-shifting electrical properties of materials is also very important in this field (Pieterson, 2009). Phase-change materials (PCM) are materials that undergo a solid-liquid phase transformation known as the melt-solidification cycle within a thermal application range within a specified temperature range. As a material changes phase from solid to liquid, although it remains at a constant temperature, it absorbs energy from its environment. Due to this absorbed energy, the energy of atoms or molecules increases and their vibration behavior increases. When the melting temperature is reached, atomic bonds relax and a phase change from solid to liquid occurs (Fig. 1). Solidification, on the other hand, is exactly the opposite of this process (Fleischer, 2015).
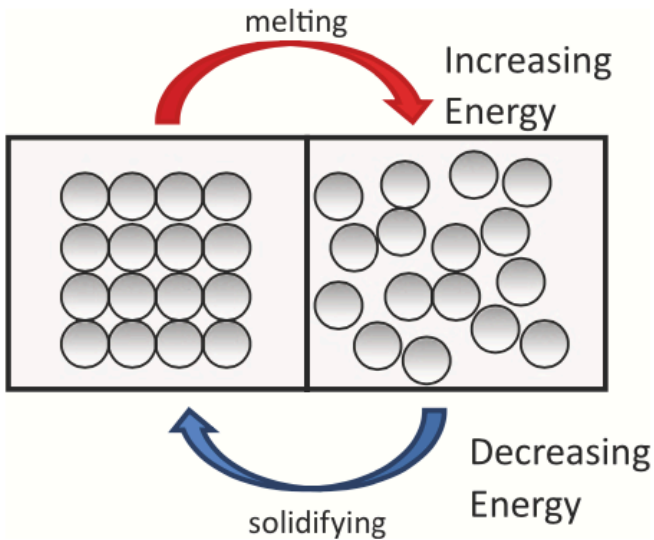
Figure 1. The melting/solidification process (Pieterson, 2009)

The energy absorbed or released during the melting-solidification cycle is called latent heat of fusion. Sensible heat, on the other hand, is the heat that causes a change in temperature within the material, unlike latent heat (Fleischer, 2015). In this sense, one of the most important forms of energy storage is thermal energy storage. Heat storage methods can be realized as latent heat, sensible heat and a combination of these two methods. Latent heat storage is based on the heat release or adsorption of a storage material during phase change. Examples of these materials are paraffin wax, salt hydrates, and fused salts. The sensible heat storage method is performed by adding energy to a material to increase its temperature without changing its phase. In the thermochemical energy storage method, which is called the combination of these two energy storage methods, the energy obtained from the breaking and dissociation reactions of chemical bonds at the molecular level is stored and can then be reversed (Delgado et al., 2019)

2.   PCM Classification

There are several types of PCM's with different melting points, divided into three categories (Fig 2.). The first classification of PCM's into three categories as organic, inorganic and eutectic was realized in 1983 (da Cunha & de Aguiar, 2020).
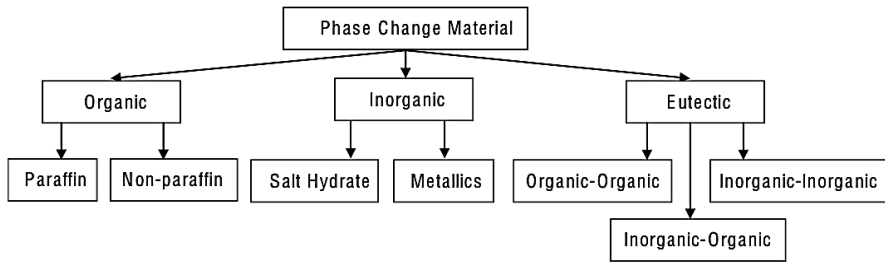
Figure 2. Classification of PCM (Memon, 2014).

2.1. Organic PCM

Organic PCMs are fatty acids, polyethylene glycol and paraffins. Although not dangerous, they show a harmonious phase change and have a good nucleation rate (Kuznik et al., 2011). Some of the advantages and disadvantages of these materials are given in Table 1.

Table 1. Advantages and disadvantages of organic PCM's (Kuznik et al., 2011).

Advantages	Disadvantages
Chemically stable	Low thermal conductivity
No segregation	Flammable
Safe and non-reactive	Low volumetric latent heat storage capacity
Compatible with traditional building materials	
Recyclable	

2.2. Inorganic PCM

Inorganic PCM's are salt hydrates (Kuznik et al., 2011). Some of the advantages and disadvantages of these materials are given in Table 2.

Table 2. Advantages and disadvantages of inorganic PCM's (Kuznik et al., 2011).

Advantages	Disadvantages
High volumetric latent heat storage capacity	High volume change
Low cost and easy availability	Supercooling
Non-flammable	Segregation
High thermal conductivity	
Sharp phase change	

2.3. Eutectic PCM

Eutectic PCMs consist of two or more organic, inorganic, or a combination of both PCM compounds. So these offer a transition temperature closer to current needs (Cabeza et al., 2011). Some of the advantages and disadvantages of these materials are given in Table 3.

Table 3. Advantages and disadvantages of
eutectic PCM's (Cabeza et al., 2011).

Advantages	Disadvantages
High enthalpy	High cost
Harmonious phase change	Limited thermophysical properties
Suitable transition temperature	Strong odor

3. Properties of PCM

Since only one material cannot be used for a perfect thermal storage environment, some properties may need to be compensated for a suitable system design. Therefore, choosing the appropriate PCM is an important issue for researchers. The choice of PCM plays an important role in the development of latent thermal storage properties. In order to realize this situation, PCM must have some thermal, physical, chemical, kinetic and economic properties (Rathod, 2018). Among the thermal properties; good thermal conductivity, worthy melting point, latent heat of fusion per unit volume can be listed. Among the physical properties; small volume variability in phase change, approving phase balance, low vapor pressure to retention problem. As kinetic properties; effective heat transfer and extreme cooling behavior can be said. Chemical properties are; non-toxic, not corroding building materials, non-flammability and non-explosive. In terms of economy, the abundance of materials, recyclability and cheapness are important features (Rathod, 2018).

4. Application of PCM in Building Area

The construction industry has a significant environmental impact. This impact originates from the life cycle of the buildings (Meggers et al., 2012). Reducing energy usage and using renewable energy technologies in buildings will help to lower CO_2 emissions and reduce harmful effect to environment. Thermal energy storage is a possible way to reduce energy consumption of buildings due to its ability to store thermal energy and also control temperature (Zhu et al., 2018). Phase change materials (PCM) have a remarkable capability that can be used as

a thermal energy storage in buildings to reduce indoor temperature swings and decrease the annual cooling/heating load (Zhu et al., 2018; Drissi et al., 2019). There are many different application areas of PCM in buildings such as in walls, floors, ceilings, roofs and as an admixture to the construction materials.

4.1. PCM Use in Walls

 Use of PCM in building walls involves PCM trombe walls, PCM wallboards and PCM building blocks (Cui et al., 2017). Both organic and inorganic phase change materials could be used in building wall (Kuznik et al., 2011). The temperature fluctuation range in a room may be reduced by using PCM wallboards which are made up of fatty acids as PCMs and traditional construction materials. In several studies it is shown that PCM walls has valuable thermal reliability and energy storage capacity (Yuan et al., 2014). However it is well known that ventilation rate, the PCM selected and its phase transition temperature, the orientation of the wall and the latent heat capacity per unit area of the wall are some components that affecting performance of PCM walls (Memon, 2014).

4.2. PCM Use in Floors

Floor has a remarkable impact on reducing indoor temperature swings because of having huge area in the building (Frigione et al., 2019). PCM can be used to improve floor boards, tiles or panels (Kośny, 2015). The idea to use PCM in floors in a building is to take advantage of the high energy storage capacity of the material. PCM applied floors provide thermal comfort and low temperature fluctuations. Moreover, consumption of electricity could be reduced since PCMs charge during night time and discharge during the day (Cui et al., 2017). The PCM floors exposed to direct sunlight could be more efficient in terms of saving heat energy (Souayfane et al., 2016). More specifically, shape-stabilized PCM (SSPCM) plates are suitable choice for radiant floor applications in buildings (Ermolli et al., 2011). SSPCM is obtained by melting and mixing of PCM and additive components at high temperature (Zhu et al., 2018).

4.3. PCM Use in Roofs

Roofs receive solar radiation more than other building elements and this could lead to thermal discomfort both in cold and hot climate regions (Mengjie et al., 2018; Ismail et al., 2015). In hot regions, roofs absorb a certain amount of solar radiation and transfer a significant amount of it to the indoor environment. On the other hand, an important amount of heat that we need in cold regions goes to

the outdoor environment (Ismail et al., 2015). Thus, PCM use in roofs is crucial to achieve thermal comfort. PCM layers and PCM integrated roofing materials could be used for this purpose (Ismail et al., 2015; Thongtha et al., 2021). Use of PCM layer in roof is a way to reduce the temperature fluctuation. Thickness of PCM layer and phase transition range of PCM are factors affecting energy saving capability of roof with PCM (Reddy et al., 2017). Incorporation of PCM into roof with conical holes lowers the heat load significantly (Cui et al,. 2017).

4.4. PCM Use in Windows and Shutters

The glazed areas are preferred widely since it provides vision and natural air ventilation. However, a large portion of heat loss in buildings comes from windows and this leads to more energy consumption due to the demand for heating in cold regions and demand for cooling in hot regions because of solar radiation. Incorporation of PCM into glass window can reduce the heat load coming into the room (da Cunha & de Aguiar, 2020; Souayfane et al., 2016). Semi-transparent solar window with PCM conserves the heat that absorbed throughout the day and release it at night (Delgado et al., 2019). As a result of comparison of the traditional double glazing unit and PCM integrated glazing unit, it is shown PCM has an important impact on thermal comfort (Kalnæs & Jelle, 2015)

Another use of PCM is its incorporation into window shutters. The aim of shutters with PCM is to lower the heat loss and reduce the energy consumption. The melting temperature of PCM affects the functionality of both PCM incorporated windows and PCM with shutters (Delgado et al., 2019).

4.5. PCM Use in Concrete and Bricks

Concrete is a most widely consumed building material. Thus, use of PCM in concrete could have a huge impact on energy saving of building. Higher density and thermal mass of concrete make it favorable for integration of PCM. However, the incorporation of PCM into concrete decreases its fire resistance. Further, thermal properties of concrete is affected by the way of integration of PCM into concrete (Adesina, 2019). PCM integration into textile reinforced concrete panels is an effective way to reduce energy consumption (da Cunha & de Aguiar, 2020).

Moreover, PCM could be integrated into bricks. PCM integration into empty parts of bricks will help to narrow the temperature fluctuation range of indoor environment (da Cunha & de Aguiar, 2020).

4.6. PCM Use in Gypsum Boards

Thermal mass of lightweight building materials like gypsum board increased by integrating PCM. Gypsum boards with PCM could be utilized in both new lightweight and renovated buildings to provide thermal comfort (Delgado et al., 2019). A major advantage of integrating PCM into gypsum board is that performance of reducing temperature fluctuations. In the literature, it is shown that PCM integrated gypsum board applied wall compared to regular wall is more efficient in terms of keeping room temperature stable (da Cunha & de Aguiar, 2020).

4.7. PCM Use in Mortar

The use of mortars in buildings is pretty wide. Their utilization includes covering surfaces and filling the gaps in the bricks. It is also used for rehabilitation works of buildings. The integration of PCM into mortars increases the need for water, hence causes increase in porosity. Further, increase in porosity causes mortars to be attacked more easily. Lime based mortars are more sensitive to incorporation of PCM compared to cement based mortars. However, it is possible to observe the ability to reduce temperature fluctuation of PCM mortars (da Cunha & de Aguiar, 2020).

5. Conclusions

In these days when the importance of energy efficiency and ecological sustainability is increasing, phase change materials are important for the sustainability of building materials. It can be advantageous to use phase change materials in specific structural areas where energy efficiency is sought, especially in applications for insulation and energy purposes. For this purpose, we believe that the theoretical and applied studies to be carried out with phase change materials will contribute to national and international scale.

References

Pieterson, L. (2009). Experimental Methods for Material Selection in Phase-change Recording. In S. Raoux, M. Wuttig (Eds.), Phase Change Materials: Science and Applications (pp. 81-98). New York, USA: Springer.

Kuznik, F., Damien D., Kevyn J., & Roux, J.J. (2011). A Review on Phase Change Materials Integrated in Building Walls. *Renewable and Sustainable Energy Reviews* 15(1):379–391.

Cabeza, L.F., Castell, A., Barreneche, C., de Gracia, A., & Fernández, A.I. (2011). "Materials used as PCM in thermal energy storage in buildings: A review." *Renewable and Sustainable Energy Reviews* 15:1675–1695.

Ermolli, S.R., Koukkari , H., & Braganca, L. (2011). Phase Changing Materials in Building Elements. In L. Braganca, H. Koukkari, R. Blok, H. Gervásio, M. Veljkovic, Z. Plewako, R. P. Borg (Eds.), Integrated Approach Towards Sustainable Constructions - Summary Report of the Cooperation Activities of COST Action (pp. 245–256). Malta: University of Malta.

Meggers, F., Leibundgut, H., Kennedy, S., Qin, M., Schlaich, M., Sobek, W., & Shukuya, M. (2012). Reduce CO2 from buildings with technology to zero emissions. *Sustainable Cities and Society* 2:29-36.

Yuan, Y., Zhang, N., Tao, W., Cao, X., & He, Y. (2014). Fatty Acids as Phase Change Materials: A Review. *Renewable and Sustainable Energy Reviews* 29:482–498.

Memon, S.A. (2014). Phase Change Materials Integrated in Building Walls: A State of the Art Review. *Renewable and Sustainable Energy Reviews* 31:870–906.

Kalnæs, S.E., & Jelle, B.P. (2015). Phase Change Materials and Products for Building Applications: A State-of-the-Art Review and Future Research Opportunities. *Energy and Buildings* 94:150–176.

Fleischer, A.S. (2015). Thermal Energy Storage Using Phase Change Materials: Fundamentals and Applications. New York ; London: Springer.

Kośny, J. (2015). PCM-Enhanced Building Components: An Application of Phase Change Materials in Building Envelopes and Internal Structures. New York ; London: Springer.

Ismail, K.A.R., Castro J.N., & Lino, F.A.M. (2015). Thermal insulation of walls and roofs by PCM: modeling and experimental validation. *International Journal of Engineering and Applied Sciences* 2:83-93.

Souayfane, F., Fardoun, F., & Biwole, P.H. (2016). Phase Change Materials (PCM) for Cooling Applications in Buildings: A Review. *Energy and Buildings* 129:396–431.

Cui, Y., Xie, J., Liu, J., Wang, J., & Chen, S. (2017). A Review on Phase Change Material Application in Building. *Advances in Mechanical Engineering* 9(6):1–15.

Reddy, K.S., Mudgal, V., & Mallick, T.K. (2017). Thermal Performance Analysis of Multi-Phase Change Material Layer-Integrated Building Roofs for Energy Efficiency in Built-Environment. *Energies* 10.

Mengjie, S., Fuxin N., Ning M., Yanxin H., & Shiming D. (2018). Review on Building Energy Performance Improvement Using Phase Change Materials. *Energy and Buildings* 158:776–793.

Rathod, M. (2018). Thermal Stability of Phase Change Material. In M. Mhadhbi (Ed.), Phase Change Materials and Their Applications (pp. 38-57). IntechOpen.

Zhu, N., Li, S., Hu, P., Wei, S., Deng, R., & Lei, F. (2018). A Review on Applications of Shape-Stabilized Phase Change Materials Embedded in Building Enclosure in Recent Ten Years. *Sustainable Cities and Society* 43:251–264.

Delgado, J.M.P.Q., Martinho, J.C., Vaz Sá, A., Guimarães, A.S., & Abrantes, V. (2019). Thermal Energy Storage with Phase Change Materials: A Literature Review of Applications for Buildings Materials. Switzerland: Springer.

Frigione, M., Lettieri, M., & Sarcinella, A. (2019). Phase Change Materials for Energy Efficiency in Buildings and Their Use in Mortars. *Materials* 12(8).

Drissi, S., Ling, T.C., Mo, K.H., & Eddhahak, A. (2019). A review of microencapsulated and composite phase change materials: Alteration of strength and thermal properties of cement-based materials. *Renewable and Sustainable Energy Reviews* 110:467-484.

Adesina, A. (2019). Use of Phase Change Materials in Concrete: Current Challenges. *Renewable Energy and Environmental Sustainability* 4:9.

da Cunha, S.R.L., & de Aguiar J. L. B. (2020). Phase Change Materials and Energy Efficiency of Buildings: A Review of Knowledge. *Journal of Energy Storage* 27.

Thongtha, A., Janyoosuk, K., & Mano, C. (2021). Integration of phase change material into fiber cement roof for reduction of heat accumulation in buildings. *ScienceAsia* 47S: 83-89.

TDR APPLICATIONS IN CIVIL ENGINEERING

Sami ARSOY[1]

[1](Prof. Dr.), Kocaeli University, Dept. of Civil Eng., Turkey
E-mail: sarsoy@kocaeli.edu.tr
Orcid: 0000-0003-0125-8612

1.   Introduction

Time Domain Reflectometry (TDR) is a well-established remote sensing technology with a relatively long history beginning with cable testing in 1930s (Cerny, 2009). TDR is based on sending a fast rising electromagnetic (EM) step pulse or impulse into an electrical cable or a transmission line and measuring the reflections due to the change of system geometry or material dielectric permittivity. Transmission lines typically consist of a co-axial cable or two parallel conductors. The transmission line is embedded within a structure or surface-mounted as a sensor to monitor the local changes in geometry or material properties.

The use of TDR has been expanded to include civil and structural engineering with a wide variety of applications such as measuring soil water content (Topp et al., 1980), landslide monitoring (Lin et al., 2009), bridge scour monitoring (Yu and Yu, 2011) and detecting-locating cracks in structural elements (Chen et al., 2005).

A typical TDR system basically consists of a high frequency step generator, a digitizing oscilloscope for signal sampling and displaying, and a transmission line (TL) for the signal. A TDR instrument generates a signal (incident test wave), usually a step voltage with an ultra-short rise time and transmits it to the TL during the measurement. While the pulse travels in the TL, the magnitude and the travel time of the reflected waves returning from the TL are recorded.

TDR has been successfully applied to a wide range of monitoring issues in civil engineering since the early 1980s. Well known applications include volumetric soil water content measurement (Topp et al., 1980; Ledieu et al., 1986; Malicki et al., 1996; Stangl et al., 2009; Arsoy et al., 2013), landslide

and slope monitoring (Lin et al., 2009), bridge scour monitoring (Yu and Yu, 2011) and detection of corrosion of steel cables and reinforcing steel in concrete structures (Liu et al., 2002). Determination of cracks in concrete has also been reported by Chen et al. (2009) and Arsoy and Özgür (2019).

2. Soil Water Content Measurements

Quantification of the soil water content (SWC) plays a key role in unsaturated soil mechanics, and it is essential to know the value of SWC for many geotechnical engineering applications such as early detection of landslide risk and compaction quality control in earthwork and highway projects. Additionally, determination of SWC is also one of the fundamental needs in the soil physics and hydrology as defining the optimal time for irrigation, estimating the infiltration rate and evaluating the potential leakage from a waste site are often needed (ASTM 6565, 2005; Heathman et al. 2012).

Several traditional methods are currently being used for determination of the SWC. Although the oven-drying method (gravimetric sampling) is the most accurate and widely known in geotechnical practice, it is time consuming and destructive (Topp et al., 1984). Radioactive methods such as neutron scattering and gamma ray attenuation are widely accepted non-destructive methods but they require special caution and licensing to operate in order to avoid possible health hazards (Noborio, 2001). As an alternative non-destructive method, Time Domain Reflectometry (TDR) became popular for measuring the volumetric soil water content (θ). Accurate, remote, rapid and automated measurement, using simple probes and measuring the dielectric permittivity directly are some of the features associated with TDR (Siddiqui and Drnevich, 1995; Nadler et al., 2002).

The early developments of TDR for SWC measurement started in 1970s (Topp et al., 2003) and furthered by Topp et al. (1980) with the retrieval of a relationship between the θ and the apparent dielectric permittivity (ε_a) of the soil. TDR measured ε_a represents the real part of the complex dielectric permittivity when the dielectric losses assumed to be negligible in the TDR bandwidth (Bittelli et al., 2008).

The TDR method for SWC determination is based on generating a fast rise-time pulsed EM signal (usually in step-wave formation) and coupling it into a probe that acts as a waveguide which is embedded in the soil under investigation. The incident and the reflected signals are recorded with a TDR system in order to perform a travel time analysis (Figure1).
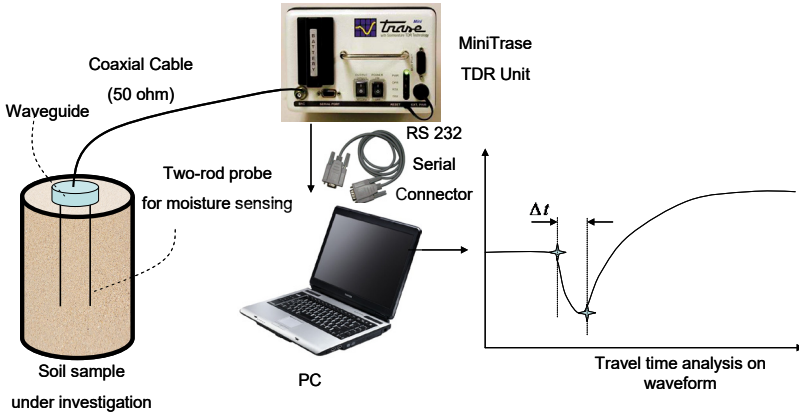
Figure 1 Sketch of TDR apparatus for laboratory measurements of SWC

The round-trip travel time (Δt) of the EM signal along the probe of length (L) depends on the ε_a of the soil surrounding the metallic conductors of the waveguide, as

$$\varepsilon_a = \left(\frac{c\,\Delta t}{2\,L} \right)^2 \tag{1}$$

where c is the velocity of light ($2.998.10^8$ ms^{-1}). Topp et al. (1980) developed probably the most cited relationship between the ε_a and the θ (Ekblad and Isacsson, 2007).

$$\theta = -0.053 + 0.0292\varepsilon_a - 5.5 \times 10^{-4} \varepsilon_a^2 + 4.3 \times 10^{-6} \varepsilon_a^3 \tag{2}$$

The above relationship was initially considered to be universal and has been concluded to be accurate, within a few per cent, for medium-textured soils, and it needs adjustment for peat and heavy clay soils (Kim et al., 2000).

An even simpler empirical relationship presented by Ledieu et al. (1986) was calibrated on loam soils of varying bulk dry densities (1.38-1.78 g/cm³).

$$\theta = 0.1138\,\varepsilon_a^{0.5} - 0.1758 \tag{3}$$

Ledieu et al. (1986) also demonstrated that using the bulk dry density (ρ_d) in the ε_a - θ relationship could improve the accuracy of the method.

$$\sqrt{\varepsilon_a} = a\,\rho_d + b\,\theta + c \tag{4}$$

where a, b, and c are calibration constants (a = 0.297, b = 8.79 and c = 1.344).

The equation proposed by Malicki et al. (1996) which contains not only the ε_a but also the ρ_d derived a higher level goodness of fit. The calibration was performed with wide ranges of soil textures and bulk dry densities.

$$\theta = \frac{\varepsilon_a^{0.5} - 0.819 - 0.168\rho_d - 0.159\rho_d^2}{7.17 + 1.18\rho_d} \tag{5}$$

The accuracy of the round-trip travel time measurement and the calibration models are the essentials in order to make a successful prediction of the θ from the ε_a measured by TDR. Tangent line fitting procedure (Topp et al., 1982) and using the apex of the first derivative of the TDR recorded waveform (Baker and Allmaras, 1990) are demand to be reliable methods to perform the travel time analysis. On the other hand, the discrepancy between the existing calibration models and the experimental results, obtained with oven-drying method (i.e., the difference of $\theta_{measured} - \theta_{predicted}$), became notable especially for soils with high clay content because of the increase in the resolution of the TDR measuring systems. The cause for this deviation has not been completely identified but the bound water effect is one of the possible reasons due to its polarization of which is mainly impeded by the charged surfaces of the clay particles. The reduced polarization results in a lower apparent dielectric permittivity for the bound water (e.g., 6 to 30 depending on the bound water layer thickness) than that of the free water (around 80 at 20 ºC), all of which will lead to measure a lower apparent dielectric permittivity. Therefore, TDR inherently underestimates the water content of soils with high clay content.

In contrast to earlier research (Keng and Topp, 1983), the bulk dry density of the soil is another possible source of error for the TDR based SWC due to its effect on the volume fraction of the bound water. Additionally the bulk apparent dielectric permittivity of the dry soils get larger as the dry density increases because the apparent dielectric permittivity of the solid soil particles is in the range of 2 to 5 versus unity for the air (Gong et al., 2003). For soils with considerable volume change potential, the effect of the bulk dry density becomes more important.

3.   Slope Monitoring

Monitoring of slope stability involves observing the displacement of a slope in time. Accurate monitoring of slopes has been conducted with varying methods like inclinometers and extensometers. However, these methods are expensive and time consuming methods. They also require trained personnel for periodical monitoring of the slopes. Naturally, such a periodical measurement

can sometimes result in missing of a movement in the slope. In addition, the obtained data by these methods needs to be carefully interpreted to determine a risk for slope stability. A schematic diagram of a TDR system used to detect movements in the slopes can be seen in Figure 2.
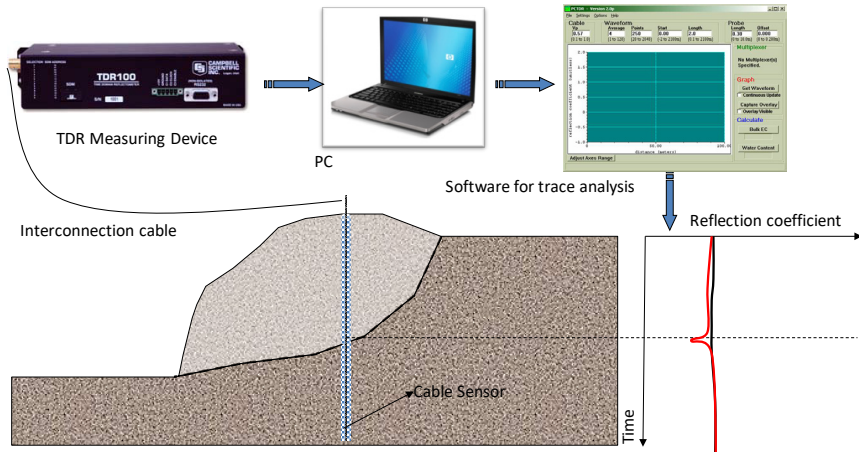

Figure 2 A typical slope monitoring system with TDR technology

As can be seen in Figure 2, the TDR device sends the EM pulse into the coaxial cable embedded in the borehole. The borehole which traverses the anticipated shear surface of a slope failure is generally grouted with a weak sand-cement grout. When the pulse encounters an anomaly or defect along the length of the cable, such as those produced by shearing, a portion of the pulse energy reflects to the TDR device. The reflection causes a spike in the reflection coefficient-time graph. The relative amplitude of the spike and the reflection time are used for determination of the magnitude of the movement and the location of the shear surface, respectively. The relative amplitude of the spike increases as the displacement due to the movement of the slope increases.

The principle advantage of the TDR system is the ability of monitoring the cable sensor remotely by data loggers or telemetry. A warning system based on TDR monitoring system provides an immediate warning when a movement occurs in the slope and critical facilities adjacent to unstable slopes can be real time monitored. TDR is also an advantageous slope monitoring method with its digital data that can be easily acquired and analyzed with suitable software.

4.   Bridge Scour Monitoring

Bridge scour, refers to the reduction of the streambed around bridge piers or abutments, is one of the major causes leading instability of bridges constructed

over waterways. According to the National Cooperative Highway Research Program (NCHRP) Report 396, score accounts for 60% of bridge failures in the United States and approximately 84% of all the 575,000 bridges require scour mitigation. Local scour caused by the interference of piers and abutments with stream flow is the most dangerous type of scour that results in holes around piers and abutments and reduces the lateral support of the surrounding soil (Yu and Yu, 2011).

The methods in practice for determination of bridge scour mainly rely on "after-the-fact" surveys such as visual inspection by trained divers. Therefore the obtained data does not reflect the real situation of the highest flow conditions due to the possible sediment inflow to the scour holes. Sonar monitoring and bathymetric radar are significantly useful methods but they have major limitations.

Using TDR technology for scour monitoring relies on the big differences between the dielectric permittivity of water and that of the air (1) or sediment soils (dielectric permittivity of dry soil varies between 2 and 7, while it increases as the degree of saturation increases), Figure 3. The EM pulse reflects from the interfaces between these material layers due to the significant difference between dielectric properties. The probe consisting of two metallic conductors is connected to the TDR device and mounted on the surface of the pier, Figure 4. When scour occurs the sediment layer thickness around the conductor of the probe differs and the cable signature changes. The difference in the layer thickness can be easily calculated with a trace analysis.
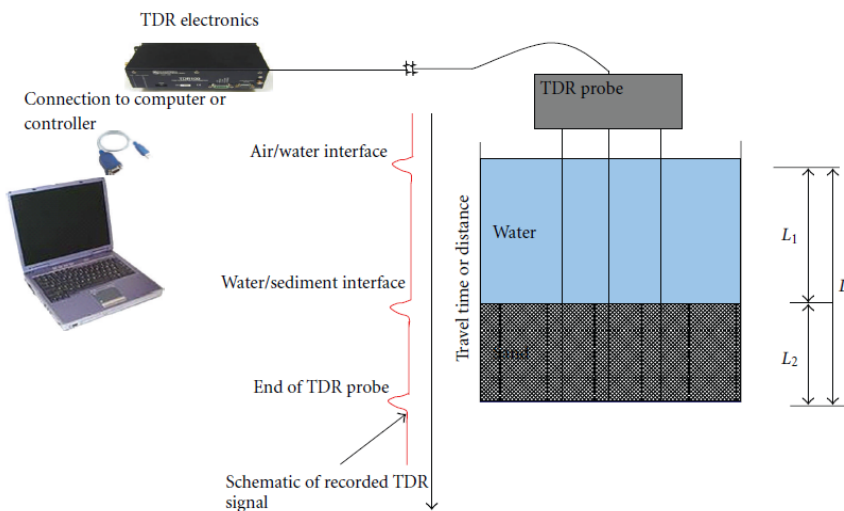

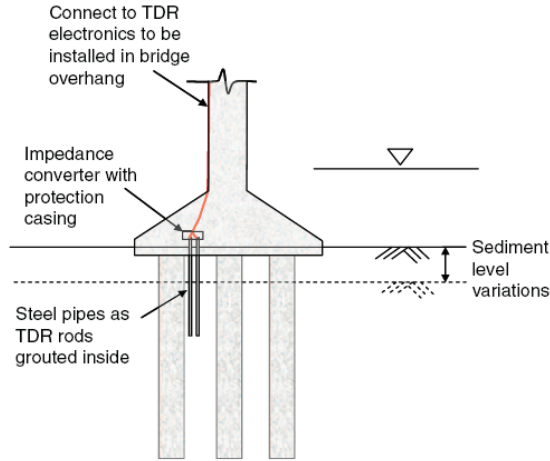**Figure 3** Determination of sediment layer thickness (Yu and Yu, 2011).

Figure 4 TDR scour monitoring system (Yu and Yu, 2009)

5.   Determination of Cracks on Structural Members

Crack detection is one of the primary concerns in health monitoring of civil infrastructures, because cracks may lead to structural degradation (Sun et al., 2009). Especially, knowing the structural integrity of deep foundations, tunnels, water tanks and similar underground structures is an expensive and time consuming process due to the lack of visual inspection.

Using TDR for damage detection on structural elements has a shorter history with a limited literature. The use of TDR on small-scale concrete specimens was first implemented by Lin et al. (1999) and showed the potential of the TDR for crack detection, and the method was further improved in a follow up study (Lin et al., 2000). Chen et al. (2004) designed a novel cable sensor with spiral shaped outer conductor, and its performance consistency was improved later (Chen et al., 2005). More recently, Zhou et al. (2016) pointed out that the limitations of the TL cables developed earlier and proposed a new topology-based cable sensor.

The ongoing studies show that well designed cable sensors can be used for proactive maintenance of structures. Sensing capability of these sensors and their ability in locating a crack provides a remarkable potential for TDR to be a real time monitoring method for structures. Conventional point sensors can easily miss a crack because heterogeneous nature of concrete inhibits to define where the crack exactly occurs. Two point sensors which measure the displacement between any two points cannot differentiate a wide open crack from many fine cracks near one another. A crack sensing method using TDR

technology has been developed for structural members without prior knowledge of crack location (Chen et al., 2009).

The ability of placing a cable sensor to several locations in a structural member and inexpensive measuring system may allow TDR to be a fruitful structural health monitoring method. The commercial coaxial cables are classified as non-sensitive for crack determination applications based on the results of the previous works. These cables consist of an inner conductor, an outer conductor, and a dielectric layer between these two conductors. Chen et al. (2009) modified a commercial cable for better crack sensing by replacing the outer conductor with a spirally wrapped conductor onto the dielectric layer and spray coating for continuity at zero strain (Figure 4a). When a crack sensor is embedded into a reinforced concrete member, a crack intercepting the sensor creates a local separation between two spirals, generating a reflected electromagnetic wave when traveling through the coaxial cable, an electromagnetic wave guide (Figure 4b).
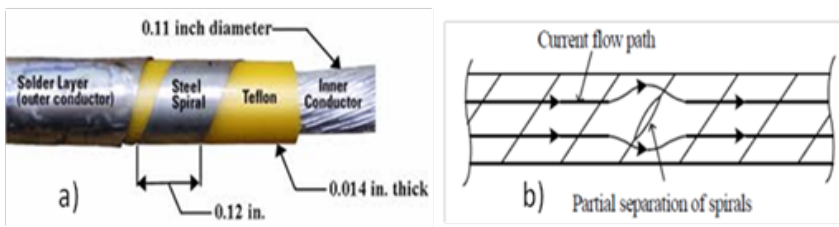

Figure 4 a) Prototype cable sensor b) Change in current
flow path (Chen et al., 2009)

Arsoy and Özgür (2019) conducted a limited experimental study and evaluated the usability of ordinary coaxial cables with a TDR equipment as a nondestructive evaluation method in terms of detecting and locating the cracks on the reinforced concrete (RC) piles. Existence and location of the cracks were derived with help of the reflected EM signals from the embedded non-modified and modified coaxial cables that serve as a damage sensor in this study.

TDR measurements in this study were carried out by using the TDR100 manufactured by Campbell Scientific, Inc. A commercial coaxial cable (RG6/U-4) was used as a potential damage sensor. In the first experiment the cable was used as is. In the subsequent experiment, a propriety modification to the cable was applied in the form of series circular notches following a propriety pattern to enhance the cracks/damage detection capability of the coaxial cable. The waveforms obtained by the TDR system for an as-is cable and for the propriety modified coaxial RG6/U-4 cable is shown in Figure 5 as an example. As seen in

Figure, the damage exerted on the pile is clearly visible on the resulting waveform obtained from the propriety modified embedded cable sensor. Comparisons of the visual inspections and the TDR measurements showed that the location of the primary crack developed on the model pile was determined with 3 cm of error.
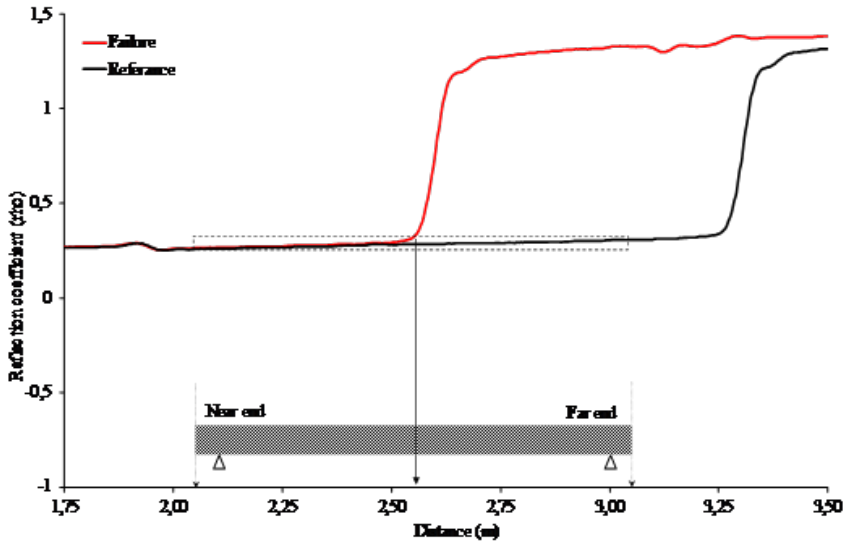

Figure 5 TDR waveforms from model piles equipped
with damage detecting cable sensor (Arsoy and Özgür, 2019).

6.   Concluding Remarks

TDR (Time Domain Reflectometry) is a rapid measurement method developed initially for finding the faults on electrical and communication cables. In recent years, the method has been applied to many civil engineering areas. TDR allows users to monitor the sensing mechanism remotely and continuously. Devices using TDR technology are usually integrated with a multiplexer, so hundreds of channels, connected to the data logger, can be monitored simultaneously. Waveforms, produced with TDR, can be digitally recorded and easily analyzed with convenient software. Features described in this writing makes TDR potentially a very suitable method for needs of real time monitoring issues in civil engineering.

Acknowledgement

References

Arsoy, S., Ozgur M, Keskin, E. and Yilmaz, C. (2013). Enhancing TDR based water content measurements by ANN in sandy soils. Geoderma 195: 133-144.

Arsoy, S.,and Özgür, M. (2019).Post-Earthquake Damage Detection in Concrete Piles with TDR Using Coaxial Cables, 5. International Conference on Earthquake Engineering and Seismology (5ICEES) 8-11 October 2019, METU Ankara, TURKEY.

ASTM, D6565, (2005). Standard test method for determination of water (moisture) content of soil by the time-domain reflectometry (TDR) method, Annual book of ASTM standards, Vol. 04.08. ASTM, West Conshohocken, Pennsylvania, USA, pp. 1118–1122.

Baker, J.M., Allmaras, R.R., (1990). System for automating and multiplexing soil moisture measurements by Time Domain Reflectometry, Soil Science Society of America Journal 54, 1-6.

Bittelli, M., Salvatorelli, F., Pisa, P.R., (2007). Correction of TDR-based soil water content measurements in conductive soils, Geoderma, 143, 133-142.

Cerny, R., (2009). Time-domain reflectometry method and its application for measuring moisture content in porous materials: a review, Measurements 42, 329–336.

Chen, G., Tang, F., Zhou, Z., (2009). Coaxial Cable Sensors and Sensing Instrument for Crack Detection in Bridge Structures – Phase I: Field Qualification/Validation Planning, NUTC R230, Missouri University of Science and Technology, Rolla, MO 65409, USA.

Ekblad, J., Isacsson, U., (2007). Time-domain reflectometry measurements and soil-water characteristic curves of coarse granular materials used in road pavements, Canadian Geotechnical Journal 44:(7), 858-872, 10.1139/t07-024.

Gong, Y., Cao, Q., Sun, Z., (2003). The effects of soil bulk density, clay content and temperature on soil water content measurement using time-domain reflectometry, Hydrological Processes 17, 3601–3614.

Heathman, G.C., Cosh, M.H., Han, E., Jackson, T.J., Mckee, L., McAfee S., (2012). Field scale spatiotemporal analysis of surface soil moisture for evaluating point-scale in situ networks, Geoderma, 170, 195–205.

Keng, J.C.W., Topp, G.C., (1983). Measuring water content of soil columns in the laboratory: A comparison of gamma ray attenuation and TDR techniques, Canadian Journal of Soil Science 63:(1), 37-43.

Kim, D.J., Choi, S.I., Ryszard, O., Feyen, J. and Kim, H.S., (2000). Determination of moisture content in a deformable soil using time-domain reflectometry (TDR). European Journal of Soil Science 51, 119–127, doi: 10.1046/j.1365-2389.2000.00284.

Nadler, A., Green, S.R., Vogeler, I. and Clothier, B.E., (2002). Laboratory horizontal and vertical TDR measurements of soil water content and electrical conductivity, Soil Science Society of American Journal 66, 735–743.

Noborio, K., (2001). Measurement of soil water content and electrical conductivity by time domain reflectometry: a review. Computers and Electronics in Agriculture 31, 213–237.

Lagasse, P. F., Richardson, E. V., Schall, J. D., and Price, G. R., (1997). Instrumentation for Monitoring Scour at Bridges. NCHRP Report 396, National Academy Press, Washington, D.C., USA.

Ledieu, J., De Ridder, P., De Clerck, P., Dautrebande, S., (1986). A method of measuring soil moisture by time-domain reflectometry. Journal of Hydrology 88, 319-328.

Lin, C., Tang, S., Lin, W., Chung, C., (2009). Quantification of cable deformation with time domain reflectometry - implications to landslide monitoring, Journal of Geotechnical and Geoenvironmental Engineering 135(1), 143-152.

Liu, W., Hunsperger R.G., Chajes M.J., Folliard, K.J. and Kunz E (2002). Corrosion detection of steel cables using time domain reflectometry. Journal of Materials in Civil Engineering 14(3): 217-223.

Malicki, M.A., Plagge, R., Roth, C.H., (1996). Improving the calibration of dielectric TDR soil moisture determination taking into account the solid soil, European Journal of Soil Science 47, 357–366.

Siddiqui, S.I., Drnevich, V.P., (1995). Use of time domain reflectometry for determination of water content an density of soil, Publication FHWA/IN/JHRP-95/09. Joint Highway Research Project, Indiana Department of Transportation and Purdue University, West Lafayette, Indiana, doi: 10.5703/1288284313342.

Stangl R, Buchan GD and Loiskandl W (2009). Field use and calibration of a TDR-based probe formonitoring water content in a high-clay landslide soil in Austria. Geoderma 150 (1-2), 23-31.

Sun, S., Pommerenke, D.J., Drewniak, J.L., Chen, G., Xue, L., Brower, M.A. and Koledintseva, M.Y., (2009). A Novel TDR-Based Coaxial Cable Sensor

for Crack/Strain Sensing in Reinforced Concrete Structures, IEEE T. Instrumentation and Measurement, Vol. 58, Nr. 8, p. 2714-2725.

Topp, G.C., Davis, J.L., Annan, A.P., (1980). Electromagnetic determination of soil water content: Measurements in coaxial transmission lines, Water Resources Research, 16(3), 574–582, doi:10.1029/WR016i003p00574.

Topp, G.C., Davis, J.L., Bailey, W.G., and Zebchuk, W.D. (1984). The measurement of soil water content using a portable TDR hand probe, Canadian Journal of Soil Science 64(3), 313-321.

Topp, C.G, Davis, J.L., Annan, A.P., (2003). The early development of TDR for soil measurements, Vadose Zone Journal Soil Science Society of America Journal 2, 492-499.

Yu X., Yu X, (2009). Time Domain Reflectometry Automatic Bridge Scour Measurement System: Principles and Potentials, *Structural Health Monitoring*, vol. 8(6), 463-476, doi: 10.1177/1475921709340965.

Yu, X.B., Yu, X., (2011). Assessment of an automation algorithm for TDR bridge scour monitoring system, Advances in Structural Engineering 14(1), 13-24, doi: 10.1260/1369-4332.14.1.13.

WELDING OF DISSIMILAR METALLIC MATERIALS

Zakaria Boumerzoug

Department of Mechanical Engineering, LMSM, University of Biskra, Algeria
E-mail: z.boumerzoug@univ-biskra.dz

I. APPLICATIONS OF DISSIMILAR WELDING

The need for producing joints of dissimilar metals which can provide appropriate mechanical properties and good cost reduction is continuously increasing due to their advantages (Guo, et al., 2014; Bozkurt and Bilici, 2013). With the development of industry, the connection between dissimilar metals plays an important role in many manufacturing fields and has become a critical technology in many areas. Connecting dissimilar metals can achieve a combination of their advantages to improve properties of products to meet the needs of automobile industry, aerospace, electronics, chemical, and shipbuilding industry (Guo, et al., 2014; Bozkurt and Bilici, 2013. Satoh and Qiu, 2013; Chen, et al., 2010; Mvola, et al., 2014; Praveen and Yarlagadda, 2005; Aizawa, et al., 2007).

II. TECHNIQUES OF DISSIMILAR METALS WELDING

A number of dissimilar metals joints have been successfully formed using various methods from fusion welding to diffusion bonding. The processes for joining of dissimilar metals are divided into three categories, fusion welding, low dilution welding, and solid state welding. The fusion welding processes include the different arc welding (shielded metal arc welding, gas metal arc, submerged arc, flux cored arc, and gas tungsten arc), and resistance spot welding. The low dilution welding includes electron beam welding, laser welding, and pulsed arc welding. The solid state welding includes friction welding (rotation friction welding, friction stir welding, linear friction welding), explosion welding, and diffusion bonding.

A. Fusion welding

Fusion welding includes traditional welding methods such as gas tungsten arc and gas metal arc. Gas tungsten arc welding is also known as tungsten inert gas (TIG) welding, and gas metal arc welding is also known as metal inert gas (MIG) welding. These processes use a filler to create the weld (Mulkerin, 2020).

B. Low-Dilution Welding

In this process, the two welded surfaces do not melt as much compared to other methods. The methods are used for joining metallic materials without the need of filler. For special applications or high-production processes, low-dilution welding is used more often than fusion welding for dissimilar metals (Mulkerin, 2020).

Laser welding is considered as low dilution welding. The principle of this process is shown in Fig. 1. The laser beam is pointed on to a joint and the beam is moved along the joint. The process will melt the metals in to a liquid, fuse them together and then make them solid again thereby joining the two pieces (Gowd and Goud, 2012). Laser welding has several advantages, such as high energy density, high cooling rate, and production of a narrowed heat-affected area. We notice that laser welding involves expensive equipment and complex welding procedures (Zhang and Song, 2011).
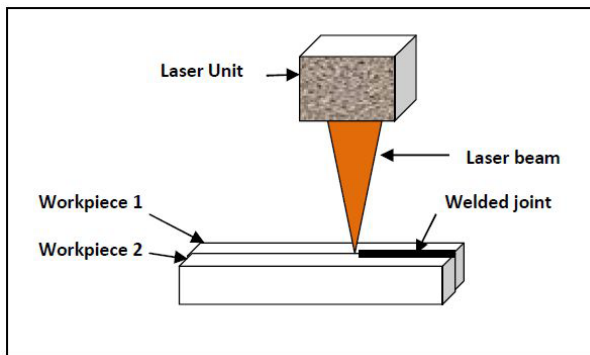

Fig.1. Principle of laser welding of two workpieces.

The second type of low dilution welding is the electron beam welding. This welding process is carried out in vacuum to prevent electron beam dispersion and oxidation of the material. The electron beam welding possesses produces a narrowed heat-affected area with a rapid cooling rate. Hence, this welding method is also widely used in aerospace, nuclear industry, and chemical fields (Sufizadeh and Mousavi, 2016; Kaur, et al., 2015; Sun and Karppi, 1996; Barreda, et al., 2010).The advantage of electron beam welding is its high depth to width ratio which results in a very strong weld. The quality of weld depends upon the parameters, namely, accelerating voltage, beam current, welding speed,

focus current, and vacuum level (Fragomeni and Nunes, 2003). The spot size of the Electron beam welding can vary between 0.2 mm and 13 mm, though only smaller sizes are used for welding. The depth of penetration is proportional to the amount of power supplied but is also dependent on the location of the focal point (Ho, 2005). This method produces very small intermetallic layer and it requires speed from the welder to execute successfully (Mulkerin, 2020).

C. Solid state welding (Non-fusion joining)

Non-fusion joining includes processes such as friction welding, diffusion bonding, soldering and explosion welding (Mulkerin, 2020). Friction stir welding (FSW) is a solid state welding method applied for joining successfully dissimilar metals. A friction stir butt weld is produced by plunging a rotating tool into the facing surfaces of two plates. The tool consists of a shoulder and a profiled pin emerging from it. As the rotating pin moves along the weld line, the material is heated up by the friction generated by the shoulder and stirred by the rotating pin in a process similar to an extrusion (Tolephih, 2011). Fig. 2 shows the schematic of its working. Fig. 3 presents an example of welded dissimilar metals by FSW (steel with aluminum alloy). FSW offer some advantages in the suppression of the formation of cracks, holes, and brittle IMCs (Kuang, et al., 2015; Mishra and Ma, 2005; Hossain, et al., 2014).
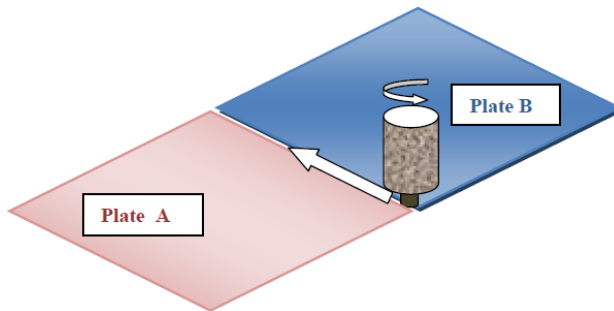

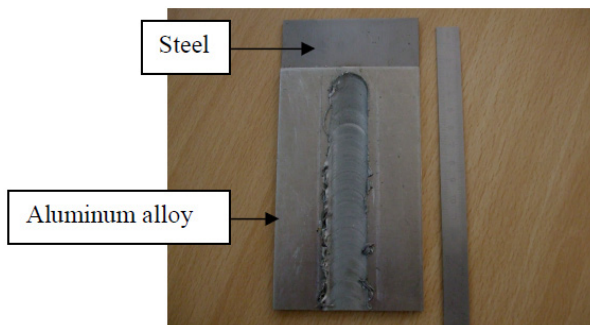Fig. 2. Schematic representation of FSW process (Boumerzoug, 2018).

Fig.3. Welded joint (Al/Steel) by FSW(Boumerzoug, 2018).

Fig. 4 presents two bars of copper and steel welded by Rotary Friction Welding (RFW) and the microstructure of the welded joint. RFW is the most commonly used method in friction welding, where welding heat is generated by friction between the surfaces of a rotating work piece and another stationary (Fig.5).
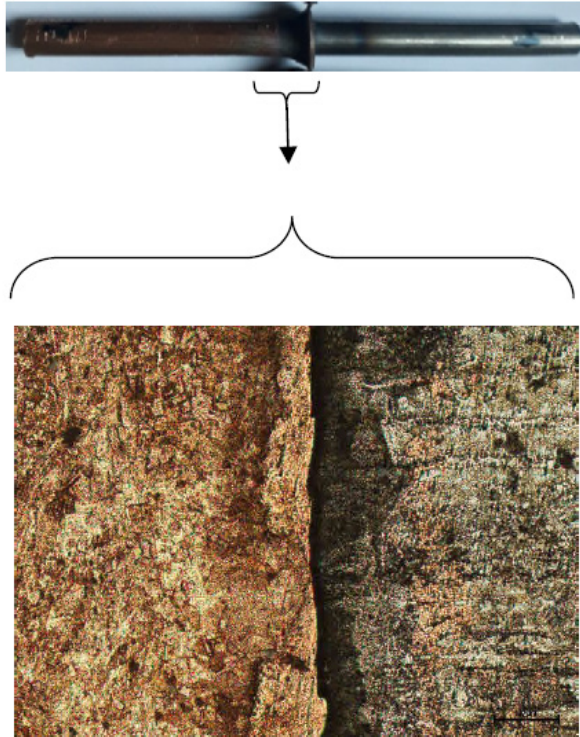

Fig. 4. Friction welded piece of copper to steel with its microstructure.

Fig.5. Friction welding of copper bar to A60 steel bar, carried out on a universal milling machine.

We notice that all these welding processes have been used for welding different dissimilar steels as presented in Table 1. The different methods of welding (traditional and recent) were applied to weld these dissimilar steels. The quality of welded joint depends on the use of the appropriate welding process.

Table 1. List of the most recent welded dissimilar
steels with the main applied welding methods.

No.	Dissimilar steels	Technique of welding	Reference
1	Ferritic-martensitic steel and 316L stainless steel	Electron beam welding (EBW)	(Liu, et al., 2019)
3	Ferritic stainless steel to austenitic stainless steel	Gas tungsten arc welding	(Ghasemi, et al., 2018)
4	AISI 430F stainless steel to AISI 304 stainless steel	Laser Welding	(Pancikiewicz; et al., 2020)
7	Austenitic stainless steel to galvanized steel	Resistance spot welds	(Pouranvari et al., 2008)
8	Stainless steel to carbon steel	Explosive Welding	(Mendes et al.,2013)
9	Duplex stainless steel to low Carbon-Manganese structural steel	Friction Stir Welding	(Rahimi, et al. , 2019)
10	Medium carbon steel (32-2Mn) to medium carbon steel (40-Cr-Ni)	Rotary friction welding	(Priymak, et al., 2020; Boumerzoug et al., 2020)

However, the combination of two techniques of welding was also adopted in recent years. For example, low carbon steel was welded to 304 austenitic stainless steel by using laser welding with tungsten inert gas welding (Chen, et al., 2019). For FSW, an optimization technique like Taguchi approach, are adopted to minimize the experimental runs during the welding of dissimilar metals (Harwani and Banker, 2014).

III   PROBLEMS AND SOLUTIONS

Welding dissimilar metals presents some difficulties. In dissimilar metal welding, the mutual solid solubility and the formation of the intermetallics are

influenced by welding method (Marya, 2008). The intermetallic zone formed in dissimilar metal welding is susceptible to cracks and corrosion (Shahid, et al. 2015). In addition, the difference in thermal properties of dissimilar metals induces the thermal stresses and forms cavities and cracks. The controlling or reducing of intermetallics formation is the main factor to achieve a weld joint with a good quality.

However, the differences in chemical composition and physical properties of the dissimilar metals are a challenge during a welding (Fang, et al., 20019). In addition, formation of large residual stress and brittle intermetallic compounds (IMCs)in welded joint of dissimilar metals is a serious problem. In order to solve this problem, intermediate interlayers were used to eliminate or inhibit the formation of brittle intermetallic reaction layers in many welding techniques, such as diffusion bonding, laser welding, electron beam welding, and other welding techniques (Fang, et al., 20019; Kurt, 2007).

IV   MAIN FACTORS CONSIDERED IN THE WELDING OF DISSIMILAR METALS

Generally, the intrinsic properties of the materials used in dissimilar welding play a major role in determining the weld quality (Sunand and Karppi, 1996). It has been reported that several factors must be considered for welding dissimilar metals (Mulkerin, 2020). The main factors are
 * Melting points of the dissimilar metals
 * Coefficients of thermal expansion of dissimilar metals
 * Electrochemical difference of the dissimilar metals
 * Solubility of each metal.

V.   DIFFERENT WELDED DISSIMILAR METALS

Some selected welded dissimilar metallic (ferrous and non ferrous) materials are being presented below.

A. Welding of dissimilar ferrous metals

The number of welded dissimilar steels increases in recent years. As presented in Table 1, it was possible to weld two dissimilar steels. However, the number of welded dissimilar steels remains limited compared to the huge number of different grades of steels in industry.

B. Welding of non-ferrous metals to ferrous metals

Table 2 gives two examples of welding of non-ferrous metals to ferrous metals. From these two examples, two metals with different chemical and mechanical properties have been successfully welded.

Table 2**.** Some welded dissimilar non-ferrous metals to ferrous metals.

Dissimilar non-ferrous metals	Applications	Ref
Aluminum to steel	Transportation industries.	(Boumerzoug and Helal, 2017; Helal and Z. Boumerzoug,2019; Khalfallah, et al., 2020)
Copper to steel	Automobile industries	(Shanjeevi, et al.,2013; Bhagi, et 2016)

C. Welding of dissimilar non-ferrous metals

Some dissimilar non-ferrous metals have been also successfully welded for specific purpose as indicated in Table 3.

Table 3**.** Some welded dissimilar non-ferrous metals.

Dissimilar non-ferrous metals	**Applications**	**Ref.**
Aluminum to magnesium alloys	Automotive and transportation industry	(Zeng, et al. ,2001; M. Paramsothy, et al. 2008)
Aluminum of different grades	Shipbuilding	(Kaufman,2003)
Aluminum to copper	High-power electronics systems Electronic devices Cables	(Wetzel,2012)
Magnesium alloys to copper	Aerospace, shipbuilding, and instrument fields.	(Mvola, et al. 2014)
Titanium to copper	Aerospace, shipbuilding, and instrument fields	(Mvola, et al. 2014)
Titanium to nickel	Aerospace industries, for instance, as static and rotating components in turbine engines	(Mvola, et al. 2014)

From the previous published works, it important to notice that the number of welded dissimilar metals increases during recent years but it remains very limited. The scientific research on welding of dissimilar metals needs more

investigations, such as the corrosion resistance, because the welded joint is a critical zone and dissimilar metal welds form galvanic couples and may initiate galvanic corrosion in aggressive environments (Shahid, et al.,2015).

CONCLUSION

Based on the review of previous studies, the below conclusions can be summarized as follows:

- Joining of dissimilar materials is very attractive for many applications such as automotive, aerospace, electronics and shipbuilding industries.
- The main challenges of welding dissimilar relate to the different properties displayed by the different materials.
- Intermetallic compounds in welded joint were identified as a significant factor to enhance the weld quality of dissimilar metal welds.
- Many different dissimilar metals can welded. However, the number of dissimilar metals welded until our days is very limited compared to huge number of metals in industry.
- The different methods of welding (traditional and recent) were applied to weld the dissimilar metals. The quality of welded joint depends on the use of the appropriate welding process.
- Optimization techniques are adopted to minimize the experimental runs during the welding of dissimilar metals.
- The scientific research on welding of dissimilar metals needs more investigations, such as the corrosion resistance

REFERENCES

Aizawa, T., Kashani M., & Okagawa, K. (2007). Aluminium alloys and SPCC steel sheet joints. *Weld. J.* 86, 119.

Barreda, J.L. Azpiroz, X. & Irisarri, A.M. (2010). Influence of the filler metal on the mechanical properties of Ti-6Al-4V electron beam weldments. *Vacuum*, 85, 1, 10–15.

Bhagi, L.K., Singh, S., & Singh, I. (2016). Application of Taguchi method for optimization of continuous drive friction welding process parameters. *Ukrainian Journal of Mechanical Engineering and Materials Science,* 2, 1, 1-10.

Boumerzoug, Z. & Helal, Y. (2017). Friction stir welding of dissimilar materials aluminium Al6061-T6 to ultra low carbon steel. *Metals*, 7, 42.

Boumerzoug, Z. (2018). Joining of dissimilar materials by friction stir welding. MATEC Web Conf. 224, *International Conference on Modern Trends in Manufacturing Technologies and Equipment* (ICMTMTE 2018).

Boumerzoug, Z., Priymak, E., Stepanchukova, A., Helbert, AL., Brisset, F., & Baudin, T. (2020). Texture of rotary-friction-welded from dissimilar medium carbon steels. *World Journal of Condensed Matter Physics*, 10, 4, 178-190.

Bozkurt, Y., & Bilici, M. K. (2013). Application of Taguchi approach to optimize of FSSW parameters on joint properties of dissimilar AA2024-T3 and AA5754-H22 aluminum alloys. *Materials and Design*, 51, 513–521.

Chen, Y., Chen, S., & Li, L. (2010). Influence of interfacial reaction layer morphologies on crack initiation and propagation in Ti/Al joint by laser welding-brazing. *Mater Des*, 31, 1, 227–233.

Chen, H.C., Ng, F.L. & Du, Z. (2019). Hybrid laser-TIG welding of dissimilar ferrous steels: 10 mm thick low carbon steel to 304 austenitic stainless steel. *Journal of Manufacturing Processes* 47, 324–336.

Fang, Y., Jiang, X., Mo, D., Zhu, D., & Luo, Z. (2019). A review on dissimilar metals' welding methods and mechanisms with interlayer.*The International Journal of Advanced Manufacturing Technology*, 102, 2845–2863.

Fragomeni J. M. & Nunes Jr. , A.C. (2003). A study of the effects of welding parameters on electron beam welding in the space environment. *Aerospace Science and Technology*, vol. 7, no. 5, 373–384.

Ghasemi, R. R., Beidokhti, B., & Fazel-Najafabadi, M. (2018). Effect of delta ferrite on the mechanical properties of dissimilar ferritic-austenitic stainless steel welds. *Arch. Metall. Mater.* 63, 1, p. 437**.**

Guo, J.F., Chen, H.C. , Sun, C.N., Bi, G. , Sun, Z. , & Wei, J. (2014). Friction stir welding of dissimilar materials between AA6061 and AA7075 Al alloys effects of process parameters. *Materials and Design*, 56, 185–192.

Harinath Gowd, G. & Venugopal Goud, E. (2012). Analysis of performance characteristics of laser beam welding. *International Journal of Engineering Science and Technology (IJEST),* 4, 05, 1925.

Harwani, D., & Banker, K., (2014). A Review: Welding of dissimilar metal alloys by laser beam welding & friction stir welding techniques. *Journal of Engineering Research and Applications*, 4,12(Part 1), 64-70.

Helal, Y. & Boumerzoug, Z. (2019). Microstructural evolution and mechanical properties of dissimilar friction stir lap welding aluminum alloy 6061-T6 to ultra low carbon steel. Energy Procedia 157, 208-215.

Ho, C. Y. (2005). Fusion zone during focused electron-beam welding," *Journal of Materials Processing Technology,* 167, 2-3, 265–272.

Hossain, M.A.M., Hasan, M.T., Hong, S.T., Miles, M. Cho, H.H., & Han, H.N., (2014). Mechanical behaviors of friction stir spot welded joints of dissimilar ferrous alloys under opening dominant combined loads. *Advanced in Materials Science and Engineering,* Vol. 2014, Janv. Article ID 572970.

Kaufman, J.G.(2003). Introduction to aluminum alloys and tempers. Ohio: *ASM International*.

Kaur, A. Ribton, C. & Balachandaran, W. (2015). Electron beam characterization methods and devices for welding equipment. *J Mater Process Technol.* 22, 225–232.

Khalfallah, F., Boumerzoug, Z., Rajakumar, S. & Raouache, E. (2020). Optimization by RSM on rotary friction welding of AA1100 aluminum alloy and mild steel. *International Review of Applied Sciences and Engineering,* 11, 1, 34-42.

Kuang, B. B., Shen, Y.F., & Chen, W.H. (2015). The dissimilar friction stir lap welding of 1A99 Al to pure Cu using Zn as filler metal with "pinless" tool configuration. *Mater. Des.* 68, 54–62.

Kurt, B. (2007). The interface morphology of diffusion bonded dissimilar stainless steel and medium carbon steel couples. *Journal of Materials Processing Technology*, 190, 1–3, 138–141.

Liu, G., Yang, S., Ding, J. , Han, W., Zhou, L., Zhang, M., Zhou, S., Misra, R.D.K., Wan, F., & Shang, C. (2019). Formation and evolution of layered structure in dissimilar welded joints between ferritic-martensitic steel and 316L stainless steel with fillers. *Journal of Materials Science & Technology*, 35, 2665–2681.

Marya, M. (2008). A brief review of challenges & Technologiesto weld dissimilar metals in two industries, the upstream oil & gas and the automotive. *Mater. Sci. Forum*, 580-582, 155-158.

Mendes, R., Ribeiro, J.B., & Loureiro, A. (2013). Effect of explosive characteristics on the explosive welding of stainless steel to carbon steel in cylindrical configuration. *Mater. Des*., 51: 182–192.

Mishra , R.S., & Ma, Z.Y. (2005). Friction stir welding and processing. *Mat Sci Eng R.* 50,1–2, 1–78.

Mulkerin, A. (2020). Dissimilar metal welding. *Technical report, ORK Sheet Metal.*

Mvola, B. Kah, P., & Martikainen, J. (2014). Dissimilar ferrous metal welding using advanced gas metal arc welding processes. *Rev. Adv.Mater.Sci.* 38, 125-137.

Pancikiewicz, K., Swierczynska, A., Hucko, P., & Tumidajewicz, M.(2020). Laser dissimilar zelding of AISI 430F and AISI 304 stainless steels. *Materials,* 13, 4540.

Paramsothy, M. , Hassan, S.F. Srikanth, N. & Gupta, M. (2008). Toughening mechanisms in Mg/Al macrocomposites : texture and interfacial mechanical interlocking. *Journal of Physics D,* 41, 175402–175410.

Pouranvari, M., Marashi, P., Amirabdollahian, S., Abedi, A. & Goodarzi, M.(2008). Microstructure and failure behavior of dissimilar resistance spot welds between low carbon galvanized and austenitic stainless steels. *Mater. Sci. Eng.,* 480, 175–180.

Praveen, P., & Yarlagadda, P. (2005). Meeting challenge in welding of aluminum alloys. *J. Mater. Process. Technol.* 164, 1106**.**

Priymak, E. Boumerzoug, Z. Stepanchukova, A. & Ji, V., (2020). Residual stresses and microstructural features of rotary friction welded from dissimilar medium carbon steels. *Physics of Metals and Metallography,* 121, 13, 119–126.

Rahimi, S., Konkova, T.N. Violatos, I., & Baker, T.N. (2019). Evolution of microstructure and crystallographic texture during dissimilar friction stir welding of duplex stainless steel to low carbon-manganese structural steel. *Metallurgical and Materials Transactions A*, 50A, 664-6687.

Satoh, G., Yao, Y.L., & Qiu, C. (2013). Strength and microstructure of laser fusion-welded Ti-SS dissimilar material pair. *Int. J. Adv. Manuf. Technol*. 66, 469–479.

Shahid, F., Khan, A. A. & Saqib Hameed, M. (2015). Mechanical and microstuctural analysis of dissimilar metal welds. *IJRRAS*, 25,1, 6-14.

Shanjeevi, C., Kumar, S., & Sathiya, P. (2013). Evaluation of Mechanical and Metallurgical properties of dissimilar materials by friction welding. Procedia Engineering 64, 1514-1523.

Sufizadeh, A.R., & Mousavi, S.A.A.A.(2016). Metallurgical and mechanical research on dissimilar Electron beam welding of AISI 316L and AISI 4340. *Adv Mater Sci Eng*, 6, 1–11**.**

Sun, Z. & Karppi, R.(1996). The application of electron beam welding for the joining of dissimilar metals: an overview. J *Mater Process Technol*. 59,3, 257–267**.**

Tolephih, M.H., Mashloosh, K. M., & Waheed, Z.(2011). Comparative study of the mechanical properties of (FS) and MIG welded joint in (AA7020-T6) aluminum alloy. *Al-Khwarizmi Engineering Journal*, 7, 2, 22 – 35.

Wetzel, H.J. (2012). Die Automobil eletronik der Zukunft—kabellose Infrastrukturen als Herausforderung oder Bedrohung. Frankfurt: In *Proceeding of the CTI Forum Automotive Wire*, 2012.

Zeng, R.C., Ke, W. & Xu, Y.B.(2001). Recent development and application of magnesium alloys. *Acta Metallurgica Sinica*, 37(7), 673–685.

Zhang, H. & Song, J. (2011). Microstructural evolution of aluminum/magnesium lap joints welded using MIG process with zinc foil as an interlayer. *Mater. Lett.* 65, 3292.